N°d'ordre NNT : 2020LYSEI062

THESE de DOCTORAT DE **L'**UNIVERSITE DE LYON
opérée au sein de
L'Institut National des Sciences Appliquées de Lyon
En cotutelle internationale avec
Université Politehnica de Bucarest

Ecole Doctorale N° EDA 162
MEGA DE LYON Spécialité

: Biomécanique

Soutenue publiquement le 18/09/2020, par :
Patricia **–** Isabela BR**Ă**ILEANU

Research on optimizing customized prostheses

Devant le jury composé de :

Bârsan Ioan-Lucian	Professeur des Universités	Université Transilvania de Braşov	Rapporteur
Massi Francesco	Professeur des Universités	Université Sapienza de Roma	Rapporteur
Gheorghe Marian	Professeur des Universités	Université Politehnica de Bucarest	Examinateur
Oujebbour Fatima-Zahra	Chargée de Recherche	C.N.E.S.T.E.N., Kenitra, Maroc	Examinatrice
Bou-Saïd Benyebka	Professeur des Universités	Université INSA Lyon	Directeur de thèse
Simion Ionel	Professeur des Universités	Université Politehnica de Bucarest	Co-directeur de thèse
Stoica Gina Florica	Professeur des Universités	Université Politehnica de Bucarest	Invitée

BUCHAREST
2020

ACKNOWLEDGMENTS

Now that the period of the doctoral studies has come to an end, but also because the PhD Thesis has been concluded, a mixture of deep feelings and happiness embraces me due to the personal satisfaction that another stage from my academic background has been completed.

In this sense, I would like to thank the people who gave me scientific support during all this period to complete this research work and to obtain satisfactory results.

I would like to express my deep gratitude to my scientific coordinators, Mr. Prof. PhD. Eng. **Ionel Simion** from *University "Politehnica" of Bucharest* and Mr. Prof. PhD. Eng. **Benyebka Bou-Saïd** from *Institut National des Sciences Appliquées de Lyon* for the continuous scientific support provided, for the opportunity offered to work in an international team of researchers at LaMCoS, INSA Lyon, where I settled my knowledge base in biomechanics, for the opportunity to work on the project with orthopedic surgeons to obtain a medical point of view for my PhD Thesis, and also for the opportunity to participate in summer schools and conferences to present my work in this doctoral field. Finally, I would like to thank them for giving me the freedom to have a personal approach on my PhD Thesis, to experiment and to exploit this field in a personal way.

I would also like to express my deep gratitude to Ms. Prof. PhD. Eng. **Gina Florica Stoica** because she believed in my potential from the beginning, when I was still a student aspiring to the title of engineer, and because she provided me study opportunities throughout my academic years.

In this way, I would like to thank to PhD. Eng. **Nicoleta Crişan** and PhD. Eng. **Florin Baciu** for the scientific help offered on the experimental part of my thesis.

My thanks to my colleagues from *Ecole Doctorale MEGA* and *TMI* team from *LaMCoS* for sharing their research interest in different fields during seminars and discussions, which helped me to broaden my area of knowledge, and to have a multidisciplinary approach on my PhD thesis. Among them, I would like to mention PhD. **Marine Menut**, **Wenyang Pan** and **Alberto Porras Vazquez**.

Finally, I would like to dedicate this research work to my family who supported me and encouraged me unconditional to fulfill my dream and finish this PhD research project.

PhD. Eng. Patricia Isabela Brăileanu

LIST OF ACRONYMS

2D – two dimensional, bidimensional
3D – three-dimensional
ABS – Acrylonitrile Butadiene Styrene
AM – Additive Manufacturing
ASCII – American Standard Code for Information Interchange
CAD – Computer Aided Design
CCN – Cervico Diaphyseal Angle
CDS – Center for Disease Control and Prevention
CLAHE – Contrast Limited Adaptive Histogram Equalization
CMD – Command Prompt
CoC – Ceramic on Ceramic
CT – Computed Tomography
CW – Clockwise
DICOM – Digital Imaging and Communications in Medicine
EFFORT – Romanian Register of Arthroplasty
ESTRN – Equivalent Strain
FE – Finite Element
FEA – Finite Element Analysis
FEM – Finite Element Method
FDM – Fused Deposition Modeling
HFS – Head First Supine
HU – Hounsfield Units
ISO – International Organization for Standardization
KVP – Peak Kilo Voltage
MoM –Metal on Metal
MoP – Metal on Polyethylene
MRI – Magnetic Resonance Imaging
NAOS – Numerical Analysis for Orthopedic Surgery
OA – Osteoarthritis
PLA – Polylactic Acid
PTFE – Polytetrafluoroethylene
RA – Rheumatoid Arthritis
ROI – Region of Interest
RP – Rapid Prototyping
SUUB – Bucharest University Emergency Hospital
SLA – Stereolithography
SLS – Selective Laser Sintering
THR – Total Hip Replacement
UHMWPE – Ultra-High-Molecular-Weight-Polyethylene
UML – Unified Modeling Language, use cased diagram
USP – United States Pharmacopeia class
VP– Virtual Prototyping
VPP – Virtual Preoperative Planning
VR – Virtual Reality
VTK – The Visualization Toolkit

TABLE OF CONTENTS

CHAPTER 1

INTRODUCTION

1.1.   Presentation of the doctoral thesis field

1.1.1. PhD thesis structure presentation

This research work was carried out between two university partners, *University "Politehnica" of Bucharest* and *Institut National des Sciences Appliquées de Lyon* as part of a "*cotutelle*" contract. To conclude the research work carried out during the doctoral years, it was then structured and divided into chapters as described below.

Chapter I offers a medical view of the human hip joint anatomical morphology and the determinative causes of hip pain with related or degenerative diseases which can occur in a patients' life, but also an engineering point of view which describes the evolution of the hip joint prostheses.

Chapter II presents the Total Hip Replacement surgery with its postoperative complications after THR, the hip joint prosthetic components with the type of bearings and categories, the traditional 2D preoperative planning that most of the orthopedic surgeons are using nowadays, and the transition trend to 3D virtual preoperative planning.

Chapter III describe a methodology of rapid prototyping of a custom femoral stem by using the patients' CT scans. The chapter goes through all the steps from the description of the medical files (DICOM files), through a bone segmentation process done in SimpleWare ScanIP and the specific algorithms used to extract the bone tissue. The refining surface preparation of the femoral CAD model, was concluded by obtaining patients' femoral landmarks in order to be used in the 3D virtual preoperative planning approach.

Chapter IV aims to analyze the mechanical behavior of a patient's hip joint that suffers of arthritis disease at different loads which may describe the patient's weight in order to observe how a poor quality bone tissue reacts to external solicitations, but also a comparative analysis between a standard femoral anatomical stem and a custom femoral anatomical stem at different loads, to observe their mechanical behavior.

Chapter V aims to develop a medical software, based on the information specified in the previous chapters, using VTK libraries to create a Multiplanar view with a perspective view of the patients' bone tissue by choosing the level of Hounsfield Units. A bone segmentation module was developed by using image processing algorithms to extract the desired bone tissue in a CAD model that can be used in the 3D virtual preoperative planning and also a changeable script of the femoral stem used as a template, in which by introducing specific dimensions can generate geometrical transformations that permits the femoral customization.

Chapter VI presents the flexibility of this customization and optimization method of the femoral stem by integrating it into the additive manufacturing sector, which represents the future and the tendency in bioengineering, offering the possibility of fast manufacturing of custom medical products. Compression tests performed on the custom prostheses made of biocompatible natural material show the possibilities, which can be exploited in future, when it comes to customization of femoral stem and AM fabrication.

Chapter VII represents the final chapter where the conclusions regarding the theoretical and practical part obtained from this research study are expressed together with future directions and possibilities to use this study in different future research works, which will take place in this orthopedic field.

At the end of the thesis are presented the reference sources used as a theoretical basis in this research study, which also includes the author's publications in specialized journals and conferences.

1.1.2. PhD thesis proposed objectives

This thesis aims to develop a virtual surgery planning methodology starting from the traditional Total Hip Replacement preoperative planning and having as final goal the realization of a template prosthesis that can be customized according to the femoral landmarks of each patient. Starting from the traditional preoperative planning of THR, which is done on the patients' X-Ray and using the same principles of obtaining femoral landmarks, the CT scans of a patient with hip joint related disease that need to undergo a THR surgery were segmented by using specific algorithms in order to extract the patients' femur and after that was imported in dedicated CAD software in which, with the help of evaluation instruments, all the patients' femoral landmarks were identified. These femoral landmarks were used to develop a custom prosthesis starting from a standard anatomical femoral stem, which was validated using FEA simulations.
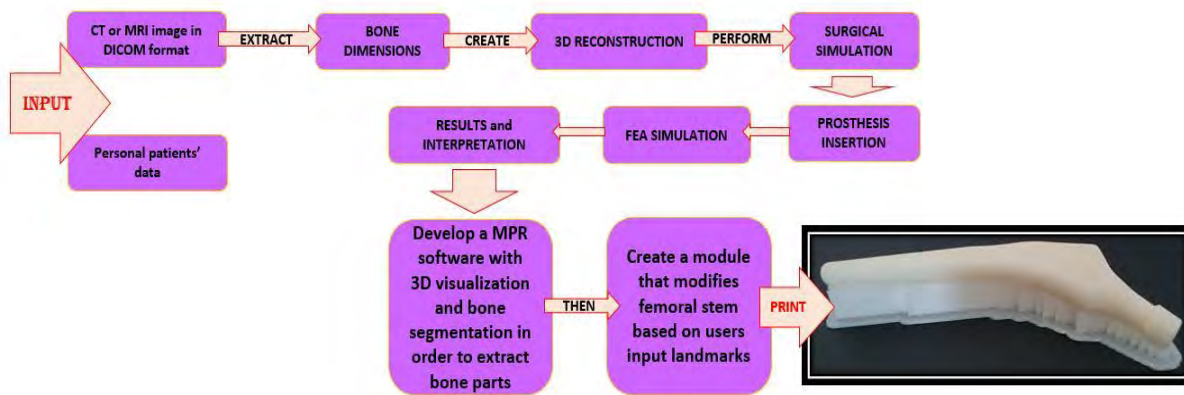
Figure 1.1. Project aim chart with its objectives

Based on the information obtained, the development of a software coded in Python language was done to create somehow a tool that allows the analysis of patients' CT scans in MPR view, but also in 3D view. It allows the bone segmentation of the affected area in order to obtain a CAD model file and perform the virtual preoperative planning in a CAD dedicated software, and finally use some of these dimensions in order to personalize a custom hip stem based on a pre-existing stem model used as basis for the desired geometrical transformations.

The work is completed by printing it with FDM technology, using a biocompatible material to demonstrate the potential of this study, the versatility and the possibility of orienting the femoral stems used in THR towards personalization and AM, avoiding the use of standard prostheses that

can lead to postoperative complications and thus leading to the elimination of prostheses "banks" due to the fact that they would no longer be necessary.

Following those described above, these objectives have been set for this research thesis:

O_1: Description of a methodology for geometric customization of the femoral stem according to patient's anatomical landmarks who is subjected to a THR surgery.

O_2: Development of a medical software meant to analyze the condition of the patient that will be subjected to a THR surgery, offering a visualization module, a segmentation module and a personalization of the femoral stem module.

O_3: Manufacture of the customized hip stem with the help of AM in order to emphasize the possibilities offered by this technology, too little exploited in the orthopedic endoprostheses field.

The results obtained from the study led to the achievement of secondary objectives, as follows:

OS_1: Bone extraction methodology applying specific image processing algorithms in Simpleware ScanIP.

OS_2: Finishing and remeshing the surfaces that define organic forms to simplify them in order to carry out FEA studies.

OS_3: Performing THR surgical simulation in a dedicated CAD software.

OS_4: Virtual simulation at different loads by using FEM having as purpose to obtain a characterization of the mechanical behavior of the prosthetic hip stem and the bone tissue interface to validate the custom femoral stem geometric shape.

OS_5: Developing a semi-automatic bone extraction code in Python language by using the Region Growing algorithm.

OS_6: Development and design of a medical software in Python coding language and proposing a user-friendly interface by using QT Designer software and library.

1.1.3. *The current state of femoral stem in the orthopedic field*

Nowadays, most of the orthopedic surgeons are using the traditional preoperative planning or surgical technique which consists in three main stages: the evaluation step, the anticipation step and the selection step.

In the evaluation stage the orthopedic surgeon are using an X-Ray of the patient that includes both hip joints in a 2D coronal view [1], begins to determines hip pathology (this can mean, for example, measuring the difference between the lower limbs), then is marking the femur center and observe its location in relation with the greater trochanter, to determine if the patient falls into a case of coxa valga or coxa vara. After the preliminary evaluation, the surgeon is drawing the diaphyseal axis of the femur and evaluates the bone support quality (sometimes uses also a left or right side X-Ray to gather information about the anteversion of the femur).

After the surgeon is concluding the first stage of the preoperative planning is starting to reconstruct the hip acetabulum by choosing an acetabular cup that fits better with the patients' needs from a standard catalog offered by the companies that produce this type of prosthesis. The same procedure is repeated in the case of the femoral component, the surgeon using a transparent template over which a femoral stem of different sizes is drawn, and overlaps it with the patient's X-Ray to find a standardized solution, as optimal as possible, to solve each patient orthopedic medical problem.

The step is concluded by adjusting the hip joint reconstruction and choosing the size of the prosthetic components from the catalog furnished by the company and finally planning a surgical technique approach that fits best with the patients' needs.
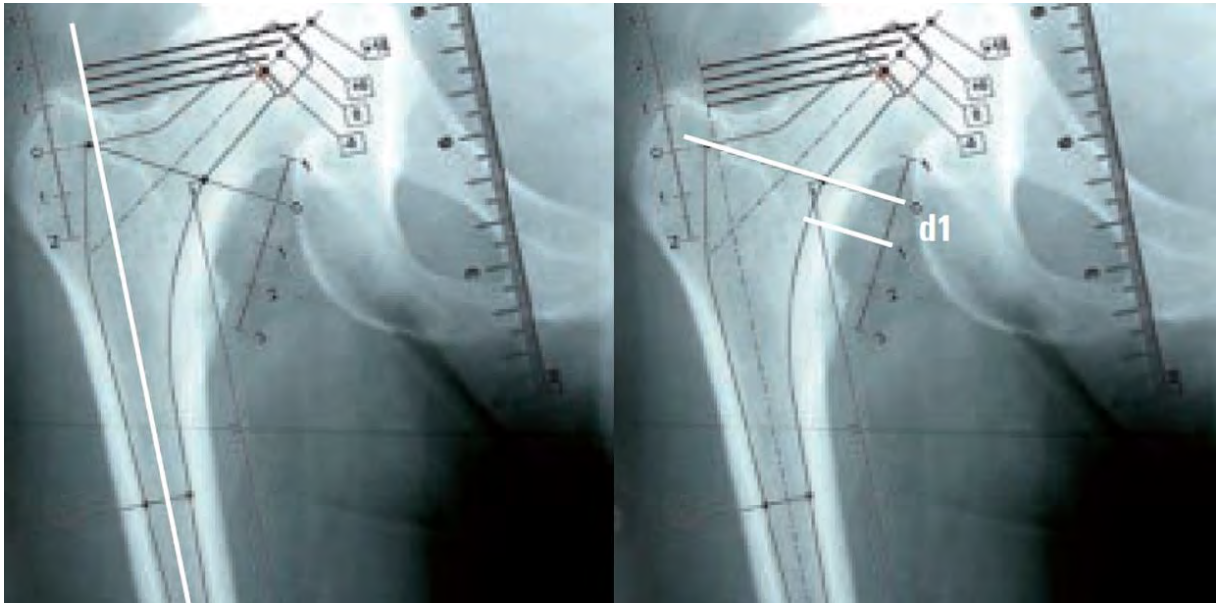
Figure 1.2. Femoral stem selection by using a stem template [2]

Standardized prostheses are kept in "prostheses banks" and they have an expiration date that usually is around 5 years. The orthopedic surgeon that is following to perform a THR surgery on a patient, use this "banks" every time to procure the prosthetic components and transport them in the hospital where it will perform the surgery.

Customized prostheses are used in exceptional situations, in which the patient has a special medical condition through which the implantation of standard prostheses would not solve or improve his medical condition. They are rarely used due to the difficult process of obtaining them, the number of specialized people involved and the production costs.

1.1.4. Current trends and research directions in THR and hip stem prostheses production

Nowadays, due to technology produced in the recent years as a result of technological advancement, researchers working in the bioengineering field together with orthopedic doctors, are forming research teams to improve prosthetic implants that meet better the patient's needs.

People are much more prone to orthopedic surgery such as THR from an early age and this happens due to the fact that in the recent years the population has begun to eat unhealthy food that predisposes them to obesity, or even they perform activities that strains excessively the hip joint articulation. For this reason, researchers are constantly trying to optimize the endoprosthesis either geometrically or the manufacturing material, to reduce the number of postoperative revisions of a patient, and thus, increase the lifespan of the endoprosthesis.

Periprosthetic osteolysis is one of the most common postoperative complications for which many patients have to undergo THR revision surgery, this taking place due to the detachment of wear particles from the polymeric components that in time eliminate proteolytic enzymes and

cytokines enzymes that eventually lead to the implant failure [4]. To slow down this wear process, the researchers realized that they can irradiate the polyethylene components with gamma rays, thus subjecting them to a treatment that makes them more resistant to wear.

Subsequently, the use of metal-on-metal couples was thought to reduce the probability of producing periprosthetic osteolysis, but this type of bearing couple also produces metal ions or metallosis, these being metal wear particles, which studies have shown to be carcinogenic, especially for patients with sensitivity and medical predispositions in this regard [5].
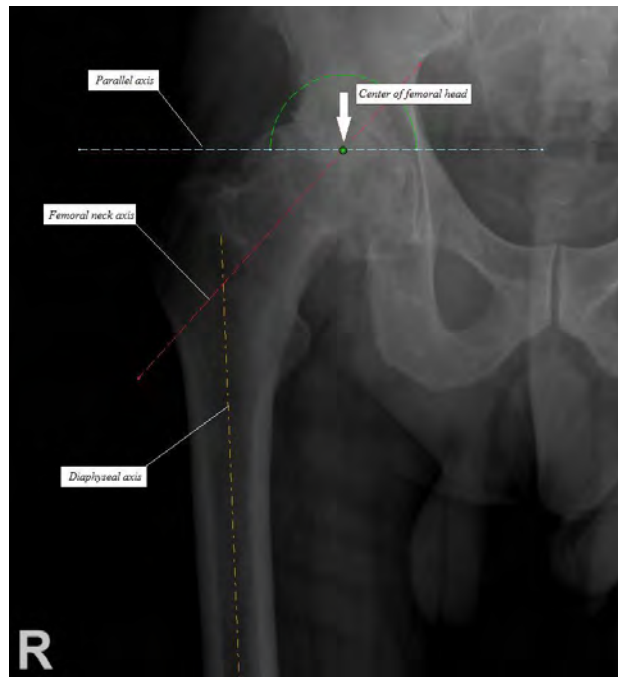
Figure 1.3. Axis tracing in 2D preoperative planning

Due to the fact that lately more and more young patients need orthopedic interventions such as THR, engineers and doctors have created implants coated with hydroxyapatite to prevent bone loss. It is usually used uncemented, and their fixation is done in time because this material allows the ingrowth of bone tissue on its surface [6].

The directions in orthopedic surgery and implicitly in THR surgery is to minimize the invasiveness of the surgery, this involves optimizing surgery time to reduce blood loss, optimizing the materials from which endoprosthesis are made, and, of course, finding optimal geometric solutions to reduce the number of surgical revisions after THR. In this sense, software engineers have started to produce software capable of performing computer-assisted surgeries in order to prepare future orthopedic surgeons, but also to prepare virtual THR surgery depending on each patient case. This can come as a solution to preview a THR intervention surgery and gives surgeons the opportunity to choose the most suitable solution for the patient who is about to undergo THR, in a virtual environment. One such software is Osso VR that allows surgeons to perform virtual surgeries that look very real because they use VR headset [7].

Designing geometric models that represent prosthetic components, which imitates or reproduce the anatomical landmarks of the patient, represents another direction of development in the orthopedic field. Because of this, researchers are trying to use femoral landmarks in order to customize prostheses and achieve better osseointegration. Among the first prostheses made by

Bohlman and Moore in the 1939 [8] were custom prostheses manufactured specifically for the patient who underwent surgery. Over time, however, with the increase of the orthopedic surgery interventions and due to limited technology, custom manufacturing has collapsed in favor of standardization of the prosthetic components because of the high production costs.

Due to technological advancement produced in recent years and especially because of the additive manufacturing industry development, researchers are performing VPPs to obtain patients' femoral landmarks directly from their CT scans, trying to customize the design of hip joint prostheses. In this sense, the trend is to use software that allows the user to choose anatomical landmarks dimensions and then generate the geometry of the implant based on algorithms. Finally, the design obtained can be manufactured using AM technology.

Recent research studies on materials used in the manufacture of prostheses try to reproduce the bone tissue to recreate a material that has the same mechanical properties and characteristics with the human bone tissue [9]. At first, both engineers and doctors considered that the use of metal prosthetic components biocompatible with the human body will solve the problem of wear, so implicitly the lifespan of the prosthesis. The introduction into the human body of a metal alloy bearing couple that has different properties from the bone tissue, with a high density, can cause damage to both femoral bone and pelvis due to high stress, which a human hip joint is exposed daily, and making patients more prone to postoperative complications, that includes also femoral bone fractures. Thus, research studies are carrying on this field to obtain a material that can be used in 3D printing and that has gradient property characteristics.

Figure 1.4. Pelvis model manufactured with AM technology

In this sense, all directions in the orthopedic field and implicitly in THR are made to obtain prosthetic components that have a design as close as possible to the anatomical structure of the human hip joint, but also at the material level, trying to imitate spongy bone tissue or cortical bone tissue, to obtain a medical product that better meets the needs of each patient who need to undergo such surgery.

1.2. The human joints

The joints are the connecting elements between the bones, which make the movements possible. Depending on the joint mobility degree, we can divide them into the following main categories: synarthrosis and diarthrosis (synovial joint).

1.2.1. Synarthrosis joints

Synarthrosis are fixed, immobile joints, which do not have articular cavity and which allow execution of reduced movements [10]. They are divided into three categories according to the type of tissue that interposes between the two articulated bones:

a. *Syndesmosis joints*: are joints joined by fibrous tissue, such as the joint between the coxal and sacral bones, joined by strong interosseous ligaments, or the sutures we encounter at the human skull;

b. *Synchondrosis joints*: are joints connected by a cartilaginous tissue layer, such as synchondrosis of the bones which form the coxal bone;

c. *Synostosis joints*: its results by ossifying syndesmosis and synchondrosis joints met at the elderly.

1.2.2. Diarthrosis / Synovial joints [11]

Synovial joints have a variable degree of mobility and are divided into the following categories:

a. *Amphiarthrosis joints*: are joints with flat or slightly concave, semi-movable surfaces, such as the joints between vertebrae;

b. *Arthrodesis / Syndesis joints*: are synovial joints with a high degree of mobility. The elements of an arthrodesis joint are the following: articular surfaces, joint capsule, synovial membrane, joint cavity, ligaments.

The *articular surfaces* can be spherical as in the femoral head case, concave as in the acetabular cavity case, or flat like the tibial plateau. These surfaces are "*coated*" with cartilage composed of hyaline cartilaginous tissue that does not contain nerves or blood vessels. Cartilage has the role of reducing the pressure exerted by body weight and protection, making easier the sliding between the bones. The cartilage destruction leads to the disappearance of movements in a joint, also called ankylosis.

The *joint capsule* contains a fibrous outer layer and a fibrous internal layer, also called the synovial membrane. The articular capsule acts as a sleeve that fits on both ends of the bones and has different thicknesses depending on the degree of mobility, for example the hip joint has a thick articular capsule. The role of the joint capsule is to protect the joints from the periarticular pathological processes and to prevent the synovial fluid spread in the neighboring tissues.

The *synovial membrane* is the deepest layer of the articular capsule formed by a thin and glossy layer that adheres to the surface of the joint capsule and which secretes the synovium (a yellow, viscous and greasy liquid that facilitates joint movements).

The *joint cavity* is a virtual space between the joint bone ends and the joint capsule with a small amount of synovial fluid. The presence of a negative pressure in the joint cavity as well as the atmospheric pressure, participates in keeping in contact with the surfaces.

The *ligaments* are fibrous formations attached to the bones, maintaining in contact the articular surfaces. When there are mismatches between the jointed surfaces, different fibrous-cartilaginous formations appear, achieving the matching of the surfaces, such as the meniscus in the knee joint.

1.3. The human hip joint movements

The human hip joint movements and mobile joint DOF (Degree of Freedom) depends on the surfaces form which are jointed, these can be made around an axis, two or three axes. We can distinguish the following movements that can be performed by human joints:

a.   *Flexion and Extension:* are movements of approaching or distance around a transverse axis of two parts;

b.   *Abduction and Adduction:* these two movements are made around a transverse axis. By adduction, we approach the limb to the median axis of the body and by abduction the limb distances from the median axis of the body.

c.   *Rotation:* it can be internal or external, depending on how the limb rotates and represents the movement made around the axis that passes through the moving segment/limb.

d.   *Circumduction:* it is a complex and compound movement which sum up flexion, extension, abduction, adduction movement and associates them with the rotation movement.

e.   *Pronation/Supination:* pronation is the rotation movement of the hand, by which the thumb rotates medially, with the palm oriented downwards, and supination is the reverse movement.

1.4. Human hip joint anatomical morphology

The hip joint, or sometimes referred as *coxa* in specialized medical terminology is the human body biggest joint. The hip joint occupies a vital position and role in the body, which, without it, locomotion would not have been possible. Being a synovial and spherical joint because the spherical head of the femur fits in the pelvic concave cavity, thus forming the hip joint capsule. The femur's head surface and the concave part (acetabulum) of the pelvis are "*coated*" with a layer of hyaline cartilage or articular cartilage, having the role of reducing the friction between the two joint elements during movement, but also of absorbing shocks that may occur during more demanding activities or even in the event of an accident.

The complex structure of the human hip joint makes possible to perform the following movements: flexion (this movement allows the thigh to approach the front part of the abdomen) and extension (this movement allows the thigh to distance the front part of the abdomen) made around a transverse axis that passes through the top of the big trochanter in the sagittal plane; abduction and adduction, made around an antero-posterior axis that passes through the center of the femoral head and it is performed in the frontal plane; external and internal rotation made around an antero-posterior axis that passes through the center of the femoral head; circumduction being

possible by combining the other movements. The components of the hip/coxofemoral joint are the following: ilium/coxal bone or pelvis, femoral/diaphyseal bone, acetabular labrum, hip joint ligaments, hip joint capsule and hip joint muscles.

1.4.1. *The pelvic girdle*

The coxal bone it is an irregular shape bone often likened to a propeller formed by three smaller bones called ilium, ischium and pubis, which all connect in the acetabulum and sutures between them at puberty, the connection lines having the appearance of a "Y" letter. The two coxal joint anteriorly forming the pubic symphysis and posteriorly with the sacrum, forming the sacroiliac joint. In the center it is located the acetabular cavity, and above it is the external face of the ilium on which is located the anterior and posterior gluteal line. Between these two lines the three gluteus muscles have the origins.

The medial face of the pelvis presents the arched line, above the arcuate line is the iliac fossa and below is the iliac tuberosity. It presents also an articular surface of the coxal bone and a flat surface corresponding to the acetabular cavity.
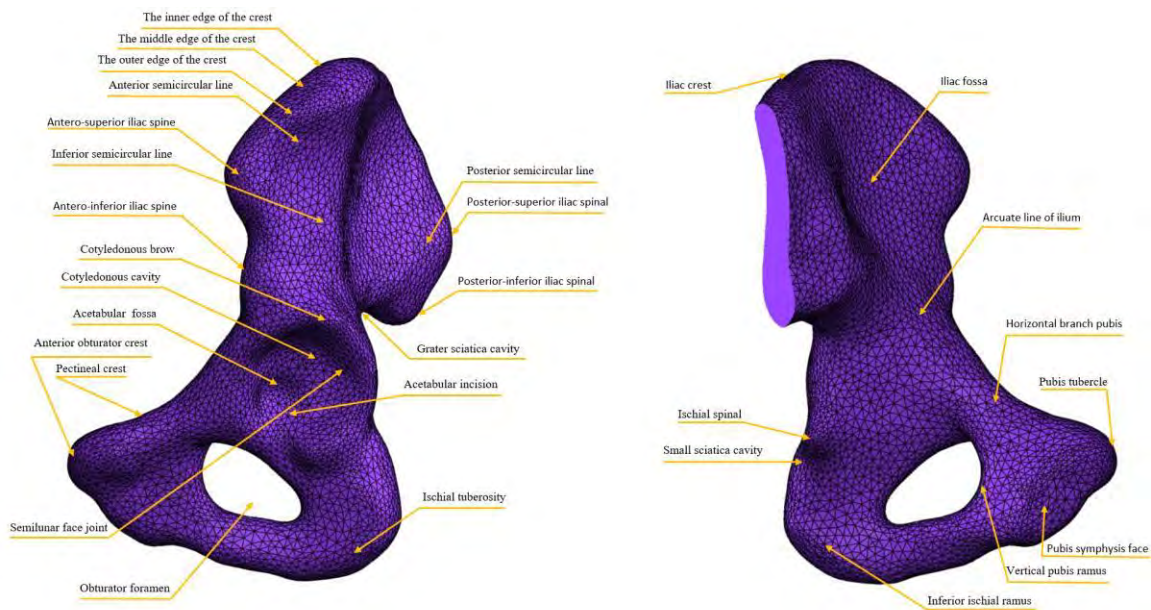
Figure 1.5. Pelvic girdle

The upper margin of the ilium is represented by the iliac crest, which has the shape of a rotated S. The inferior margin presents an anterior segment that joints with the other coxal forming the pubis symphysis and a posterior segment represented by the ischiopubic ramus. Anterior margin presents antero-superior iliac spine, antero-inferior iliac spine, the iliopubic eminence, the pectineal line and the pubis tubercle. The lower margin of the pelvis shows the posterior-superior iliac spinal, the posterior-inferior iliac spinal, the large ischial cavity, ischial spine, the small ischial cavity and the ischial tuberosity.

1.4.2. Diaphyseal bone

The diaphyseal bone, commonly known as femur is compounded by three parts: one named diaphysis, an extremity called proximal epiphyses and another one called distal epiphyses. The proximal epiphysis contains the femoral head, the femoral neck and the two tuberosities, the greater and the lesser trochanter. The femoral head is 2/3 of the sphere and articulates with the acetabular cavity of the coxal bone. The greater and lesser trochanter are united posteriorly by the intertrochanteric crest and anteriorly by the intertrochanteric line.
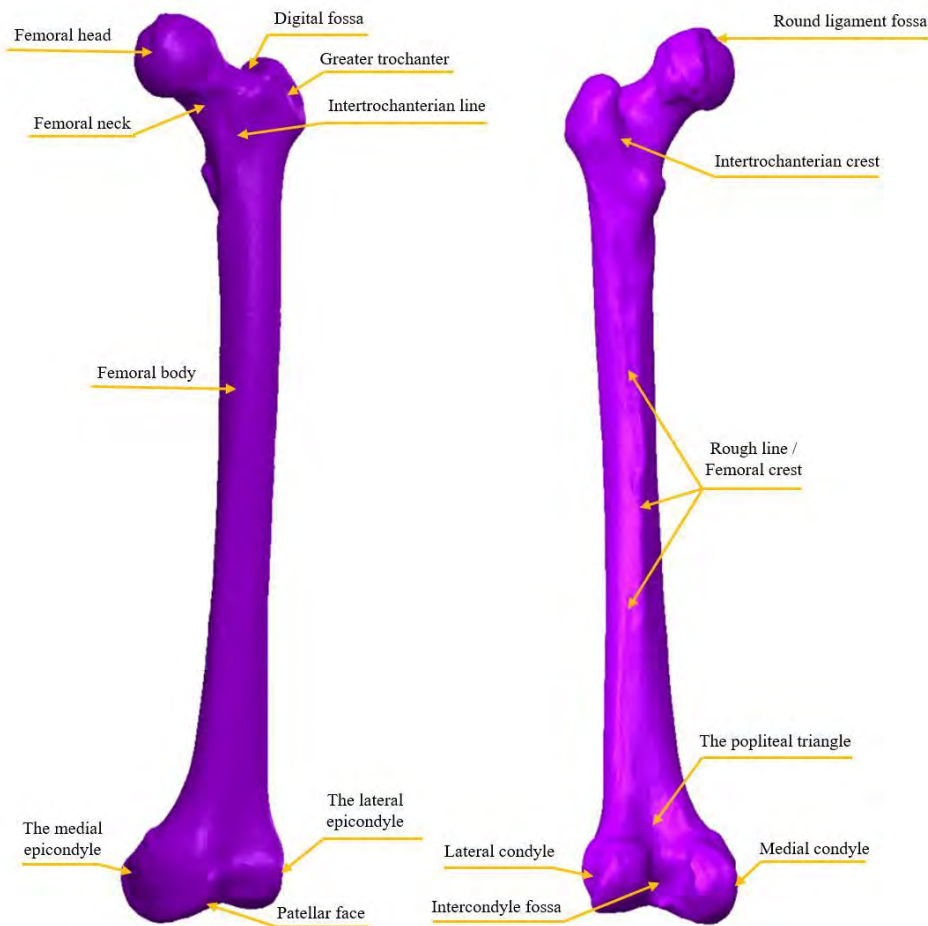
Figure 1.6. Femoral bone

The diaphysis has a prismatic geometry, having an anterior face, a medial and a lateral one. At the union of the medial and lateral faces, the rough line is observed, which, at the top is divided in three and at the bottom in two.

The distal epiphyses presents two articular surfaces called femoral condyles. Between the two condyles the patellar surface is located and posteriorly the intercondylar fossa. Above the medial part is the medial epicondyle and above the lateral condyle, the lateral epicondyle.

1.4.3. Acetabular labrum

Acetabular labrum is a ring made of fibrous cartilage, fixed on the acetabulum circumference.

1.4.4. Hip ligaments

Ligaments are a fibrous or fibro-conjunctival formation which fixes and reinforce the hip joint components (iliofemoral, ischiofemoral, pubofemoral which are extracapsular ligaments and the only intracapsular ligament called the femoral head ligament).

1.4.5. Hip joint capsule

Hip joint capsule is a longitudinal and circular fibrous ring which forms a reinforcement around the femoral neck.

1.4.6. Hip joint muscles

Hip joint muscles are a contractile tissue formed by muscular cells, which make possible the following hip joint movements: extension (semimembranosus, semitendinosus, biceps femoris and gluteus maximus muscles acts to achieve this type of movement), flexion (sartorius, rectus femoris, pectineus and iliopsoas muscles acts to achieve this type of movement) , adduction (pectineus, gracilis, adductors longus, brevis and magnus muscles acts to achieve this type of movement), abduction (tensor fascia latae, gluteus medius and minimus and piriformis muscles acts to achieve this type of movement), lateral rotation (obturators, piriformis, biceps femoris, gluteus maximus, gimili and quadratus femoris muscles acts to achieve this type of movement) , medial rotation (gluteus minimus and medius and tensor fascia latae muscles acts to achieve this type of movement).

1.5. Causes of hip joint pain and related illnesses

1.5.1. Patient group risk

One of the most common orthopedic surgeries today is THR because of the increased number of people affected by various diseases or traumas that need to be removed/solved by such surgery. The patients who present the highest risk group and who are more prone to such orthopedic surgery are elderly patients, age being a determining factor due to bone tissue degradation and the reduced ability of cell regeneration that generates structural changes in the bone tissue, causing the appearance of so-called bone demineralization.

Following the statistics from Swedish Hip Register (1992-2003), one of the most spread hip joint disease affecting people aged under 50 is the primary osteoarthritis (52%), for the people aged between 59 and 50 the primary OA affects them in 78.2%, for the individuals aged between 75 and 60 the OA affects them in 80.5% and for the individuals aged over 75 the primary OA affects them in a percent of 66.9%.

There are also other factors, of which patients end up undergoing THR surgery, these being: excessive sports activities that require repetitive movements or that stress excessively the individual hip joint, morbid obesity, lack of physical activity, accidents from which results injuries or trauma at the hip joint level, venereal diseases or hereditary inheritance, etc. Due to such factors, degenerative diseases such as bursitis or other inflammatory diseases led to THR a percentage of 4.6% of the patients, a percentage of 11.4% of patients who suffered bone fractures undergo THR, 1.6% of the patients who suffered various diseases in childhood went through THR surgery, 2.9% of patients with avascular necrosis undergo THR and 0.4% of patients who were diagnosed with a tumor went through THR surgery [19].

The main risk factors which trigger arthritis are:

a.   *Gender:* the exact causes that influence arthritis onset is still unknown, but studies have shown that women are more exposed to rheumatoid arthritis and osteoarthritis than men; instead men are more exposed to develop gout [20].

b.   *Heredity:* if there are cases of arthritis in family history exists a high probability that the disease will be genetically transmitted to children [21].
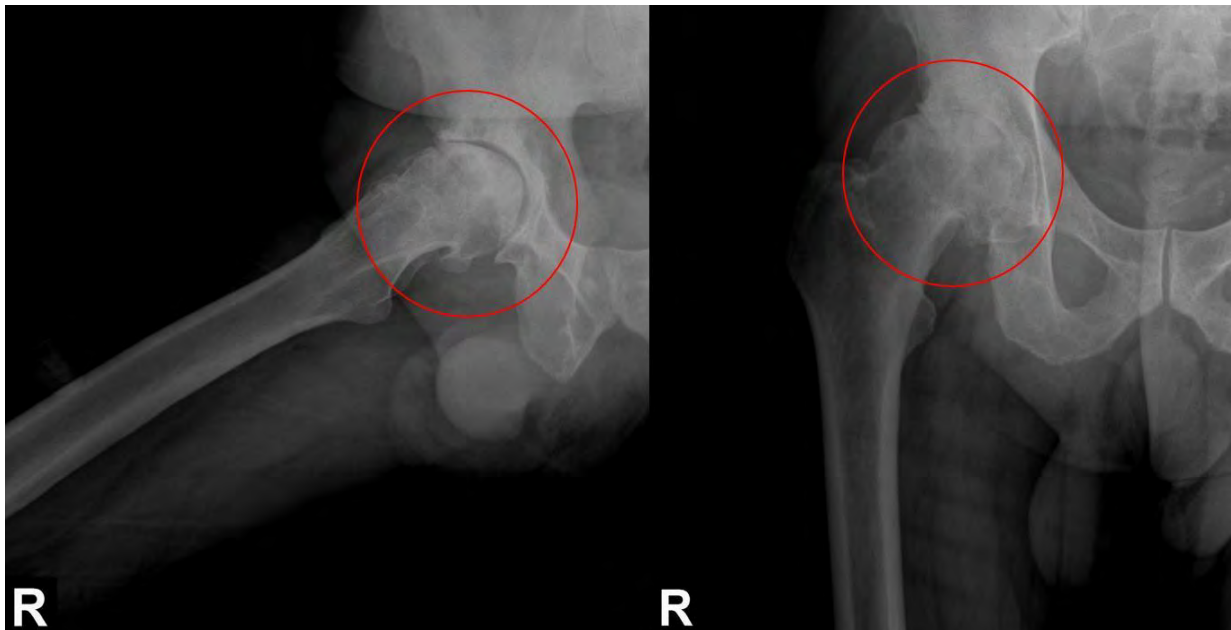
Figure 1.7. Osteoarthritis disease affecting a patient hip joint [Image Source: SUUB]

c.   *Obesity and overweight:* the weight puts high pressure on the hip joint during daily activity [22].

d.   *Hip joint physical trauma:* some of the injuries that occurs in the hip joint area can lead to arthritis and people which are more exposed to hip joint trauma are the professional athletes [23].

e.   Job: people whose work involves repetitive movements of the pelvis associated with osteoarthritis [24].

f.   *Smoking:* studies have shown that smokers presents an increasing risk of rheumatoid arthritis or it may worsen the situation of a patient diagnosed with arthritis [25].

g.   *Age:* with age patients are more exposed to any type of arthritis [26].

Symptoms varies depending on the type of disease, but most of the common signs that may indicate arthritis installation are hip joint pain, joint stiffness, swelling in the area of the hip joint, hip sensitivity and local heat sensation. Usually, in the morning hip joints may be more stiffened and the pain can be accompanied by fatigue of moving.

The treatments can be surgical or non-surgical which can be accompanied by physiotherapy, alternative medicine treatments, even healthy diets meant to slow down the process of hip joint degradation, but in most cases the disease progresses over time and with aging the hip joints are so degraded that they require urgent treatment measures such as surgeries.
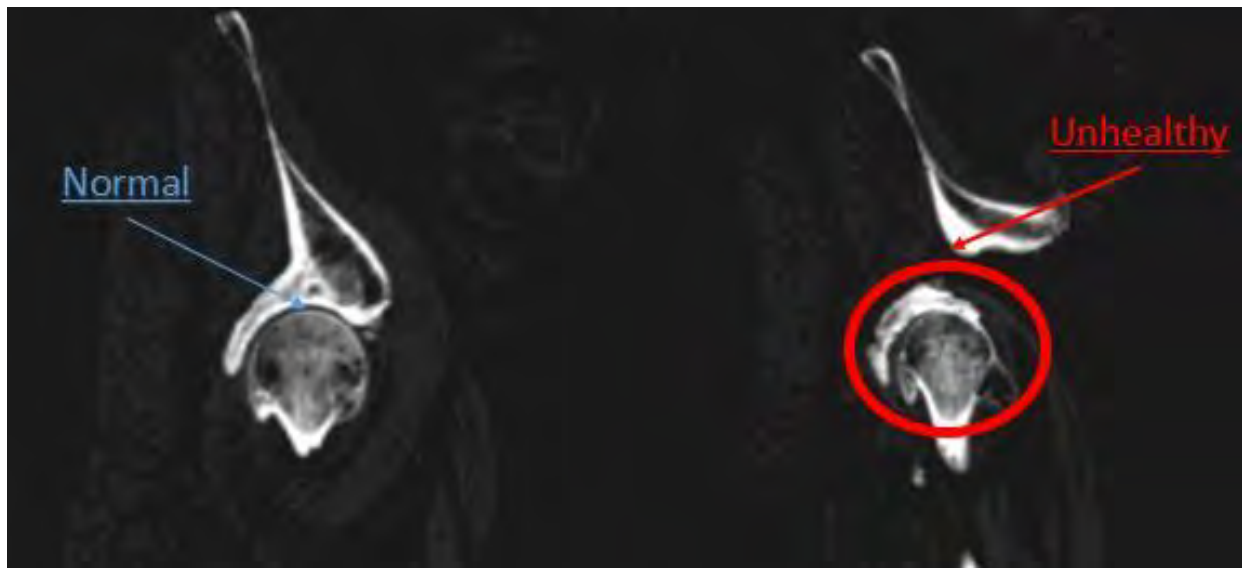

Figure 1.8. Comparison between a healthy and diseased hip joint of a 77 year old female patient

1.5.2. Arthritis pathology

Arthritis is a pathological disease which involves articular inflammation that occurs as the acetabular labrum wearing that over comes in time. As the disease progresses the cartilage is diminished excessively until it disappears and, in time, leads to bone deformation that causes hip pain.

Nowadays it exists around one hundred arthritis affections which, depending on the disease stage or progress can lead in time to surgical interventions. The most common forms of arthritis are rheumatoid arthritis or RA (a very painful arthritis form, an autoimmune disease) [27] and osteoarthritis or OA (occurs at the appearance of acetabular labrum wear, especially with aging) [28]. If arthritis affects more joints at the same time it is known as polyarthritis [29] and it is usually associated with autoimmune diseases that can occur at any age.

The causes of arthritis may vary, depending of the heredity, medical history and predisposition of the patient, the rheumatoid arthritis arises because the patient's immune system start to produce antibodies which attacks their own tissues that at the beginning results as an inflammation, but in time the inflammation spreads to the cartilage, muscles, tendons, ligaments and finally to the bones that starts to deform and wear. This autoimmune disease affects around 1% of the world population being nine times more frequent at women. Osteoarthritis / osteoarthrosis instead, occurs with aging

and it is a degenerative disease that appears in time. Because of the hip cartilage wear, frequent cause severe hip pain and disability among elderly patients.
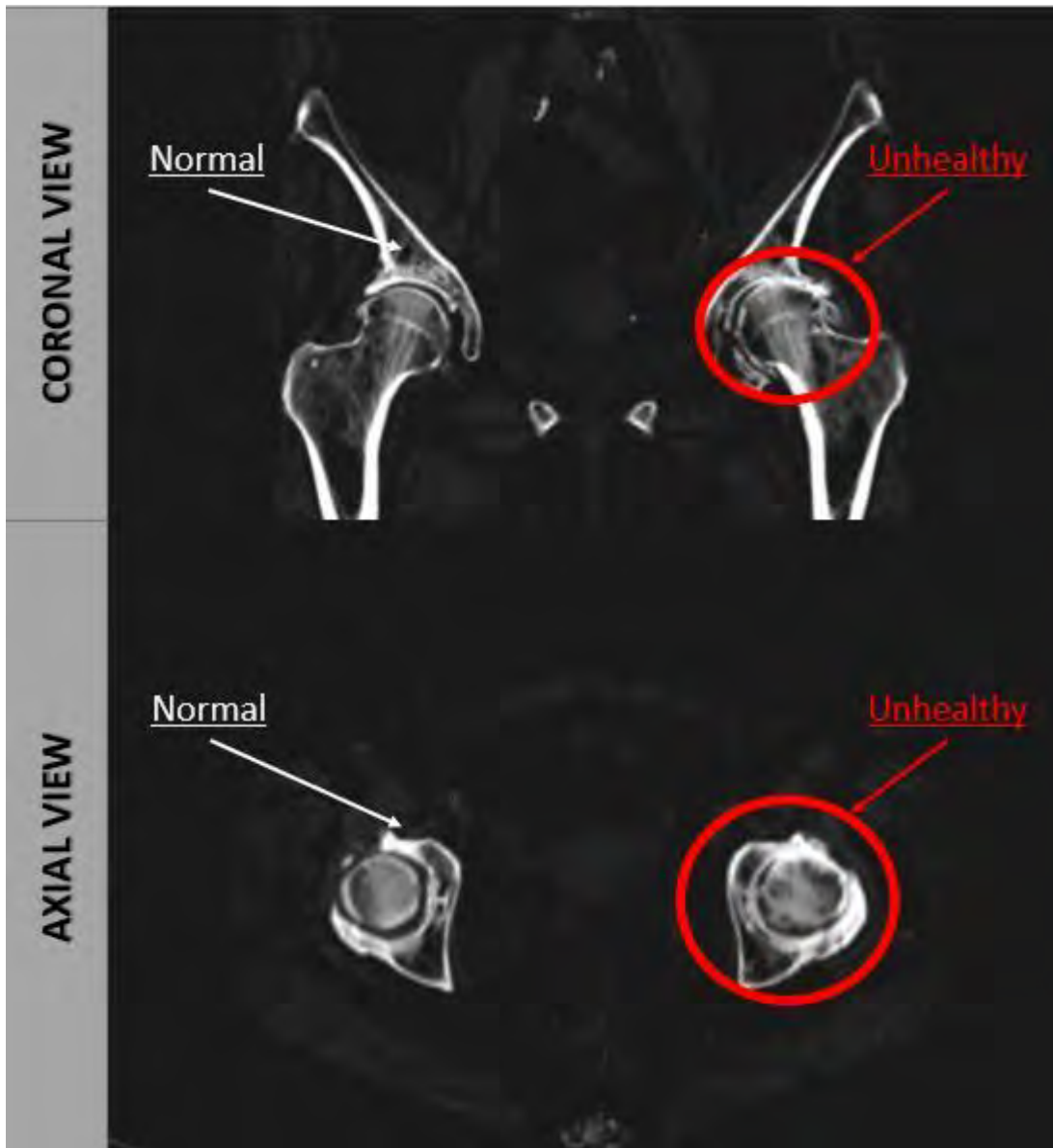
Figure 1.9. Affected hip joint identification in the coronal and axial view of the studied patient case

In the USA the Center for Disease Control and Prevention called CDC collects data in order to establish an average annual arthritis prevalence for people which are more than 8 years old. Between 2013 and 2015 around 22.7%, the equivalent of 54.4 million adults were diagnosed with arthritis diseases. Due to the unhealthy lifestyle, pollution, lack of physical exercises and other factors, CDC expects an increase of arthritis diagnosed patients in the following decades, so in the 2040s around 25.9% of the US adult population will be diagnosed with arthritis, the equivalent of 78.4 million adults will be diagnosed with this disease, with 24 million people more, than between 2013 – 2015 (2/3 from the population diagnosed with arthritis it is estimated to be women) [30].

Figure 1.10. Statistics on the US population diagnosed with arthritis according to ethnicity

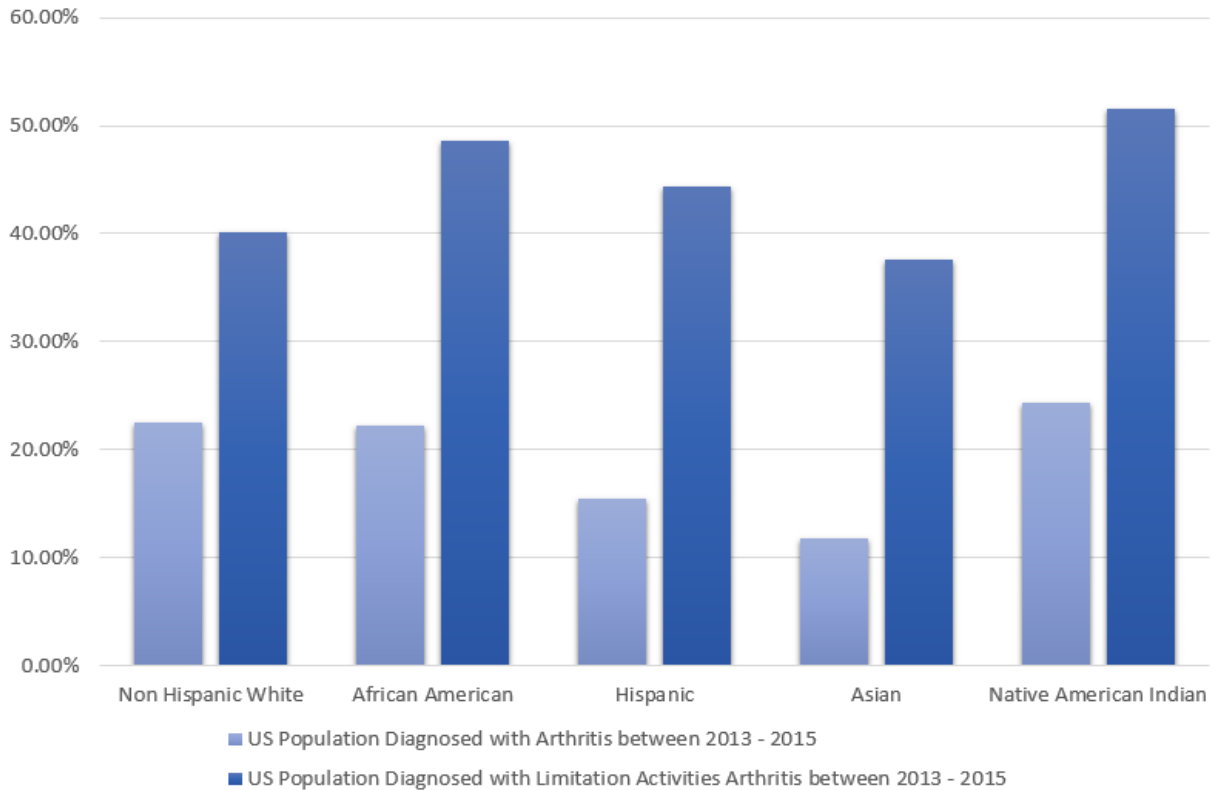CDC also published a racial/ethnic data realized by National Health Interview Survey during 2013 – 2015, which shows that non–Hispanic white population was diagnosed with arthritis in a percentage of 22.6%, African American population was diagnosed with arthritis in a percentage of 22.2%, Hispanic population was diagnosed with arthritis in a percentage of 15.4%, Asian population was diagnosed with arthritis in a percentage of 11.8% and Native American Indian was diagnosed with arthritis in a percentage of 24.4%, which shows that in this case the white non-Hispanic race along the Native American Indian are the most prone to develop rheumatoid arthritis during life. Instead the percentage of adults diagnosed with arthritis who presents limitations of activities based on race/ethnicity are the following: 40.1% for the white, non-Hispanic, 48.6% for the African American, 44.3% for the Hispanic, 37.6% for the Asian and 51.6% for the Native American Indian [31].

Due to patients percentage who are predisposed to diseases such as arthritis the probability that they will undergo surgery to substitute the affected joints is constantly growing, thus, engineers and orthopedic surgeons are working together to optimize the current prosthetic implants in sense of : geometry/design, mechanical material properties , the osseointegration capacity of the implant and its durability/life spam.

1.6.   Evolution of the hip joint prostheses

During the life of an individual, multiple factors can determine the appearance of joint diseases and for this, researchers have constantly worked on optimizing the prosthetic components that are

used in THR. Due to the anatomical shape of the femur and pelvis bone, but also to the movement produced by this joint, the prosthetic elements have been designed to achieve a spheroidal contact with the aim of making movements as close as possible to those of a healthy hip joint, but also to absorb the shocks and the body weight transmission in a static position or during demanding activities.

The oldest exoprosthesis in the world was located in Luxor in the 2000s and is a thumb toe made of wood dated between 950-710 B.C. [32, 33]. Although exoprostheses enjoyed such an early evolution, implants/endoprosthesis on the other hand appeared much later, because the people had limited knowledge of the human body at that time and the idea of biocompatibility was completely unknown, many attempts resulted in total failures.

Before orthopedics became as we know today, amputation was the safest and most convenient way to save suffering patients, because of this, in the 1860 orthopedic surgeons began testing various techniques to save patients with bone tumors from amputation, but unfortunately all their attempts failed at that time [34]. However, orthopedic surgeons were aware of the need for a prosthesis which reproduce the hip joint, and between 1881 and 1890, Themistocles Gluck succeeded in performing a surgery that involved replacing a femoral head with a component made of ivory for a patient, and this technique proved to be a real success [35]. Later, in the same year, he decided to introduce methacrylate cement into his technique to create a better fixture of the prosthetic components [36].

Over time, different bearing couples were developed in an attempt to find the best prosthetic component combination, but Charnley's implementation of "*low-friction arthroplasty*" led to the emergence of a bearing couple called MoP, which is still the most spread today [37].

In the 1930s, it was developed by Philip Wiles the first MoM bearing couple, both components being made of steel and fixed into the bone with screws. Later, in 1953, this bearing couple was improved by two orthopedic surgeons Ring and McKee, by using a modified Thompson hip stem prosthesis, and McKee's method proved to be a real success because the lifespan of his prosthesis was around 28 years [38].

The researchers' attempt to make the most reliable version of the hip joint prosthesis, it was a long process, which in 1925, in an attempt to implement more accessible materials M. Nygaard Smith-Petersen, an American orthopedic surgeon performed the first mold arthroplasty which proved to be a failure because the prosthetic components were made of glass and due to material fragility, the components of this material were very brittle [39].

Total Hip Replacement is as we know it today because of the British orthopedic surgeon Sir John Charnley, who introduced the principle of "*low-friction arthroplasty*" and since then, both engineers and surgeons have been working together to develop a more feasible bearing couples than the one made by Charnley and based on MoP bearing couple [40, 41].

In the 1970s, Boutin made a ceramic bearing couple due to the known high biocompatibility with the human body of these materials, and which was called CoC bearing couple [42].

1.7.   Chapter conclusion

All human beings are complex and unique organisms, each one presenting anatomic particularities that need to be considered if the patient must undergo a surgery. Although hip prostheses evolved later than exoprostheses due to the limited knowledge of the human body that scientists knew at that time, starting with surgeon Carnochan, who in 1840 came up with the idea of replacing an affected hip joint with an artificial one, hip prostheses are experiencing a relatively

rapid rise that has taken place with technological advancement and the understanding of biocompatibility. Nowadays, the technology promises countless directions for the development and modernization of this field of orthopedics, and THR surgery can now be planned in a virtual environment. Along with the AM technology, the ways to personalize the prosthetic components can be opened, trying to imitate as well as possible the anatomy of each patient in an attempt to reproduce a model as "*biofidel*" as possible.

CHAPTER 2

TOTAL HIP REPLACEMENT SURGERY AND PREOPERATIVE PLANNING

2.1.   Overview of Total Hip Replacement surgery

Degenerative diseases over time can affect the patient's joints and one of the most predisposed joints of the body is the hip joint due to repetitive movements and daily activities. With age and with the progression of the disease, the patient experiences discomfort at the joint level, and later, more and more intense pain, so in the end the patient must undergo surgery.

Total hip replacement or THR is a surgery that completely replaces the damaged hip joint of a patient as a result of its irreversible deterioration with an artificial mechanical hip joint meant to restore the mobility and the movements that the patient initially was able to make before the onset of the disease, in the most natural way possible. THR is one of the most successful orthopedic surgery worldwide due to the continuous development of the medical technique, of the research performed in this field for the hip prostheses optimization, from a geometric point of view and in terms of used biomaterials, the tendency being to ensure quality prostheses, suitable for patients, made of durable materials, so that surgical revisions interventions to be diminished.
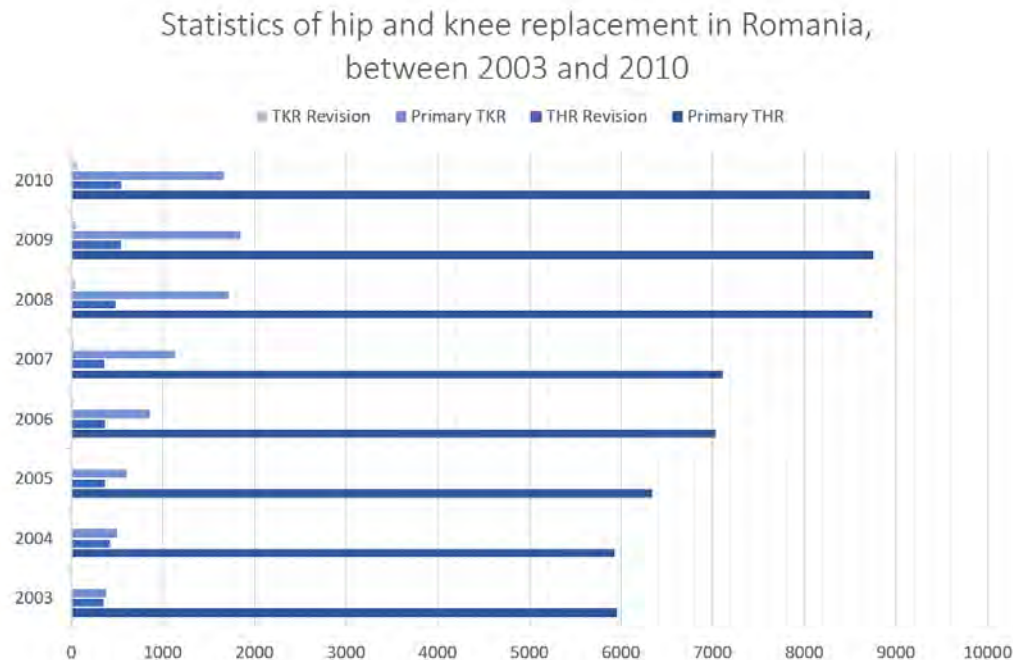

Figure 2.1. Statistics of hip and knee replacement in Romania, between 2003 and 2010 according to Romanian Arthroplasty Register under E.F.O.R.T. Supervision [43]

THR has become a common surgery due to the frequent pathology which affects the hip joints. Normally, the patient undergoes a rigorous preoperative preparation, and the hospitalization is

usually performed one day before the intervention if there are no other health problems, which involves a different surgery approach. The average duration of a THR is approximately one hour, and during the intervention the patient is permanently monitored by specialists. The day after the surgery the patient starts the postoperative recovery program, and the average hospitalization duration is about one week.

According to Romanian Arthroplasty Register under E.F.O.R.T. Supervision, which collects general information in the orthopedic field, has made a statistic between 2003 and 2010 that registered a number of 695 188 patients hospitalized in the orthopedic department, of which 455 108 of them underwent surgery. The statistic shown that primary hip replacement is the most common orthopedic surgery with a total of 58 591 patients, followed immediately by total knee replacement with a total of 8 690 patients. We can observe an uneven distribution of the bipolar THR across age groups, with female patients being more prone to degenerative diseases such as primary coxarthrosis or femoral fractures (66.78% of female patients) than male patients (57.64% of male patients) [43].

2.2.   Hip joint prosthetic components

The total hip prostheses consist of three elements that connect with each other, usually by press fit, meant to make a spherical contact that allows the movements of flexion, extension, abduction, adduction and external or internal rotation of the hip.
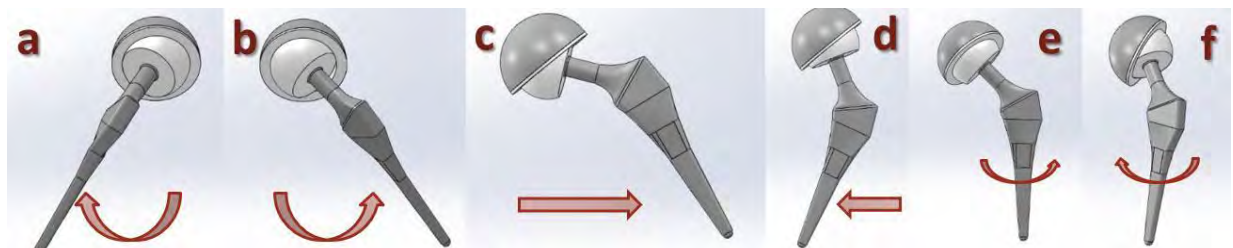

Figure 2.2. Hip joint prosthesis allowed movements (a. Flexion; b. Extension; c. Abduction; d. Adduction, e. External rotation; e. Internal rotation)

Both the hip joint prostheses and the surgical approach are performed based on the particularities related to the patient's hip joint morphology and the medical history, so surgeons look for the best standardized hip prosthesis type for each individual patient and the most appropriate surgical medical technique to achieve a successful intervention without postoperative complications.

2.2.1.   *Femoral hip stem*

The hip stem is the component inserted into the patient's femoral canal after the femur has been sectioned to remove the damaged area. It is made of special alloys, such as titanium, to ensure the best biocompatibility. Usually they are coated with hydroxyapatite to facilitate the growth of bone tissue on the load-bearing surface which leads to a better osseointegration and implicitly a good stem fixation. Also, the femoral stem can be cemented (usually used for patients with poor bone quality, such as elderly patients who have bone tissue demineralization) or uncemented (commonly

used for young patients, or active patients who may subsequently undergo hip replacement surgery in order to replace the old hip prosthesis without damaging the femur) [44].
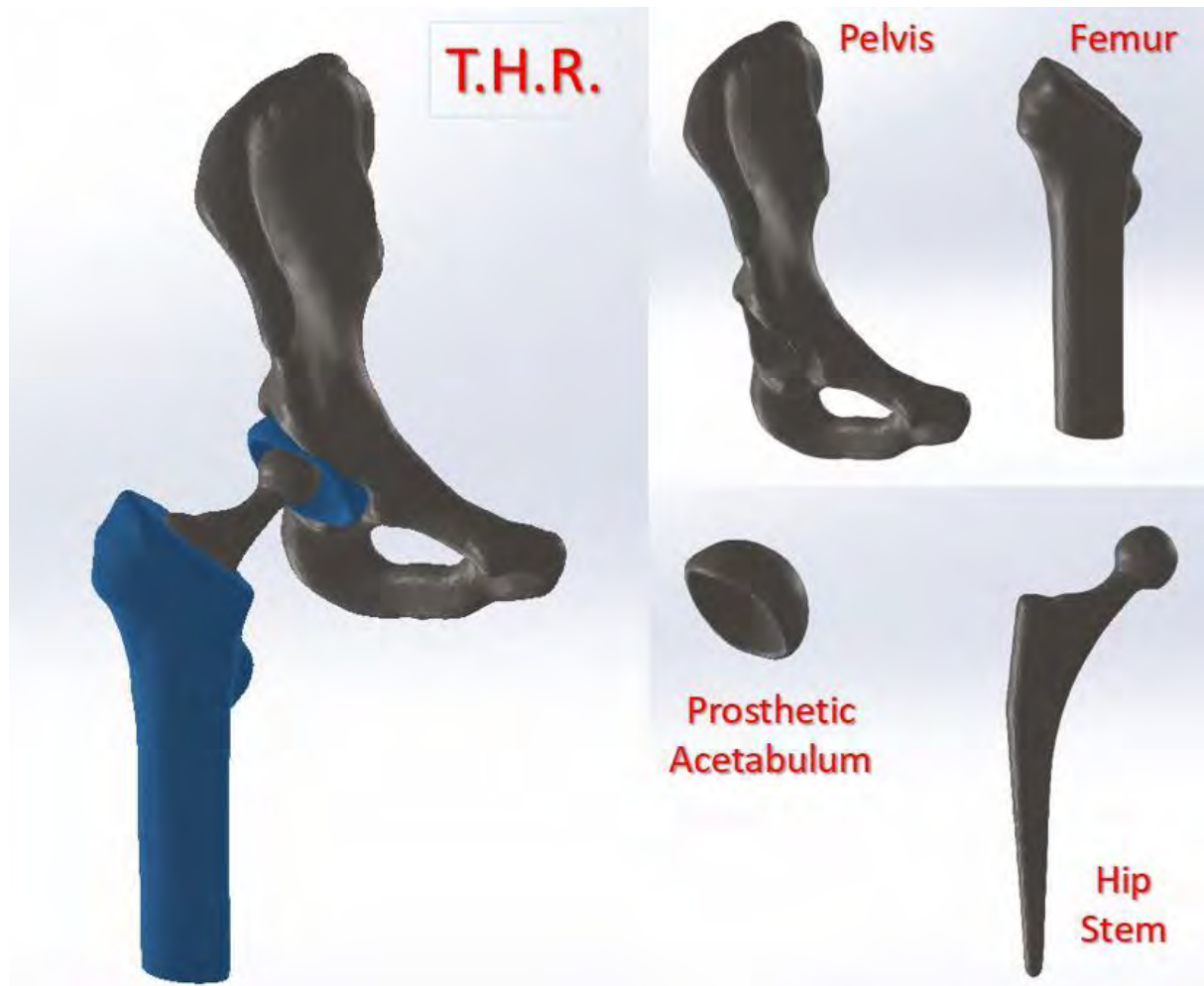

Figure 2.3. THR prosthetic main components

2.2.2. Acetabular prosthetic cup

The acetabular cup it is the prosthetic component fixed with the help of special screws in the pelvis, having the form of a hemisphere made of special alloy or other biocompatible materials. The acetabular cups can be created for both cemented and uncemented mounting having standard diameters [45].

2.2.3. Acetabular prosthetic liner

The acetabular liner it is the element intended to mimic human cartilage, usually made of polymeric material such as High-Density Polyethylene (UHMWPE, for example) [46].

2.2.4. Femoral prosthetic head

The femoral head is a component that has a spherical shape fixed to the femoral stem, inserted into the acetabular component and forming a spherical contact [47].

2.3. Hip joint prostheses type of bearings

There are a variety of bearings used in THR, and as science advances, they become more and more effective, biomaterials trying to mimic bone tissue or facilitate osseointegration of prosthetic components. Hip prostheses are made of specially selected and tested materials that have the quality of being biocompatible with the human body, because the human body can identify the prosthesis as a foreign object and reject it after THR. The human body is a harsh, corrosive environment and therefore the material from which the hip prostheses are made must be resistant to corrosion and wear, in this way to produce less wear particles as possible over time, and of course, to withstand repetitive activities and motion cycles. Because of the movements, between the two surfaces of the prosthetic components that come into contact and due to the absence of natural lubrication of the hip joint, after the implantation of the prosthetic components begins their wear process. During the movement cycle due to friction, particles on the prosthetic components surface detach from them, so these particles called generic *debris* can cause serious postoperative complications leading to prosthetic failure

2.3.1. Metal on Metal bearing (MoM)

Figure 2.4. Anatomical femoral stem made of TC4 and coated with hydroxyapatite from TORNIER, Inc.

MoM type of bearing it is composed of a metal femoral stem head and an acetabular prosthetic part made of metal, which defines the contact between the components. These type of bearing have not been shown good results over time. MoM wearing in time develops a large amount of metallic debris that can cause disastrous effects over time. Therefore, this type of prosthesis is no often used.

The most used materials in the MoM bearing couples are alloys such as: Ti_6Al_4V which is a titanium alloy highly biocompatible with the human body, also called TC4 [48], stainless steel, cobalt-chromium-molybdenum, a cobalt-chromium alloy, which lately orthopedic surgeons are avoiding to implant it because there are studies who put this alloy in the category of those who can cause cancer [49].

2.3.2. Metal on Polyethylene bearing (MoP)

MoP bearing couple involves the use of an acetabular cup made of polyethylene, or one of the most used, UHMWPE with a femoral stem made of a metal alloy. This bearing couple was developed by Sir Charnley that at the beginning used components made of PTFE and cobalt-chromium alloy, then fixed them with methacrylate cement, later on, he replaced the PTFE component with one made of UHMWPE and cement them. In 1971 another researcher named Oonishi continued the studies on the same materials, producing an ultra-high-molecular-weight polyethylene of 1000KGy and Grobbellar used in 1978 the same material, but of 100KGy [50].

Although it is one of the most used bearing couple type in THR, the most major disadvantage of this bearing involves the production of residual particles called debris, due to the aggressive environment to which the implant is subjected, implicitly due to the components wear.

2.3.3. Ceramic on Ceramic bearing (CoC)

The CoC bearing couple used in THR involves the use of an acetabular cup and a femoral hip stem made of ceramics, usually alumina oxide (Al_2O_3) or zirconium oxide (ZrO_2) [54]. This bearing couple was developed in order to increase the lifespan of prosthesis, especially for young and active patients, but also in order to reduce the wear particles and other postoperative complication, such as aseptic decimation.

2.4. Categories of hip joint prostheses

Depending on the prosthetic component fixation type, they are divided into the following categories:

a.   *Cementless femoral hip stem fixation* involves the use of a prosthetic component pressing technique. This type of fixation is used for young and active patients, which is supposed to undergo another THR surgery to replace the initial hip prosthesis with a new one during their lifetime. In order to facilitate the osseointegration of the femoral hip stem most of this prosthesis presents a so-called coatead surface which facilitate the ingrowth of bone tissue on hip stem surface in order to realize also a better prosthesis fixation in the femoral canal [55].

b.   *Cemented femoral hip stem fixation* involves the use of additional materials that are added around the femoral prosthesis to achieve better fixation and to prevent the appearance of the micro movements. This technique is often used in older patients with poor bone quality, which are less

active, and of course, because there are expected fewer replacement surgeries of the initial prosthesis during their lifetime [56].

Depending on the geometric shape of the femoral stem, it is divided into two categories:

a.   *Straight hip stem* it is most often used for elderly patients with poor bone quality and who have suffered a femoral neck fracture, requiring a special fixation of the prosthesis [57]. After analyzing the contact between the straight hip stem and the patient's femoral canal, the researchers established that in the case of this typology of prosthesis the contact is made in three points, thus, the load distribution is not uniform and in the event of intense activity or accidents may occur cracks that may lead to femur fractures. Usually, these types of hip stem are cemented and have holes through which they can be reinforced by clamping it with the femur, as well as having standard removable necks.

Figure 2.5. Contact between the right hip stem and the femoral canal

b.   *Anatomical hip stem* it is a prosthesis that follows the morphology of the human femur, having a curvature that molds on the inner femoral canal. Due to this fact the contact surface between the stem and the inner femoral canal is determined by a curved surface, which evenly distributes the loads in the hip joint [58]. This type of hip stem is one of the most commonly used in the recent years, especially for young patients with good bone quality. They can be used cemented or uncemented, and are usually coated with hydroxyapatite to facilitate bone growth on the prosthesis surface.
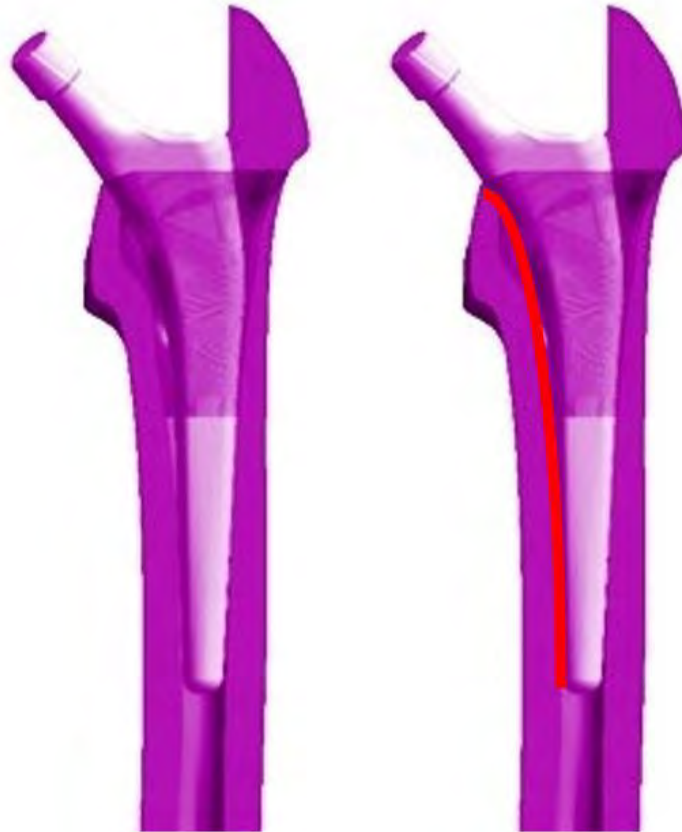
Figure 2.6. Contact between the anatomical hip stem and the femoral canal

2.5.   Postoperative THR surgery complications

One of the largest human body articulations is the hip joint, and is designed in such a way to resist repetitive movements. The bones are making a perfect fit, allowing the synovial fluid to continuously lubricate the articulation. Because of the increase in outdoor sports activities, junk food consumption, and body trauma, or just because of ageing, hip pain is a commonly encountered problem that occurs in the case of many people nowadays. The exact location of hip pain can provide valuable clues about the hip pain causes. Depending on the hip joint affection or illness, the patient can be prescribed a treatment, or in more serious situations, has to undergo a THR surgery [59], which can be partial (hemi-arthroplasty) or full (bipolar hemi-arthroplasty), hip resurfacing surgery, arthroscopy or osteotomy.

Focusing on Primary Total Hip Replacement, engineers and surgeons identified the main postoperative complications, which are faced by a large number of patients: early and late intraprosthetic dislocation, periprosthetic osteolysis, after THR impingement and heterotopic ossification. Postoperative complications may appear due to various reasons, but some of them are directly related to the prosthetic component design, such as early and/or late intraprosthetic dislocation, and after THR impingement [60].

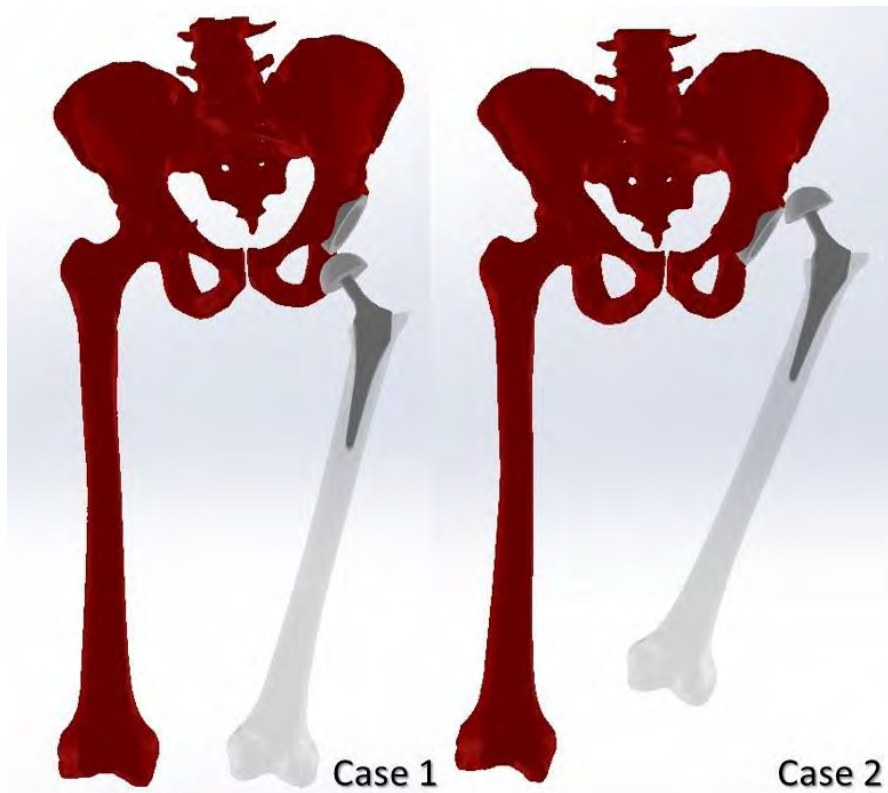### 2.5.1. *Early intraprosthetic dislocation*

Figure 2.7. THR most common early intraprosthetic dislocation scenario

Early intraprosthetic dislocation is the third cause of revision surgeries [61] and can occur at 5% of patients that undergo a THR as shown by the Swedish Hip Arthroplasty Registry [62], after the aseptic decimation (which represents 75% of cases) and deep infection (which represent 7.5% of cases). Early intraprosthetic dislocation can appear more or less after five weeks from the surgery, but, for the majority of patients, it appears three months after the surgery.

Causes of occurrence vary and may be combined, as component malposition (about 50% of the dislocation, especially the acetabular cup orientation), the anteversion angle (anterior and posterior), the femoral shaft angle and muscular factors (muscular diseases). The circumstances of early intraprosthetic dislocation can be traumatic (accidents) but also positional, which it is even more dangerous if taking into account the fact that it can appear in a normal life situation.

Researchers studied the main factors that influence the occurrence of early intraprosthetic dislocation in order to develop new solutions that can solve, or at least reduce, the percentage of patients that are affected.

Surgical factors that can lead to early intraprosthetic dislocation are the path approaches, that can be grouped into four families: pure anterior (Hueter) [63], which represents 1.8% of the risk, antero-side (Watson-Jones, Hardinge), which represents 1.7% of the risk, pure side (Ollier, Gibson) and postero-side (Moore) that represents 4.3% of risk, and the implant orientation, that is directly related to the experience of the surgeon.

The main mechanical factors that can affect the postoperative situation of the patient are: friction torque calibration, large or very large femoral head, the type of implant used and the

geometrical approach. In the case of friction torque calibration, the dislocation risk decreases, as the caliber of the prosthetic head increases. On the other hand, if we take into account the movement and mobility, not only does the risk increases with the femoral head caliber, but also the wear rate of the components, hence the surgeon has to make a compromise, by trying to use femoral components, having a diameter between 6 and 28mm. Another mechanical factor that increases dislocation was demonstrated by Harris in 1991 by using large or very large femoral heads, with extension. One of the most important mechanical factors that can lead to early intraprosthetic dislocation is the type of implant used, alongside its design. Because of the particularities of human morphological aspects, most of the implants doesn't properly fit the patients' anatomy, and risk can appear; that is the reason why the postoperative dislocation in most patients is due to the fact that the surgeon chose a large head, with a thick neck stem prosthesis for THR.

While trying to avoid a postoperative complication and keep every risk in balance, the surgeons have to make compromises in order to achieve several THR goals (prosthetic hip mobility, stretching of the prosthetic joint contact surface and its stability). By combining a horizontal acetabular component with small acetabular and femoral anteversion, leads to large contact surface with limited mobility for flexion and abduction movements. If the acetabular cup is positioned vertically at an angle greater than 45° with a normal bow and femoral anteversion we limit the contact surface, but also adduction and rotational hip movements, instead flexion, extension and abduction movements are increasing and also the stability. If we realize a more horizontally anteversed acetabular cup, this can reduce the posterior dislocation risk, but increase the anterior instability.

Taking into account all the postoperative risks that can appear, most of the surgeons consider that the best compromise is an acetabular cup positioned at an angle between 45° and 50° from abduction, and between 25° and 30° from anteversion, with a femoral component anteversed at 10°, for optimal stability, global mobility and surface contact.

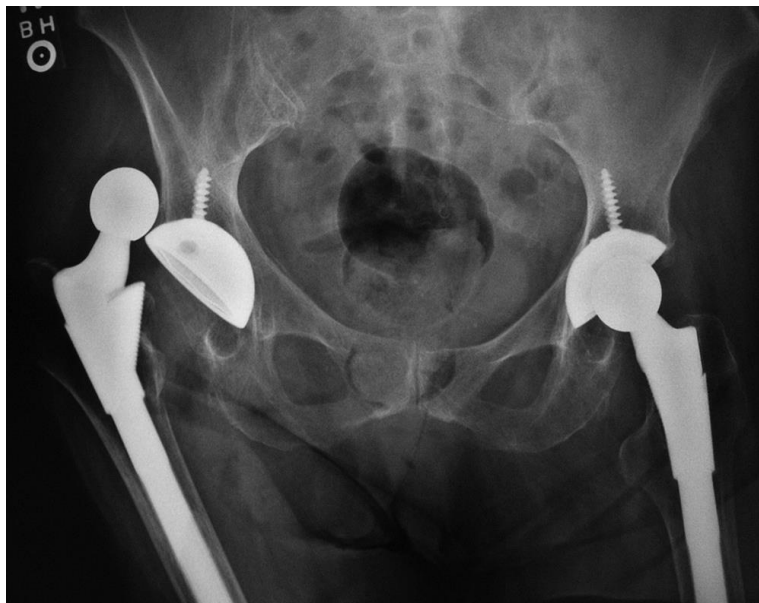### 2.5.2. Lately intraprosthetic dislocation

Figure 2.8. Lately intraprosthetic dislocation appearance of a patient's right hip [65]

Lately intraprosthetic dislocation it is defined as the early intraprosthetic dislocation, with the difference that it appear usually after approximately five years after surgery [64]. The frequency of this postoperative complication it is of 2.7% from the patients that undergo a THR surgery, most of the women, with an average of 66 years old.

2.5.3. *Impingement after THR surgery* [66, 67, 68]

Impingement postoperative complication after surgery, is one of the THR failures that cause high pain at the hip level, instability which favors luxation and accelerates the wearing process of the prosthetic components.

Impingement can be avoided by correctly positioning the acetabular cup and the femoral stem, especially recreating the right anteversion angle by selecting an appropriate ratio for the femoral head stem and femoral neck stem (it should normally be >2.0), which can restore the normal offset of the hip (the lower is the ratio, the higher is the risk of impingement appearance).

Impingement postoperative complication appearance, is favored by: incorrect positioning of the acetabular cup or hip stem, failure to comply the anatomical positioning of the prosthesis rotation center, femoral head stem and hip stem ratio < 2.0, incorrect positioning of the acetabular liner cup margins, short offset, hip stem geometry, incorrect CCN angle. The standard CCN angle of a femoral stem it is 131°, but sometimes, in order to restore the original offset a varus angle of 121° is needed.
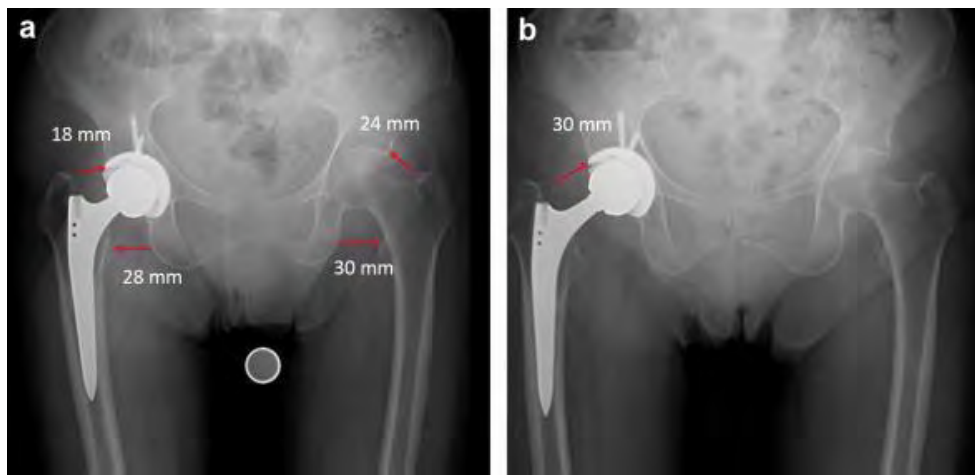

Figure 2.9. Postoperative impingement appearance of a patient's right hip [69]

2.6. Total Hip Replacement preoperative planning

2.6.1. *Traditional 2D preoperative planning*

I.   X-Rays

The X-rays were first discovered in 1895 by Professor Wilhelm Conrad Röntgen, who conducted experiments using a Crookes tube when he noticed that a barium salt-coated screen was

glowìng every time it was a discharge in the Crookes tube. He placed his hand next to the fluorescent spot and the palm outline and its bones appeared.

Figure 2.10. The first X-ray of Wilhelm Conrad Röntgen's wife's hand with her finger ring [70]

On December 28, 1895 Röntgen announced his invention, and researchers from around the world realized the impact of this discovery in the medical field. Over time, the technology is developed and improved so that patients undergoing such medical examination are less exposed to radiation, but also the medical imaging is improved in order to obtain clearer images of the examined tissues or body part.

The radiography is a special medical imaging technique obtained with the help of X gamma radiation with a wavelength between 0.06 and 8 Å (angstrom). This type of medical imaging collector allows the examination of opaque objects by penetrating them with radiation and collecting the image of the object on a photographic film.

Radioscopy is the simplest and the cheapest radiological method examination that consists in observing the Röentgen screen where the X-ray beam form an image after crossing an anatomical part, following properties like penetrability level, straight line propagation and an unequal fluorescence and absorption . The advantages of this radiological technique is the reduced cost and the possibility of examining the global functionality and morphology of patient's organs, instead the disadvantage is that we cannot identify small lesions, the radiation is high compared to the other imagistic method and the method can be quite subjective.

In orthopedics, X-rays are used either to identify a medical problem such as fractures or diseases that affect bone tissue over time, as well as to check the prosthesis positioning and osseointegration, or to observe the healing of a fracture. Currently, orthopedic surgeons use X-rays to diagnose the patient and to perform preoperative planning for THR surgery. This THR

preoperative planning is performed based on a two-dimensional X-ray that we can called it pre-operative 2D planning.
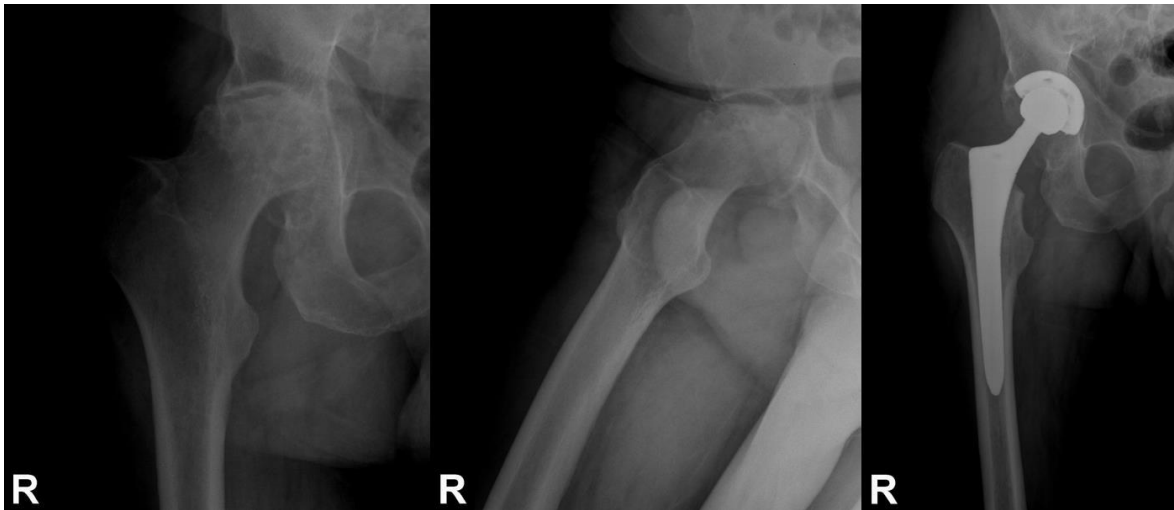

Figure 2.11. X-rays of a patient who underwent THR surgery at the right hip [Image source: Bucharest University Emergency Hospital-SUUB]

I.   Identification of the femoral and pelvis morphological parameters [71, 72, 73]

In order to proceed the THR preoperative planning the clinicians are using antero-posterior pelvic X-rays but also a lateral hip X-Ray called Löwenstein view as we can observe in *Figure 2.12*.

THR preoperative planning begins with establishing the main morphological landmarks such as vertical or the horizontal reference line that help us to understand if the patient has a difference between the lower limbs, if they are aligned. The horizontal reference line is determined by uniting the lowest ischial tuberosity of the pelvis, instead the vertical reference line is a median drawn at the horizontal reference line.
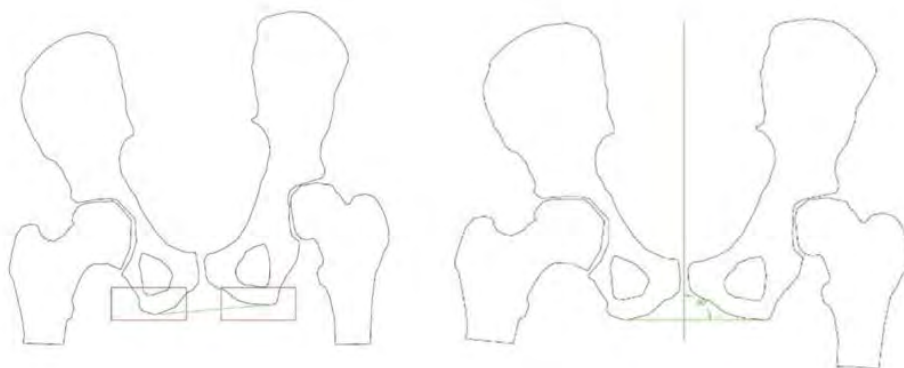
Figure 2.12. Identification of horizontal reference line (left image) and vertical reference line (right image)

After defining the reference lines surgeons are passing to the next step, which is the acetabulum template. They measure the femoral head and find an acetabular component closer to the patient's landmark, after fixing the acetabulum component into the most optimal position, surgeons mark the rotation center by trying to restore the initial hip rotation center of the patient in most of the cases, if it is possible.
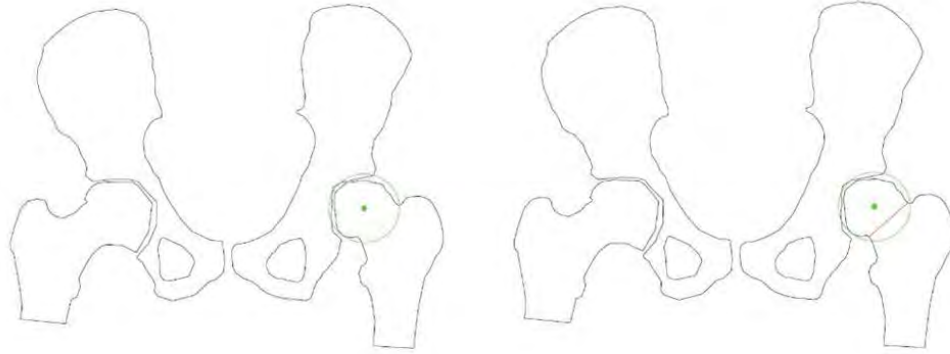

Figure 2.13. Determination of rotation center (left image) and acetabular axis (right image)

The next step into traditional preoperative planning, after the acetabulum prosthetic cup template is to measure patient's femoral landmarks in order to find the most appropriate hip stem. The main femoral landmarks considered by the orthopedic surgeons in THR are the following:

a.   Femoral neck axis

The femoral neck axis is determined by starting from the center of the femoral head where we identify two points on the femur neckline. To identify the axis well, the two points must be one on the concave side and the other one on the convex side of the neck contour; the result is a segment whose median is the femoral neck axis.
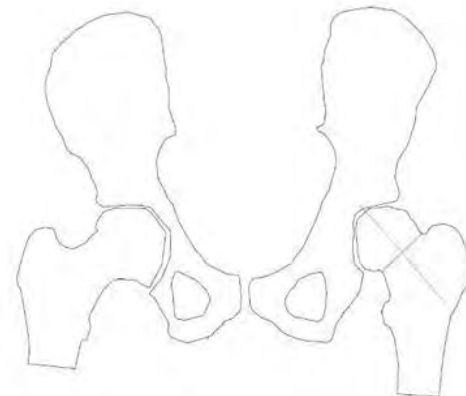
Figure 2.14. Femoral neck axis determination
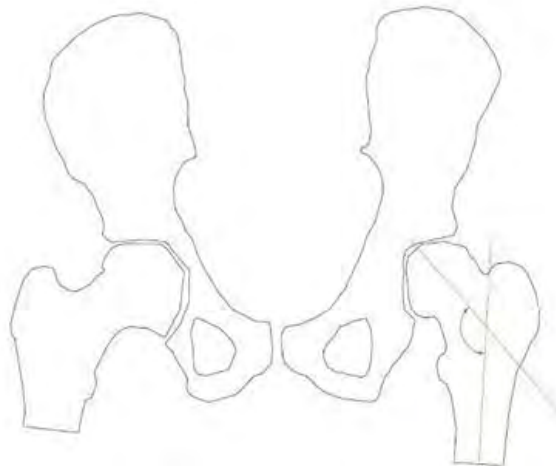
b.   Femoral diaphyseal axis

The femoral diaphyseal axis is determined by identifying two points along the femoral contour and unite them, the result is a segment, whose median is the femoral axis.
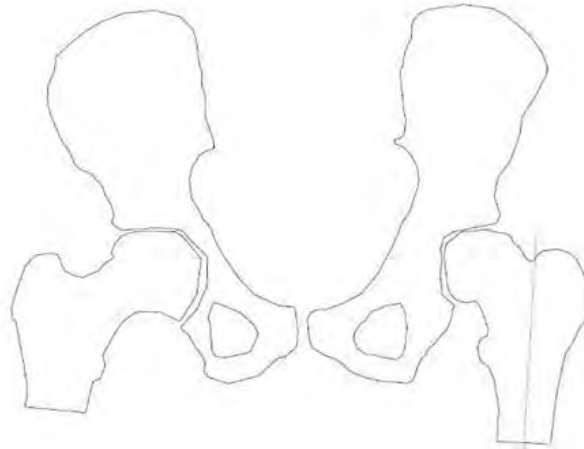
Figure 2.15. Femoral diaphyseal axis landmark determination

c.   Cervico-diaphyseal angle (CCN)

The cervico-diaphyseal angle is identified on patient's radiography at the intersection formed by the femoral neck axis with the femoral diaphyseal axis. Most of the individuals present a CCN angle between 120° and 130°, which we identify as a normal CCN angle, but there are also patients who have a CCN angle which is not included in this range, for this case we got two typology of cervico-diaphyseal angle: coxa vara with an angle <120° and coxa valga with an angle >130°.

Figure 2.16. Cervico-diaphyseal angle femoral landmark determination

Depending on these main anatomical parameters determined by the orthopedic surgeons, but also taking into account other patient's morphological landmarks such as the anteversion angle or the medical history, they manage to identify the best standard hip stem variant that fits into the patient's femur by using templates received from companies that produce stems and overlapping these templates on the patient's radiographs in order to determine the stem dimensions as shown in *Figure 2.17*.

The company TORNIER exemplified and realized a selection of the main stages of preoperative planning such as measuring the pathological hip landmarks (i.e. observing if the patient presents differences between the lower limbs, fixing the center of motion, drawing the diaphyseal axis, measuring the anteversion and shaft angles), reconstructing the acetabulum by choosing the size and tilting it at a 40°- 45° angle and marking the new center of motion, choosing the femoral implant by positioning the company's template on the diaphyseal axis and femoral axis. In order to make this step easier, the template usually presents some perforations for helping surgeons in understanding where the femur must be cut. The shaft distance and angle can be chosen at this stage, in order to solve the differences between the lower limbs. After adjusting the new hip sketch, the surgeon must choose the most suitable implant for the patient.
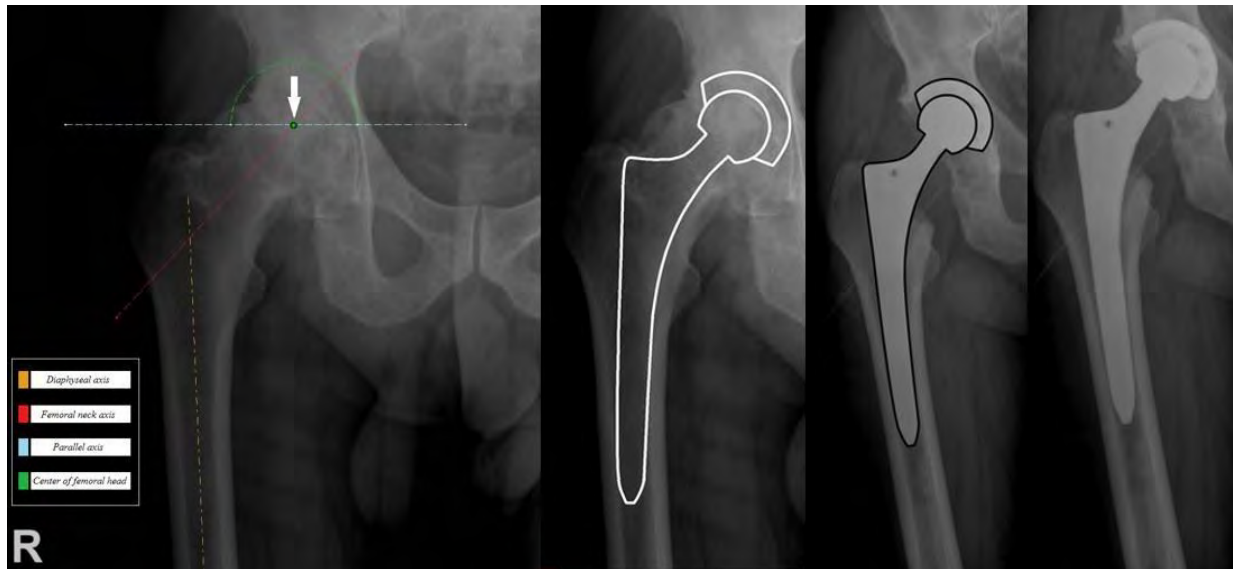
Figure 2.17. THR preoperative planning done on patient's radiographs [Image source: Bucharest University Emergency Hospital-SUUB]

2.6.2. 3D virtual preoperative planning (VPP)

I.   Computer Tomographic (CT scans)

CT scans or Computed Tomography is one of the most revolutionary discoveries in medicine made by two researchers, GodsFrey Hounsfield a British engineer and the physicist Allan Cormack with South African origin, invention who received the Nobel Prize in 1979 [74]. The name of

tomography comes from the Greek word "tomos" which means slice and from the word "graphia" which means writing.

The CT works on the principle of reconstructing the image of a body starting from its projection, thus realizing a two-dimensional reproduction of the patient's body; it measures the attenuation of an X-ray fascicle that crosses the patient's body and calculates its attenuation coefficient so that the radiological density of the tissues can be identified. The patient exposure risk in case of CT scan is minimal because of the small amount of radiation exposure during examination, presenting an optimal level of safety and a minimum exposure time [75].

To determine a problem at the hip joint level, radiologists use as ROI the patient pelvic area in order to lessen the exposed body zones, extracting only the necessary information for diagnosis and also for the procedures which helps in organizing the surgery, such as 3D THR preoperative planning.

Engineers have found the solution to convert and store these types of images or CT scans as DICOM files. DICOM files represent a coded way and transfer of medical and associated images obtained from special medical devices such as CT, MRI or ultrasounds.
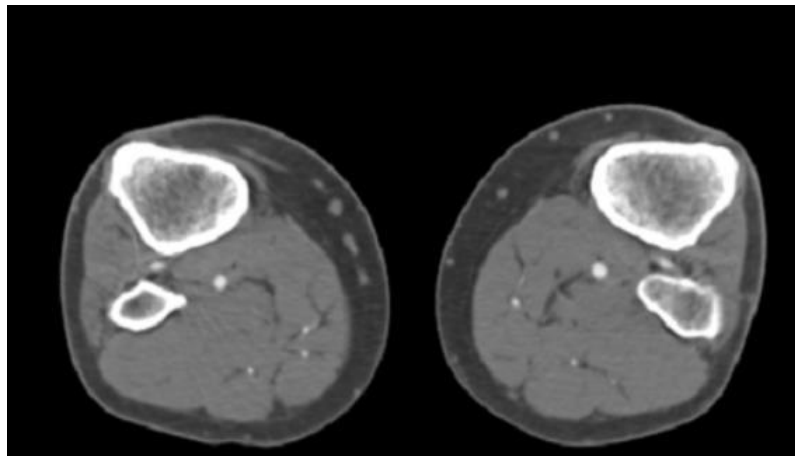
Figure 2.18. Axial view of a patients' CT scans

In order to realize virtual preoperative planning for THR, the patient's CT images were used, with a different number of frames of the whole body or pelvic part, from which bone tissue can be extracted.

II.   Identification of femoral and pelvis morphological parameters for virtual preoperative planning [76, 77, 78, 79, 80, 81]

Nowadays, more and more surgeons prefer a virtual alternative for preoperative planning which involves bone segmentation and working with Computer Aided Design files that offer a three-dimensional overview of the surgical and virtual preoperative planning. In order to obtain the femur CAD is mandatory to make a bone segmentation from the patient's scans by using dedicated software, such as Simple Ware ScanIP.

After obtaining the femoral model, it is imported in a CAD software and VPP is performed by determining the femoral parameters that orthopedic surgeons use to determine which prosthesis suits the patient's needs. Thus, the landmarks needed to achieve a complete VPP are: femoral shaft

angle, femoral neck axis, center of the femoral head, diaphyseal axis, femur's neck diameter, femur length, the femur's anteversion angle and the width of the femoral canal.

a.   Femoral neck axis

Starting from the middle of the femur's head, two points were identified, one in the convex area of the femoral neck and another one in the concave area of the femoral neck, in this way the femoral neck axis can be determined in a more accurate manner, obtaining more exact representation as in the case of 2D preoperative planning.
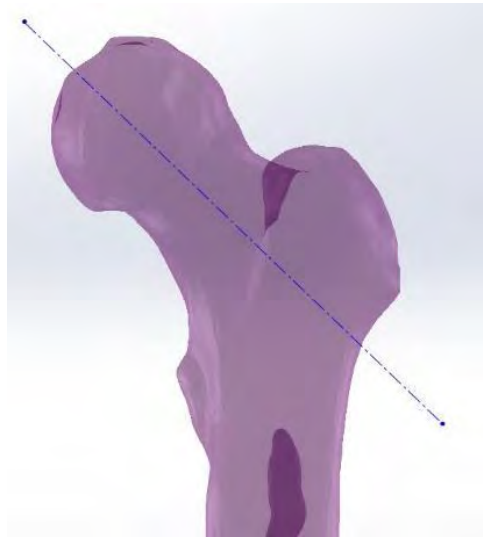
Figure 2.19. Femoral neck axis landmark in 3D preoperative planning

b.   Femoral head center

Because the femur's head is an irregular form, it can be approximated with a sphere tangent at the femur's surface. The femoral head center is a femoral landmark which determines the new motion center of the artificial joint and can give natural lower limb movement.
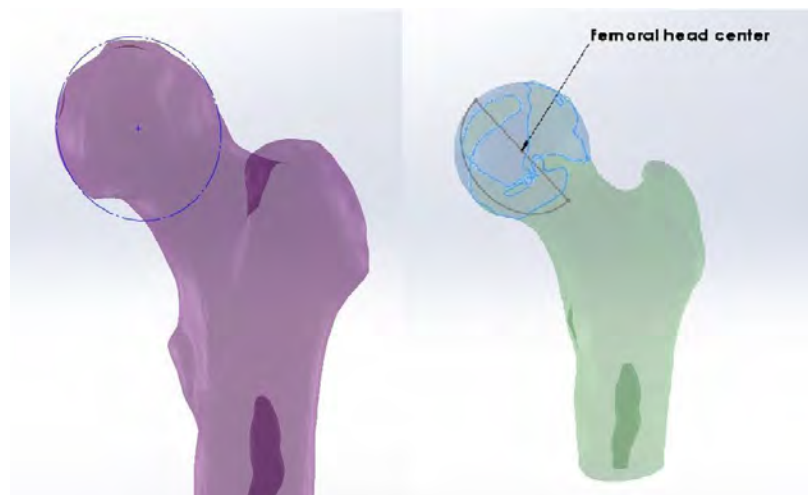
Figure 2.20. Femur's head center landmark in VPP

c. *Femur neck diameter*

The diameter of the femoral neck can be compared to a cylindrical form, having the base perpendicular to the axis of the femoral neck, for example, in *Figure 2.21* the diameter of the femoral neck is ~ 47.5mm.
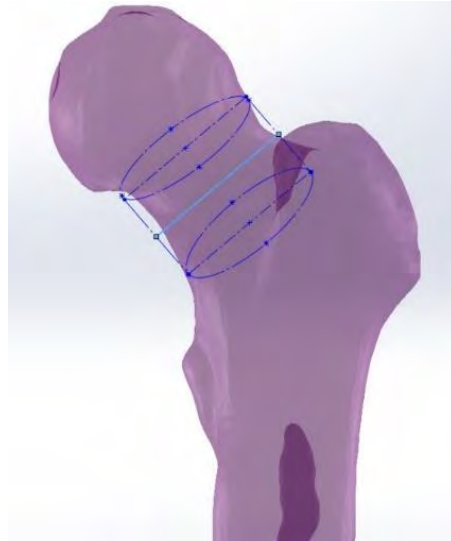
Figure 2.21. Femoral neck diameter landmark in 3D preoperative planning

d. *Femur's diaphyseal axis*

The femur can likewise be approximated with a cylindrical shape whose tallness is the diaphysis axis, it can be identified by determining two points in various zones along the femur, situated in the femoral width center of the picked area.
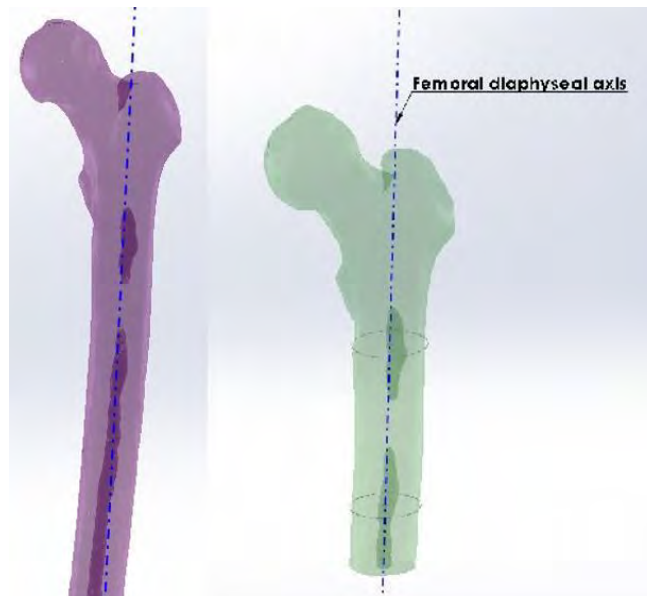
Figure 2.22. Femoral diaphyseal axis landmark in 3D preoperative planning

The CCN angle is identified at the convergence between the neck axis and the diaphyseal axis of the femur. The neck shaft angle can determine in which case the patient is situated: coxa valga, normal shaft angle or coxa vara. Many patients who have a dimensional difference between the lower limbs are in one of the cases outside the normal range of the angle.
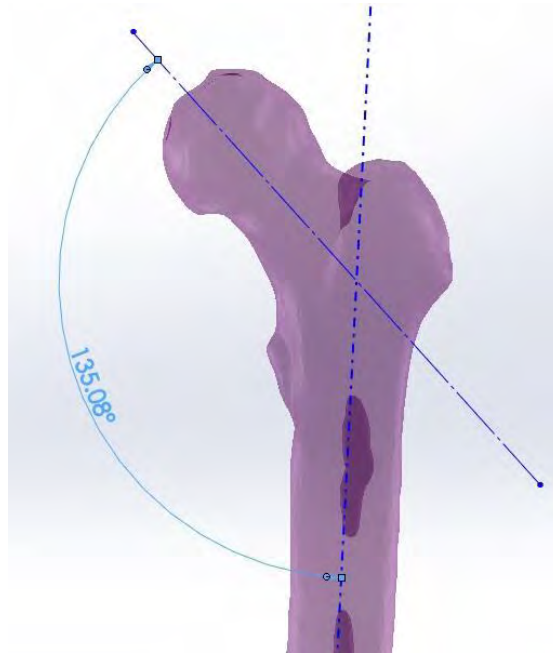
Figure 2.23. Shaft angle landmark of the femur in 3D preoperative planning

f. *Total length of the femur*

The femoral total length can be measured as shown in *Figure 2.24*, in this care is ~505mm, which normally can be identified as a male femur due to its dimensions.
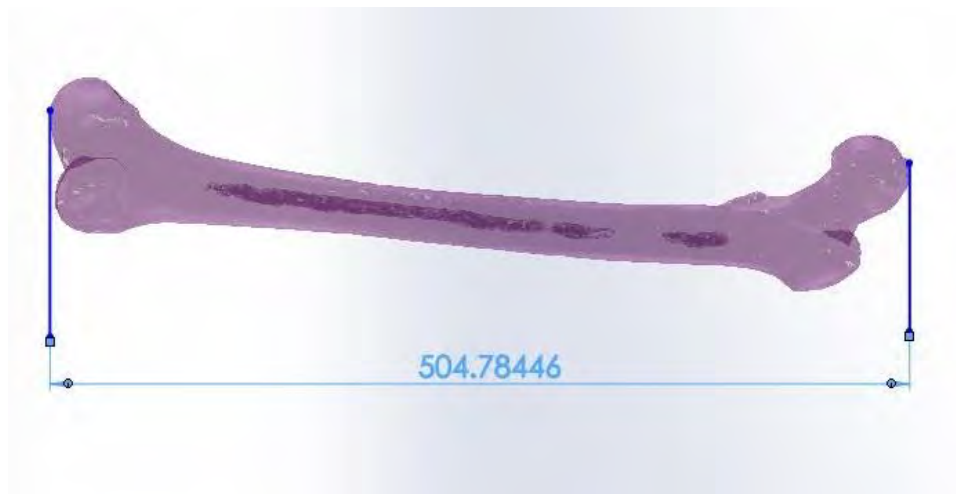
Figure 2.24. Femoral length landmark in 3D preoperative planning

In order to determine the angle of anteversion it must be built an axis by joining two points located in the posterior femoral condyles, the angle formed between this axis and the axis of the femoral neck determines the angle of anteversion which in *Figure 2.25* is about 15°.

One of the most common causes of postoperative complications that produce after THR pain to the patient, increase the wear degree between the prosthetic components and causes unnatural walk to the patient, is the incorrect identification of the anteversion angle, and implicitly defective positioning of prosthetic components, which determine the patient to undergo new revision surgeries to resolve the problem.
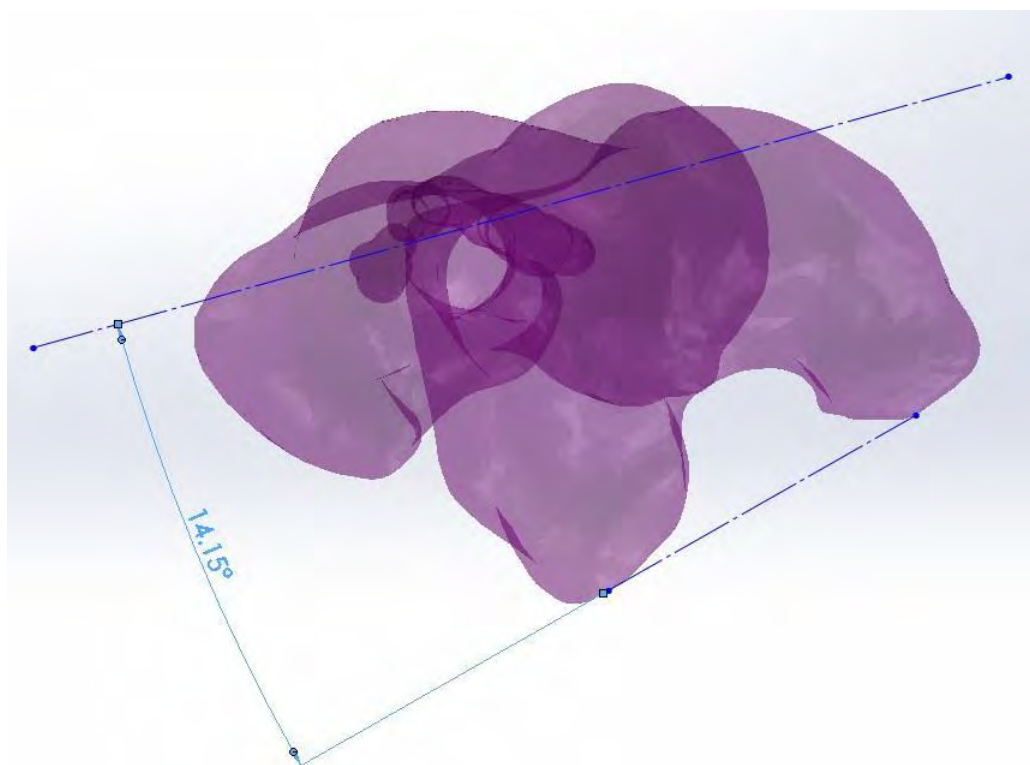
Figure 2.25. Femur anteversion angle landmark in 3D preoperative planning

h. *Femur width above the lesser trochanter*

This femoral landmark can be identified by creating a construction axis at 20mm above the lesser trochanter and determine the width of the femoral canal in the section, by measuring it on the construction line.

i. *Femur width at the lesser trochanter level*

This femoral landmark can be identified by creating a construction axis at the level with the lesser trochanter and determine the width of the femoral canal in the section, by measuring it on the construction line.
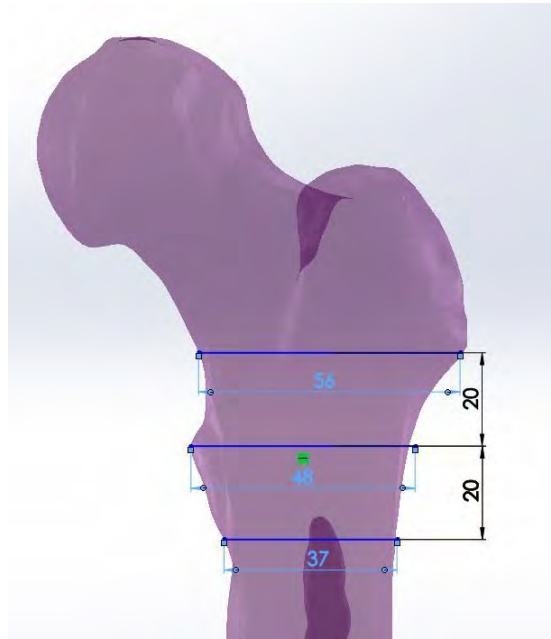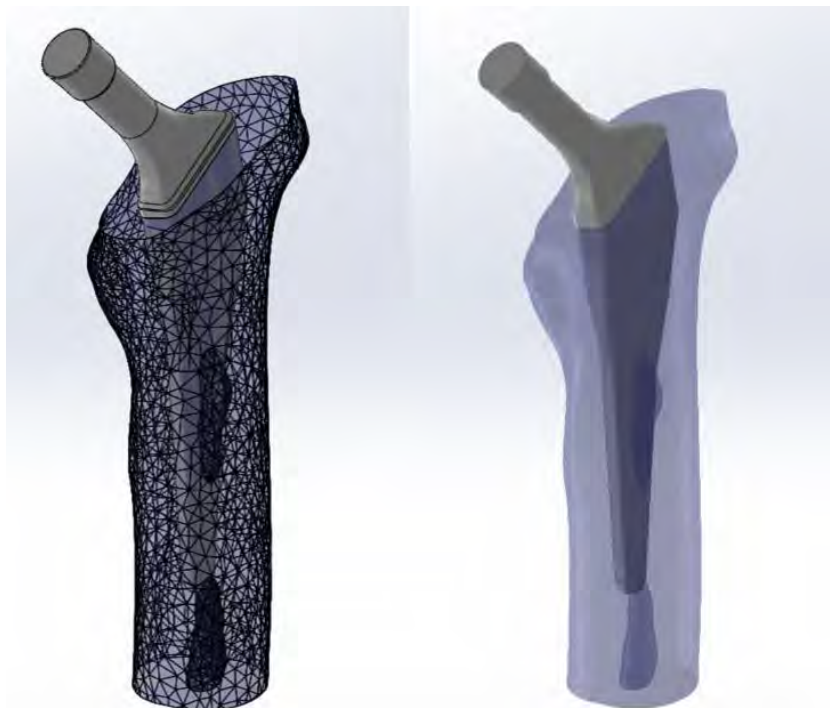
Figure 2.26. Femur width at the lesser trochanter level, above and below lesser trochanter in VPP

j. Femur width below the lesser trochanter

This femoral landmark can be identified by creating a construction axis at 20mm below the lesser trochanter and determine the width of the femoral canal in the section, by measuring it on the construction line.

Figure 2.27. 3D preoperative planning of a femur with the femoral stem inserted

Once the femoral morphological parameters have been determined, the 3D models of the standardized prostheses can be inserted using the previously determined axes as a guideline and seek the best solution regarding the recreation of the hip motion center and the anteversion angle.

2.7.   Chapter conclusion

The human organism is a very complex organic machine with subsystems that work in perfect harmony one with each other conserving energy and protecting us from potential interferences that may emerge from the outside. The use of the particular landmarks which are unique for any individual that must undergo a THR orthopedic surgery, helps to increase not only the eventual prosthetic life, but also to reduce postoperative complication such as early intra prosthetic dislocation, related also to prosthesis geometry.

VPP is a modern method of measuring the femoral parameters of the patient that must undergo a THR surgery. By performing this THR planning in a virtual, three-dimensional environment, the orthopedic surgeon can plan the surgery approach, choose a suitable prosthesis for the patient and better understand his medical condition.

Each patient must be treated in an individual manner and the reverse engineering method can help us establish the femoral parameters of each patient, helping to change the standard procedures, treating each patient case differently because all of us has unique particularities, although they may seem similar at first glance.

CHAPTER 3

VIRTUAL PROTOTYPING FOR CUSTOM FEMORAL STEM PROSTHESIS

3.1. CT scans data acquisition

For this study, were used the CT scans of a female patient aged 77 years old at the date of the examination procedure, obtained from Imagerie Médicale Clinique du Parc, Lyon, France. The patient was diagnosed with hip joint arthritis subsequently undergoing a THR surgery to improve the patient's life quality and eliminate the pain caused due to hip joint mechanical wear.
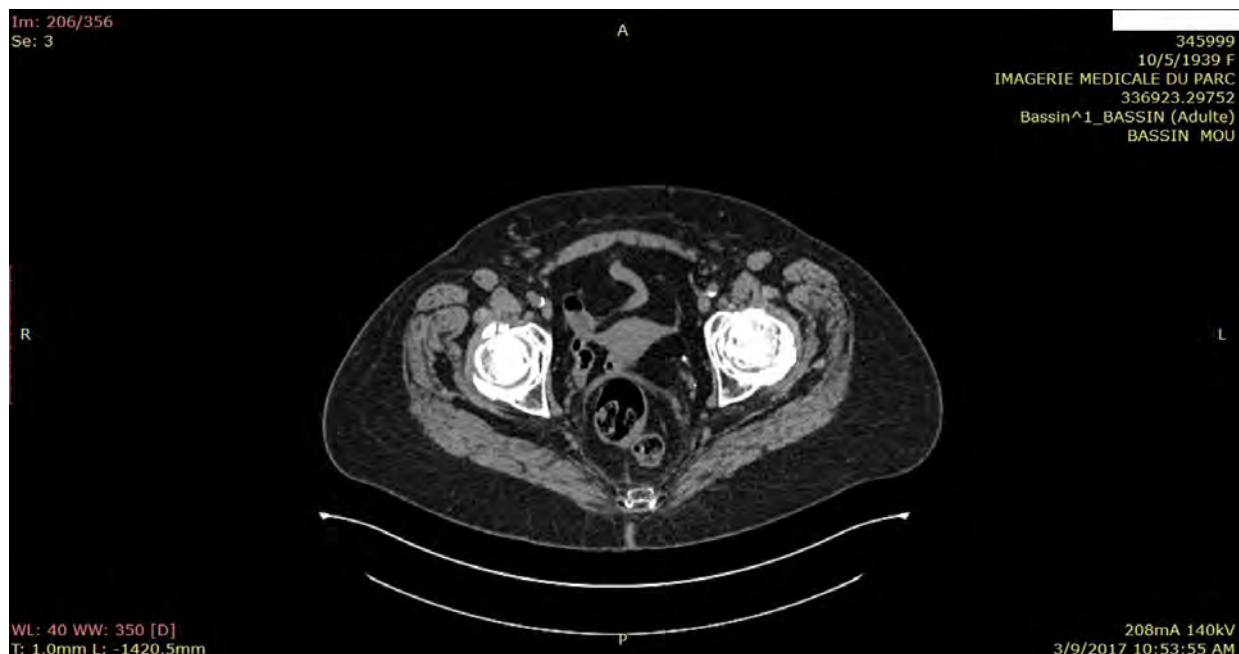
Figure 3.1. Patient's CT scans in axial view

Acquisition of DICOM images was made with the help of Siemens Somatom Definition AS in CT modality, the body part examined being set to the pelvic region with a nominal slice thickness called also slice thickness of 1mm, the patient position was set to HFS, with a flat filter type, the peak kilo voltage or KVP of 140mA·s, 34kW generator power, data collection diameter of 500mm and a reconstruction diameter of 474mm, table height set up at 173.5mm, distance source detector of 1085.6mm and distance source to patient of 595mm, exposure time of 1000m·sec, rotation direction in CW, the X-Ray tube current of 190mA, a 0.6mm single collimation width with a total of 12mm collimation width, 0.55 spiral pitch factor value, with a total number of 356 DICOM image files. The table speed moves with 6.5(9)mm in one second in order to collect image data and the table feed per rotation is also about 6.5(9)mm during a complete rotation around the fixed orbit and in image collection was used an equal number of 512 rows and column in the image, being the multiples of the vertical or horizontal down sampling factor if any of them are encoded in the vertical or horizontal direction. Regarding pixel tag settings the spacing between each pixel center

was set at ~0.93mm with a 16 bits allocated for every pixel and a total of 12 bits used to store each pixel, with a number of 11 high bits which represents the most significant pixel data bit. The largest image pixel value of data acquisition is about 2251 and the smallest image pixel value is represented by 0, the rescale intercept set up to -1024, type 1 measured in HU, the window center for display set to 40\400 and window width 350\2000.

3.2. Bone segmentation process in Simpleware ScanIP

Bone segmentation is the particular operation with which we can reconstruct body parts, usually organs by overlaying the voxels and separating the soft tissue of bone tissue in order to extract the parts, which this study needs. There are different image algorithms used in particular cases in order to reach the final segmentation results: Otsu algorithm (by calculating the binary threshold) [82] [83], connected threshold [84] (evaluating the intensity in a particular interval), neighborhood connected [85] (it determines if a pixel from a close area belongs or not to the particular area in which this filter is applied), Watershed algorithm [86] (is a delimitation and separation of the grayscale level), isolated connected algorithm [87] (connecting the pixel with another by identifying if it belongs to the same area), level set segmentation algorithm [88] (is able to detect two different shapes and split them in two parts) and confidence connected algorithm [89] (relying on statistics from the selected area).

Today, there are multiple dedicated software programs which realize bone segmentation in an automatic way by applying multiple image processing algorithms and extracting directly the bone tissue, or in semi-manual way, requiring user's intervention, usually prepared or trained to use the specific software [90]. In this chapter the femur of a patient, which suffers of arthritis need to be extracted and because of the patient condition an automatic bone segmentation software will not extract only the femur, but also the pelvis in a same CAD file due to the hip joint wearing, the threshold algorithm couldn't identify the difference between the two bone parts. Because of this condition this study was realized in Simpleware ScanIP Version 7.0 +FE software, dedicated to the processing of medical images, having a complex basis of image processing algorithms which can be applied to obtain a better surface and a better CAD model in order to perform virtual analysis or even preparing a 3D printing model.

The principle of bone tissue extraction from medical images is based on voxels (is the equivalent of a pixel in a three-dimensional space) identification from region of interest by applying various image processing algorithms on each CT scan, slice by slice, so that the 3D anatomical model can be recreated [91].

The model accuracy obtained after image processing can also be influenced by the digital image quality, which are often affected by a specific phenomenon called noise. Noise in images occurs due to imperfections of medical capture devices, scanning systems or optical systems when transferring data and can be of several types: additive, Rician, multiplicative, Gaussian or white etc. [92] If the situation requires, these images can be processed with the purpose of imperfections and noise reduction, thus, the following algorithms can be applied: histogram equalization by adaptive filtering with contrast limitation or CLAHE, linear contrast adjustment, image filtering, Wavelet transform, Fourier transform, image binarization etc. [93] All these medical image adjustments can help clinicians to better isolate and identify the patient's medical problem by increasing the visibility of the studied areas.

To start the image process the DICOM images were imported by selecting the DICOM directory and add all the frames: a crop and resample window will pop-up where the user can

choose a pixel rescaling, a pixel skip and if the user wants to crop the files or not. After importing the data, a four windows view called generically MPR view (Multi Planar View) will appear and in this way the user has the possibility to work in axial view, coronal view or sagittal, and verify the applied algorithms by refreshing the perspective view.
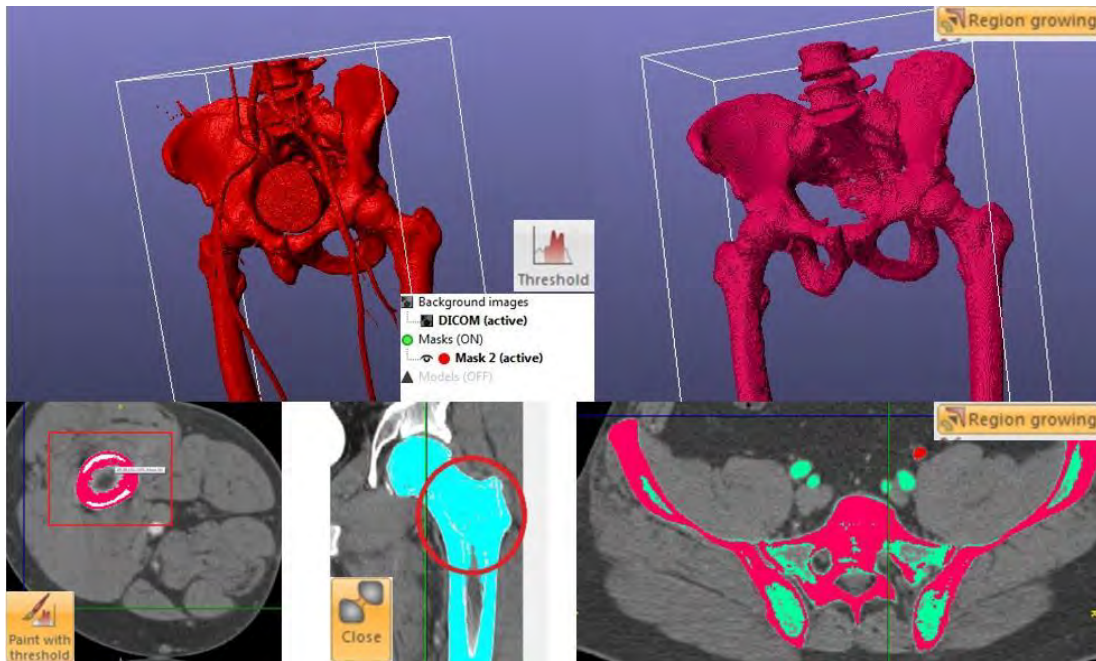

Figure 3.2. The main image processing algorithms used for bone segmentation in Simpleware ScanIP, MPR view and Perspective view

The main important steps performed in order to obtain the CAD femur file are:

a.   *Threshold* image processing algorithm (perform segmentation based on lower and upper greyscale boundaries, by creating a histogram in order to extract only the bone tissue and prosthesis components) with a lower value of +400 HU and an upper value of +2000 HU, this value allows to extract specific tissue. In radiology each voxel from the CT scan has a value which is measured in Hounsfield units, a quantitative unit scale used to describe the radio density, every voxel having a number of 4096 possible values that it can take, this value being arranged on a scale from -1024 HU to + 3071 HU [94].   In DICOM files, a value is directly related to the linear attenuation coefficient for the X-Ray and is usually calibrated and set to 0 HU for water and to -1024 HU for air, studies have shown that values around -120 HU corresponds to fat, +40 HU corresponds to muscle and +400 HU corresponds to bone tissue [95].

b.   *Region growing* algorithm (growing a region from a voxel by using statistics) is used to identify neighboring voxels and to select whether they belong to the region of interest. If voxels belonging to the region are still not selected *Paint with threshold* tool can be chosen so each DICOM can be repaired separately.

c.   *Island removal* algorithm is applied because of residues remained from other organs around the main part, thus applying this algorithm the user can eliminate island size threshold or isolated voxels.

d.   *Close morphological algorithm* which is closing the small holes inside the mask part by uniting the voxels.
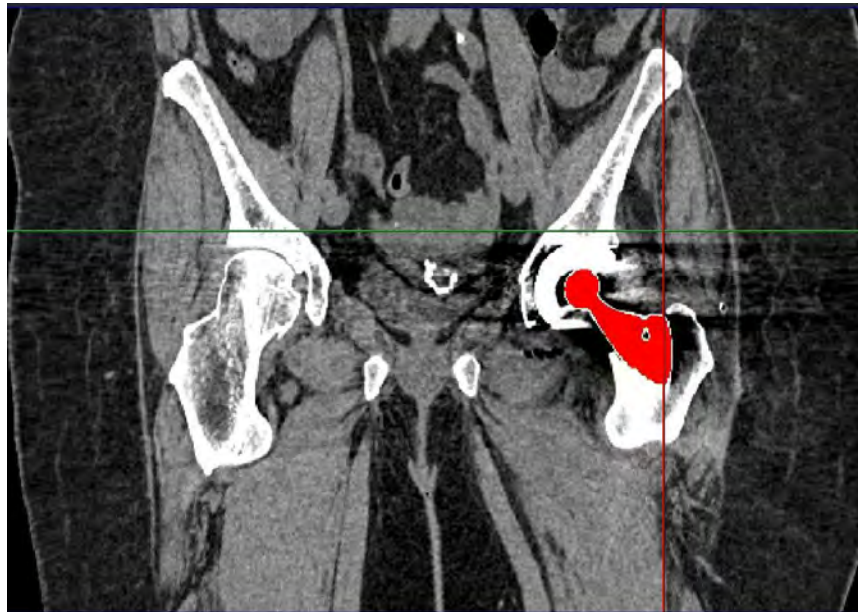
Figure 3.3. Threshold mask of a hip stem performed in Simpleware ScanIP in coronal view

In order to extract the femur more accurately, the image processing was done in two MPR views (in the horizontal plane/axial view and in the vertical plane/coronal view), starting by using the *Threshold* tool, choosing a lower and an upper value and selecting the option *Profile line* with, which two points can be selected along the entire hip and the software will automatically separate most of the soft tissue from the bone tissue. In order to isolate the femur and eliminate the body part that we don't need the *Crop tool* can cut the 3D image by using reference planes, so in this way the user can focus on the specific area that wants to extract it from the CT scans.
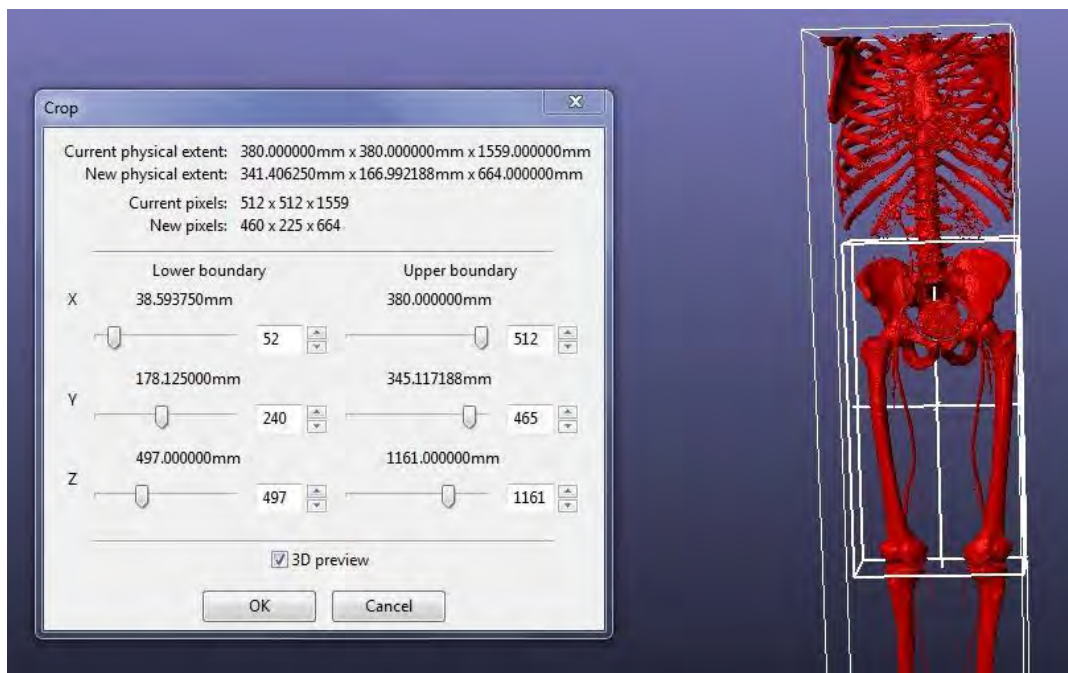
Figure 3.4. Threshold image processing for bone segmentation in Simpleware ScanIP example

In most cases after the *Threshold* algorithm residues of other tissues that interfere with the profile line will appear, and this effect was eliminated by using the *Island Removal* tool with a specific voxels size that we can choose depending on the situation, in this way *Island Removal* algorithm helps us to "clean" the 3D image of small residual particles.

Usually we can notice that the algorithm applied selects also the femoral arteries, the user can proceed through processing the image by using a *Region Growing* tool, and selecting the femur in a particular view, which offers good visibility such as the axial view in our case, where we can distinguish well the femur. By using this tool in the active view area and creating a new mask overlapped on the initial mask, the entire femur can be isolated and recreated in all the frames by applying the algorithm a several times, until the bone is fully covered by the mask.
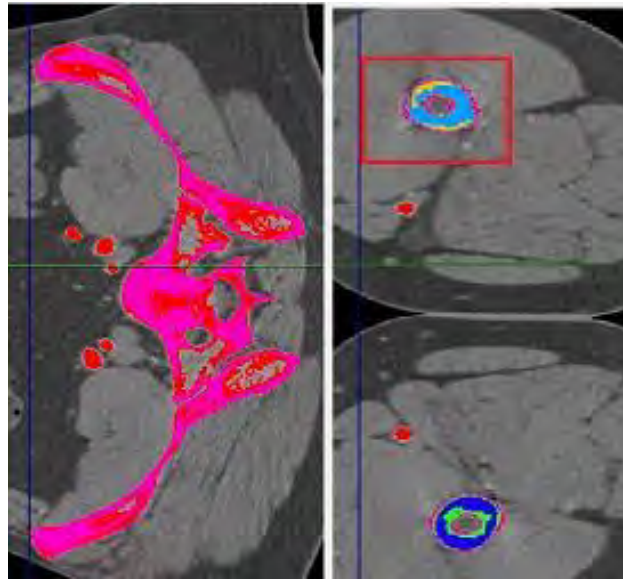
Figure 3.5. Simpleware ScanIP Region Growing algorithm

After checking the other frames we can observe that the new mask didn't cover all the bone tissue and there were still pixels in the initial mask that weren't covered by the new created mask: in order to fix this problem, the user can increase the multiplier and the initial neighborhood (voxels), and select the areas where the second mask didn't cover the initial one.

Since the need to obtain a model as accurate as possible is high, Simpleware ScanIP offers the *Paint with Threshold* tool which helps the user to select each voxel, in order to cover all the bone tissue for every DICOM image frame.

For the femur part finishing the *Close* tool with cubic values for the active mask was used, in order to close all the small gaps between the voxels and to define better the final surface, but also a *Recursive Gaussian* with cubic values algorithm, in order to provide more smoothness to the femur part surface.

After arriving at the desired results the femur model surface can be generated and export it as a binary in *.stl (Stereolithography) file extension, which can be used to import it in other software.

In most cases after extracting the bone tissue in Simpleware ScanIP, the surface needs to be re-mesh because of its complexity. For this purpose, additional simple software can be used to reduce the mesh, or redefining the surface, otherwise the surface complexity can slow the system or easily crashed it.
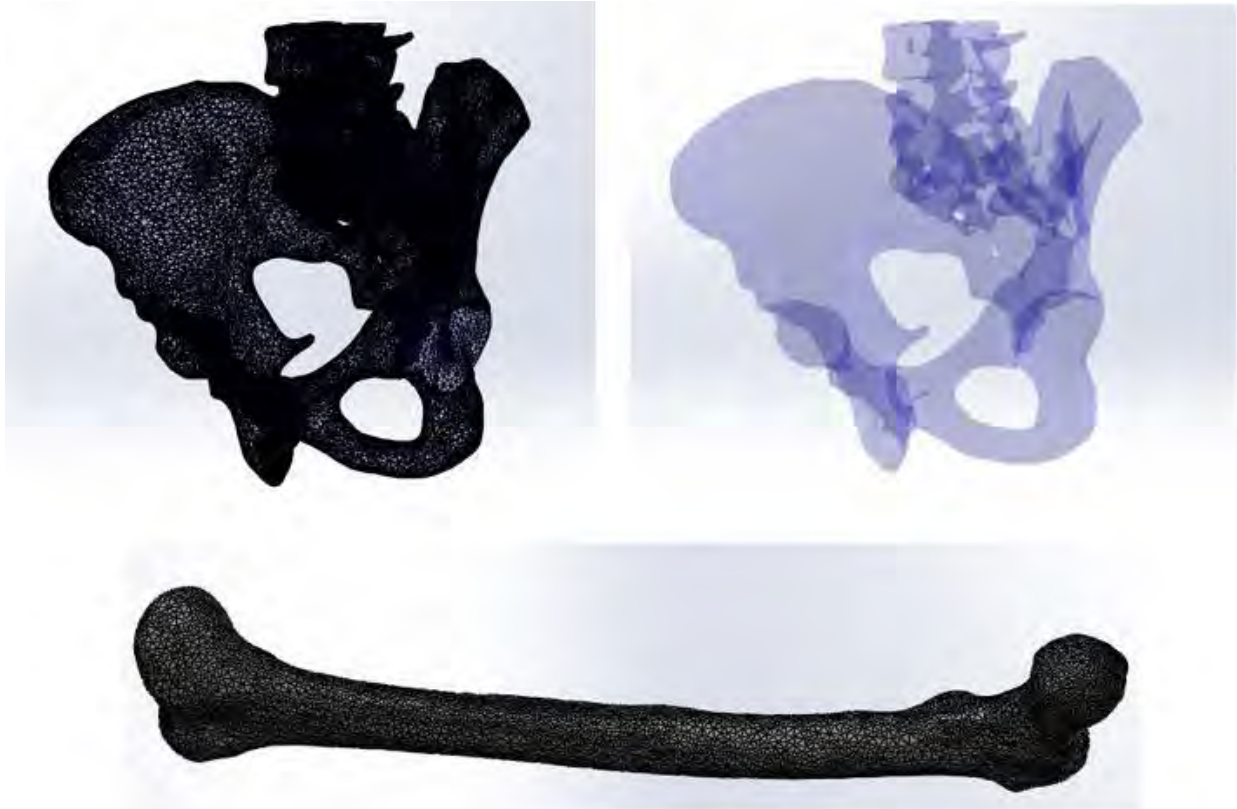
Figure 3.6. CAD raw models of the pelvis and femur example extracted with Simpleware ScanIP

3.3.   CAD refining and surface preparation

For finishing the exported raw model from Simpleware ScanIP, MeshLab 2016 was used, an open source software dedicated to edit and improve triangular meshes that offers a large palette of tools to clean and edit, inspect, render and even convert meshes.

In order to clean each 3D model, filters from the Cleaning and Repairing category was applied, such as: Merge Close Vertices, Remove Duplicate Faces and Remove Duplicate Vertex. This filter allows to remove unnecessary geometric elements, small elements that are not referenced or that are duplicated.

Anatomical surfaces of any kind have a high complexity due to the irregular geometric shape, which therefore directly affects the analysis time of the CAD model, but also the requirements regarding the performance of the computer. For this purpose, the models are simplified, re-meshed and refined, in order to obtain a surface with reduced geometry model complexity, thus optimizing the model analysis times [96]. To simplify mesh from the toolbar the re-meshing option can be selected, simplification and reconstruction category, the Quadric Edge Collapse Decimation filter was used to reduce the number of faces. As the number of polygons increases, the simulation accuracy or details increases, but the model complexity increases as well, so as a repercussion the virtual simulations, for example, tends to be as simple as possible by keeping the essential parts with an agreeable number of elements.

Original raw file	Processed file in MeshLab 2016

N° of faces: 13044 (19 044 with the duplicate faces) N° of vertices: 39 132 (42 132with the duplicate vertices)	N° of faces: 2000 (0 duplicate faces) N° of vertices: 1000 (0 duplicate vertices)

Figure 3.7. Femur CAD model before and after mesh simplification and refinement

In order to provide a more refined surface with MeshLab software, the user can also reconstruct surface decimation, in this way it can reduce the number of elements by using the algorithm of Taubin Smooth in order to remove residuals as in E. P. Ravera et al. study [97].

After the surface optimization and finishing process was concluded, the model was exported in the extension *.stl, after it can be imported in CAD software programs that can perform finite element analysis (FEA).

3.4.   Identification and measurement of patient's femoral landmarks

The foremost imperative part in characterizing the geometry of a hip stem prosthesis is represented by the femoral landmarks of the patient, which were presented in the previous chapter. These landmarks offer support to adjust the standard geometric shape of a femoral prosthetic component so that it matches with patient's morphology. Each landmark has a purpose in the construction of the hip stem prosthesis, but also in its orientation when inserted into the femoral canal.

The performance of a virtual preoperative planning can be realized in most CAD type software that allow the import of a 3D file and which can be manipulated (Catia V5, Solidworks, Solid Edge, Inventor). In this study, Solidworks 2017 software was used in order to measure patient's femoral parameters.

After the *.stl file has been imported in Solidworks 2017 it was proceeded by determining the femoral diaphyseal axis by creating first a reference plane coincident with the lower sectioned surface of the patient's femur. In this plane, a tangent ellipse was made at the transverse contour of the femur and its center is becoming the first reference point that will be used in the achievement of the diaphysis axis. In the same manner, the second reference plane was realized which includes the second ellipse tangent to the transverse contour of the femur and which is parallel to the previous plane. The two ellipse centers were used as reference points to construct a reference axis, namely femoral diaphyseal axis as *Figure 3.8* shows.
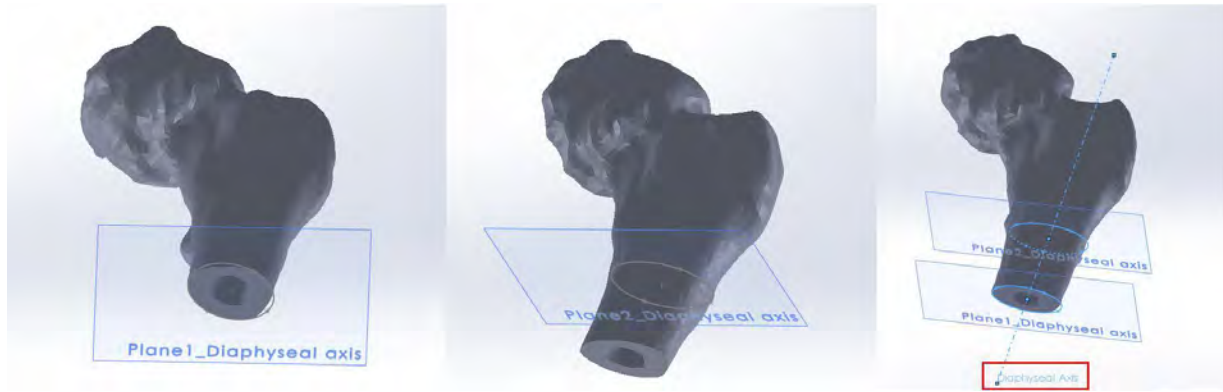
Figure 3.8. Patient's femoral diaphyseal axis determination

For the femoral neck axis determination, the same principle as the previous one was used, but this time the first reference plane was constructed using two collinear edges at the base of the femoral neck. In order to facilitate the construction of the ellipse, a section of the femur was created by the respective plane. After constructing a plane and an ellipse tangent to the transverse profile of the femoral neck the process was repeated in another parallel plane that was created at the opposite end of the femoral neck. By joining the two centers of the ellipses, the axis of the femoral neck is determined as in *Figure 3.9*.
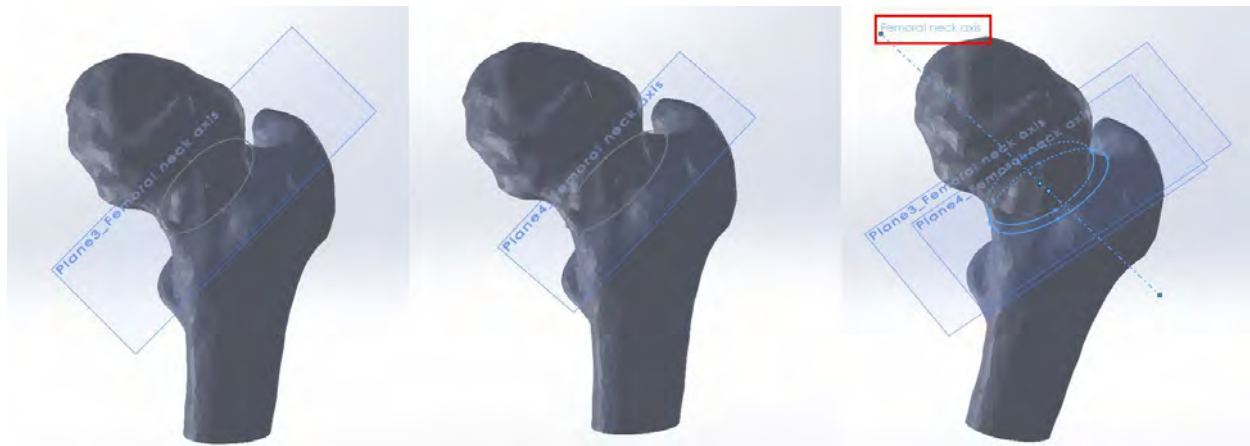
Figure 3.9. Patient's femoral neck axis determination

In order to determine the new patient's motion a new reference plane coinciding with the axis of the femoral neck and being perpendicular to one of the reference planes used to determine the axis of the femoral neck was needed, and inside this plane was made a sketch of a half sphere that is approximately tangent to the surface of the patient's femoral head. Using the *revolved boss/base* command we generated a spheroid that is approximately tangent to the femoral head as *Figure 3.10* shows, but it is worth mentioning that the femur is damaged due to arthritis and because of this the surface of the femur cannot be perfectly enclosed in a sphere.

The center of this spheroid is the femoral head center or the new center of motion.
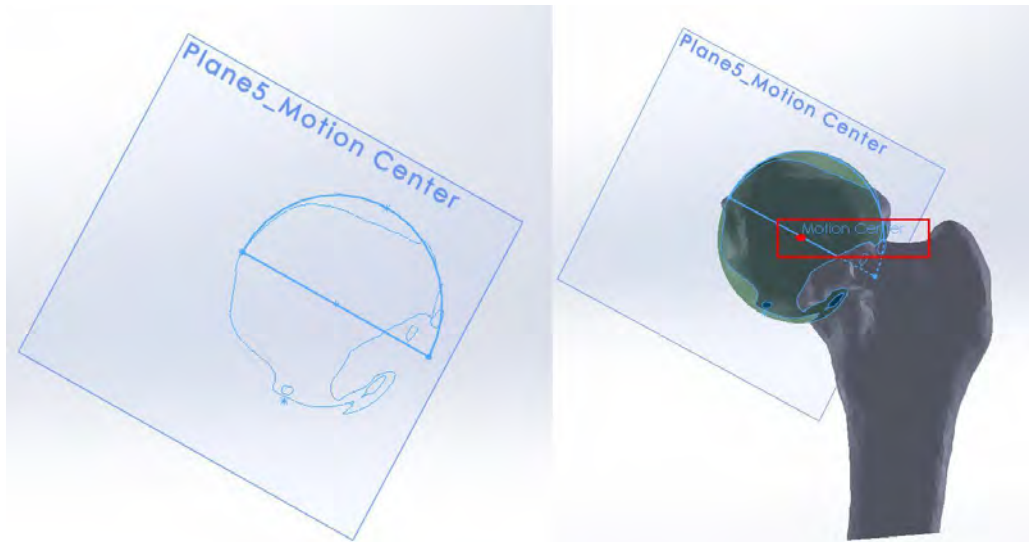
Figure 3.10. Patient's motion center determination

To determine the neck shaft angle, it just needs to be measured the angle between the femoral diaphyseal axis and the femoral neck axis, which were constructed before. In this case the CCN angle measures ~114.29°, which includes the patient in a coxa vara case as the *Figure 3.11* shows.

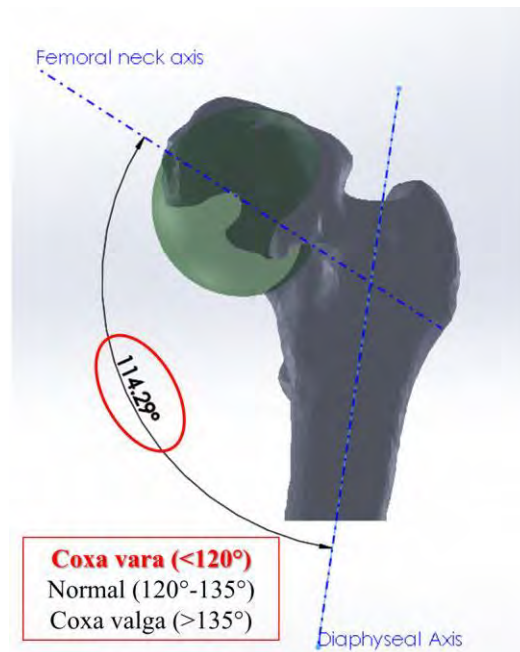*Figure 3.11. Patient's neck shaft angle determination*

The femoral neck width was measured by constructing an ellipse in a reference plane situated approximately in the middle of the femoral neck the parameters of the ellipse determining the neck width of ~36.9mm as shown in *Figure 3.12*.
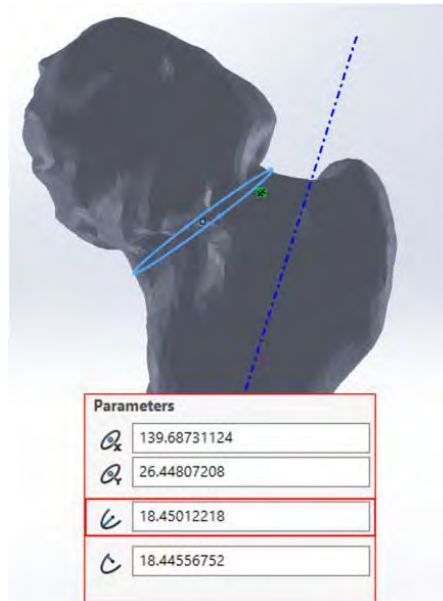
Figure 3.12. Patient's femoral neck width determination

In order to determine the thickness parameters of the femoral canal, it was proceeded by constructing a reference plane that passes through the femoral diaphyseal axis and the femoral neck axis and perpendicular to one of the diaphyseal axis reference planes. The femur was sectioned with the help of the new reference plane created that cuts the femur in two pieces and next to the lesser trochanter were measured the femoral canal width as shown in *Figure 3.13*.
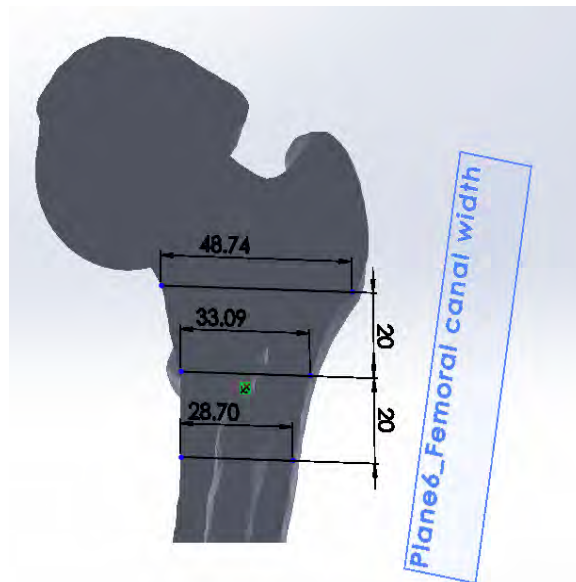

Figure 3.13. Patient's femoral canal width determination

In order to determine stem's offset, it was proceeded by measuring the distance between the femoral neck center and the diaphyseal axis as shown in *Figure 3.14*, which in this case measures approximately 39.64mm.
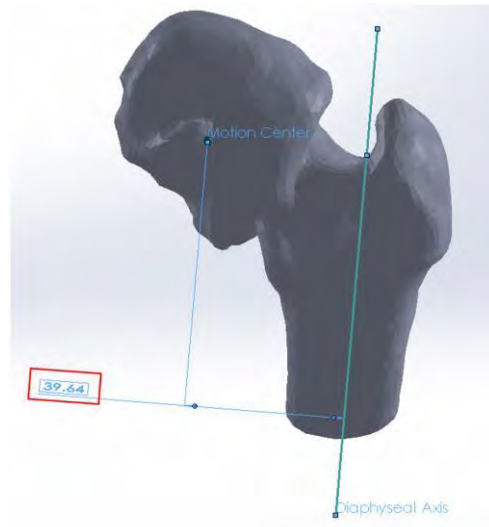
Figure 3.14 .Stem offset determination

After determining the patient's femoral landmarks, the next step on virtual prototyping of a custom stem is to build a personalized hip stem prosthesis using patient's landmarks and trying to mold it as much as possible on the femoral canal surface.

3.5. Developing a custom hip stem *[98]*

The foremost commonly femoral stems utilized in THR surgeries, if we take into account the stems geometry, are the anatomical and the right hip stems shape. The considerable distinction between them is the contact mode realized between the hip stem and the femoral inner wall cavity that clearly is influencing the way in which the loads are distributed.
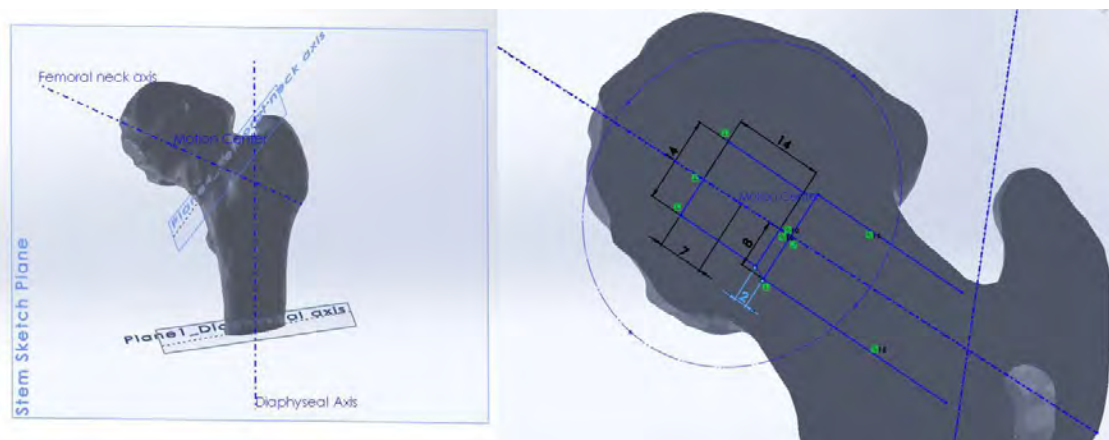
Figure 3.15. Custom hip stems starting sketch

Since the anatomical stem shows a curved contact surface along the femoral internal cavity, which implicitly helps to a better load distribution that can occur in hip joint, it was decided to develop a customized anatomical stem model, according to the patient's femoral landmarks.

Once the primary step of the femoral landmark determination was done, the femoral prosthetic stem's length was chosen to be about 130mm in accordance with the patient's femoral geometric shape. An inappropriate choice of the femoral stem total length can cause postoperative complications and over time a very long stem can cause fracture of the femur, therefore the length of the femoral stem is chosen taking into account the anatomical landmarks of the patient and his age.

The femoral stem offset is determined as shown in *Figure 3.16*, being about 40mm in this studied case. Then, by using a construction line angled at about 45°, the femoral cutting line is marked, this practically represents the line marked by the orthopedic surgeon to determine which part of the patient's femur is removed in order to insert the femoral hip stem. This reference line is necessary because the anteversion angle of the femoral prosthesis component changes its inclination in this area, achieving an anteversion of ~16°.
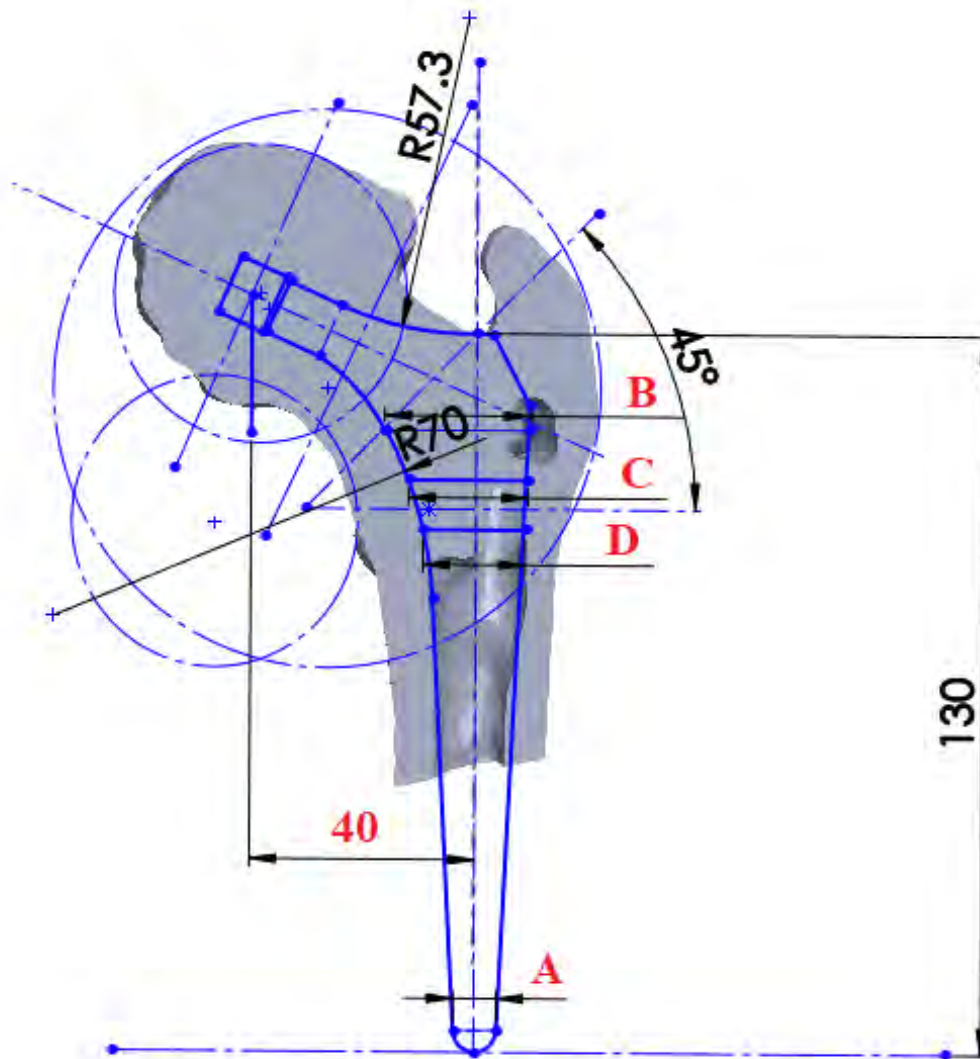
Figure 3.16. Patients' custom hip stems sketch

Using as reference the patient's femoral cavity in section, three widths A, B, C and D are identified as we can see in *Figure 3.16*, these being necessary to mark the width of the femoral hip stem in different areas of it (the dimensions are measured in the area of the lesser trochanter, below and above it).

Each of us presents unique features of the body, implicitly the curvature of the femur has a distinct radius that gives us a certain way of walking, different from one individual to another. In this study was assumed that the patient has a healthy hip joint and a damaged one, for which he must undergo THR surgery. If a femoral prosthesis is implanted with a standard CCN angle of 135° that is completely different from the patient's healthy hip joint, it can create a difference between his hip joints and obviously between their kinematics, and although it may seem unimportant it may be one of the factors that triggers postoperative complications. In order to optimize the femoral component of the hip prosthesis and to create the possibility to reduce eventual postoperative complications that a patient could go through, but also in an attempt of trying to restore the patient's initial kinematics, it was decided to develop a prosthetic femoral component using these patient's landmarks.
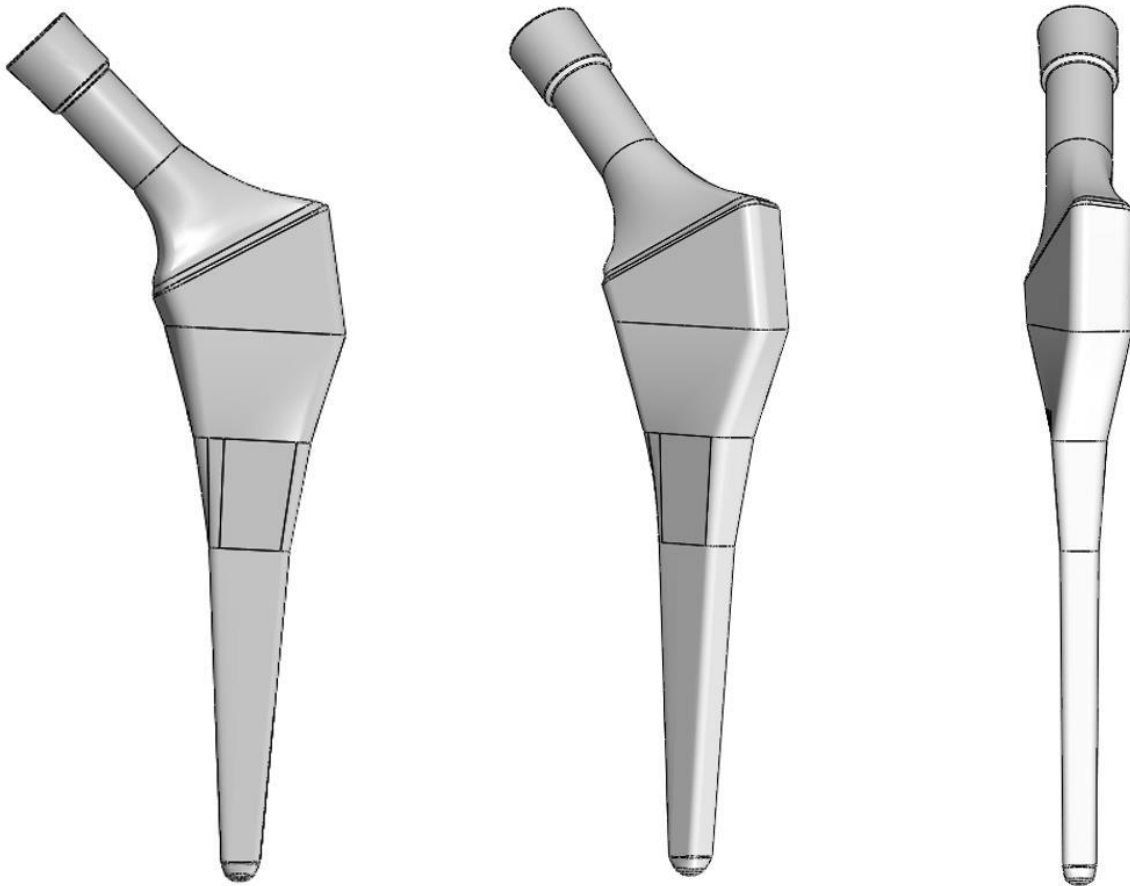
Figure 3.17. Patient's custom hip stem CAD

Because it was wanted to reproduce the femoral curvature of the patient in an attempt to make a prosthesis as "*biofidel*" as possible, a construction circle tangent to the outer surface of the femur,

in the area of the lesser trochanter was drawn, which was offset until its intersection with the construction line represented by the B segment. Was proceeded in the same manner with the outer part of the great trochanter to acquire the outer part of the femoral stem prosthesis. By joining the segments, the thickness of the femoral prosthetic component was determined, its curvature being obtained through the circle arches made with the help of the construction circles, as shown in *Figure 3.16*.

By constructing the two curvatures of the prosthetic femoral component so as to imitate those of the patient, but also using these radii to produce a gradual transition from the body of the prosthesis to its neck, a personalized prosthesis can be developed according to the patient's anatomical landmarks.

To transform this sketch into a 3D model, the two spline curves and a profile perpendicular to these curves and tangent at the same time is used. In order to achieve the anteversion angle of 16°, a tilted reference plane is created at the same angle, in which the transition profile is inserted. With the help of the loft tool from the Solidworks software, material can be added between the created profiles, respecting the guidance of the curves that define the thickness of the femoral prosthetic component.

Postoperative complications such as impingement after THR can also be determined by the design of the femoral prosthetic component, and making customized prostheses can reduce some of the factors that lead to these complications. Orthopedic surgeons are aware of this determining factor, and having only standardized prosthetic components at their disposal tries to avoid the occurrence of such postoperative complications by positioning them so as to create a compromise in the patient's favor.

3.6.   Developing a femoral stem template with changeable parameters *[99]*

The greatest challenge is to decrease the manufacturing cost of these personalized medical products. Prosthesis standardization is a quick and permissible way to restore the hip joint of a patient who is suffering from hip pain or has related joint disease, but although these prostheses are developed to restore an initial patient's condition, unfortunately it does not fully meet the needs of the patient because each bone system contains unique features depending on the individual.

That is why orthopedic surgeons and engineers are motivated to develop prostheses that faithfully mimic the human femur through their design, increase the lifespan of the medical product, and being manufactured from a biocompatible material to reduce the percentage of patients who have to undergo a revision surgery shortly after THR.

Thus, the femoral parts that lead to the prosthetic components wear can be modified and improved so that the patient is less exposed to postoperative complication, so the need to customize the prosthetic femoral component becomes more and more important.

Making a custom prosthesis as by following the steps explained in the previous sub-chapter takes time, trained personnel and of course it involves validating the prosthesis once it is built. Because of this laborious work from designing to production and implantation implicitly, the manufacturing involves high costs and extended time compared to selecting a standard prosthesis. For this reason, it was chosen to develop a CAD femoral stem template that could be modified according to the certain patient's morpho-anatomical landmarks. This contributes to the semi-automation process of making a femoral stem and can reduce the time, but also the costs of production, giving the possibility of using additive manufacturing.

Figure 3.18. Standard Femoral Hip stem Linea® Anatomical TORNIER© model

The modeling work that we carry out as part of this thesis is the modification of the existing Linéa® anatomical femoral stem model marketed by the company Tornier©.

3.6.1. *Femoral stem sketches construction*

Developing a femoral stem template is a laborious work done in a CAD mechanical software, which in our case was done in Solidworks 2017. Due to the complex shape but also to the anteversion angle, the femoral stem was divided into 13 cross sections which contains 13 profiles of a standard prosthesis. In order to be able to design the sketches of each initial profile, 13 reference plans were constructed, each of them being located at a certain distance from each other and at a certain angle as exemplified in the *Figure 3.19*. The first plane was chosen to coincide with the top plane, the second plane is an offset plane of the top one at a distance of 3.55mm, the 3rd plane was chose to be parallel with the top plane and situated at a distance of 68.25mm, the 4th plane is also an offset plane of the top one at a distance of 92.25mm, from the 5th plane the angulation is started to be change thus it's making an angle of ~10.5° with the 4th plane, the 6th plane is making an angle of ~27.5° with the 4th plane, the 7th plane is a offset of the 6th one at a distance of ~1.80mm, the 8th plane forms an angle of 42° with the 4th one, the 9th plane forms an angle of 46.5° with the 4th plane, the 10th, 11th, 12th and 13th plane is an offset of the 9th plane at a distance of approximately 8.15mm, 9.15mm and 20.80mm. These data were processed based from a standardized prosthesis with a normal CCN angle of 135° and an average stem length.
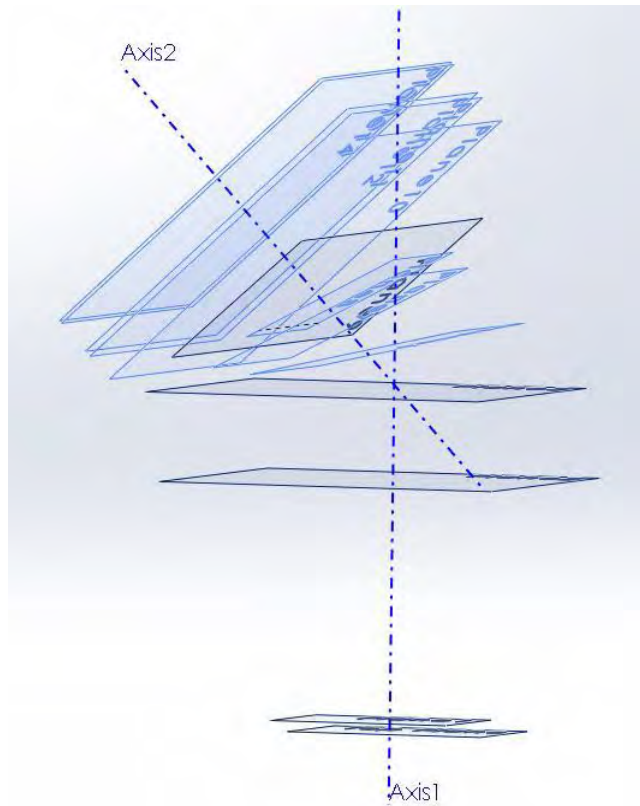
Figure 3.19. Reference planes for femoral stem template

Axis 1 and Axis 2 from *Figure 3.19* represents a normal CCN angle of 135°, which will be used in the femoral stem template construction as a reference, but it can also be changed if we want to modify the angle in order to custom the hip stem.
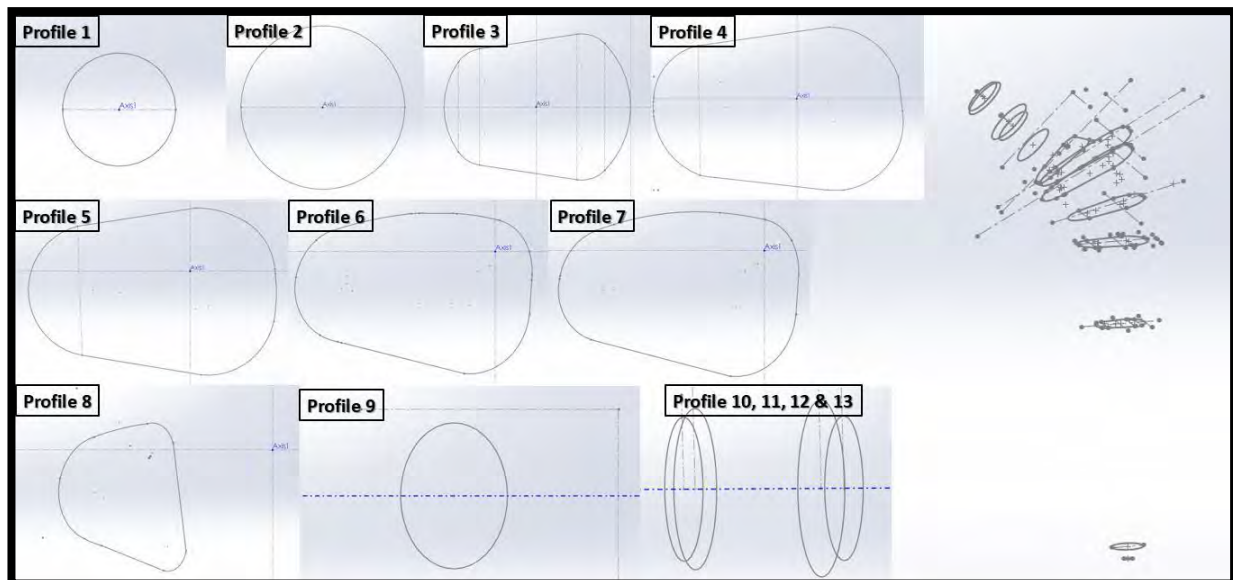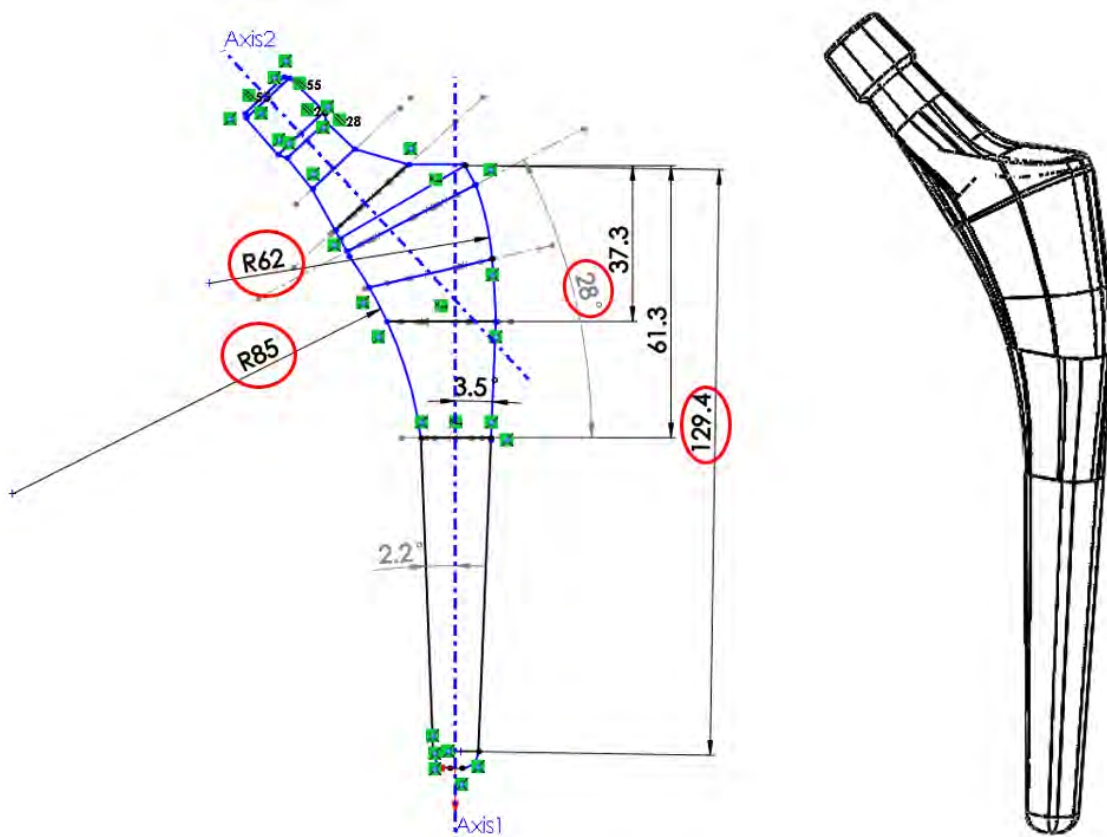

Figure 3.20. Femoral stem template profiles sketch

After the plane's construction it was proceeded by realizing a stem profile sketch in each one by using as a reference the Axis 1 and 2, but also a point created at the intersection of construction axis located in the first top plane as represented in *Figure 3.20*.

3.6.2. *Femoral stem spline curves*

Figure 3.21. Hip stem template with adaptive geometry

To obtain the final curvature of the femoral stem two curves tangent at the stem profiles were realized, generically called paths, which serve as a guide for the final instrument applied in order to obtain the final model, called *loft* (an instrument that adds material between all the profiles in order to create the final feature). The radii of these curves that coincide with the curvature of the femur shown in *Figure 3.21* can be modified according to the femoral morphological landmarks of the patient by accessing the 3D sketch from the template file. A femoral stem with a geometry that tends to fuse on the femoral inner canal may facilitate a better fixation and thus reduce postoperative complication such as impingement after THR.

At the same time, by accessing the 2D sketches, we can change the total length of the stem according to the size of the patient's femur, neck diameter, neck shaft angle and hip stem offset. Depending on the patient's femoral landmarks we can customize a hip stem prosthesis that it fits much better with the patient's needs. Adaptive geometry and a suitable surgical approach can reduce post-operative complications, increase the life span of the femoral stem, and thus reduce the number of THR revisions during the patient's lifetime.

3.7. Chapter conclusion

One of the main causes that increase the early prosthesis dislocation is the geometrical aspect of the hip stem and acetabular components. In order to create a more suitable anatomical hip stem that tends to fuse with the patient's femur, patient's femoral landmarks and femoral curvatures were used to develop a personalized hip stem prosthesis. The difference between the standard hip joint prosthesis and a personalized one is that in case of personalized hip joint prosthesis the shaft angle and the anteversion angle (which influence the probability of early intra prosthetic postoperative complication) can be the same as the initial one that the patient had when the hip joint was healthy; instead if we talk about the standard hip joint prosthesis we can choose between a limited number of angles.

With the help of Additive Manufacturing Technology, the costs of manufacturing personalized hip joint prosthesis can be decreased, and the opportunity to develop specific medical products for any individual becomes more and more possible and feasible.

Because of a significant improvement of pre-clinical validation in the last years, numerical models and experiments in vivo can replicate nowadays most of failure scenarios of hip joint prosthesis. However, there are still many factors that are very difficult to consider like: patient's anatomy, bone and muscles characterization and activity level or other biological interferences. In this sense, in the next chapter, a virtual validation was performed with the help of FEM in order to observe the mechanical behavior of a standardized prosthesis and a customized prosthesis.

CHAPTER 4

FINITE ELEMENT ANALYSIS OF HIP JOINT FEMORAL STEM

Finite element analysis is a numerical method of reproducing in a simplified or complex manner a physical phenomenon helping us to describe and understand the virtual model behavior when submitted to external loads. Virtual models tend to reproduce the object, organ or cells as accurately as possible [100], but most of the times they are simplified, so the analysis can be reduced only to the area of interest because in the case of a complex model it takes more time and more resources to solve the equations and to give an analysis result. A biological model has a higher degree of difficulty due to its irregular shape and surface, so a mesh in this case can be more complex and the FEA study can take longer.

Even though this method has incredible potential in terms of the experimental side the results obtained from the analysis remain approximations of the CAD models mechanical behavior because they depend on the model parameters. Usually the errors that appear when solving are related to the simplification of the geometry model commonly named as discretization errors (they occur because of the element size or shape, which is in relation of interdependence with the structure, anatomical morphology or model thickness), but also due to a displacement field called interpolation error.

Although the human body is a complex "biological machine", this method allowed specialists to predict prosthesis or organs mechanical behavior and to evaluate them, in order to decide if the virtual model can pass at the ex vivo experimental test.
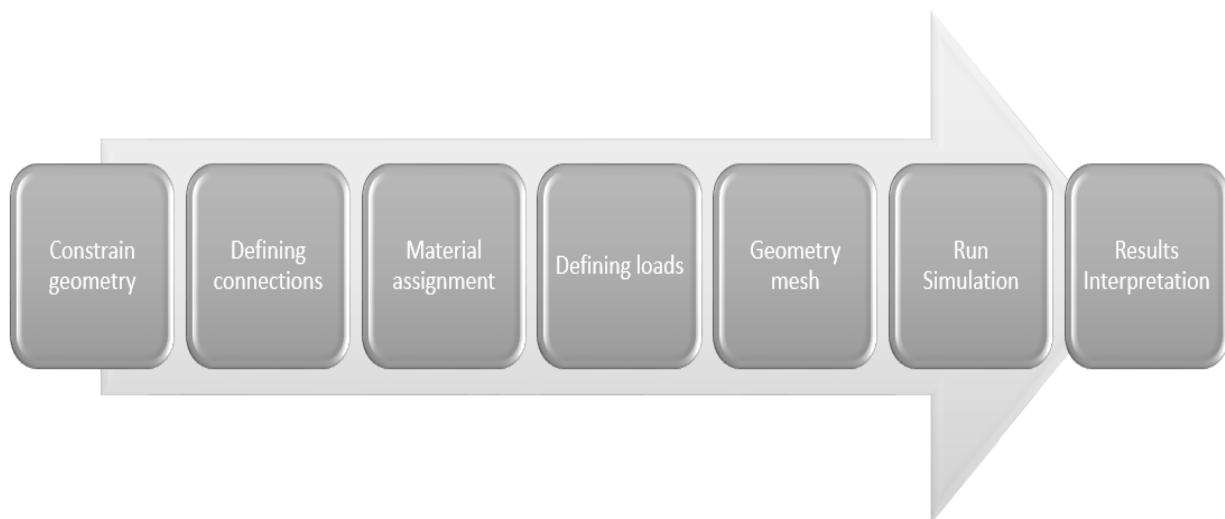
Figure 4.1. Main stages of a FEA study

4.1. Mechanical properties of the human bone tissue

The FEM studies are a convenient alternative to understand the mechanical behavior of bones at different loads or specific situations that can occur in the daily life activities. Bones are not composed of a homogeneous and isotropic material and they have the characteristics of a non-uniform "solid" that consists of two types of bone tissue: cortical bone (hard bone or compact bone) tissue and spongy bone (trabecular bone or cancellous bone) tissue, each tissue having different mechanical properties [100].

4.1.1. Cortical bone tissue

The cortical bone tissue, also called compact or lamellar bone because of its osteon's distribution is represented by the outer part of the bone. It is a hard tissue which support the structure of the human body, with a lamellar structure that is in a continuous transformation, developing in the areas where higher mechanical loads appear. Thus, the cortical bone tissue represents most of the bone mass due to its high density. The cortical bone tissue commonly referred as compact bone contains secondary osteons with diameter between 100 and 300µm having around Haversian canals recessed in the remains of old osteons. Studies performed on corpses, but also by simple CT scan analysis demonstrate that compact bone tissue has superior mechanical properties compared to spongy bone tissue [102].

The table below illustrates the most important mechanical characteristics of the cortical bone tissue:

Table 4.1. Cortical Bone Tissue Main Mechanical Properties [103]

Cortical Bone Tissue		
Mechanical Properties	**Unit Measure [SI]**	**Value**
Young Modulus	GPa	17.9
Poisson coefficient	N/A	0.3
Density	g/cm³	0.90

However, studies have shown that cortical bone tissue mechanical properties may vary from patient to another, so we can find an elastic modulus ranging from 3.9GPa to 17.9GPa with a Poisson coefficient between 0.62 and 0.26 determined by the patient's medical history, age and bone quality tissue [103].

4.1.2. Trabecular bone tissue

Trabecular bone tissue, also called cancellous or spongy bone is a porous tissue located inside the bone, having an irregular structure, with the role of giving flexibility to the bone and taking over the external loads and equally distributing them. Studies have shown that spongy bone tissue

has lower mechanical characteristics than compact bone tissue, which makes it more fragile, representing a small percentage of total bone weight [104].

The table below illustrates the main mechanical characteristics of the trabecular bone tissue:

Table 4.2. Trabecular Bone Tissue Main Mechanical Properties [105, 106]

Trabecular Bone Tissue		
Mechanical Properties	**Unit Measure [SI]**	**Value**
Young Modulus	GPa	0.76
Poisson coefficient	N/A	0.3
Density	g/cm³	0.30

As in the case of cortical bone tissue, trabecular bone tissue can have a range of values depending on the patient's bone quality and age, studies showing that the young modulus of a trabecular bone can have a range between 0.76 and 10GPa [105, 106].

Ultimately numerical simulation studies have been conducted in this field such as FEM analysis to estimate the mechanical properties of bone tissue, mostly for spongy bone. In this sense studies were conducted to determine the stress at a spongy level by using FEM to provide more information about the fracture appearance and predicting bone failure *(B. Depalle et al., 2012* [107]).

Despite the heterogeneity and anisotropy presented by different bone tissues, it is common in the biomechanical modeling of bone-prosthesis assemblies interaction to make the assumption that the bone tissues are isotropic homogeneous materials and that they follow a linear behavior law, hypothesis confirmed also by David Mitton during the Devos project held in 2013 [108].

4.1.3.   *Bone quality at elderly patients*
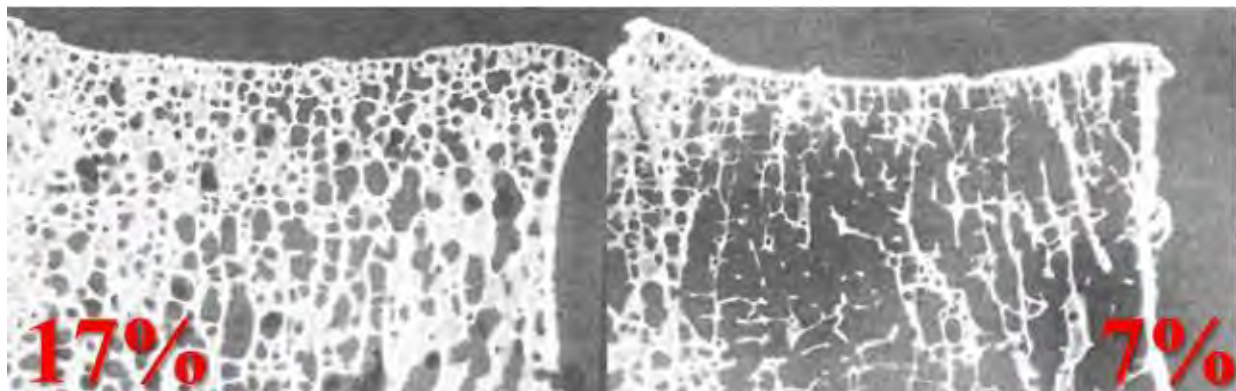
Figure 4.2. Bone tissue density affected by osteoporosis, 55 years old woman left and 86 years old women right [Vajjhala et al., 2000]

As we grow older, the ability to restore bone cells slows down, our metabolism is transformed and the capacity to recover in case of complications and fractures is diminished, all these changes affect patient bone quality. Bone loss or bone demineralization occurs with aging or in case of diagnosing with disease causing this effect, which affects the population both men and women. Although the loss of bone mass can affect regardless of gender, studies have shown that women

are more exposed with aging at diseases such as osteoporosis or osteoarthritis (OA) [109], a disease which affects bone quality, making patients more susceptible to fractures, slow healing or medical complications.

For the mechanical behavior simulation of an arthritic hip joint study, it was assumed that both the femur and the pelvis contain a homogeneous and isotropic material. Cortical tissue was chosen to be used because of better mechanical qualities. With age the cortical bone tissue loses its quality, becoming more porous and transforming into a tissue almost like the trabecular one. Following the cortical tissue analysis of the femur in case of females over 70 years old, studies have shown that Young's modulus can be 0.96±0.19GPa, tensile strength can be 0.019±0.0014GPa and compressive strength can be 0.096±0.00083Gpa [110, 111]. The values show a significant deterioration of the bone quality compared to the average in case of a young and clinically healthy patient, thus in this case study, the values were chosen because the analyzed patient can be included in the age range and gender group statistics.

4.2. Mechanical behavior simulation of an arthritic hip joint

4.2.1. Constrain / fixture geometry
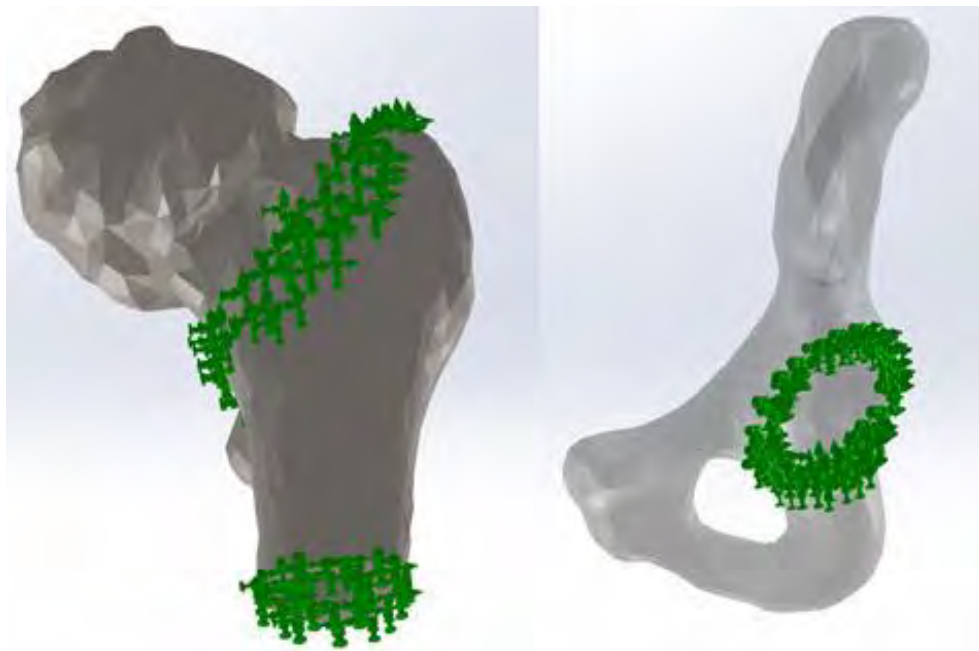
Figure 4.3. Femur and Pelvis fixture in Solidworks 2017

Fixing the geometry helps to maintain and support a CAD model, whether it is a functional part or not of an assembly, is a mandatory step to perform FEM analysis. In order to fix the hip joint anatomical parts geometry, the constraints were simplified as follows: in case of the pelvis the acetabulum labrum area was fixed and in case of the femur, the inferior part of it was fixed, but also the margins of the femoral neck. This type of constraint helps us to perform a static analysis of the anatomical parts to understand how the hip joint models behaves when receiving external loads of different intensities.

4.2.2. Assigning material to CAD model

Table 4.3. Mechanical properties of the cortical bone tissue used in the FEA study of an arthritic hip joint [99, 103]

Property	Value	Unit Measure [SI]
Elastic Modulus	11.6	GPa
Poisson's Ratio	0.26	N/A
Mass Density	1440	kg/m^{-3}
Tensile Strength	21.13	MPa
Compressive Strength	97.19	MPa

Another mandatory condition for running an FEA study is to assign a type of material to the studied geometry. Because the study wants to recreate the mechanical behavior of a patient that has suffered bone loss due to arthritis, the material is not standardized, thus, a custom material can be created in a CAD software, for example Solidworks. In this study it was assumed that the material applied to both, pelvis and femur CAD models is homogeneous, linear, elastic, and isotropic. Cortical bone tissue was used due to the superior properties and the mechanical property data of the femoral cortical bone tissue of a female aged over 70 years were extracted from Raviraj Havaldar et al. [110] study on effects of tensile and compressive loadings on human femur bone.

4.2.3. Boundary condition
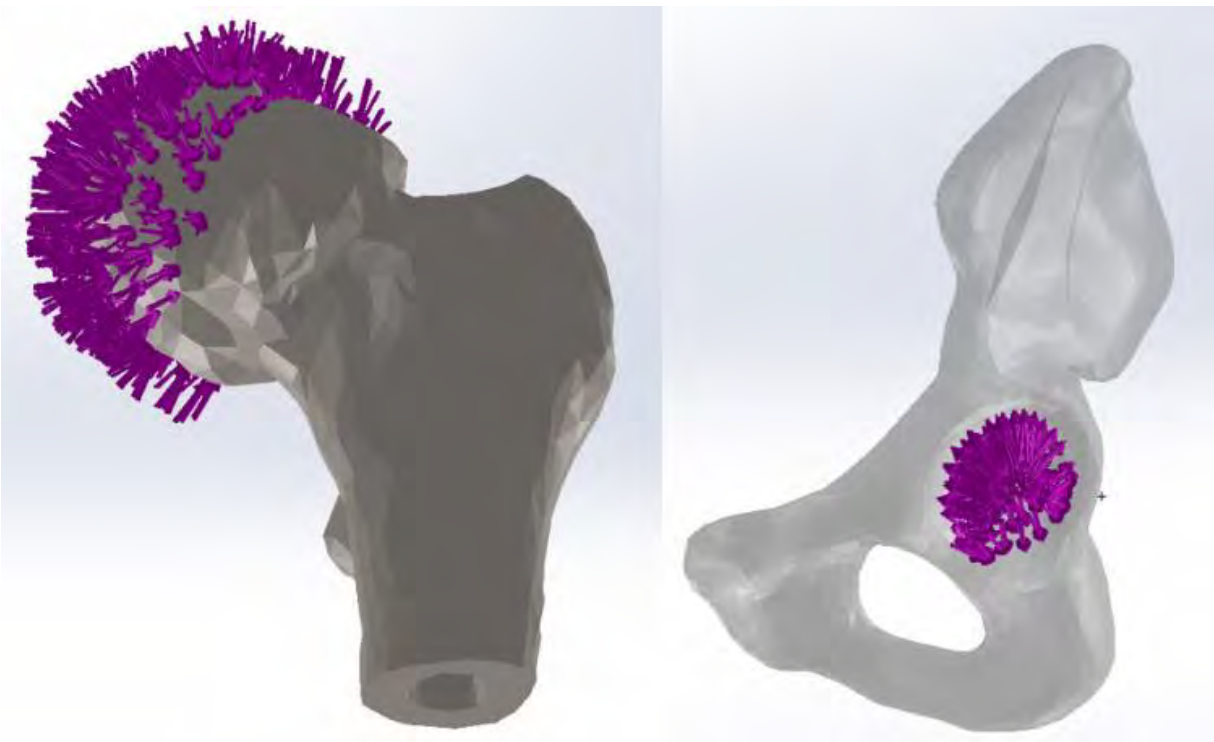
Figure 4.4. Femur and Pelvis boundary condition area in Solidworks 2017 [purple]

The human hip joint is daily subjected to repetitive movements and external loads as a result of the activities that we perform, thus, during more demanding activities such as stairs, walking or running, the human hip joint can be subject to stress up to ten times higher than during a normal gait cycle or a static position (upright bipedal stance or biped-erect posture) [112].

High stress can appear in the human hip joint, due to patient's weight and can affect the coxofemoral articulation by increasing the applied load. In this study, simulation were performed on both pelvis and femur model by applying ten types of forces, some of them representing approximately the equivalent of the weight of a patient can have, and some of them, respectively 2000 N, 2500 N and 3000 N, representing the equivalent of a shock received in the hip joint in case of accidents.

Table 4.4. Forces applied in the FEA study of a female arthritic hip joint

Load	Value [N]	Equivalent in kgf
F_1	686.46	70
F_2	784.53	80
F_3	882.59	90
F_4	980.66	100
F_5	1078.73	110
F_6	1176.79	120
F_7	1274.86	130
F_8	2000	204
F_9	2500	255
F_{10}	3000	306

4.2.4. Model mesh properties

In this study, solid models of the pelvis and femur affected by arthritis were used, with a curvature based solid mesh type and 4 Jacobian points. The CAD pelvis model having a maximum element size of 7.62mm and a minimum element size 7.61mm, with a total number of 29 177 nodes and 18 608 elements, presenting a high mesh quality plot. The CAD femur model contains a 5.23mm maximum element size and a 5.22mm minimum element size, with a total number of 23 494 nodes and 15 298 elements with a high mesh quality plot.

4.2.5. Stress analysis results

The general von Mises simplified equation used in multi-axial 3D stress is the following:

$$\sigma_v = \left\{ \frac{[(\sigma_1 - \sigma_2)^2 + (\sigma_2 - \sigma_3)^2 + (\sigma_1 - \sigma_3)^2]}{2} \right\}^{\frac{1}{2}} \qquad (1)$$

Where σ_1, σ_2, σ_3 represents the principal stress.
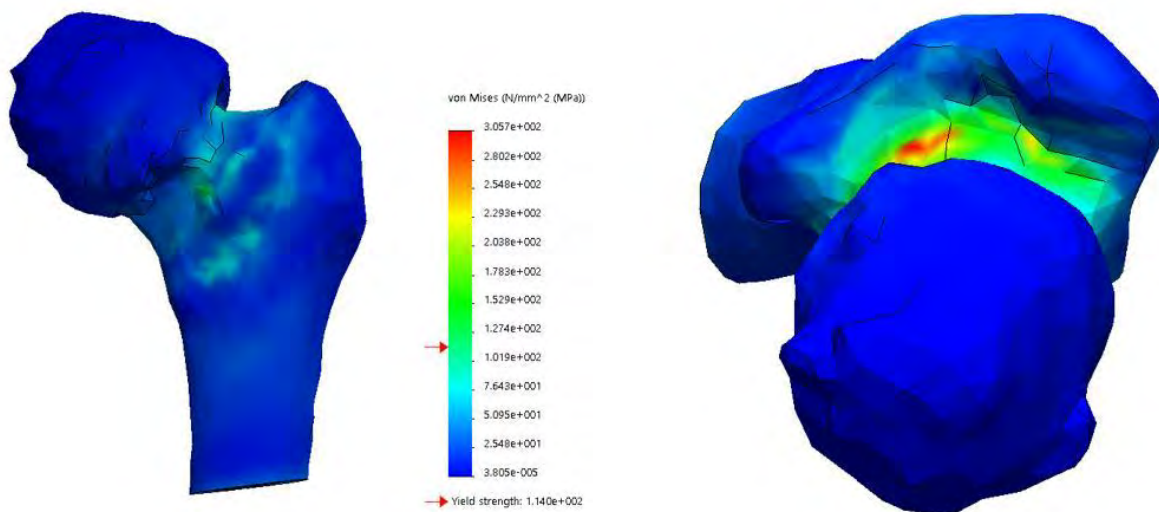
I.   Stress analysis results in case of the ischium CAD model

Following the FEA study performed in each load case applied inside the acetabulum, the results have shown a minimum stress located in the node 6904 and a maximum stress located on node 8013, in the pelvis model in all FEA studies.

In *Figure 4.6* we can identify the minimum and maximum stress values resulting from each analysis.

From the analysis of the evolution of both, minimum stress and maximum stress, the FEA study results of the patient's pelvic model who suffered bone loss due to arthritis disease shown a linear increase of the load values from 686.46N to 1274.86N, however, with the application of loads greater than 2000N, stress increases considerably.

Figure 4.5 contains the graphical representation of Von Mises and how it is distributed on the virtual pelvic model (N/mm^2 or MPa).

Acetabulum margin is the most affected area, containing the maximum stress area that increases in the same time with the load, showing critical values especially in the case of 3000N force applied.
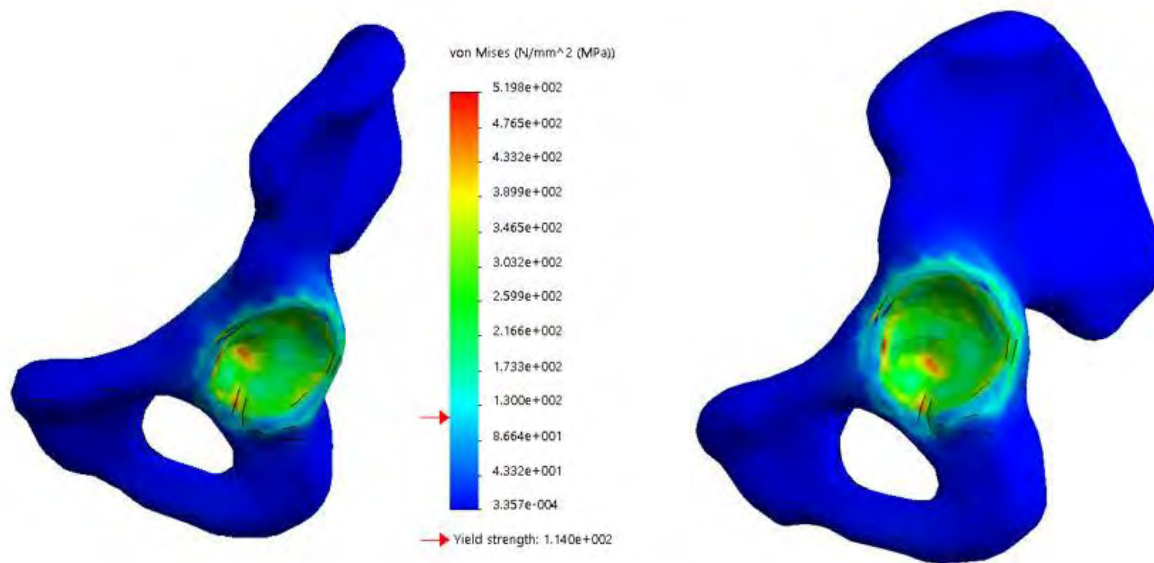
Figure 4.5. The coxofemoral model stress analysis results for F_{10} in case of an older patient diagnosed with arthritis
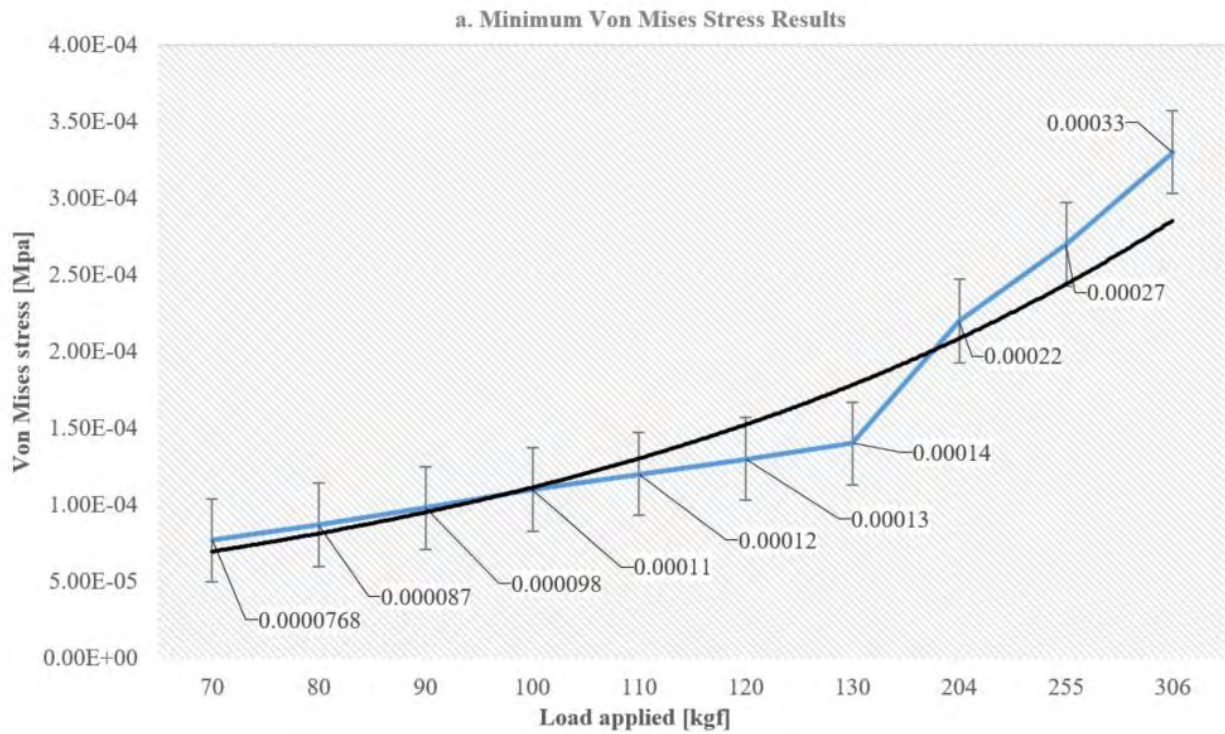
Figure 4.6. Minimum and maximum Von Mises Stress results [MPa] obtained in case of the pelvis CAD model

II.   Stress analysis results in case of the femur CAD model

Following the FEA study performed in each load case applied to the femoral head, results have shown a minimum stress located in the node 5511 and a maximum stress located on node 4758, in the femur model, in all FEA studies.

In *Figure 4.8* we can identify the minimum and maximum stress values resulting from each analysis.

From the analysis of the evolution of both minimum stress and maximum stress, FEA study results of the femur model of a patient who suffered bone loss due to arthritis disease, have shown a linear increase of the load values.

Figure 4.7 contains the graphical representation of Von Mises stress on the femur virtual model. Femoral neck is the most affected area, containing the maximum stress area that increase in the same time with the load and showing higher values especially in the case of high loads applied.

Figure 4.7. The femur model stress analysis results for F_{10} evolution in case of an older diagnosed with arthritis

a. Minimum Von Mises Stress Results
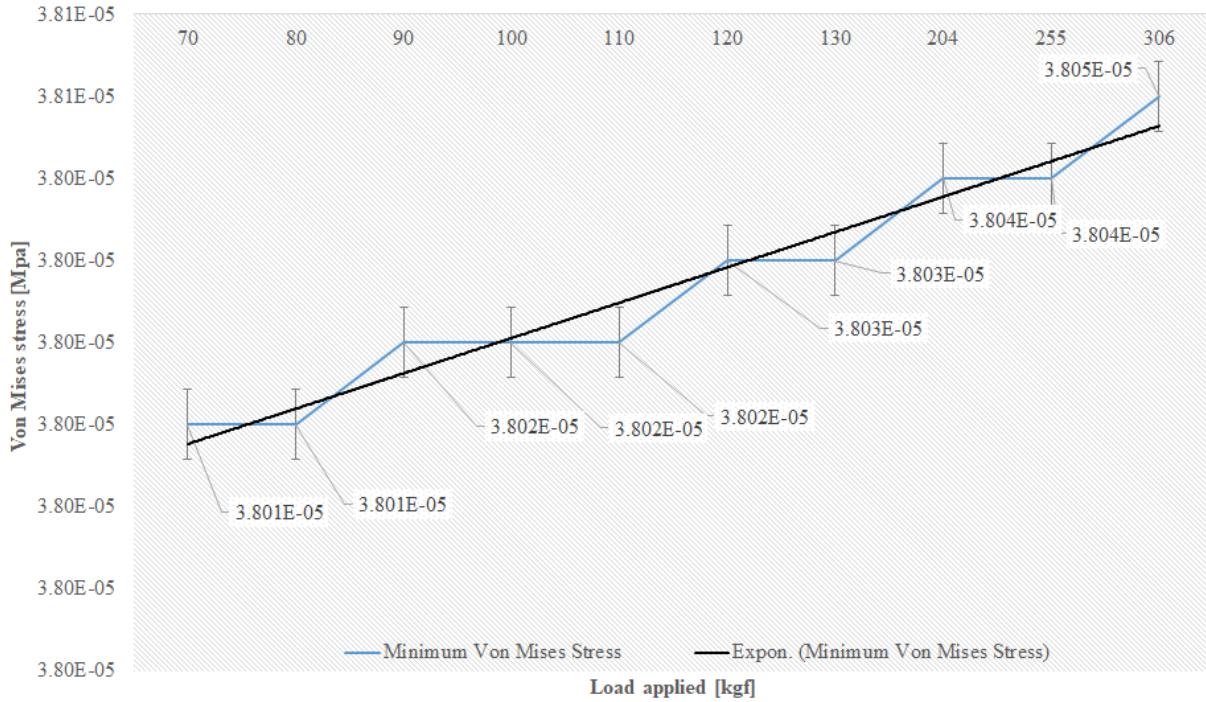
b. Maximum Von Mises Stress Results
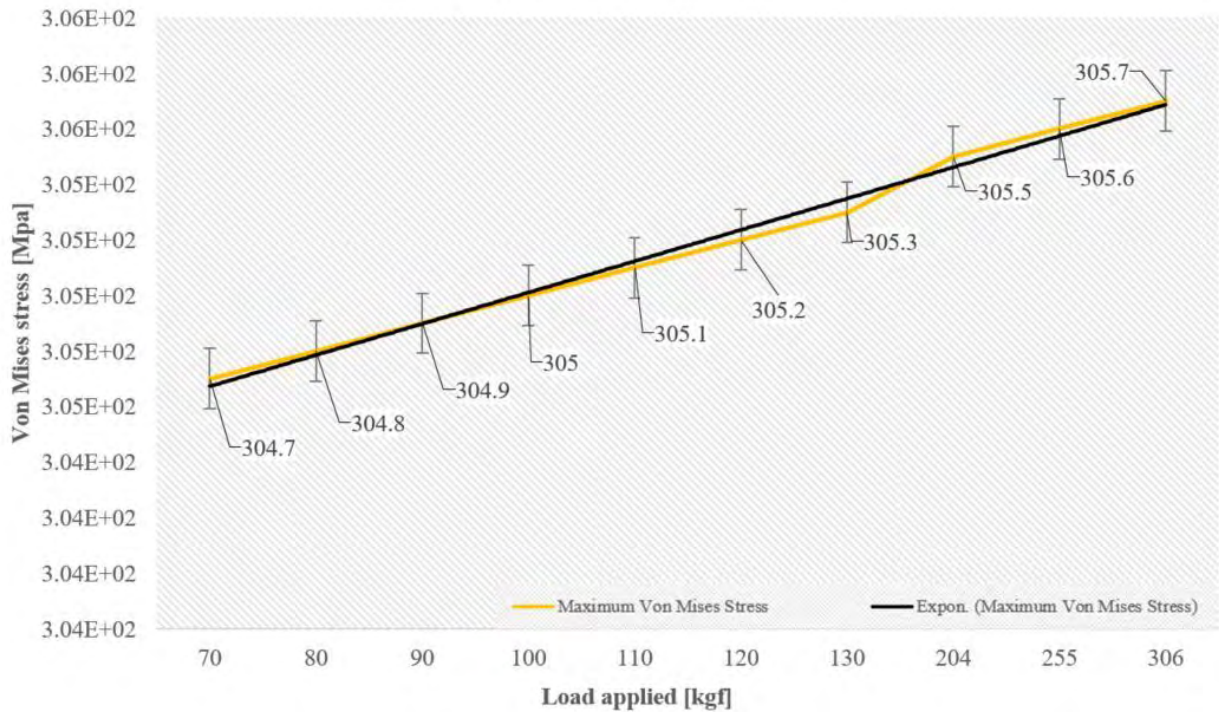
Figure 4.8. Minimum and maximum Von Mises Stress results [MPa] obtained in case of the femur CAD model

4.2.6. *Displacement analysis results*

I. *Displacement analysis results in case of the ischium CAD model*

     Following the FEA study performed in each load case applied inside the acetabulum, the results have shown a minimum displacement (0mm) located in the node 727 and a maximum displacement located in the node 8331, in the pelvis model in all FEA studies. In *Figure 4.9* we can identify the minimum and maximum displacement values resulting from each analysis.

     From the analysis of the minimum displacement and maximum displacement evolution results from the FEA studies of the pelvis model of a patient who suffered bone loss due to arthritis disease, we can observe a linear deformation for the first eight cases, with an increasing of the deformation in the case of applying a load which exceeds a value of 2000N.

     Figure 4.10 contains the graphical representation of displacement results and how deformations affect the pelvis virtual model. The acetabulum part is the most affected area, especially its center, displacement values increasing at the same time with the value of the load applied. Although the deformations may appear small, in case of an elderly patient suffering from arthritis and bone loss, a simple crack can rapidly degenerate into a fracture or other medical complications that can make it undergo surgery.
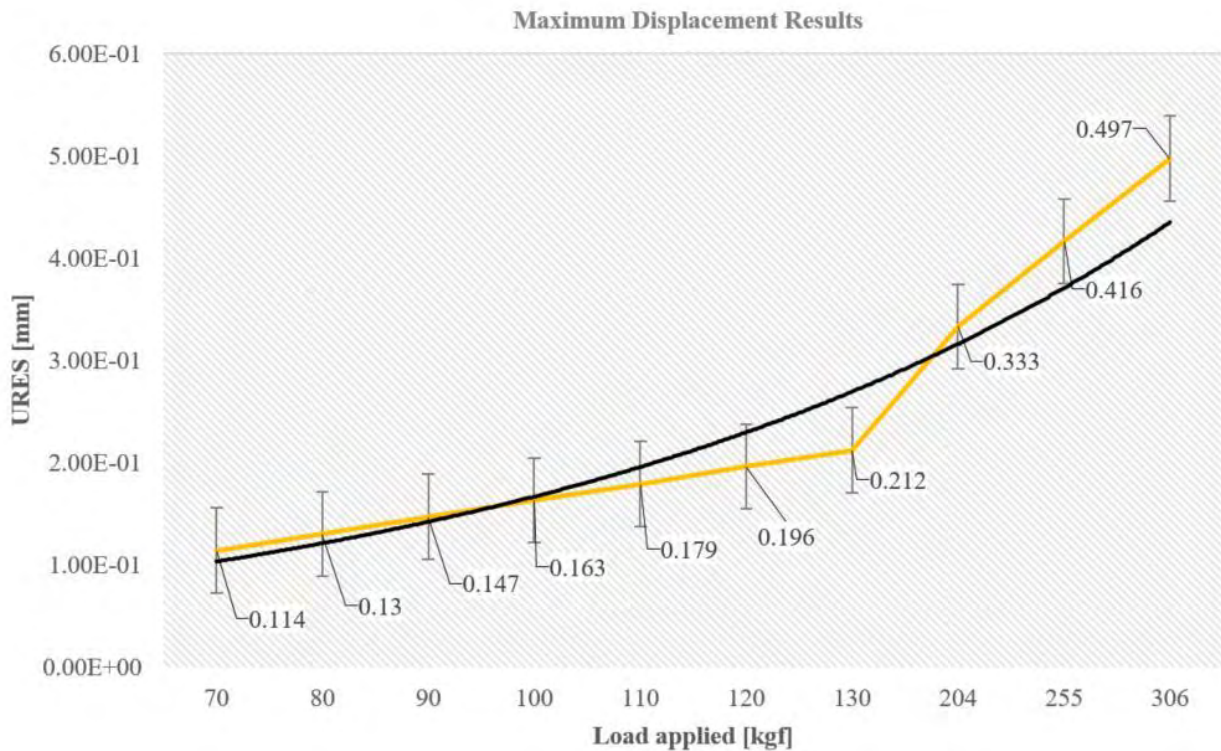
Figure 4.9. Maximum displacement results [mm] obtained in the case of the pelvis CAD model
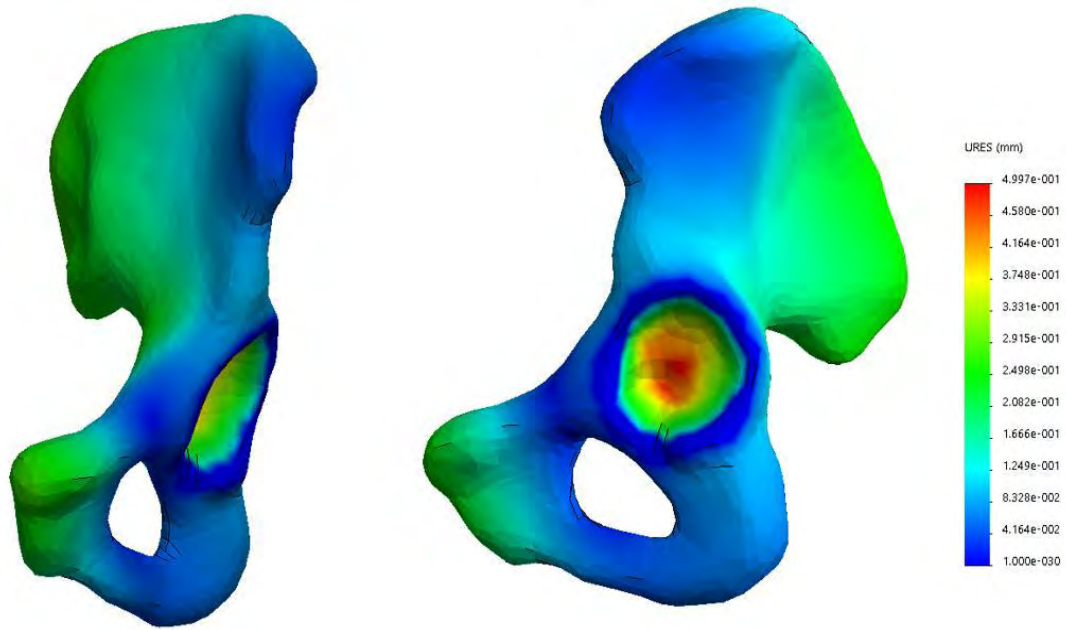
Figure 4.10. The pelvis model displacement analysis results of F_{10} in case of an older patient diagnosed with arthritis

II. Displacement analysis results in case of femur CAD model
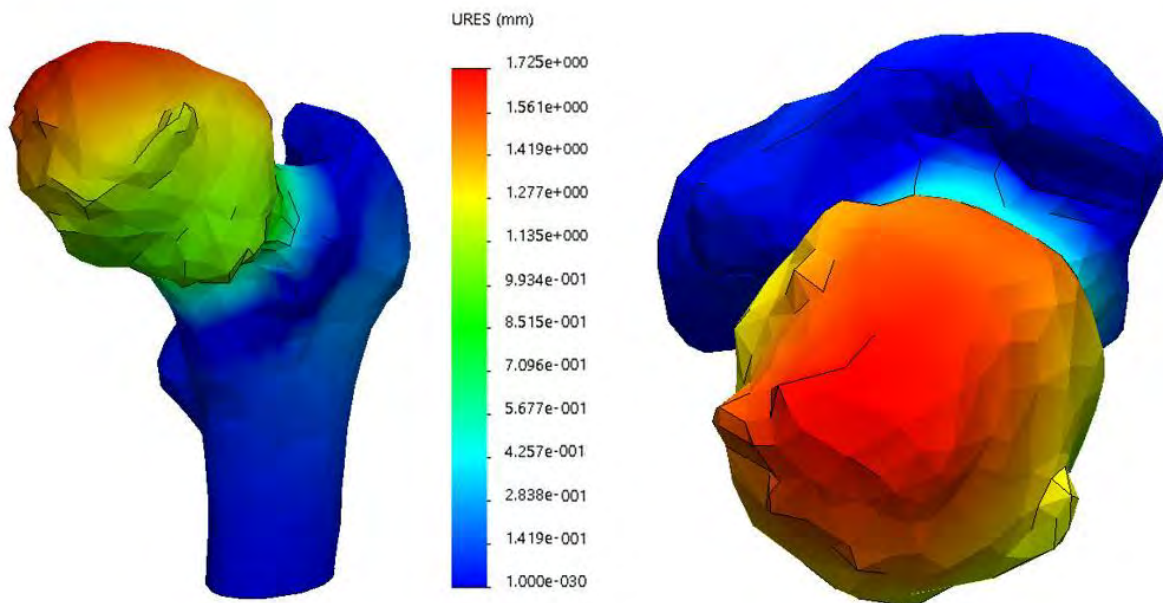
Figure 4.11. Femur model displacement analysis results of an elderly patient in case of F_{10} load
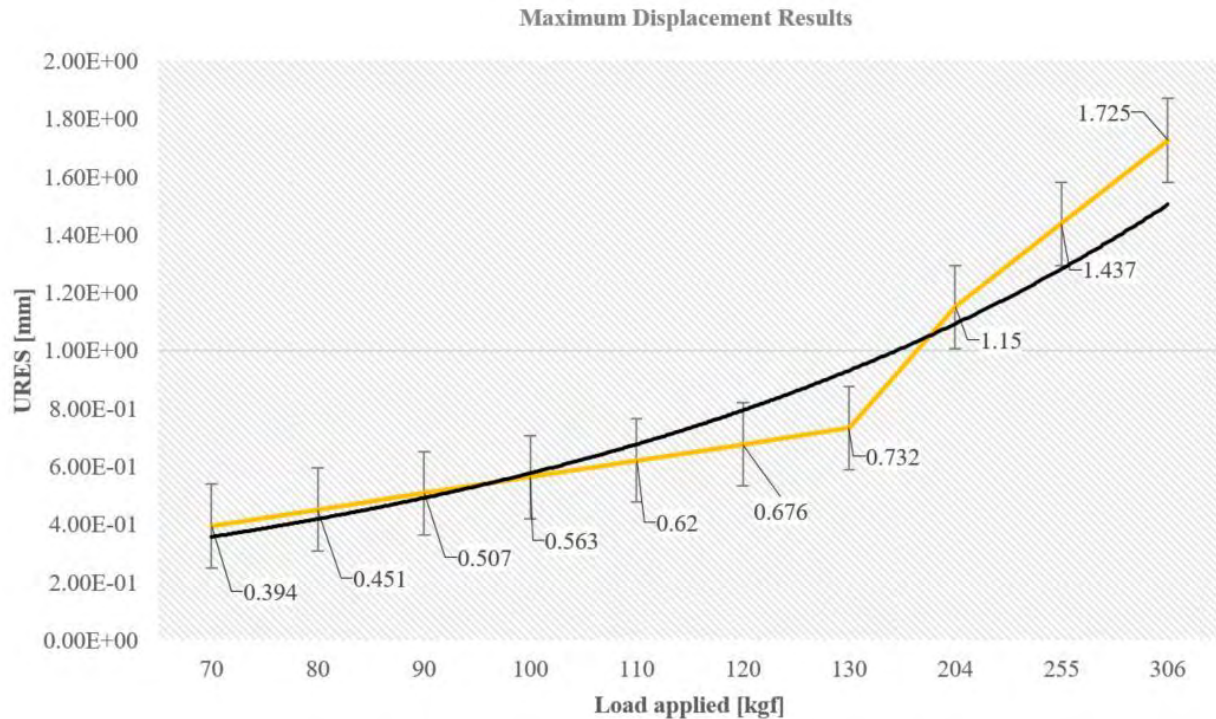
Figure 4.12. Maximum displacement results [mm] obtained in the case of the femur CAD model

The FEA study performed in each load case applied on the femoral head has shown a minimum displacement located in the node 175 and a maximum displacement located node 4, in all load cases. In *Figure 4.12* we can identify the minimum and maximum displacement values resulting from each analysis.

Figure 4.11 contains the graphical representation of displacement results and how deformations affect the femur virtual model. Femoral head part is the most affected area, displacement values increasing at the same time with the value of the applied load. Such displacement results in the case of an elderly patient suffering from arthritis and bone loss, can cause fractures of the femur which can conduct to a THR surgery.
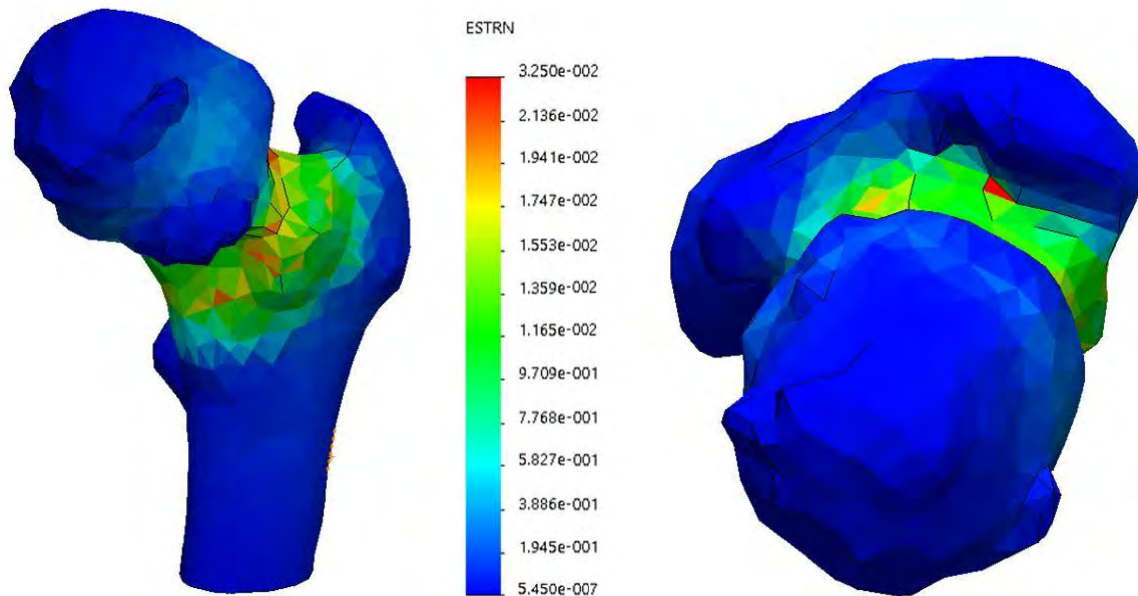
4.2.7. Strain analysis results

I. Strain analysis results in case of the ischium CAD model

The FEA study results have shown a minimum strain located in the element 8605 and a maximum strain located in the element 13 693 for the pelvis model, in all FEA studies. In *Figure 4.13* we can identify the minimum and maximum strain values resulting from each analysis.

From the analysis of the minimum and maximum FEA strain results evolution of the pelvis model of a patient who was diagnosed with arthritis, we can observe a linear strain increasing, with higher values in case of 3000N force applied in the acetabulum area.

b. Maximum Strain Results
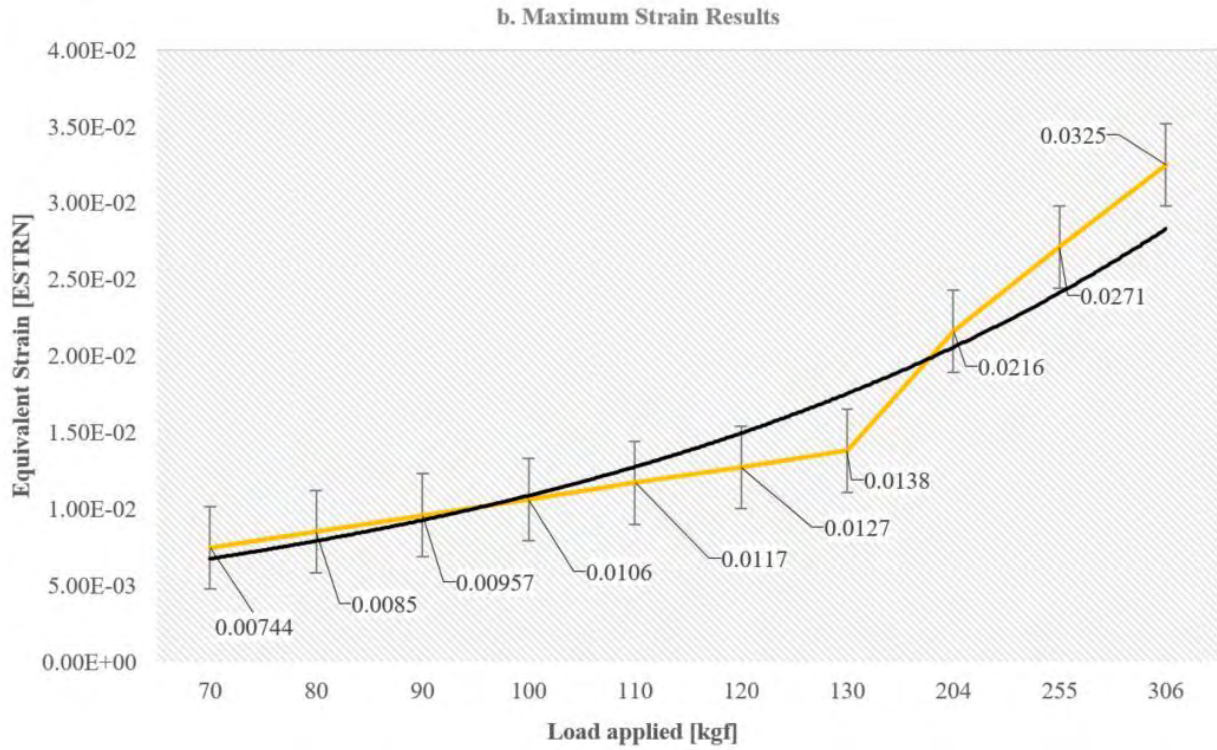
Figure 4.13. Minimum and maximum strain results [Equivalent Strain] obtained in the case of the pelvis CAD model
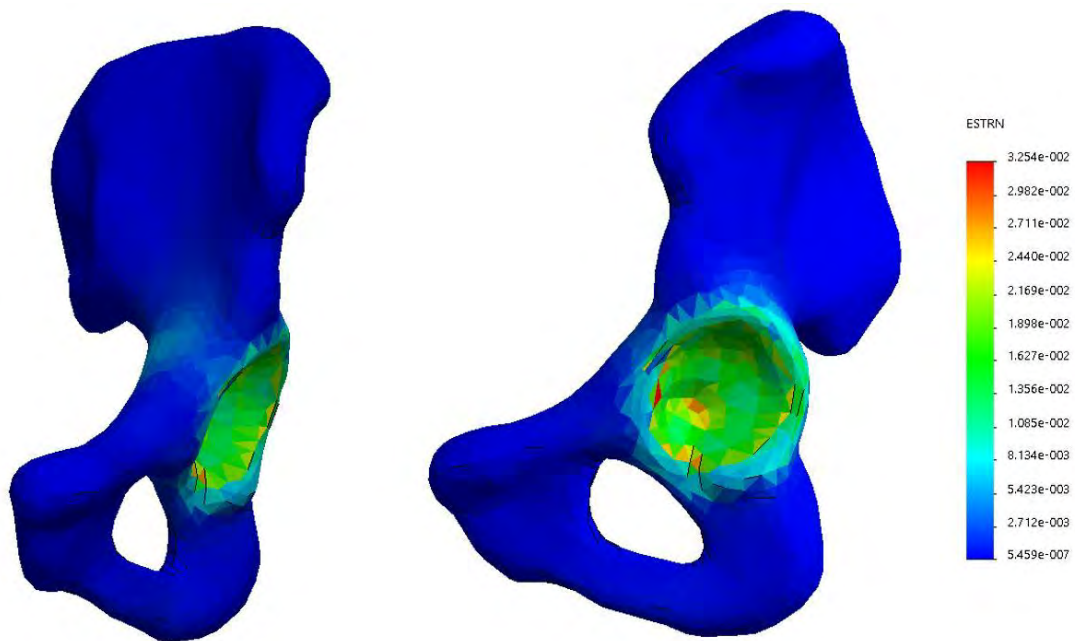
Figure 4.14. Hip model strain analysis results of F_{10} in case of an older patient diagnosed with arthritis

Figure 4.14 contains the graphical strain distribution in the hip virtual model, the most areas affected being the acetabulum interior with critical values on the acetabulum margin.
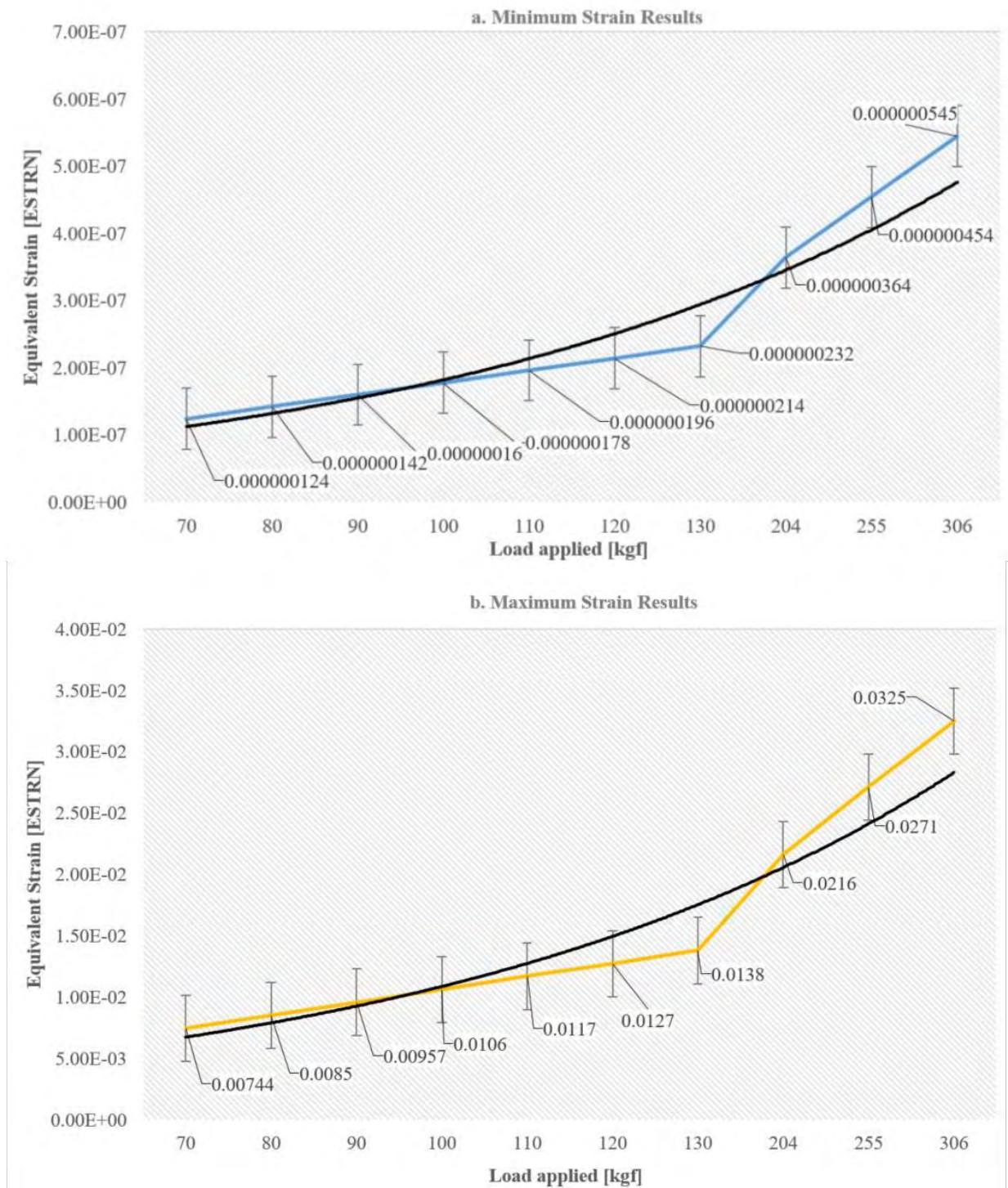
Figure 4.15. Minimum and maximum strain results [Equivalent Strain] obtained in the case of the femur CAD model

The FEA study results have shown a minimum strain located in the element 3676 and a maximum strain located in the element 6508, in the femur model in all FEA studies. In *Figure 4.15* we can identify the minimum and maximum strain values resulting from each analysis.

From the analysis of the evolution of both, minimum and maximum FEA strain results of the femur we can observe higher strain values in case of 2000N, 2500N and 3000N forces applied on the femoral head.

Figure 4.16 contains the graphical strain distribution in the femur virtual model, the most areas affected being the entire femoral neck with critical values on the femoral neck inferior margins.

Figure 4.16. Femur model strain analysis results of F_{10} in case of an elder patient diagnosed with arthritis

4.2.8. *Mechanical behavior simulation of an arthritic hip joint results interpretation*

Using CT scans of an elderly female patient diagnosed with arthritis at the left hip joint, bone segmentation was performed in order to obtain CAD models, which were used for static FEA studies at different loads in the pelvis acetabulum and on the femoral head, where normally stress may occur due to daily activities or as a result of injuries. The results of the study have shown that both, pelvic and femoral models present high stress values, which can occur due to the poor cortical bone tissue mechanical properties corresponding to female patients over 70 years old. Comparing the analyzed results obtained from the pelvis and femur models, was conclude that the femur is more prone to cracks and fractures than the pelvis, especially in the area of the femoral neck, due to its shape and load distribution capacity. Although virtual bone FEA studies are simplified due

to the complexity and uniqueness of each patient, they still can provide valuable information regarding bone failure prediction.

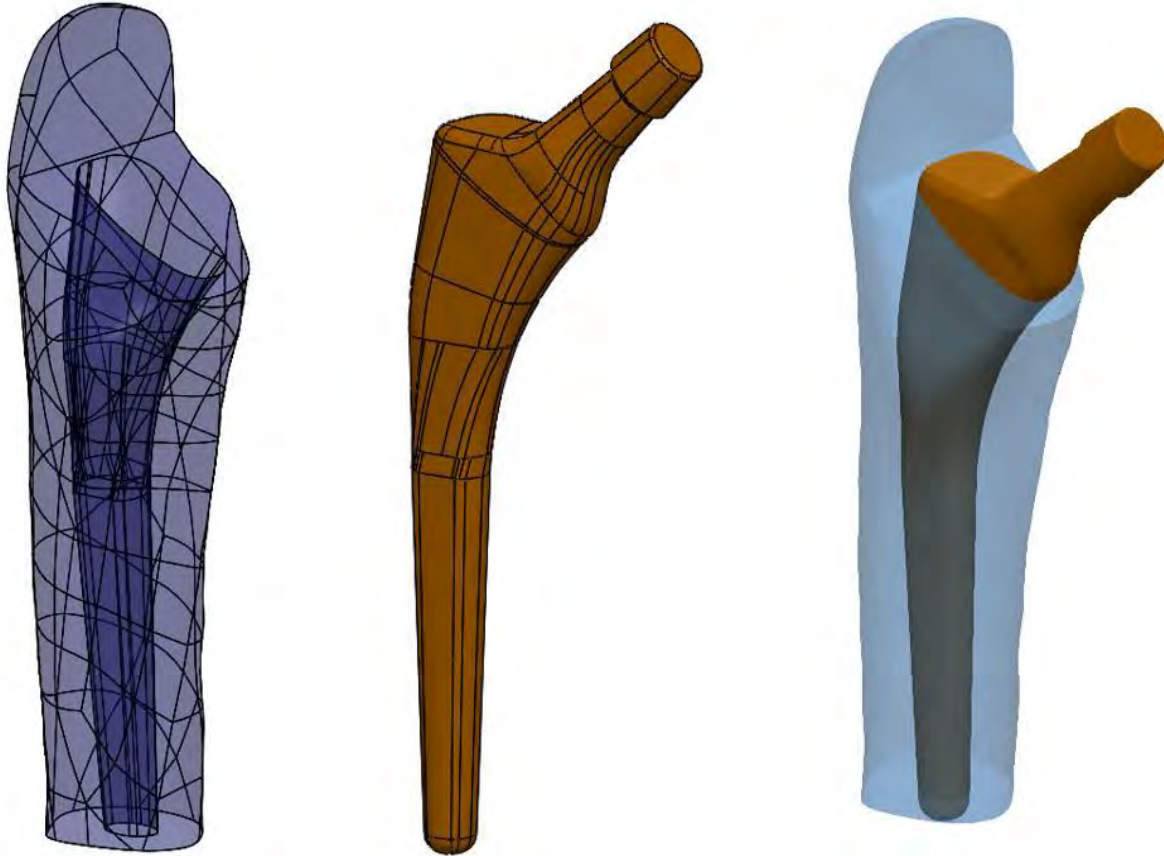## 4.3. Mechanical behavior simulation of a standard femoral stem

Figure 4.17. Femur and standard femoral stem assembly in Solidworks 2017

The simulations were carried out on Solidworks 2017 CAD software with a finite element extension called *Solidworks Simulation*, because is particularly recognized for its excellent contact management. In this part, the images used to illustrate the method come from the assembly of the standard femur and the standard anatomical hip stem.

After performing the bone segmentation process, which was explained in the previous chapter, the femur was exported into *.stl file to refine the mesh in MeshLab. After refining the mesh of the femur, the file was exported another time into *.stl extension and imported as geometry in Soldidworks 2017.

The standard anatomical femoral stem was built based on a *Linea Anatomica Tornier* femoral hip stem, to use it as a benchmark in the study of a custom hip stem prosthesis.

In order to perform the assembly and perform a virtual THR surgery, a new assembly file was created and the femur was imported and used as a basis geometry. Orthopedic surgeons are using femoral landmarks to choose the most suitable hip stem prosthesis. Using the same idea the diaphyseal axis and femoral neck axis of the femur was used in order to create a mate with the diaphyseal axis and the neck axis of the hip stem. After constraing both parts the virtual surgery is performed by cutting the femur with a reference plane at the same level with the angled femoral

stem. Depending on the bone quality, or patient's medical condition, surgeons can cut all the superior femoral part, or usually they let a part of the grater trochander, following the same procedure a small part of the grater torchander was still kept in this study. The stem insertion was created by using the create cavity feature, which practically is creating a gab inside the femur that fits with the geometry of the femoral stem inserted. At the same time, separate static simulations were performed on the femur and on the femoral hip stem in order to observe the individual mechanical behavior of each part.

4.3.1. Contact definition

Within this model one contact type was consider, the contact between the cortical bone (of a young patient and of an older patient) and the femoral stem. The management and definition of these contacts are detailed below. Defining constraints between the parts of an assembly is possible in Solidworks Simulation, *Connections, Contact Sets*. In this study, the femoral stem is in contact with the cortical bone, contact must therefore be defined between the cavity of the cortical bone and the femoral hip stem. In this sense, the interfering faces were identified automatically and set up a contact which allow penetration between the femoral cavity and the femoral hip stem with a global bonded contact between both parts, assuming that the contact between parts is a dry, ideal surface contact.

In the case of individual static studies for the femur and standard hip stem the contact were bonded because we do not have other parts involved in the simulation.

4.3.2. Fixing geometry

When modeling the femur involving only the upper part of the diaphysis and the proximal end, the boundary conditions are applied directly to the lower face of the sectioned femur. Since this face does not constitute a real limitation and the diaphyseal part is continuously up to the distal end, there is no possible translation or rotation at this face relative to the rest of the bone. In the same way for individual studies the geometry of the femur was fixed as in the assembly, but the femoral standard stem was fixed on the entire surface which is in contact with the cortical bone.
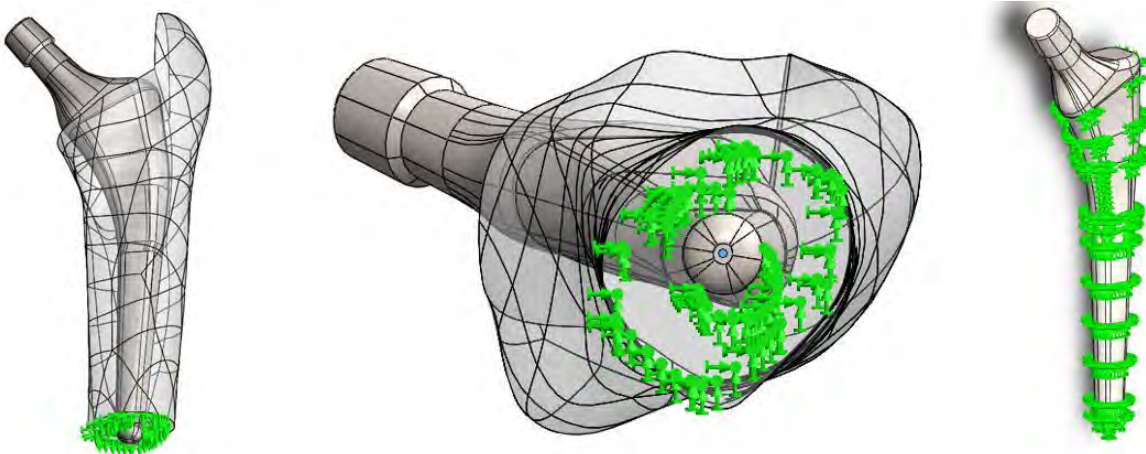
Figure 4.18. Femur and standard prosthesis assembly fixture and standard hip stem fixture for the individual part study

4.3.3. Boundary condition

In order to model the application of the loads in a realistic way, it was chosen to distribute the efforts evenly on the upper part of the femoral head, corresponding approximately to the bipedal position of a patient who undergo a THR surgery. As in the previous study, ten types of load were applied (*Table 4.4*), as a normal to the femoral head faces, and distributed over the entire surface on which it acts. For the study performed on the assembly between the femur and the standard stem, the loads were applied to the femoral head of the stem, as well as on the individual study of the standard femoral hip stem, but for the individual study of the femur the force was applied to the entire cavity created by the standard stem insertion (*Figure 4.19*).
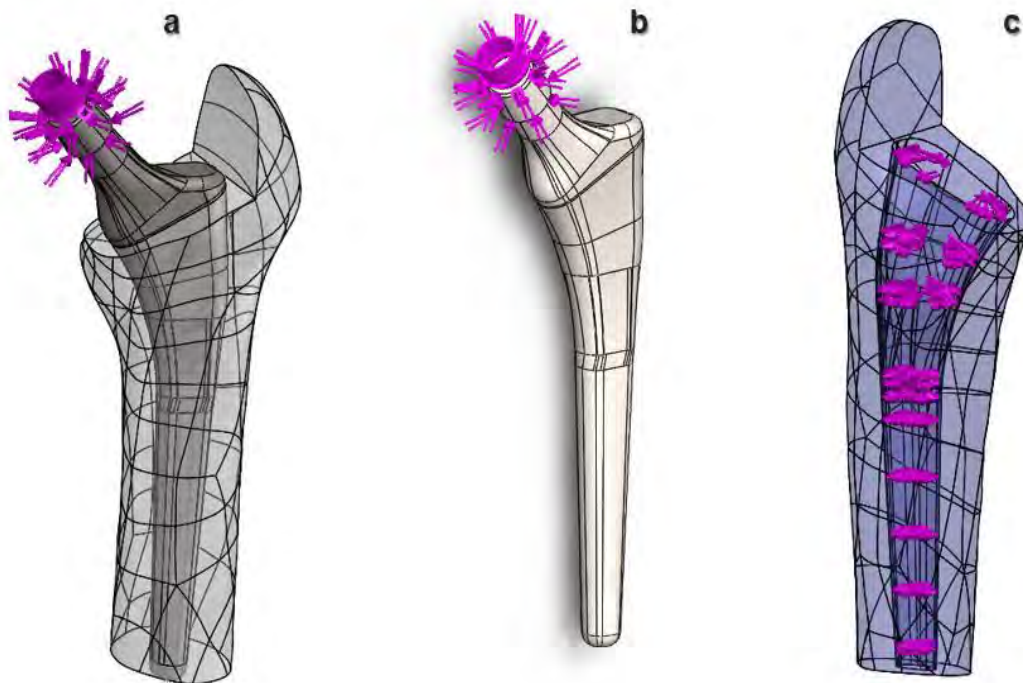
Figure 4.19. Boundary condition in case of assembly study (a), standard hip stem study (b) and femoral study (c)

A pressure distributed on the entire outer surface of the femur equal to 24MPa was applied, representing the external pressure exerted by soft tissues such as muscles on the femoral bone. Determining the value of this pressure to apply is overly complex and would require carrying out a much more in-depth bibliographic study, which was carried out on the subject within the framework of this project. This study was based on the articles of Bensamoun et al. (2006), Debernard et al. (2011) and Larsen et al. (2008), from which we can conclude that the muscle stiffness of the thigh muscles used in 20% of the voluntary muscle contraction was around 8MPa on average. In addition, knowing that during a climb of stairs, the muscles are stressed at around 60% maximum, was decided to raise this value to 24MPa, with the specification that this value is only an approximate order of magnitude because muscle behavior is far from being so linear. However, we still wanted to keep this boundary condition which seemed essential for the modeling as realistic as possible.
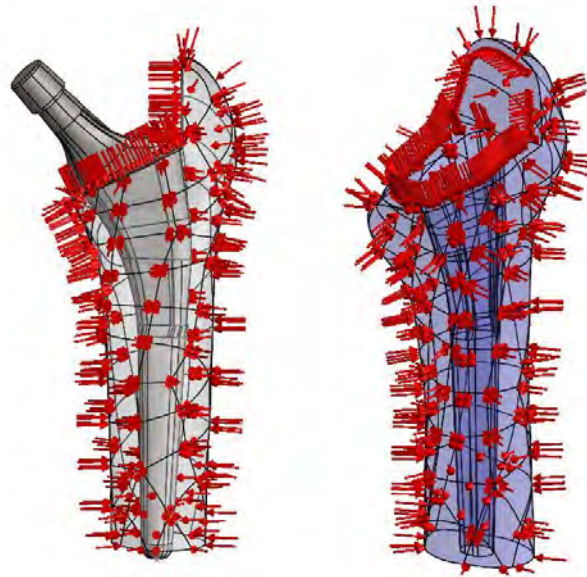
Figure 4.20. Femur applied pressure

4.3.4. Material assigning

Table 4.5. Mechanical properties of the material used in the FEA study

Property	Healthy cortical bone tissue	Elder cortical bone tissue	Titanium alloy (Ti$_6$Al$_4$V)	Units SI
	Value	Value	Value	
Elastic Modulus	15000	11600	115000	MPa
Poisson's Ratio	0.3	0.26	0.3	N/A
Shear Modulus	3300	3300	44000	kg/m^3
Mass Density	1800	1440	4400	MPa
Tensile Strength	133	21.13	950	MPa
Compressive Strength	205	97.19	970	MPa
Yield Strength	114	114	880	MPa

This study was performed with two types of bone tissue, one with healthy cortical bone tissue and one with cortical bone tissue having a lower quality, equivalent to the elderly patients, in order to compare the results and to observe how different both tissues behave in certain conditions.

Regarding the FE analysis performed on the whole femur and the standardized femoral stem, the material applied to the standard stem was the same in both types of study, the one performed with healthy cortical bone and the lower quality cortical bone tissue. To test the femoral prosthetic component, a biomaterial widely spread in medical applications called TC4 was used, a titanium alloy containing between 3.5 and 4.5% vanadium and between 5.5 and 6.5% aluminum and other impurities [113]. It was considered to implement the hypothesis that this material is homogeneous and isotropic with an elastic and linear behavior.

4.3.5. Mesh properties

The standard hip stem was treated as a solid body with a high quality solid mesh, 4 Jacobian points, minimum element size of ~1.24mm and a maximum element size of ~6.18mm, 18254 total nodes, 11421 total elements and a maximum aspect ratio of 281.08. Also the femur model was treated as a solid body with a high quality solid mesh, 4 Jacobian points, minimum element size of ~1.83mm and a maximum element size of ~9.16mm, 31526 total nodes, 20582 total elements and a maximum aspect ratio of 77.41. The entire femoral and standard hip stem assembly was treated as a solid body with a high quality solid mesh plot, 4 Jacobian points, minimum element size of ~2mm and a maximum element size of ~10.01mm, 33543 total nodes, 21720 total elements and a maximum aspect ratio

4.3.6. FEA resultant forces

Table 4.6. Assembly Femur-Standard hip stem in case of healthy and elder bone tissue resultant forces

N°	Load Value [N]	Reaction force [kgf]			
		X	Y	Z	Resultant
F_1	686.46	164.4	538.9	690	890.9
F_2	784.53	165.1	537.1	691.9	891.4
F_3	882.59	165.8	535.3	693.8	891.9
F_4	980.66	166.6	533.5	695.7	892.4
F_5	1078.73	167.3	531.7	697.6	892.9
F_6	1176.79	168.1	529.1	699.5	893.5
F_7	1274.86	168.8	528.1	701.4	894.1
F_8	2000	174.3	514.8	715.4	898.5
F_9	2500	178.1	505.7	725.1	901.8
F_{10}	3000	181.8	496.5	734.7	905.3

Table 4.7. Standard femoral hip stem resultant forces

N°	Load Value [N]	Reaction force [kgf]			
		X	Y	Z	Resultant
F_1	686.46	13.30	3.05	13.30	19
F_2	784.53	15.15	3.50	15.15	21.7
F_3	882.59	17.04	3.90	17.04	24.4
F_4	980.66	18.93	4.36	18.93	27.1
F_5	1078.73	20.83	4.80	20.83	29.8
F_6	1176.79	22.72	5.23	22.72	32.6
F_7	1274.86	24.61	5.66	24.61	35.3
F_8	2000	38.61	8.88	38.60	55.3
F_9	2500	48.26	11.10	48.26	69.2
F_{10}	3000	57.92	13.32	57.91	82.9

In case of the femur model resultant forces of the FEA static study for both materials healthy and elder cortical bone tissue are represented in *Table 4.8*.

Table 4.8. Femur resultant forces in case of healthy and elder bone tissue

N°	Load Value [N]	Reaction force [kgf]			
		X	Y	Z	Resultant
F_1	686.46	255.43	535.70	677.01	900.3
F_2	784.53	255.45	535.30	677.69	900.6
F_3	882.59	255.47	534.90	678.37	900.9
F_4	980.66	255.49	534.50	679.05	901.1
F_5	1078.73	255.50	534.10	679.73	901.4
F_6	1176.79	255.52	533.70	680.40	901.7
F_7	1274.86	255.54	533.30	681.08	902
F_8	2000	255.67	530.33	686.10	904.1
F_9	2500	255.75	528.28	689.55	905.5
F_{10}	3000	255.84	526.24	693.01	907

The resultant forces which acts in the assembly model, but also in the femur and standard hip stem model in the situation of both types of bone materials was summarized in *Table 4.6*. With loads increasing, resultant forces increase. However, we can individualize a more significant leap from F_8 to F_{10}, which is due to the high value of this loads.

4.3.7. FEA stress results
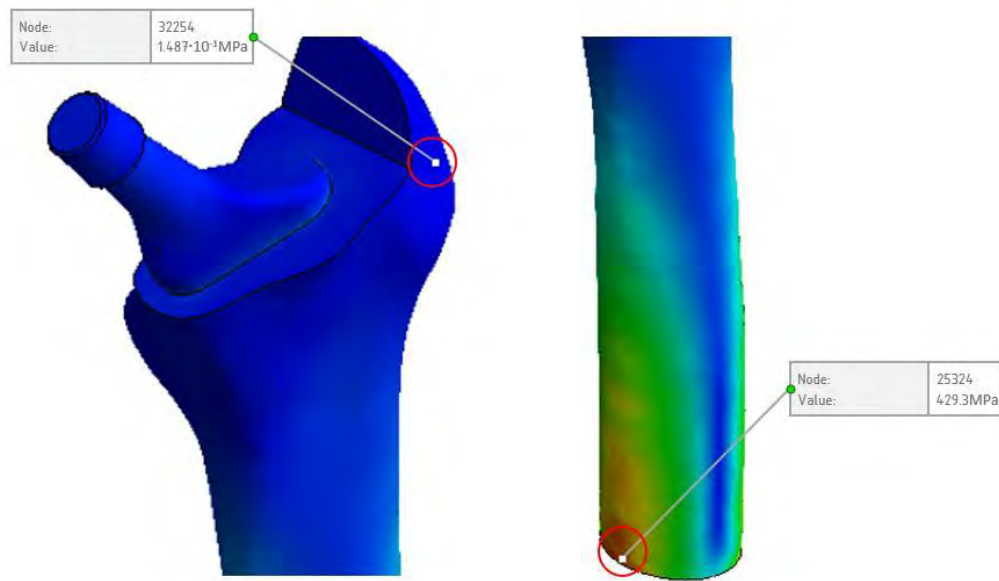
Figure 4.21. Minimum (left) and maximum (right) Von Mises Stress nodes location of the standard hip stem and femur assembly

Following the FEA study performed in each load case for the assembly have shown a minimum stress located in the node 32254 and a maximum stress located node 25324 (*Figure 4.21*). In *Table 4.9* we can identify the minimum and maximum stress values resulting from each analysis for both tissue cases.

In *Figure 4.22* we can observe the graphic evolution of stress results in the assembly study for both, healthy and an elderly patient cortical bone tissue.
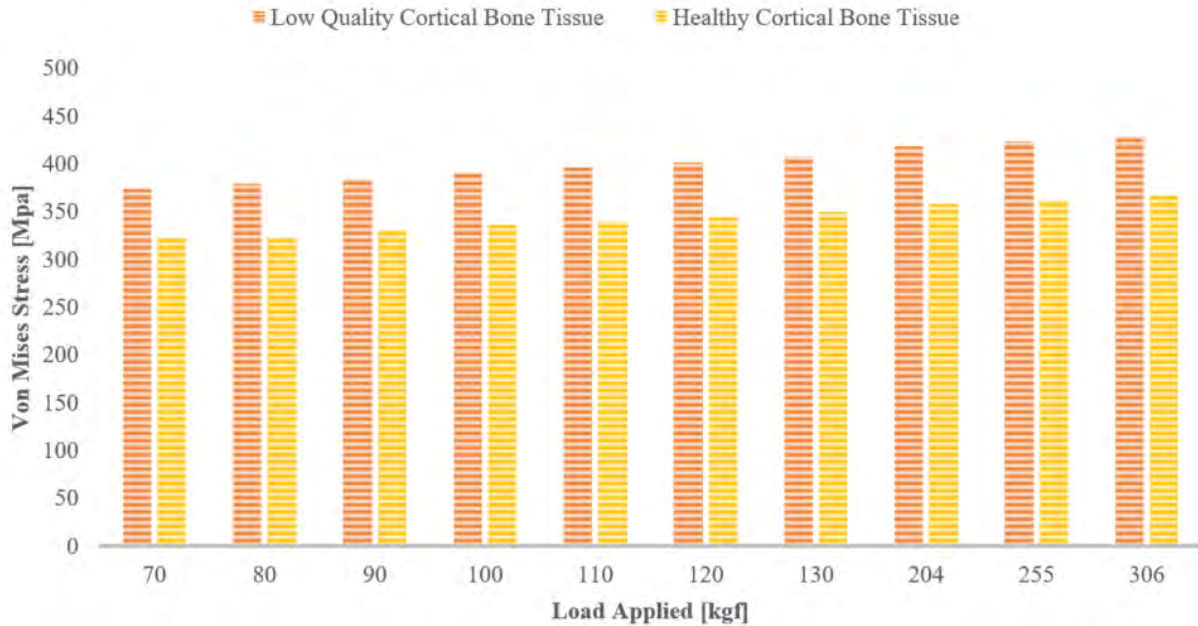

Figure 4.22. Maximum stress results of the femur and standard hip stem assembly

Table 4.9. Femur and standard femoral stem assembly stress results for healthy and elder cortical bone tissue. Stress Results VON: von Mises Stress [MPa]

N°	Load [N]	Assembly femur with elderly patient's cortical bone tissue & standard stem		Assembly femur with healthy cortical bone tissue & standard stem	
		Minimum	**Maximum**	**Minimum**	**Maximum**
F_1	686.46	$1.936 \cdot 10^{-1}$	373.8	$1.487 \cdot 10^{-1}$	322.1
F_2	784.53	$2.107 \cdot 10^{-1}$	379.4	$1.770 \cdot 10^{-1}$	322.6
F_3	882.59	$2.109 \cdot 10^{-1}$	385.0	$1.768 \cdot 10^{-1}$	331.2
F_4	980.66	$2.110 \cdot 10^{-1}$	390.6	$1.768 \cdot 10^{-1}$	335.7
F_5	1078.73	$2.111 \cdot 10^{-1}$	396.1	$1.768 \cdot 10^{-1}$	340.2
F_6	1176.79	$2.113 \cdot 10^{-1}$	401.7	$1.769 \cdot 10^{-1}$	344.7
F_7	1274.86	$2.114 \cdot 10^{-1}$	407.3	$1.769 \cdot 10^{-1}$	349.3
F_8	2000	$2.103 \cdot 10^{-1}$	418.0	$1.771 \cdot 10^{-1}$	357.8
F_9	2500	$2.103 \cdot 10^{-1}$	423.6	$1.771 \cdot 10^{-1}$	362.5
F_{10}	3000	$2.104 \cdot 10^{-1}$	429.3	$1.772 \cdot 10^{-1}$	367.1
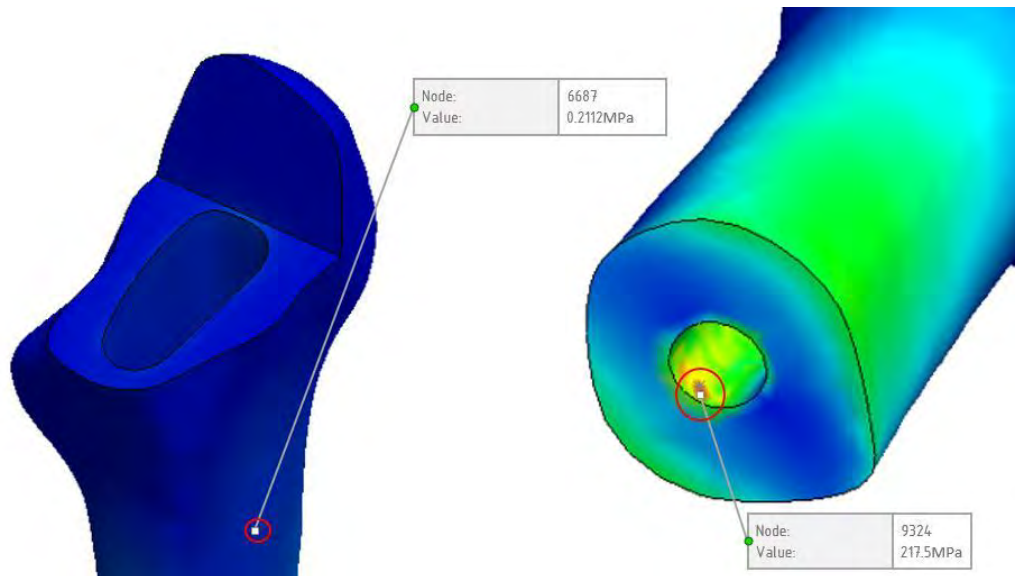
Figure 4.23. Minimum (left) and maximum (right) Von Mises Stress nodes location of the femur model

FEA studies performed in each load case for the femur has shown a minimum stress located in the node 6687 and a maximum stress located in node 9324 (*Figure 4.23*).

Table 4.10. Femur model stress results for healthy and elder cortical bone tissue. Stress Results VON: von Mises Stress [MPa]

N°	Load [N]	Femur with elderly patient's cortical bone tissue		Femur with healthy cortical bone tissue	
		Minimum	Maximum	Minimum	Maximum
F_1	686.46	0.3079	213.7	0.2112	211.1
F_2	784.53	0.3075	213.9	0.2114	211.2
F_3	882.59	0.3078	214.1	0.2116	211.4
F_4	980.66	0.3081	214.2	0.2118	211.5
F_5	1078.73	0.3084	214.4	0.212	211.7
F_6	1176.79	0.3087	214.5	0.2123	211.9
F_7	1274.86	0.3090	214.7	0.2125	212
F_8	2000	0.3119	215.8	0.2141	213.2
F_9	2500	0.3134	216.7	0.2152	214
F_{10}	3000	0.3149	217.5	0.2162	214.8

In *Table 4.10* we can identify the minimum and maximum stress values resulting from each analysis for both tissue cases.

Results have shown that in case of elderly patient cortical bone tissue the stress results are higher for each load applied compared to healthy cortical tissue.
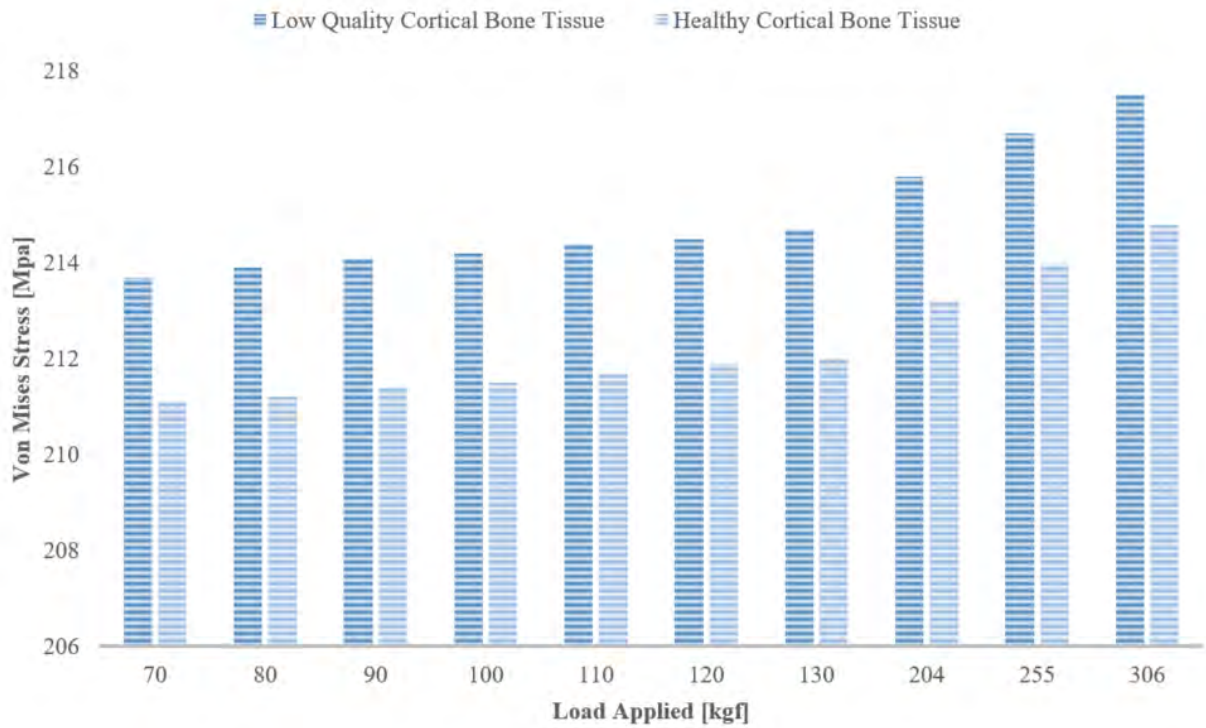
Figure 4.24. Maximum stress results of the femur model

In *Figure 4.24* we can observe the graphic evolution of stress results in the femur study for both, healthy and an elderly patient cortical bone tissue.

| Node: | 4447 |
| Value: | 9.039MPa |

| Node: | 12192 |
| Value: | $2.61 \cdot 10^{-10}$ MPa |
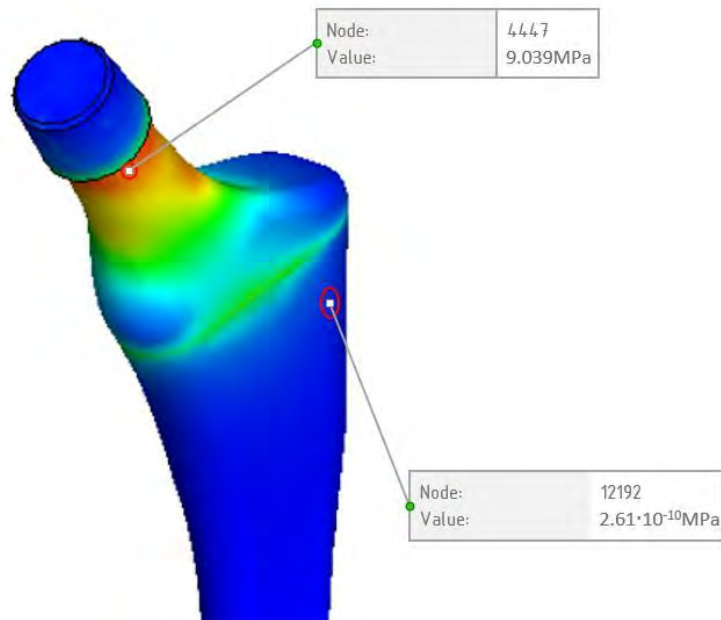
Figure 4.25. Minimum (bottom) and maximum (top) Von Mises Stress nodes location of the standard hip stem

The FEA studies performed in each load case for the standard femoral hip stem have shown a minimum stress located in the node 12192 and a maximum stress located in node 4447 (*Figure 4.25*). In *Table 4.11* we can identify the minimum and maximum stress values resulting from each analysis.

Table 4.11. Standard femoral stem model stress results. Stress Results VON: von Mises Stress [MPa]

N°	Load [N]	Standard femoral hip stem	
		Minimum	Maximum
F_1	686.46	$2.61 \cdot 10^{-10}$	2.068
F_2	784.53	$2.99 \cdot 10^{-10}$	2.364
F_3	882.59	$3.36 \cdot 10^{-10}$	2.659
F_4	980.66	$3.73 \cdot 10^{-10}$	2.955
F_5	1078.73	$4.11 \cdot 10^{-10}$	3.25
F_6	1176.79	$4.48 \cdot 10^{-10}$	3.546
F_7	1274.86	$4.85 \cdot 10^{-10}$	3.841
F_8	2000	$7.61 \cdot 10^{-10}$	6.026
F_9	2500	$9.51 \cdot 10^{-10}$	7.732
F_{10}	3000	$1.14 \cdot 10^{-9}$	9.039

In *Figure 4.26* we can observe the graphic evolution of stress results of the femoral standard hip stem study, in case of each load. Due to standard stem geometry fixture, but also to the biomaterial used in the FEA study, the maximum stress is much lower compared to the studies performed on the cortical bone tissue.
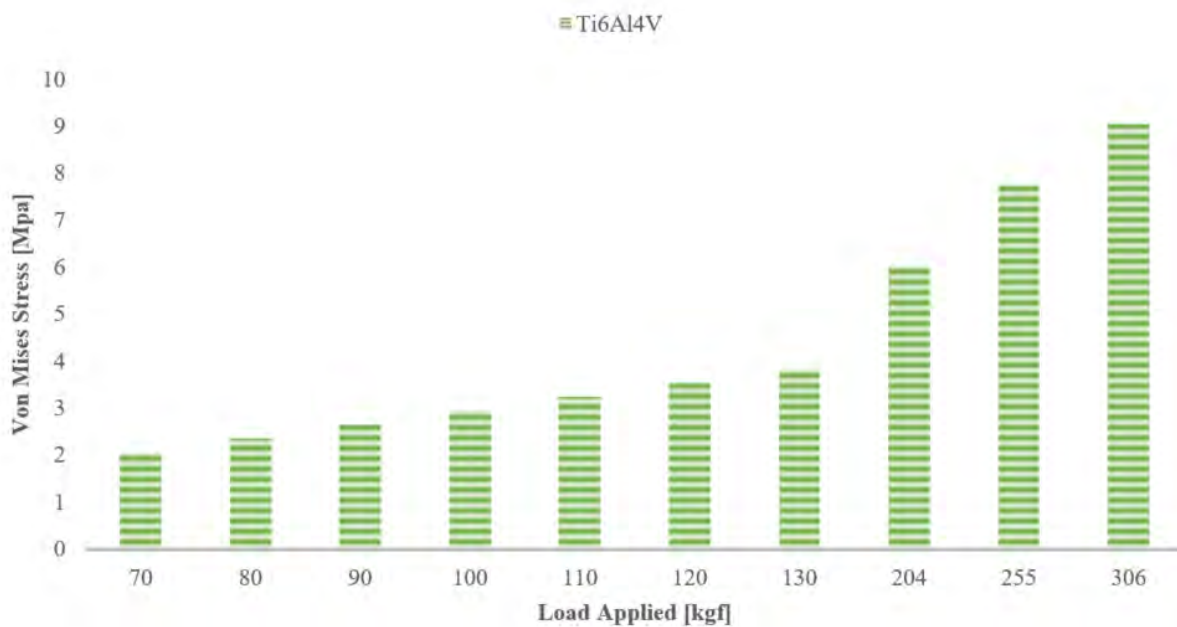
Figure 4.26. Maximum stress results of the standard femoral hip stem

In *Figure 4.27* we can observe the stress distribution on the assembly, but also in all individual parts, in case of F_{10} load application.
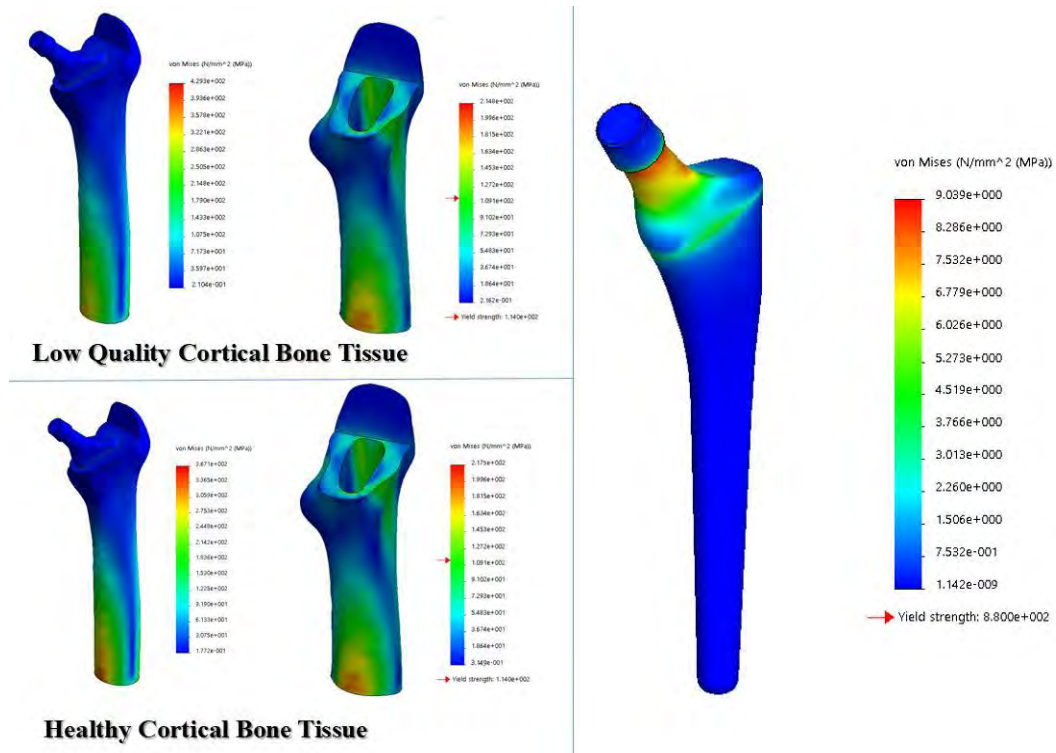
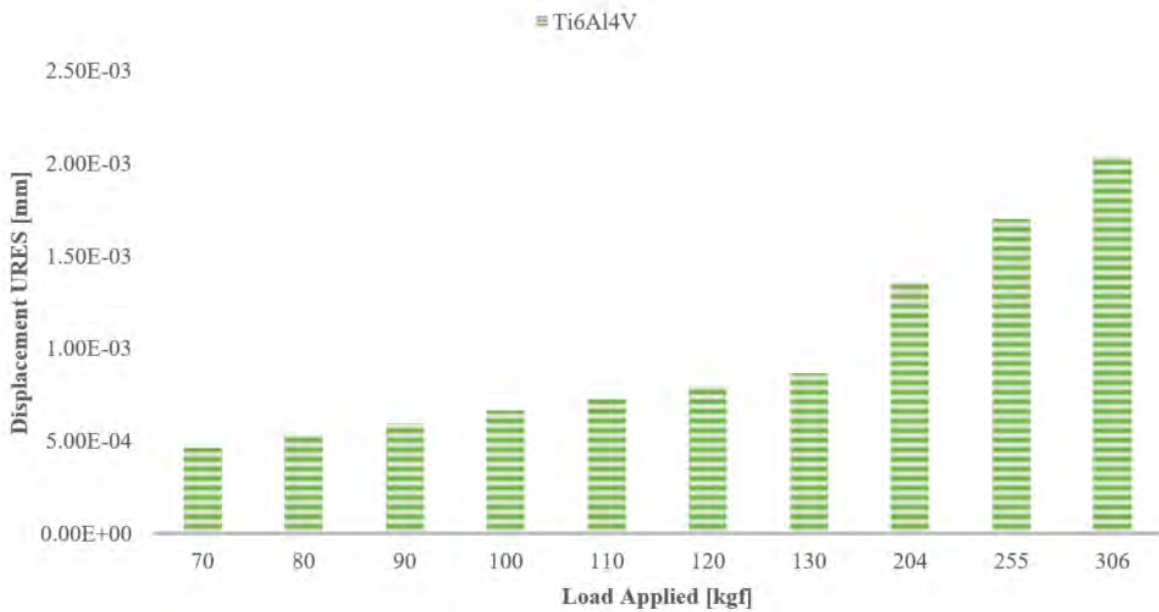*Figure 4.27. Stress results distribution in case of 3000N load applied*

4.3.8. FEA displacement results
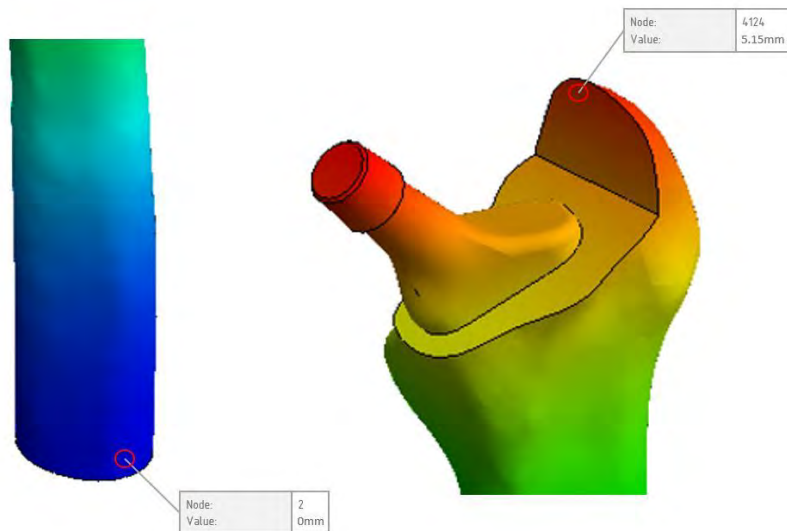
Figure 4.28. Minimum (left) and maximum (right) displacement nodes location of the standard hip stem and femur assembly

Table 4.12. Femur and standard femoral stem assembly displacement results [mm] for healthy and elderly patient cortical bone tissue

N°	Load [N]	Assembly femur with elderly patient's cortical bone tissue & standard stem		Assembly femur with healthy cortical bone tissue & standard stem	
		Minimum	Maximum	Minimum	Maximum
F_1	686.46	0	5.56	0	4.42
F_2	784.53	0	5.55	0	4.41
F_3	882.59	0	5.53	0	4.40
F_4	980.66	0	5.51	0	4.31
F_5	1078.73	0	5.49	0	4.37
F_6	1176.79	0	5.48	0	4.35
F_7	1274.86	0	5.46	0	4.34
F_8	2000	0	5.33	0	4.24
F_9	2500	0	5.24	0	4.16
F_{10}	3000	0	5.15	0	4.01

Following the FEA study performed in each load case for the assembly have shown a minimum displacement located in the node 2 and a maximum displacement located on node 4124 (*Figure 4.28*).
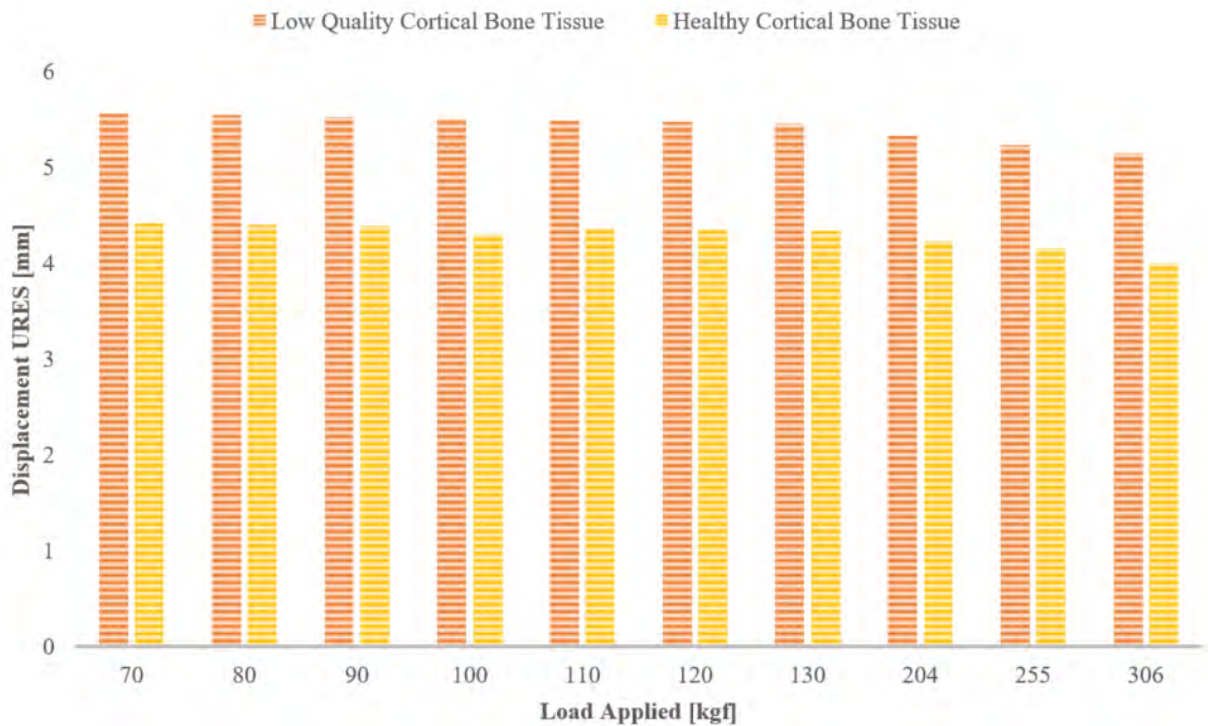
Figure 4.29. Maximum displacement results of the femur and standard hip stem assembly
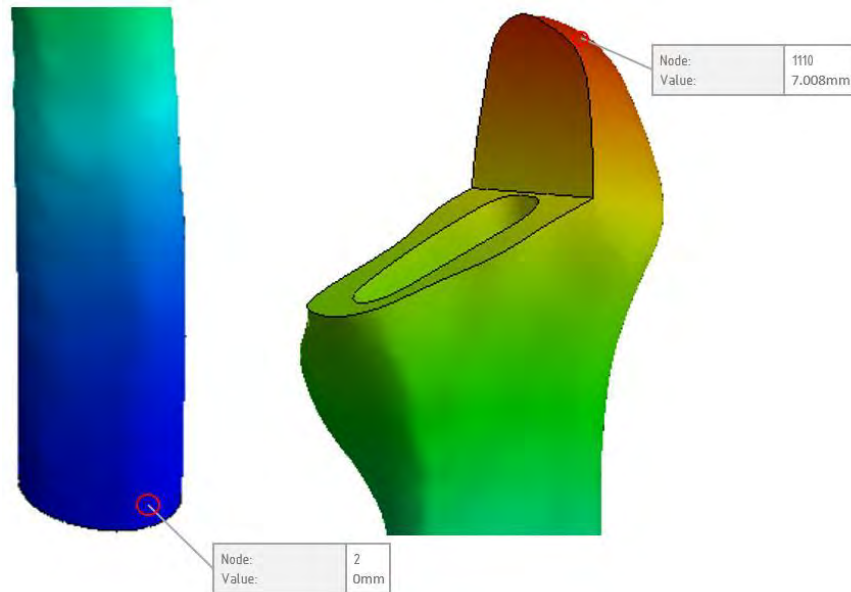
Figure 4.30. Minimum (left) and maximum (right) displacement nodes location of the femur model

In *Figure 4.29* we can observe the graphic evolution of displacement results in the assembly study for both, healthy and an elderly patient cortical bone tissue.

Table 4.13. Femur displacement results [mm] for healthy and elderly patient cortical bone tissue

N°	Load [N]	Femur with elderly patient's cortical bone tissue		Femur with healthy cortical bone tissue	
		Minimum	Maximum	Minimum	Maximum
F_1	686.46	0	6.889	0	5.308
F_2	784.53	0	6.894	0	5.312
F_3	882.59	0	6.899	0	5.316
F_4	980.66	0	6.904	0	5.320
F_5	1078.73	0	6.909	0	5.324
F_6	1176.79	0	6.914	0	5.328
F_7	1274.86	0	6.919	0	5.330
F_8	2000	0	6.957	0	5.358
F_9	2500	0	6.983	0	5.378
F_{10}	3000	0	7.008	0	5.398

The FEA study performed in each load case for the femur has shown a minimum displacement located on node 2 and a maximum displacement located node 1110 (*Figure 4.30*).

In *Table 4.13* we can identify the minimum and maximum displacement values resulting from each analysis for both materials used.

In *Figure 4.31* we can observe the graphic evolution of displacement results in the femur study for both, healthy and low quality cortical bone tissue.

Results have shown that in case of elderly patient cortical bone tissue the displacement results are higher for each load applied compared to healthy cortical tissue. Also, due to the method of fixing the femur geometry displacement may appear higher.
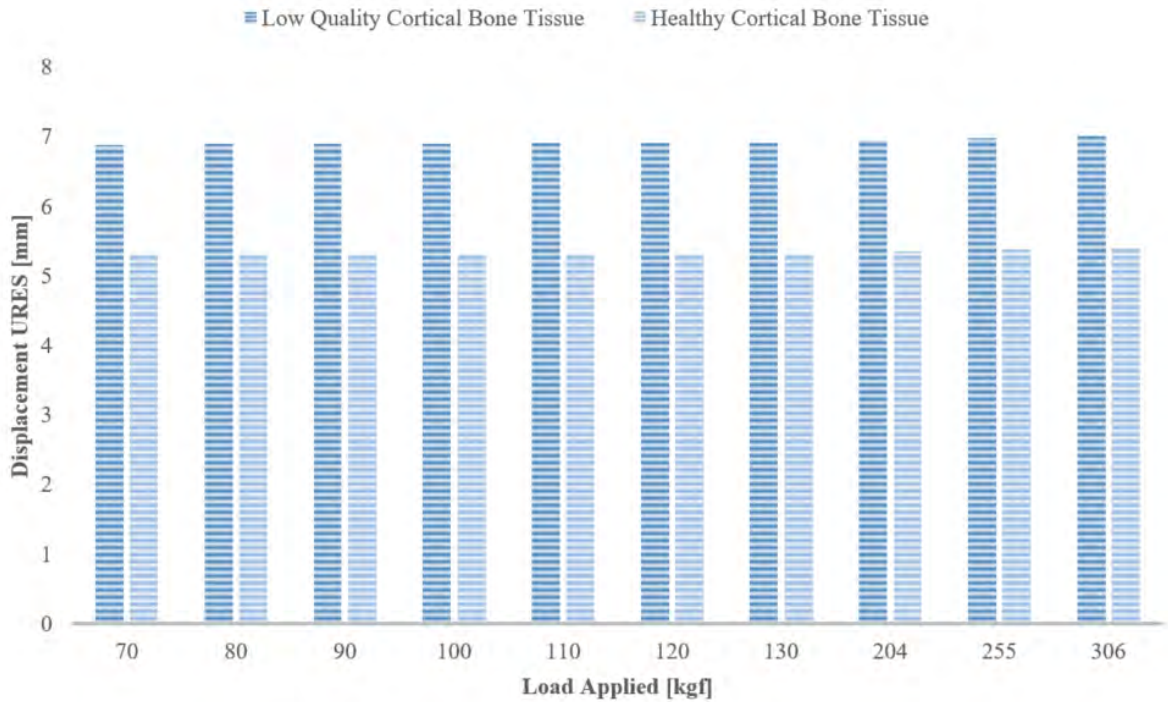
Figure 4.31. Maximum displacement results of the femur model

The FEA study performed in each load case for the femoral hip stem has shown a minimum displacement located on node 1 and a maximum displacement located node 260 (*Figure 4.32*).

Table 4.14. Standard femoral stem model displacement results [mm]

N°	Load [N]	Standard femoral hip stem	
		Minimum	Maximum
F_1	686.46	0	$4.66 \cdot 10^{-4}$
F_2	784.53	0	$5.32 \cdot 10^{-4}$
F_3	882.59	0	$5.99 \cdot 10^{-4}$
F_4	980.66	0	$6.65 \cdot 10^{-4}$
F_5	1078.73	0	$7.32 \cdot 10^{-4}$
F_6	1176.79	0	$7.98 \cdot 10^{-4}$
F_7	1274.86	0	$8.65 \cdot 10^{-4}$
F_8	2000	0	$1.36 \cdot 10^{-3}$
F_9	2500	0	$1.70 \cdot 10^{-3}$
F_{10}	3000	0	$2.04 \cdot 10^{-3}$
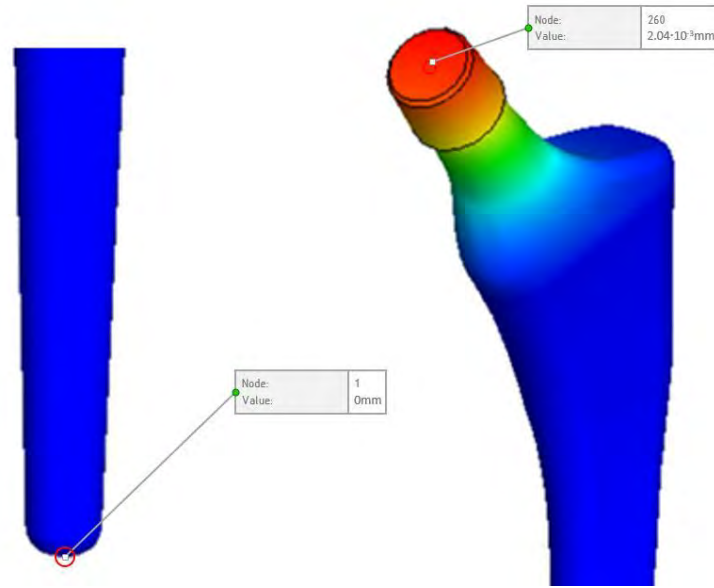
Figure 4.32. Minimum (bottom) and maximum (top) displacement nodes location of the standard hip stem

In *Table 4.14* we can identify the minimum and maximum displacement values resulting from each analysis. In *Figure 4.33* we can observe the graphic evolution of displacement results in the femoral hip stem study in case of each load. Because of the standard hip stem geometry fixture, the maximum displacement is much lower compared to the studies performed on the cortical bone tissue. In *Figure 4.34* we can observe the displacement distribution on the assembly, but also in all individual parts as a result of F_{10} load application.

Figure 4.33. Maximum displacement results of the standard femoral hip stem
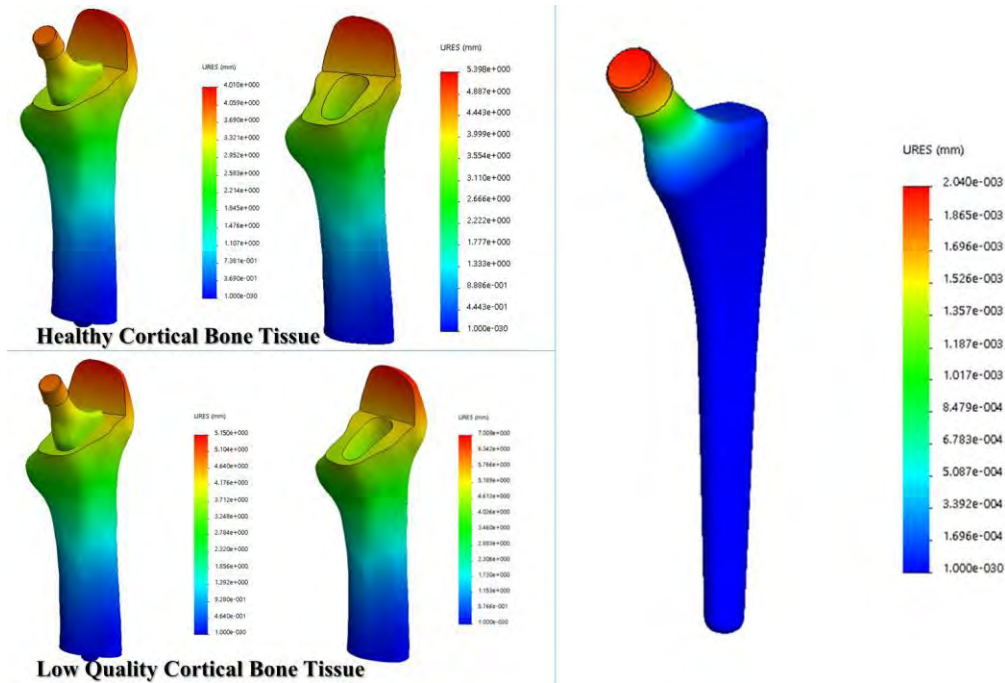
Figure 4.34. Displacement results distribution in case of 3000 N load applied

4.3.9. FEA strain results

The general equivalent strain or ESTRN equation used in the FEA simulation is the following:

$$E\square\square\square N = 2 \left[\frac{(\varepsilon_1 + \varepsilon_2)}{3}\right]^{\frac{1}{2}} \qquad (2)$$

Where is calculated as following:

$$\varepsilon_1 = \frac{1}{} \left[(EP\square\square - {}^*)^2 + (EP\square\square - \varepsilon^*)^2 + (EP\square\square - \varepsilon^*)^2\right] \; (3)$$

$$\varepsilon \qquad \qquad 2$$

EPSX, EPSY and EPSZ is representing the normal strain in the X direction, Y direction and Z direction for the geometry analyzed.

$$\varepsilon_2 = \frac{[(GM\square\square)^2 + (GM\square\square)^2 + (GM\square\square)^2]}{4} \qquad (4)$$

GMXY, GMXZ and GMYZ is representing the shear strain in the Y direction for [YZ] plane, Z direction for [YZ] plane and Z direction for [XZ] plane.

$$\varepsilon^* = \frac{[EPS⬚ + EPS⬚ + EPS⬚]}{3} \qquad (5)$$

Figure 4.35. Maximum strain results of the femur and standard hip stem assembly

Following the FEA study performed in each load case for the assembly have shown a minimum strain results located in element number 18614 and a maximum strain results located in element number 9555 (*Figure 4.36*). In *Table 4.15* we can identify the minimum and maximum strain values resulting from each analysis for both tissue cases.

Table 4.15. Femur and standard femoral stem assembly strain results [ESTRN: Equivalent Strain] for healthy and elderly patient cortical bone tissue

N°	Load [N]	Assembly femur with elderly patient's cortical bone tissue & standard stem		Assembly femur with healthy cortical bone tissue & standard stem	
		Minimum	Maximum	Minimum	Maximum
F_1	686.46	$2.50 \cdot 10^{-8}$	$1.209 \cdot 10^{-2}$	$2.51 \cdot 10^{-8}$	$9.69 \cdot 10^{-3}$
F_2	784.53	$2.80 \cdot 10^{-8}$	$1.213 \cdot 10^{-2}$	$2.87 \cdot 10^{-8}$	$9.73 \cdot 10^{-3}$
F_3	882.59	$3.21 \cdot 10^{-8}$	$1.217 \cdot 10^{-2}$	$3.23 \cdot 10^{-8}$	$9.76 \cdot 10^{-3}$
F_4	980.66	$3.57 \cdot 10^{-8}$	$1.221 \cdot 10^{-2}$	$3.59 \cdot 10^{-8}$	$9.79 \cdot 10^{-3}$
F_5	1078.73	$3.92 \cdot 10^{-8}$	$1.226 \cdot 10^{-2}$	$3.94 \cdot 10^{-8}$	$9.83 \cdot 10^{-3}$
F_6	1176.79	$4.28 \cdot 10^{-8}$	$1.230 \cdot 10^{-2}$	$4.30 \cdot 10^{-8}$	$9.86 \cdot 10^{-3}$
F_7	1274.86	$4.63 \cdot 10^{-8}$	$1.234 \cdot 10^{-2}$	$4.66 \cdot 10^{-8}$	$9.89 \cdot 10^{-3}$
F_8	2000	$7.26 \cdot 10^{-8}$	$1.262 \cdot 10^{-2}$	$7.30 \cdot 10^{-8}$	$1.02 \cdot 10^{-2}$
F_9	2500	$9.07 \cdot 10^{-8}$	$1.284 \cdot 10^{-2}$	$9.12 \cdot 10^{-8}$	$1.03 \cdot 10^{-2}$
F_{10}	3000	$1.08 \cdot 10^{-7}$	$1.306 \cdot 10^{-2}$	$1.09 \cdot 10^{-7}$	$1.05 \cdot 10^{-2}$

Element: 18614
Value: 2.50·10⁻⁸ESTRN

Element: 9555
Value: 1.306·10⁻²ESTRN
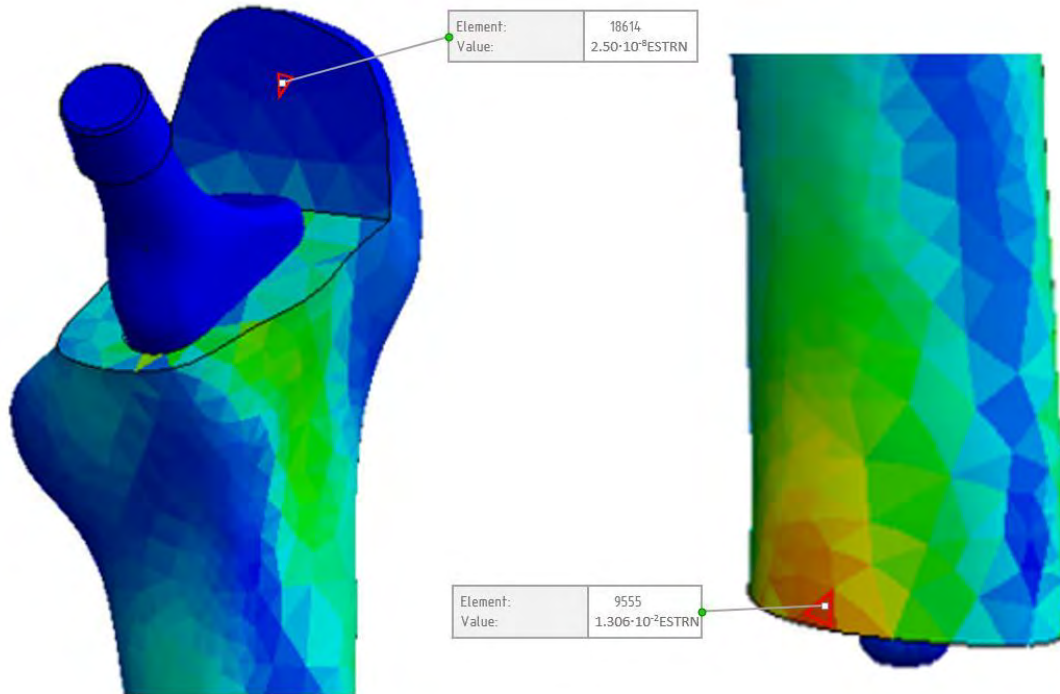
Figure 4.36. Minimum (left) and maximum (right) strain nodes location of the standard hip stem and femur assembly

In *Figure 4.35* we can observe the graphic evolution of the strain results in the assembly study for both, healthy and an elderly patient cortical bone tissue.

Element: 14071
Value: 3.215·10⁻⁵ESTRN

Element: 16027
Value: 1.390·10⁻²ESTRN
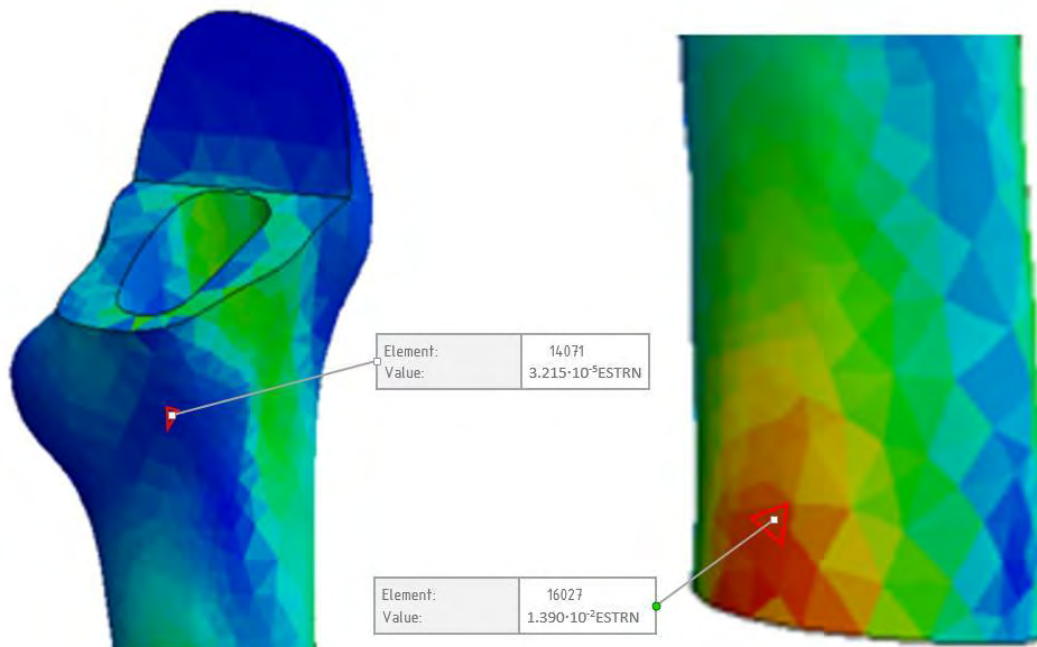
Figure 4.37. Minimum (left) and maximum (right) strain nodes location of the femur model

Table 4.16. Femur strain results [ESTRN: Equivalent Strain] for healthy and elderly patient cortical bone tissue

N°	Load [N]	Femur with elderly patient's cortical bone tissue		Femur with healthy cortical bone tissue	
		Minimum	**Maximum**	**Minimum**	**Maximum**
F_1	686.46	$2.827 \cdot 10^{-5}$	$1.366 \cdot 10^{-2}$	$3.215 \cdot 10^{-5}$	$1.078 \cdot 10^{-2}$
F_2	784.53	$2.829 \cdot 10^{-5}$	$1.367 \cdot 10^{-2}$	$3.217 \cdot 10^{-5}$	$1.079 \cdot 10^{-2}$
F_3	882.59	$2.831 \cdot 10^{-5}$	$1.368 \cdot 10^{-2}$	$3.220 \cdot 10^{-5}$	$1.080 \cdot 10^{-2}$
F_4	980.66	$2.833 \cdot 10^{-5}$	$1.369 \cdot 10^{-2}$	$3.222 \cdot 10^{-5}$	$1.081 \cdot 10^{-2}$
F_5	1078.73	$2.835 \cdot 10^{-5}$	$1.370 \cdot 10^{-2}$	$3.224 \cdot 10^{-5}$	$1.082 \cdot 10^{-2}$
F_6	1176.79	$2.837 \cdot 10^{-5}$	$1.371 \cdot 10^{-2}$	$3.226 \cdot 10^{-5}$	$1.083 \cdot 10^{-2}$
F_7	1274.86	$2.839 \cdot 10^{-5}$	$1.372 \cdot 10^{-2}$	$3.229 \cdot 10^{-5}$	$1.084 \cdot 10^{-2}$
F_8	2000	$2.853 \cdot 10^{-5}$	$1.379 \cdot 10^{-2}$	$3.246 \cdot 10^{-5}$	$1.089 \cdot 10^{-2}$
F_9	2500	$2.863 \cdot 10^{-5}$	$1.385 \cdot 10^{-2}$	$3.257 \cdot 10^{-5}$	$1.093 \cdot 10^{-2}$
F_{10}	3000	$2.963 \cdot 10^{-5}$	$1.390 \cdot 10^{-2}$	$3.269 \cdot 10^{-5}$	$1.097 \cdot 10^{-2}$

FEA studies performed in each load case for the femur has shown a minimum strain located in the element 14071 for the lower quality cortical bone case and in element 14135 for the healthy cortical bone tissue, with a maximum strain results located in the element 16027 in both cases (*Figure 4.37*).

In *Table 4.16* we can identify the minimum and maximum strain values resulting from each analysis for both study cases.
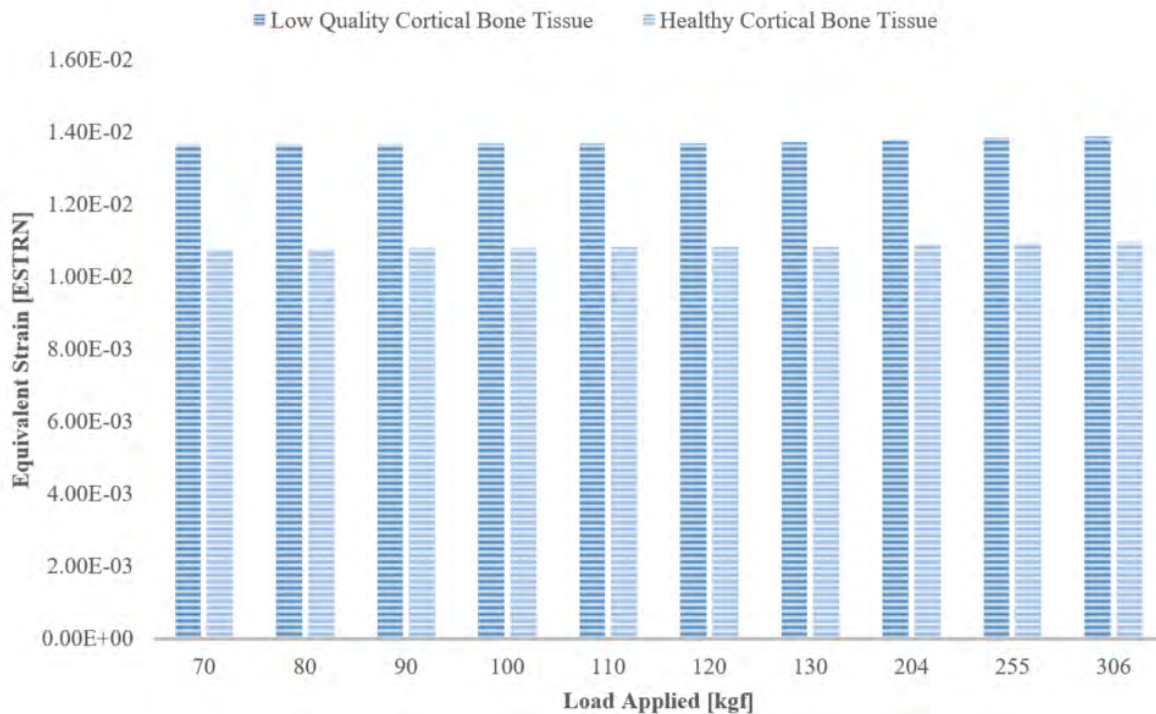
Figure 4.38. Maximum strain results of the femur model

In *Figure 4.38* we can observe the graphic evolution of the strain results in the femur study for both, healthy bone tissue and low quality bone tissue.

The FEA studies performed in each load case for the femoral hip stem have shown a minimum strain located in the element 379 and a maximum strain located in the element 8646 (*Figure 4.39*). In *Table 4.17* we can identify the minimum and maximum strain values resulting from each analysis.

Table 4.17. Standard femoral stem model strain results [ESTRN: Equivalent Strain]

N°	Load [N]	Standard femoral hip stem	
		Minimum	**Maximum**
F_1	686.46	$2.39 \cdot 10^{-15}$	$1.46 \cdot 10^{-5}$
F_2	784.53	$2.74 \cdot 10^{-15}$	$1.66 \cdot 10^{-5}$
F_3	882.59	$3.08 \cdot 10^{-15}$	$1.87 \cdot 10^{-5}$
F_4	980.66	$3.42 \cdot 10^{-15}$	$2.08 \cdot 10^{-5}$
F_5	1078.73	$3.76 \cdot 10^{-15}$	$2.29 \cdot 10^{-5}$
F_6	1176.79	$4.10 \cdot 10^{-15}$	$2.49 \cdot 10^{-5}$
F_7	1274.86	$4.45 \cdot 10^{-15}$	$2.70 \cdot 10^{-5}$
F_8	2000	$6.97 \cdot 10^{-15}$	$4.24 \cdot 10^{-5}$
F_9	2500	$8.72 \cdot 10^{-15}$	$5.30 \cdot 10^{-5}$
F_{10}	3000	$1.05 \cdot 10^{-14}$	$6.36 \cdot 10^{-5}$

In *Figure 4.40* we can observe the graphic evolution of the strain results in the femoral hip stem study in case of each load.
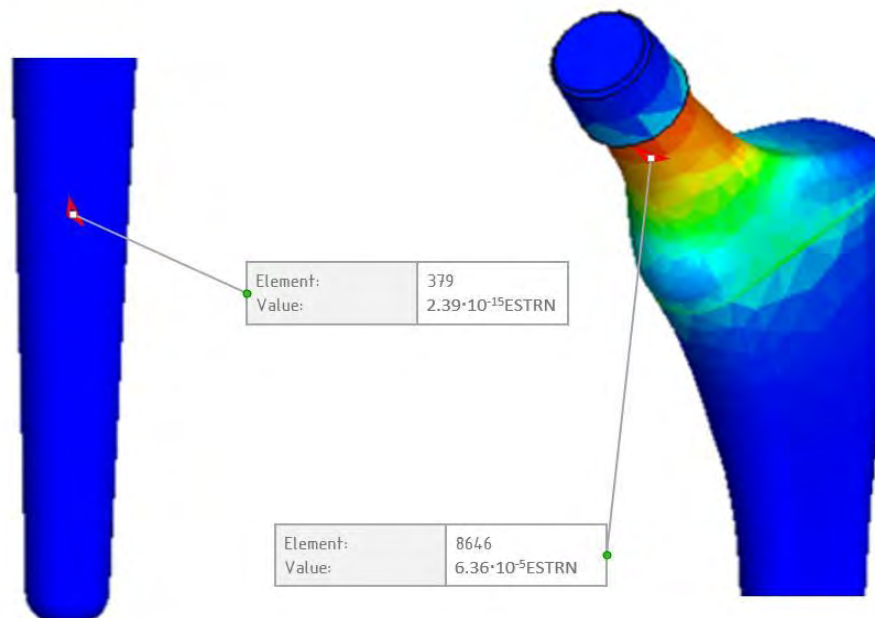
Figure 4.39. Minimum (left) and maximum (right) strain nodes location of the standard hip stem
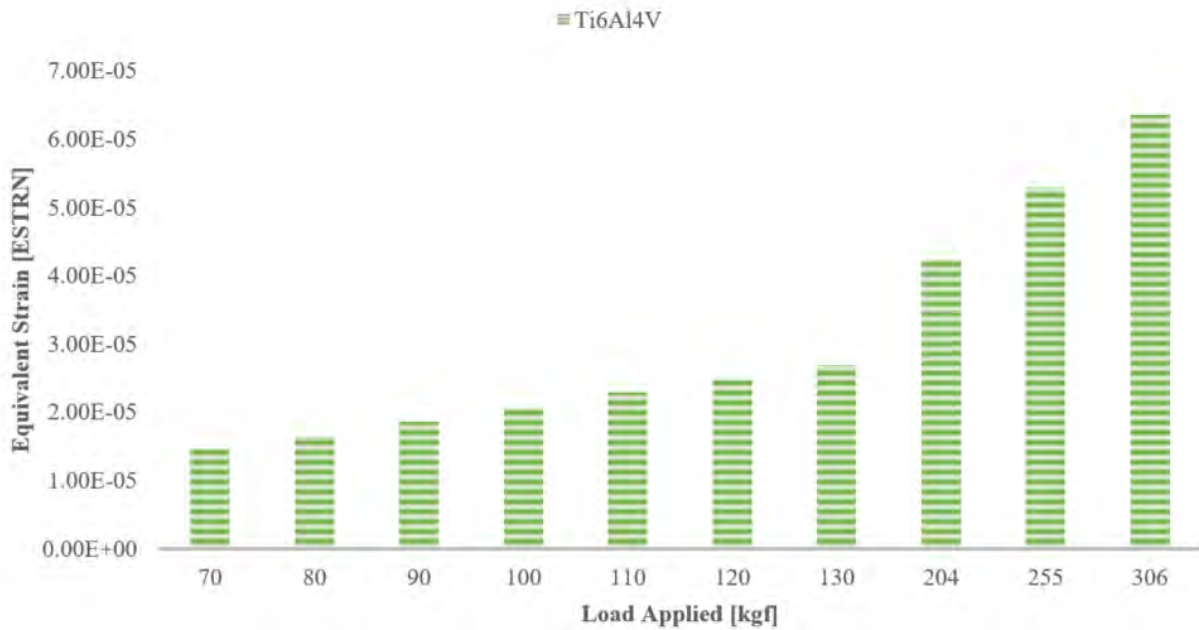
Figure 4.40. Maximum strain results of the standard femoral hip stem

In *Figure 4.41* we can observe the strain distribution on the assembly, but also in all individual parts as a result of F_{10} load application.

Healthy Cortical Bone Tissue

Low Quality Cortical Bone Tissue
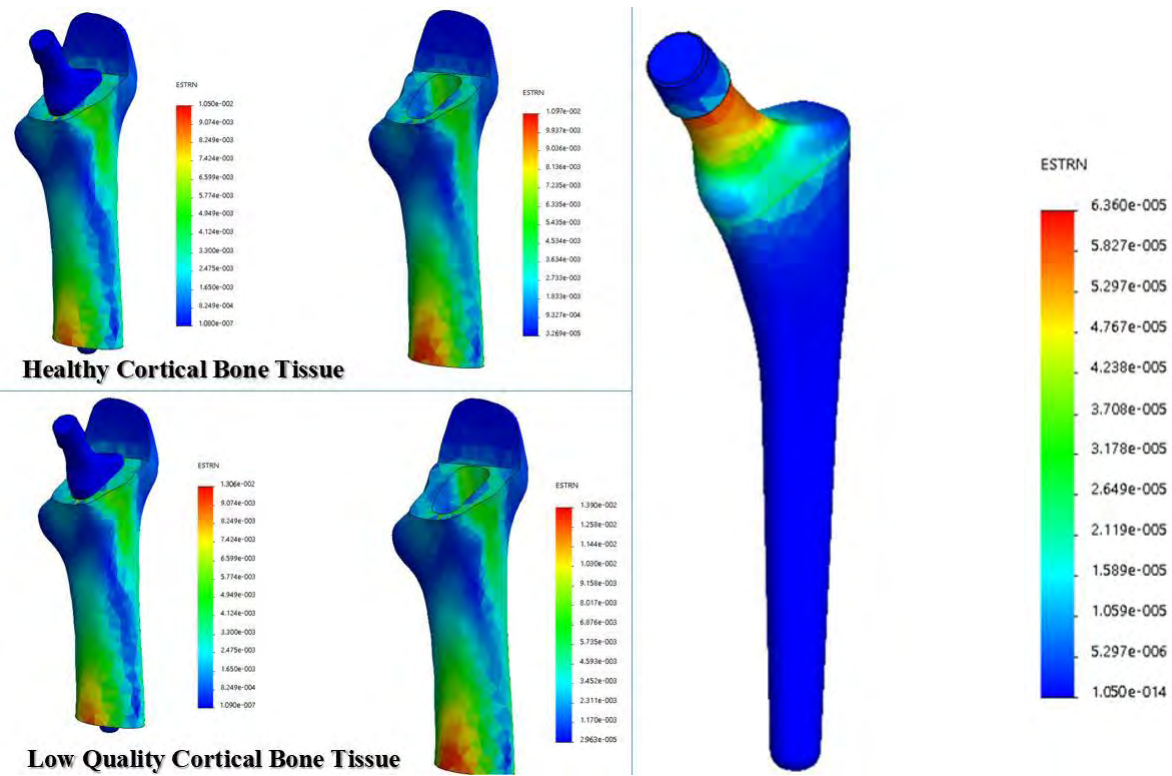
Figure 4.41. Strain results distribution in case of 3000 N load applied

4.4. Mechanical behavior simulation of a custom femoral stem

Following the same principles as in the case of finite element analysis of a femur and a standardized hip stem, a new set of simulations was performed in order to observe the mechanical behavior of the prosthesis and whether its geometry can effect a better load discharge in case of healthy cortical bone tissue and in case of low quality cortical bone tissue. In this sense, the contact was defined as in the subpoint *4.3.1*, fixing the geometry was done as well as in the subpoint *4.3.2,* the boundary condition was the same established in *4.3.3* subpoint, and the material assign was done in the same way as in the anterior simulation.

4.4.1. Mesh properties

The custom hip stem was treated as a solid body with a high quality solid mesh, 4 Jacobian points, minimum element size of ~1.20mm and a maximum element size of ~6.00mm, 34744 total nodes, 21821 total elements and a maximum aspect ratio of 72.67.

The femur model was treated as a solid body with a high quality solid mesh, 4 Jacobian points, with an element size of ~4.72mm, tolerance of 0.24mm, 19795 total nodes, 12657 total elements and a maximum aspect ratio of 36.41.
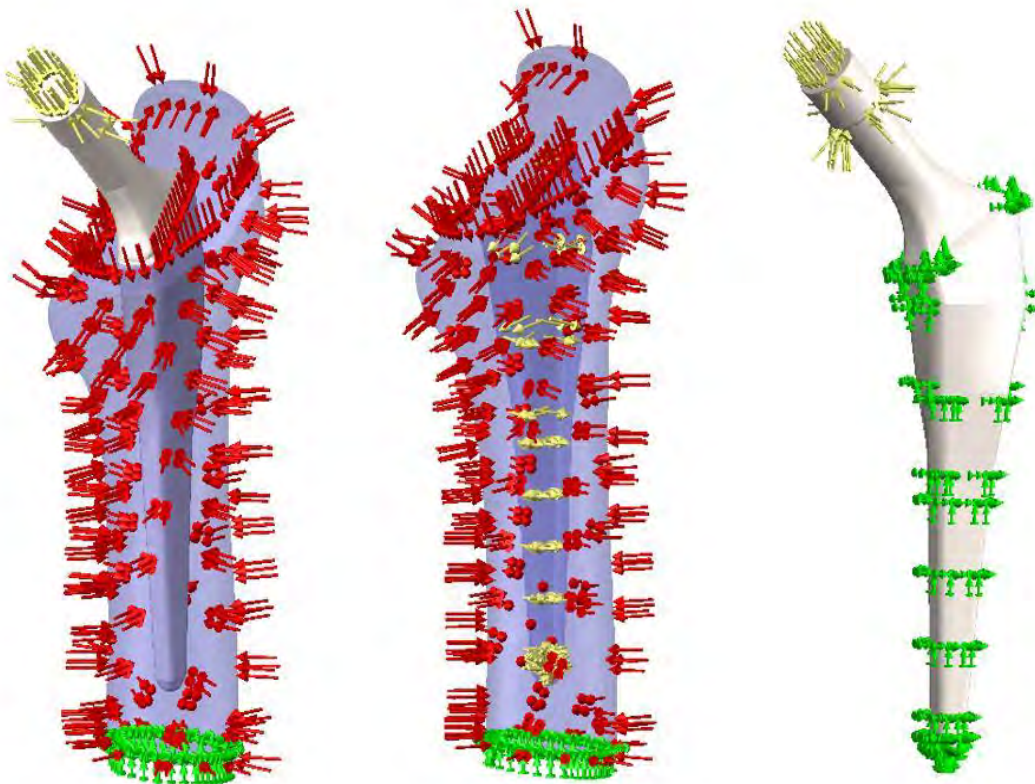
Figure 4.42. Fixture (green), load (yellow) and pressure (red) set up for CAD models used in the custom hip stem FEA study

The entire femoral and standard hip stem assembly was treated as a solid body with a high quality solid mesh plot, 4 Jacobian points, minimum element size of ~4.08mm and a maximum element size of ~20.4mm, 21755 total nodes, 13338 total elements and a maximum aspect ratio of 111.48.

4.4.2. FEA resultant forces

The resultant forces which act in the assembly model, but also in the femur and custom hip stem model in the situation of both types of bone materials was summarized in *Table 4.18*.

The resultant forces in case of the FEA static study of the custom femoral hip stem are represented in *Table 4.19*.

Table 4.18. Assembly Femur-Custom hip stem in case of healthy and elder bone tissue resultant forces

N°	Load Value [N]	Reaction force [kgf]			
		X	Y	Z	Resultant
F_1	686.46	-302.708	135.051	1100.9	1149.72
F_2	784.53	-300.275	151.045	1116.79	1166.27
F_3	882.59	-297.843	167.037	1132.67	1183.03
F_4	980.66	-295.411	183.017	1148.55	1199.97
F_5	1078.73	-292.979	199.01	1164.44	1217.11
F_6	1176.79	-290.547	215.002	1180.32	1234.43
F_7	1274.86	-288.115	230.995	1196.21	1251.92
F_8	2000	-270.131	349.251	1313.68	1385.89
F_9	2500	-257.731	430.791	1394.68	1482.27
F_{10}	3000	-245.332	512.332	1475.67	1581.23

In case of the femur model resultant forces of the FEA static study of both materials healthy and elder cortical bone tissue with custom hip stem cavity, are represented in *Table 4.20*.

Table 4.19. Custom femoral hip stem resultant forces

N°	Load Value [N]	Reaction force [kgf]			
		X	Y	Z	Resultant
F_1	686.46	-0.0188	-7.4796	7.4791	10.577
F_2	784.53	-0.0215	-8.5481	8.5476	12.088
F_3	882.59	-0.0215	-8.5481	8.5476	12.088
F_4	980.66	-0.0215	-8.5481	8.5476	12.088
F_5	1078.73	-0.0215	-8.5481	8.5476	12.088
F_6	1176.79	-0.0323	-12.8222	12.8222	18.1328
F_7	1274.86	-0.035	-13.8908	13.8899	19.6439
F_8	2000	-0.055	-21.7918	21.7905	30.8174
F_9	2500	-0.0687	-27.2398	27.2381	38.5218
F_{10}	3000	-0.0825	-32.6878	32.6857	46.2261

Table 4.20. Femur with custom hip stem cavity resultant forces in case of healthy and elder bone tissue

N°	Load Value [N]	Reaction force [kgf]			
		X	Y	Z	Resultant
F₁	686.46	-252.319	24.793	819.357	857.687
F₂	784.53	-252.278	25.159	820.033	858.330
F₃	882.59	-252.237	25.525	820.708	858.974
F₄	980.66	-252.196	25.890	821.383	859.618
F₅	1078.73	-252.155	26.256	822.058	860.262
F₆	1176.79	-252.115	26.622	822.733	860.907
F₇	1274.86	-252.074	26.987	823.409	861.552
F₈	2000	-251.771	29.691	828.401	866.325
F₉	2500	-251.562	31.556	831.844	869.623
F₁₀	3000	-251.354	33.420	835.287	872.926

4.4.3. FEA stress results

In *Table 4.21* we can identify the minimum and maximum stress values resulting from each analysis of both cortical bone tissues.
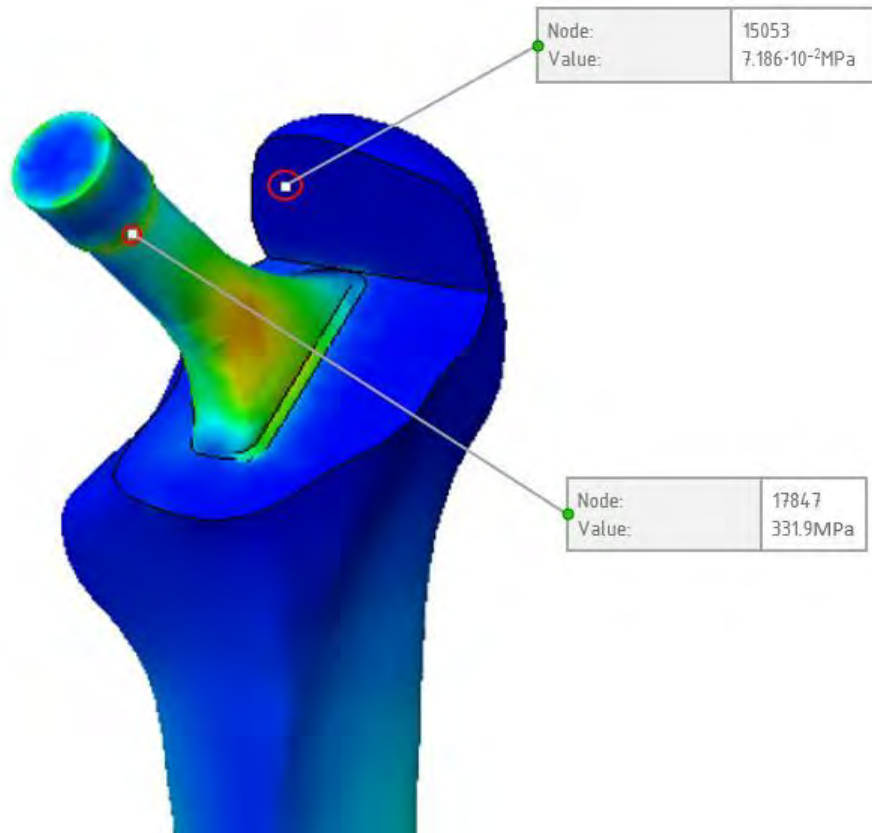
Figure 4.43. Minimum (top) and maximum (bottom) Von Mises Stress nodes location of the custom hip stem and femur assembly

Table 4.21. Femur and custom femoral stem assembly stress results for healthy and low quality cortical bone tissue. Stress Results VON: von Mises Stress [MPa]

N°	Load [N]	Assembly femur with elderly patient's cortical bone tissue & standard stem		Assembly femur with healthy cortical bone tissue & standard stem	
		Minimum	Maximum	Minimum	Maximum
F_1	686.46	$8.379 \cdot 10^{-2}$	136.2	$7.186 \cdot 10^{-2}$	115.4
F_2	784.53	$8.776 \cdot 10^{-2}$	137.2	$7.423 \cdot 10^{-2}$	119.7
F_3	882.59	$9.124 \cdot 10^{-2}$	143.5	$7.585 \cdot 10^{-2}$	127.0
F_4	980.66	$9.406 \cdot 10^{-2}$	151.8	$7.803 \cdot 10^{-2}$	134.4
F_5	1078.73	$9.187 \cdot 10^{-2}$	160.2	$8.071 \cdot 10^{-2}$	141.9
F_6	1176.79	$8.972 \cdot 10^{-2}$	168.6	$8.386 \cdot 10^{-2}$	149.5
F_7	1274.86	$8.792 \cdot 10^{-2}$	177.2	$8.741 \cdot 10^{-2}$	157.1
F_8	2000	$8.706 \cdot 10^{-2}$	241.4	$1.187 \cdot 10^{-1}$	214.4
F_9	2500	$9.976 \cdot 10^{-2}$	286.5	$1.109 \cdot 10^{-1}$	254.5
F_{10}	3000	$1.186 \cdot 10^{-1}$	331.9	$1.093 \cdot 10^{-1}$	295.0

Following the FEA study performed in each load case for the custom hip stem assembly, has shown a minimum stress located on the node 15053 and a maximum stress located in node 17847 (*Figure 4.43*). In *Figure 4.44* we can observe the graphic evolution of stress results in the assembly study for both, healthy and an elderly patient cortical bone tissue.
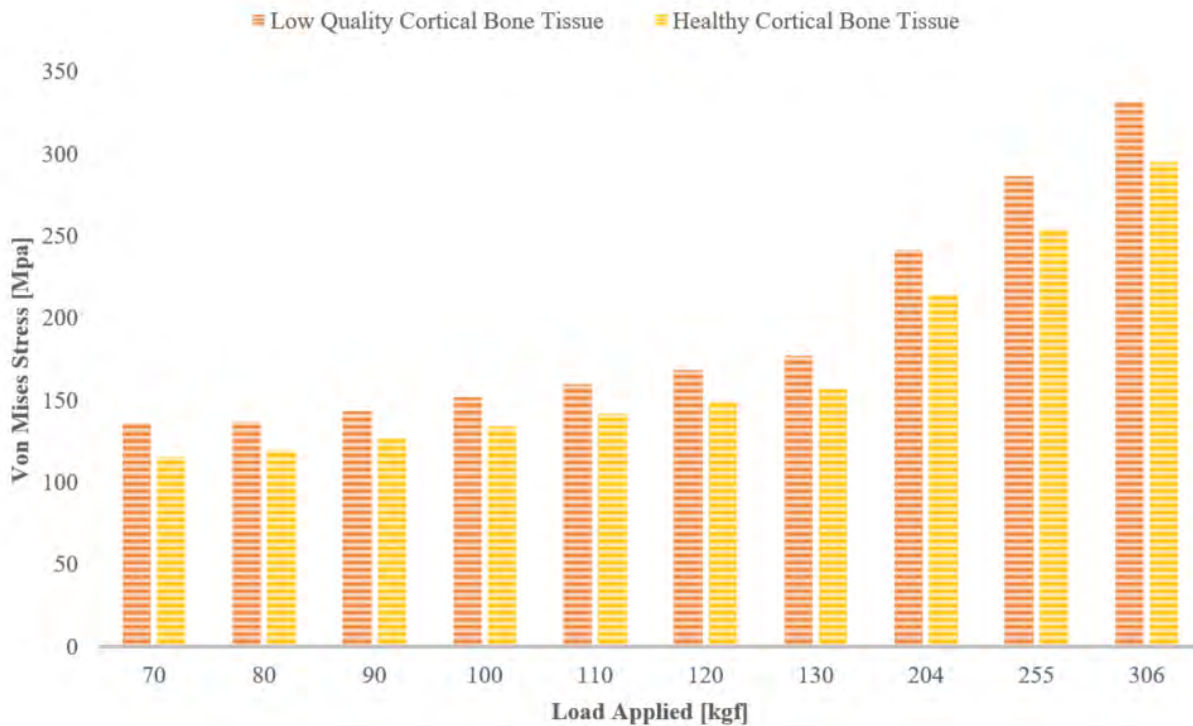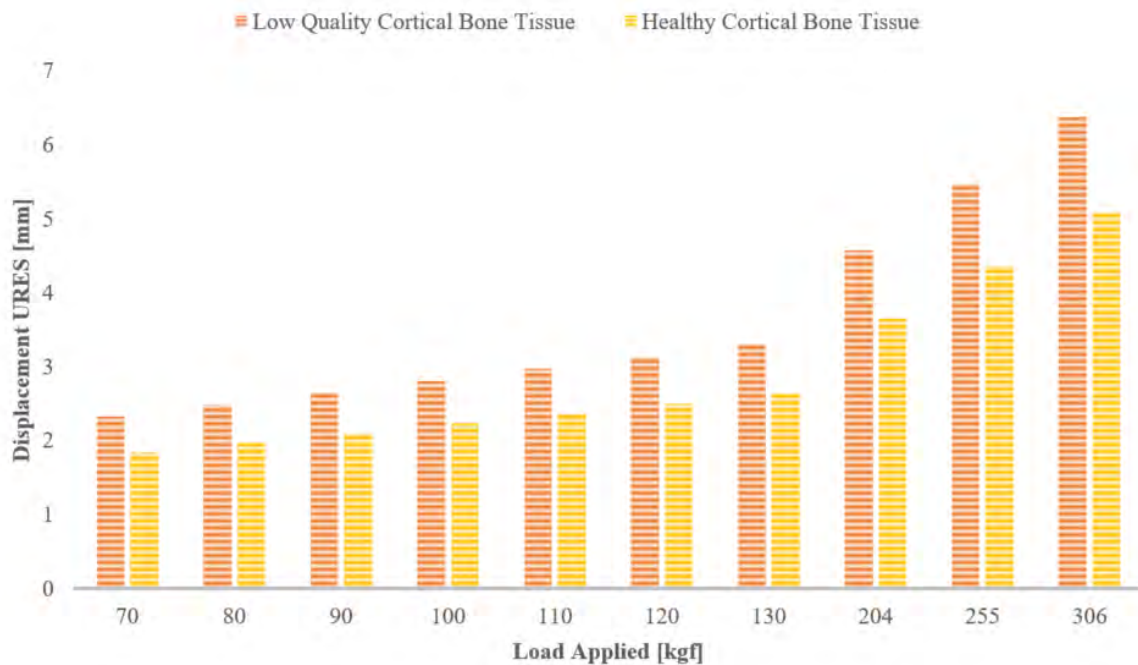

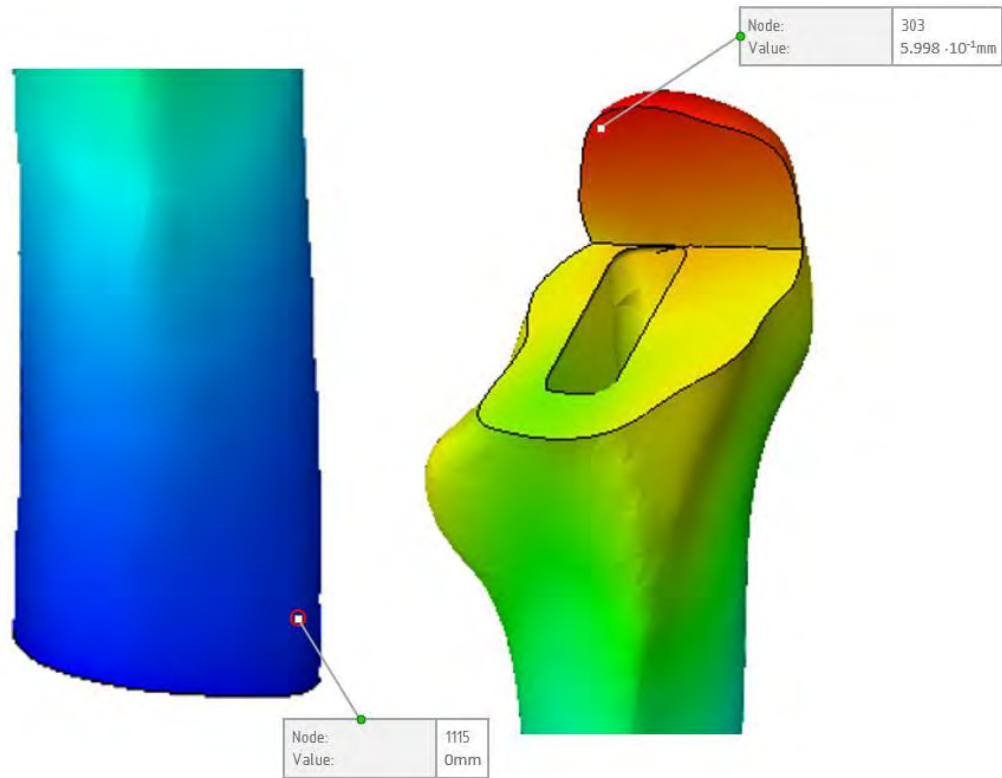*Figure 4.44. Maximum stress results of the femur and custom hip stem assembly*
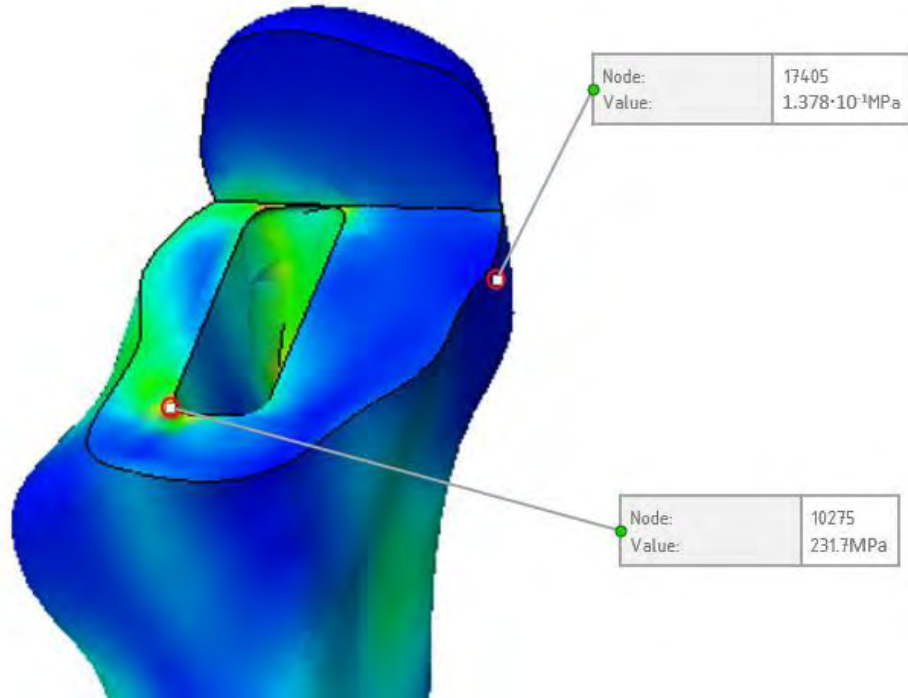
Figure 4.45. Minimum (top) and maximum (bottom) Von Mises Stress nodes location of the femur model with custom stem cavity

FEA studies performed in each load case for the femur with custom hip stem cavity has shown a minimum stress located on the node 17405 and a maximum stress located node 10275 (*Figure 4.45*). In *Table 4.22* we can identify the minimum and maximum stress values resulting from each analysis for both tissue cases.

Table 4.22. Femur custom stem cavity model stress results for healthy and low quality cortical bone tissue. Stress Results VON: von Mises Stress [MPa]

N°	Load [N]	Femur with elderly patient's cortical bone tissue		Femur with healthy cortical bone tissue	
		Minimum	Maximum	Minimum	Maximum
F_1	686.46	$1.419 \cdot 10^{-1}$	194.9	$1.378 \cdot 10^{-1}$	192.9
F_2	784.53	$1.419 \cdot 10^{-1}$	195.1	$1.379 \cdot 10^{-1}$	193.1
F_3	882.59	$1.419 \cdot 10^{-1}$	195.3	$1.381 \cdot 10^{-1}$	193.3
F_4	980.66	$1.419 \cdot 10^{-1}$	195.5	$1.383 \cdot 10^{-1}$	193.5
F_5	1078.73	$1420 \cdot 10^{-1}$	195.7	$1.385 \cdot 10^{-1}$	193.6
F_6	1176.79	$1.420 \cdot 10^{-1}$	195.9	$1.387 \cdot 10^{-1}$	193.8
F_7	1274.86	$1.420 \cdot 10^{-1}$	196.1	$1.389 \cdot 10^{-1}$	194.0
F_8	2000	$5.666 \cdot 10^{-1}$	230.3	$4.806 \cdot 10^{-1}$	211.7
F_9	2500	$5.700 \cdot 10^{-1}$	231.0	$6.371 \cdot 10^{-1}$	225.7
F_{10}	3000	$5.733 \cdot 10^{-1}$	231.7	$6.408 \cdot 10^{-1}$	226.3
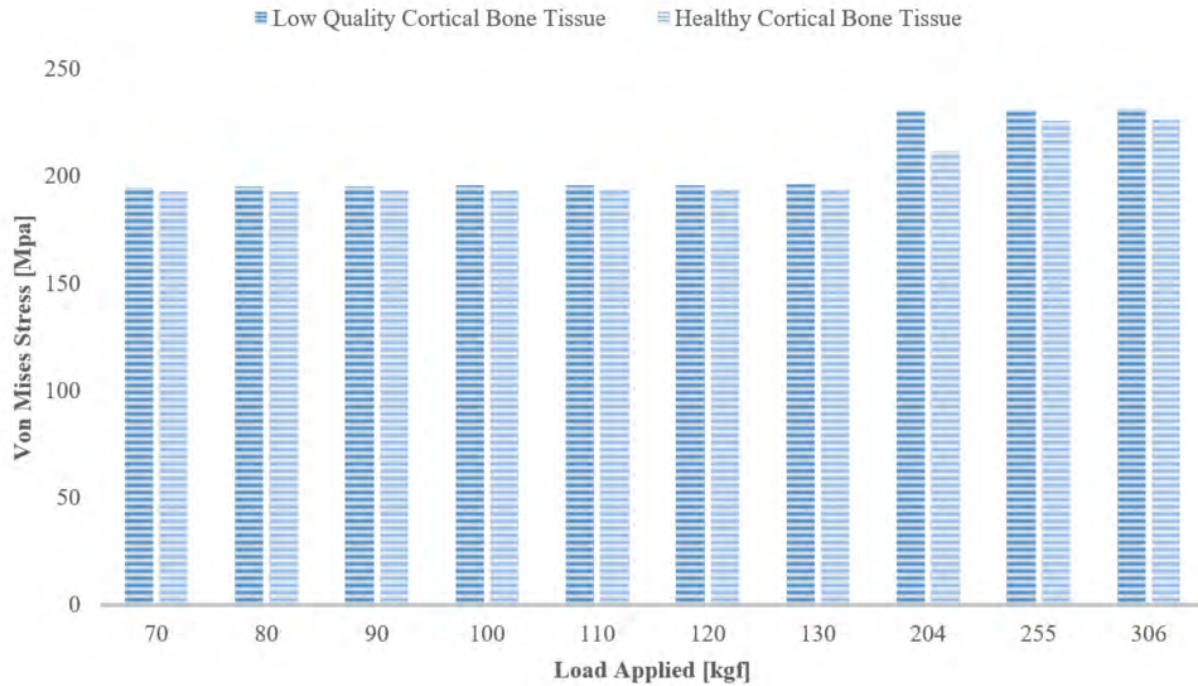
Figure 4.46. Maximum stress results of the femur model with custom hip stem cavity

In *Figure 4.46* we can observe the graphic evolution of stress results in the femur study for both, healthy and an elderly patient cortical bone tissue.

Results have shown that in case of elderly patient cortical bone tissue the stress results are higher for each load applied compared to healthy cortical tissue.
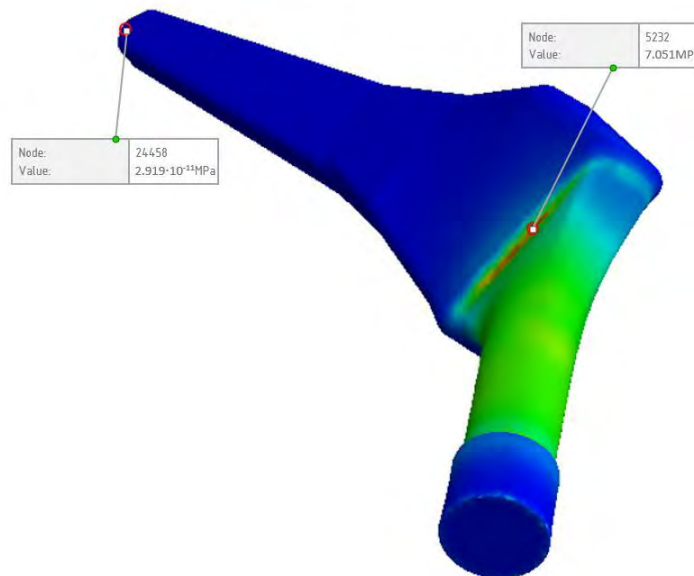
Figure 4.47. Minimum (hip stem bottom) and maximum (hip stem neck base) Von Mises Stress nodes location of the femur model with custom stem cavity

The FEA studies performed in each load case for the custom femoral hip stem have shown a minimum stress located in the node 24458 and a maximum stress located node 5232 (*Figure 4.47*). In *Table 4.23* we can identify the minimum and maximum stress values resulting from each analysis.

Table 4.23. Custom femoral stem model stress results. Stress Results VON: von Mises Stress [MPa]

N°	Load [N]	Custom femoral hip stem	
		Minimum	Maximum
F_1	686.46	$2.919 \cdot 10^{-11}$	1.613
F_2	784.53	$3.336 \cdot 10^{-11}$	1.844
F_3	882.59	$3.753 \cdot 10^{-11}$	2.074
F_4	980.66	$4.170 \cdot 10^{-11}$	2.305
F_5	1078.73	$4.587 \cdot 10^{-11}$	2.535
F_6	1176.79	$5.004 \cdot 10^{-11}$	2.766
F_7	1274.86	$5.422 \cdot 10^{-11}$	2.996
F_8	2000	$8.505 \cdot 10^{-11}$	4.701
F_9	2500	$1.063 \cdot 10^{-10}$	5.876
F_{10}	3000	$1.276 \cdot 10^{-10}$	7.051

In *Figure 4.48* we can observe the graphic evolution of stress results in the custom femoral hip stem study in case of each load. In *Figure 4.49* we can observe the stress distribution on the assembly, but also in all individual parts, in case of 3000N load application.
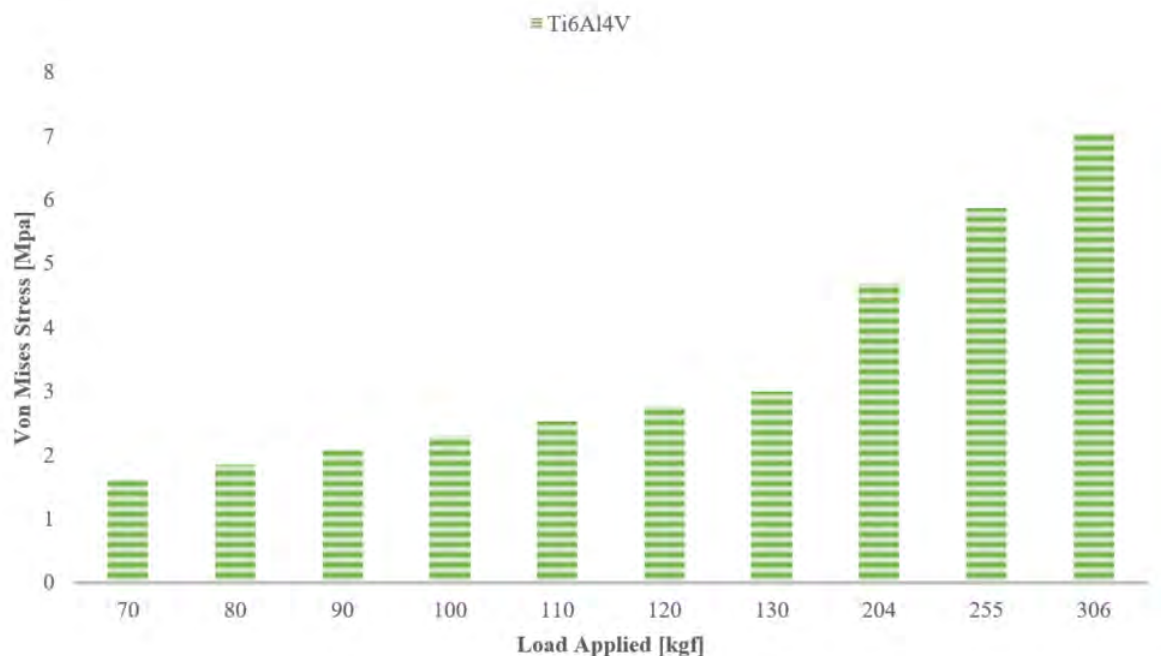
*Figure 4.48. Maximum stress results of the custom femoral hip stem*
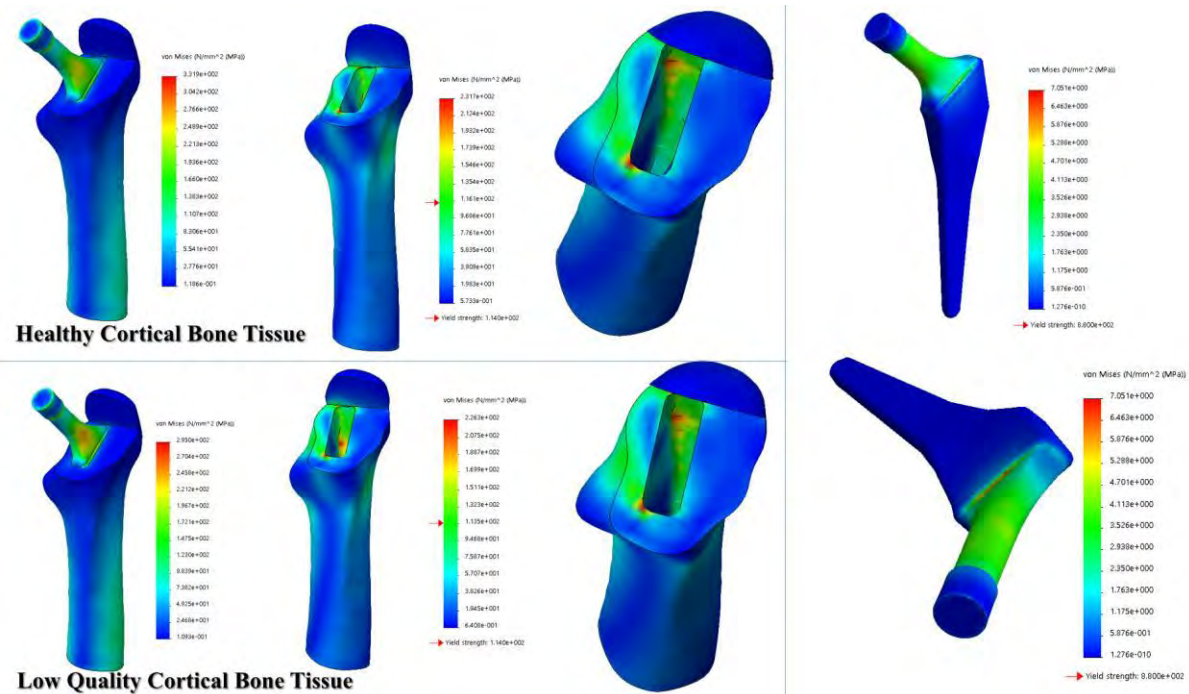
Figure 4.49. Stress results distribution in case of 3000 N load applied

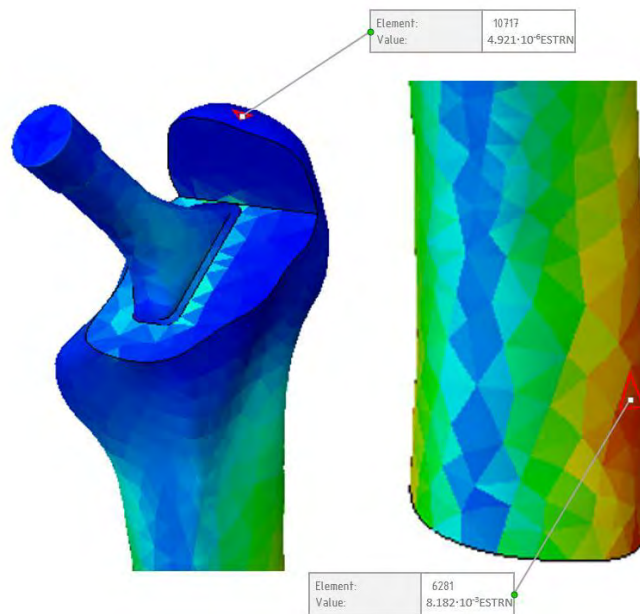## 4.4.4. FEA displacement results
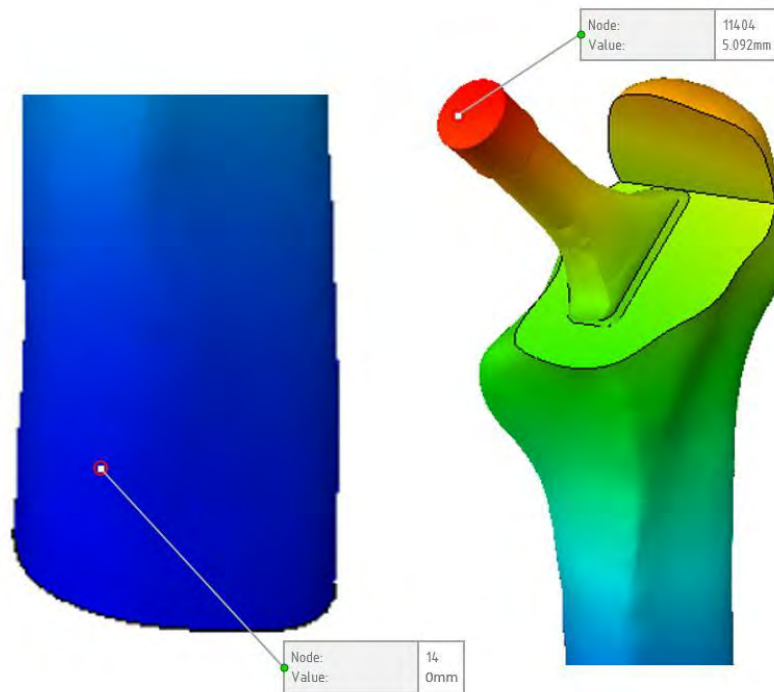
Figure 4.50. Minimum (left) and maximum (right) displacement nodes location of the custom hip stem and femur assembly

Table 4.24. Femur and custom femoral stem assembly displacement results [mm] for healthy and low quality cortical bone tissue

N°	Load [N]	Assembly femur with elderly patient's cortical bone tissue & standard stem		Assembly femur with healthy cortical bone tissue & standard stem	
		Minimum	Maximum	Minimum	Maximum
F_1	686.46	0	2.325	0	1.845
F_2	784.53	0	2.483	0	1.972
F_3	882.59	0	2.645	0	2.101
F_4	980.66	0	2.808	0	2.232
F_5	1078.73	0	2.973	0	2.364
F_6	1176.79	0	3.140	0	2.498
F_7	1274.86	0	3.309	0	2.633
F_8	2000	0	4.583	0	3.653
F_9	2500	0	5.478	0	4.370
F_{10}	3000	0	6.380	0	5.092

Following the FEA study performed in each load case for the custom hip stem and femur assembly has shown a minimum displacement located in the node 14 and a maximum displacement located on node 11404 (*Figure 4.50*). In *Table 4.24* we can identify the minimum and maximum displacement values resulting from each analysis for both applied materials. In *Figure 4.51* we can observe the graphic evolution of displacement results in the assembly study for both, healthy and elderly patient cortical bone tissue.

Figure 4.51. Maximum displacement results of the femur and custom hip stem assembly

Figure 4.52. Minimum (left) and maximum (right) displacement nodes location of the femur with custom hip stem cavity
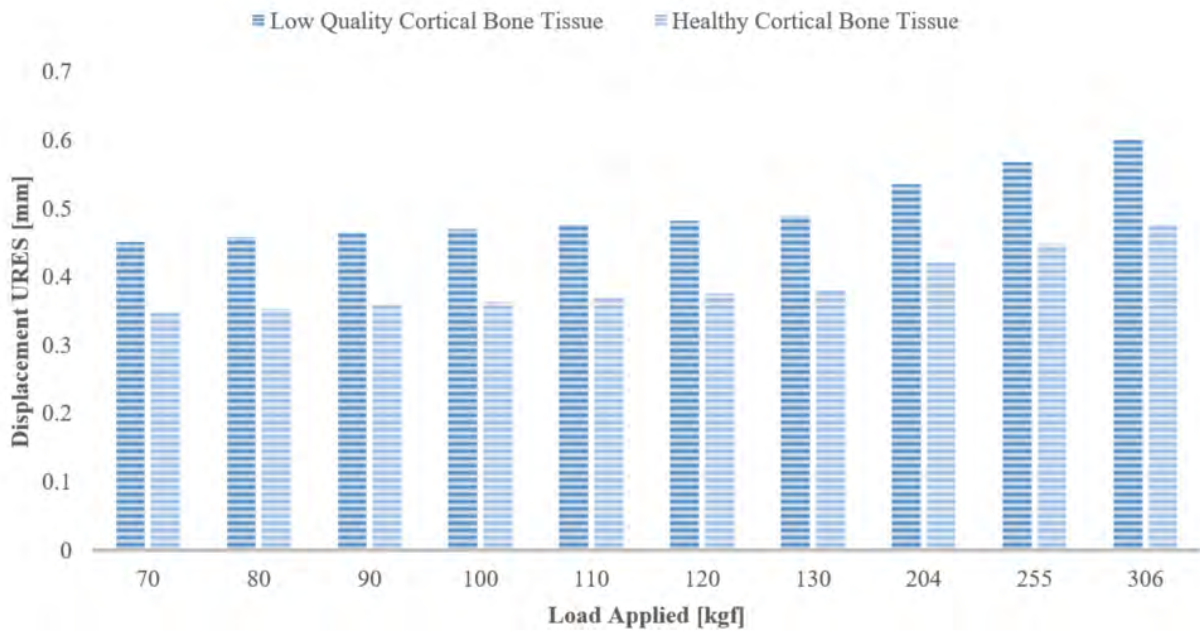
Figure 4.53. Maximum displacement results of the femur custom cavity model

Table 4.25. Femur custom stem cavity displacement results [mm] for healthy and low quality cortical bone tissue

N°	Load [N]	Femur with elderly patient's cortical bone tissue		Femur with healthy cortical bone tissue	
		Minimum	Maximum	Minimum	Maximum
F_1	686.46	0	$4.517 \cdot 10^{-1}$	0	$3.481 \cdot 10^{-1}$
F_2	784.53	0	$4.579 \cdot 10^{-1}$	0	$3.536 \cdot 10^{-1}$
F_3	882.59	0	$4.641 \cdot 10^{-1}$	0	$3.590 \cdot 10^{-1}$
F_4	980.66	0	$4.704 \cdot 10^{-1}$	0	$3.645 \cdot 10^{-1}$
F_5	1078.73	0	$4.766 \cdot 10^{-1}$	0	$3.699 \cdot 10^{-1}$
F_6	1176.79	0	$4.829 \cdot 10^{-1}$	0	$3.753 \cdot 10^{-1}$
F_7	1274.86	0	$4.892 \cdot 10^{-1}$	0	$3.808 \cdot 10^{-1}$
F_8	2000	0	$5.356 \cdot 10^{-1}$	0	$4.211 \cdot 10^{-1}$
F_9	2500	0	$5.677 \cdot 10^{-1}$	0	$4.489 \cdot 10^{-1}$
F_{10}	3000	0	$5.998 \cdot 10^{-1}$	0	$4.767 \cdot 10^{-1}$

The FEA study performed in each load case for the femur with custom stem cavity, has shown a minimum displacement located on node 1115 and a maximum displacement located on node 303 (*Figure 4.52*). In *Table 4.25* we can identify the minimum and maximum displacement values resulting from each analysis for both tissue cases.
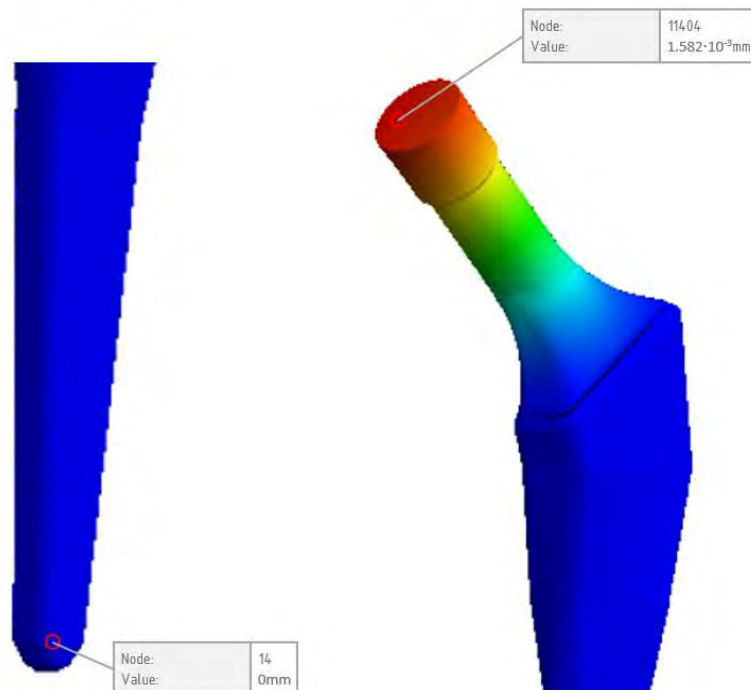
Figure 4.54. Minimum (left) and maximum (right) displacement nodes location of the custom hip stem

In *Figure 4.53* we can observe the graphic evolution of displacement results in the femur study for both, healthy and elderly patient cortical bone tissue.

In *Table 4.26* we can identify the minimum and maximum displacement values resulting from each simulation.
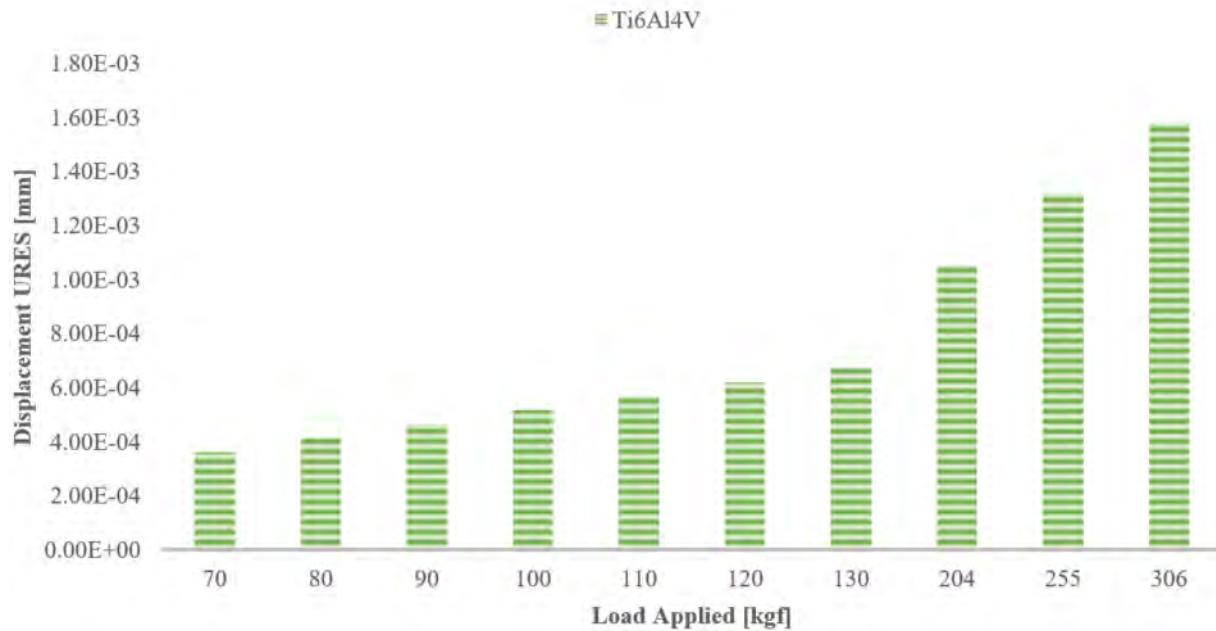
Figure 4.55. Maximum displacement results of the custom femoral hip stem

In *Figure 4.55* we can observe the graphic evolution of displacement results in the femoral hip stem study in case of each load. In *Figure 4.56* we can observe the displacement distribution on the custom hip stem a femur assembly, but also in all individual parts, as a result of 3000N load applied.

Table 4.26. Custom femoral stem model displacement results [mm]

N°	Load [N]	Custom femoral hip stem	
		Minimum	Maximum
F_1	686.46	0	$3.620 \cdot 10^{-4}$
F_2	784.53	0	$4.137 \cdot 10^{-4}$
F_3	882.59	0	$4.654 \cdot 10^{-4}$
F_4	980.66	0	$5.171 \cdot 10^{-4}$
F_5	1078.73	0	$5.688 \cdot 10^{-4}$
F_6	1176.79	0	$6.205 \cdot 10^{-4}$
F_7	1274.86	0	$6.722 \cdot 10^{-4}$
F_8	2000	0	$1.055 \cdot 10^{-3}$
F_9	2500	0	$1.318 \cdot 10^{-3}$
F_{10}	3000	0	$1.582 \cdot 10^{-3}$

The simulation performed in each load case for the femoral hip stem has shown a minimum displacement located on node 14 and a maximum displacement located in node 11404 (*Figure 4.54*).
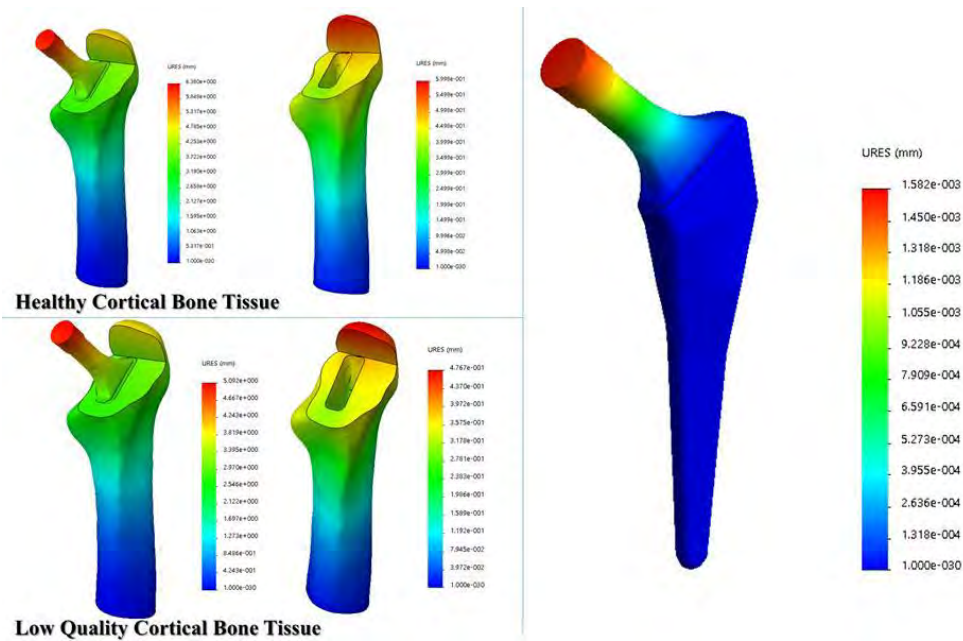
Figure 4.56. Displacement results distribution in case of 3000 N load applied

4.4.5. FEA strain results

Figure 4.57. Minimum (left) and maximum (right) strain nodes location of the custom hip stem and femur assembly

Table 4.27. Femur and custom femoral stem assembly strain results [ESTRN: Equivalent Strain] for healthy and elderly patient cortical bone tissue

N°	Load [N]	Assembly femur with elderly patient's cortical bone tissue & standard stem		Assembly femur with healthy cortical bone tissue & standard stem	
		Minimum	Maximum	Minimum	Maximum
F_1	686.46	$5.781 \cdot 10^{-6}$	$6.414 \cdot 10^{-3}$	$4.921 \cdot 10^{-6}$	$3.992 \cdot 10^{-3}$
F_2	784.53	$6.035 \cdot 10^{-6}$	$6.437 \cdot 10^{-3}$	$4.972 \cdot 10^{-6}$	$4.010 \cdot 10^{-3}$
F_3	882.59	$6.305 \cdot 10^{-6}$	$6.461 \cdot 10^{-3}$	$4.963 \cdot 10^{-6}$	$4.029 \cdot 10^{-3}$
F_4	980.66	$6.589 \cdot 10^{-6}$	$6.484 \cdot 10^{-3}$	$4.963 \cdot 10^{-6}$	$4.049 \cdot 10^{-3}$
F_5	1078.73	$6.686 \cdot 10^{-6}$	$6.507 \cdot 10^{-3}$	$4.971 \cdot 10^{-6}$	$4.069 \cdot 10^{-3}$
F_6	1176.79	$6.558 \cdot 10^{-6}$	$6.531 \cdot 10^{-3}$	$4.989 \cdot 10^{-6}$	$4.089 \cdot 10^{-3}$
F_7	1274.86	$6.435 \cdot 10^{-6}$	$6.555 \cdot 10^{-3}$	$5.015 \cdot 10^{-6}$	$4.109 \cdot 10^{-3}$
F_8	2000	$5.715 \cdot 10^{-6}$	$6.739 \cdot 10^{-3}$	$3.774 \cdot 10^{-6}$	$4.886 \cdot 10^{-3}$
F_9	2500	$5.691 \cdot 10^{-6}$	$7.054 \cdot 10^{-3}$	$2.945 \cdot 10^{-6}$	$5.559 \cdot 10^{-3}$
F_{10}	3000	$5.663 \cdot 10^{-6}$	$8.182 \cdot 10^{-3}$	$2.675 \cdot 10^{-6}$	$6.412 \cdot 10^{-3}$

Following the FEA study performed in each load case for the custom hip stem and femur assembly has shown a minimum strain results located in element number 10717 and a maximum strain results located in element number 6281 (*Figure 4.57*). In *Table 4.27* we can identify the minimum and maximum strain values resulting from each analysis for both tissue cases.

Figure 4.58. Maximum strain results of the femur and custom hip stem assembly

The FEA study performed in each load case for the femur has shown a minimum strain located in the element 10518 and the maximum strain located in the element 3808 in both cases (*Figure 4.59*).
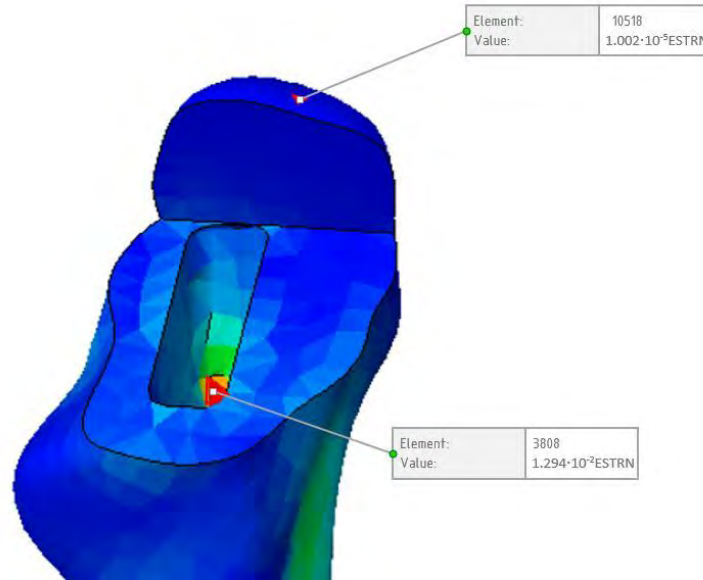
Figure 4.59. Minimum (top) and maximum (inside femur's cavity) strain nodes location of the femur with custom hip stem cavity

In *Figure 4.58* we can observe the graphic evolution of the strain results in the custom hip stem and the femur assembly study for both, healthy and an elderly patient cortical bone tissue.

In *Table 4.28* we can identify the minimum and maximum strain values resulting from each simulation for both study cases.

In *Figure 4.60* we can observe the graphic evolution of the strain results in the femur analysis for both, healthy bone tissue and low quality bone tissue.

Table 4.28. Femur with custom stem cavity strain results [ESTRN: Equivalent Strain] for healthy and elderly patient cortical bone tissue

N°	Load [N]	Femur with elderly patient's cortical bone tissue		Femur with healthy cortical bone tissue	
		Minimum	Maximum	Minimum	Maximum
F_1	686.46	$1.342 \cdot 10^{-5}$	$1.093 \cdot 10^{-2}$	$1.002 \cdot 10^{-5}$	$8.592 \cdot 10^{-3}$
F_2	784.53	$1.342 \cdot 10^{-5}$	$1.094 \cdot 10^{-2}$	$1.002 \cdot 10^{-5}$	$8.602 \cdot 10^{-3}$
F_3	882.59	$1.342 \cdot 10^{-5}$	$1.095 \cdot 10^{-2}$	$1.002 \cdot 10^{-5}$	$8.613 \cdot 10^{-3}$
F_4	980.66	$1.342 \cdot 10^{-5}$	$1.097 \cdot 10^{-2}$	$1.002 \cdot 10^{-5}$	$8.623 \cdot 10^{-3}$
F_5	1078.73	$1.342 \cdot 10^{-5}$	$1.098 \cdot 10^{-2}$	$1.001 \cdot 10^{-5}$	$8.634 \cdot 10^{-3}$
F_6	1176.79	$1.342 \cdot 10^{-5}$	$1.099 \cdot 10^{-2}$	$1.100 \cdot 10^{-5}$	$8.644 \cdot 10^{-3}$
F_7	1274.86	$1.342 \cdot 10^{-5}$	$1.100 \cdot 10^{-2}$	$1.100 \cdot 10^{-5}$	$8.655 \cdot 10^{-3}$
F_8	2000	$1.646 \cdot 10^{-5}$	$1.287 \cdot 10^{-2}$	$9.493 \cdot 10^{-5}$	$9.784 \cdot 10^{-3}$
F_9	2500	$1.641 \cdot 10^{-5}$	$1.290 \cdot 10^{-2}$	$9.042 \cdot 10^{-5}$	$1.016 \cdot 10^{-2}$
F_{10}	3000	$1.636 \cdot 10^{-5}$	$1.294 \cdot 10^{-2}$	$9.021 \cdot 10^{-5}$	$1.019 \cdot 10^{-2}$
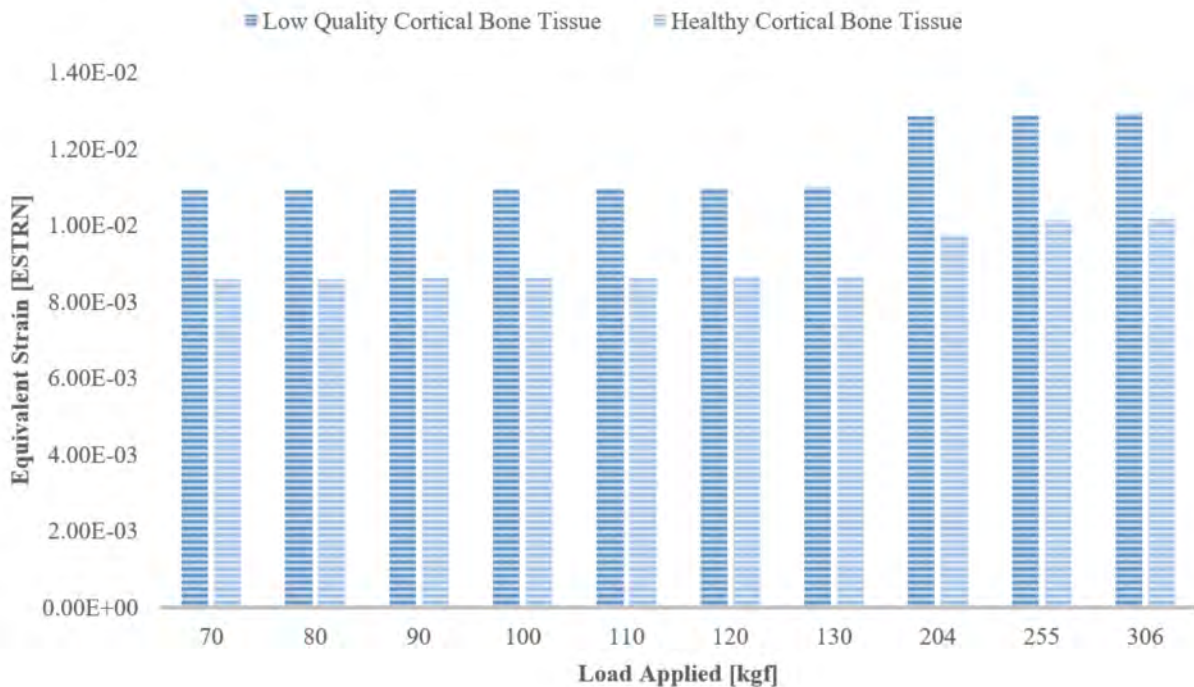
Figure 4.60. Maximum strain results of the femur model with custom hip stem cavity

The FEA study performed in each load case for the custom femoral hip stem has shown a minimum strain located in the element 7457 and a maximum strain located in the element 11596 (*Figure 4.61*). In *Table 4.29* we can identify the minimum and maximum strain values resulting from each analysis.

In *Figure 4.62* we can observe the graphic evolution of the strain results of the custom femoral hip stem study in case of each load applied. In *Figure 4.63* we can observe the strain distribution on the custom hip stem and femur assembly, but also in all individual parts as a result of 3000N load application.

Table 4.29. Custom femoral stem model strain results [ESTRN: Equivalent Strain]

N°	Load [N]	Custom femoral hip stem	
		Minimum	Maximum
F_1	686.46	$2.876 \cdot 10^{-16}$	$1.085 \cdot 10^{-5}$
F_2	784.53	$3.287 \cdot 10^{-16}$	$1.240 \cdot 10^{-5}$
F_3	882.59	$3.698 \cdot 10^{-16}$	$1.395 \cdot 10^{-5}$
F_4	980.66	$4.109 \cdot 10^{-16}$	$1.550 \cdot 10^{-5}$
F_5	1078.73	$4.520 \cdot 10^{-16}$	$1.705 \cdot 10^{-5}$
F_6	1176.79	$4.931 \cdot 10^{-16}$	$1.806 \cdot 10^{-5}$
F_7	1274.86	$5.342 \cdot 10^{-16}$	$2.015 \cdot 10^{-5}$
F_8	2000	$8.380 \cdot 10^{-16}$	$3.161 \cdot 10^{-5}$
F_9	2500	$1.047 \cdot 10^{-15}$	$3.951 \cdot 10^{-5}$
F_{10}	3000	$1.257 \cdot 10^{-15}$	$4.741 \cdot 10^{-5}$
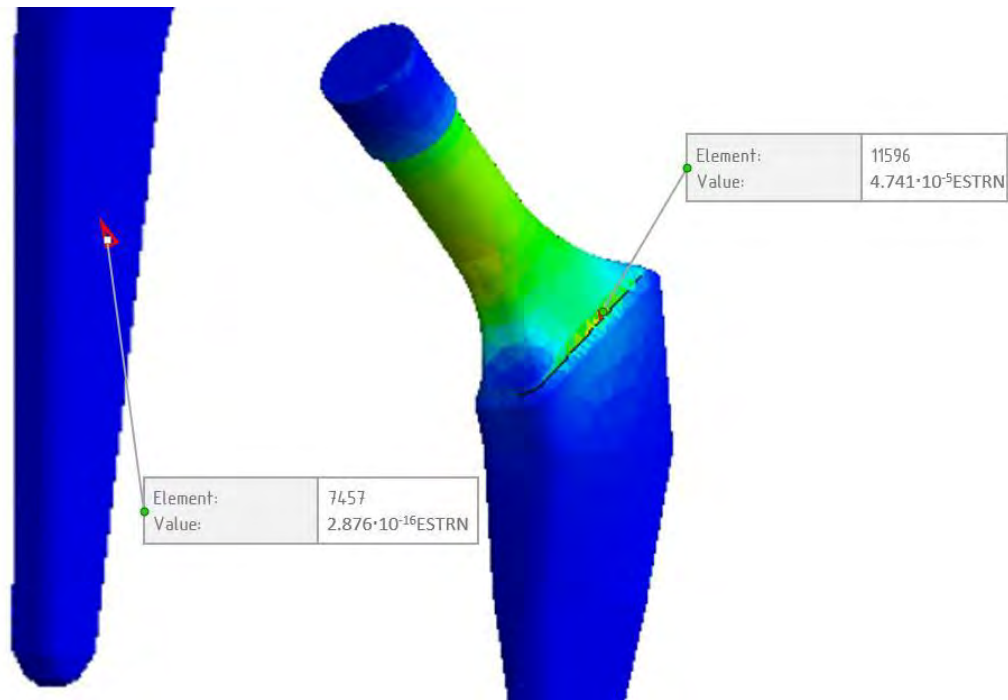
Figure 4.61. Minimum (left) and maximum (right) strain nodes location of the custom hip stem
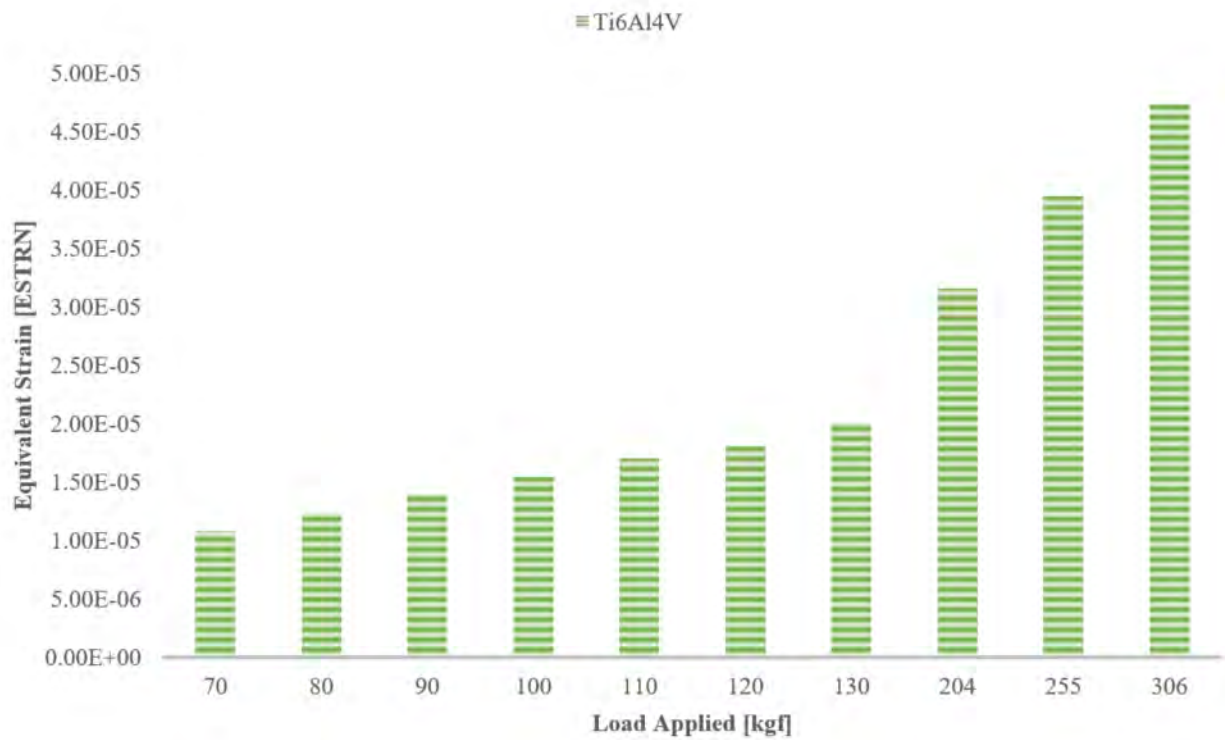
Figure 4.62. Maximum strain results of the custom femoral hip stem

Healthy Cortical Bone Tissue

Low Quality Cortical Bone Tissue
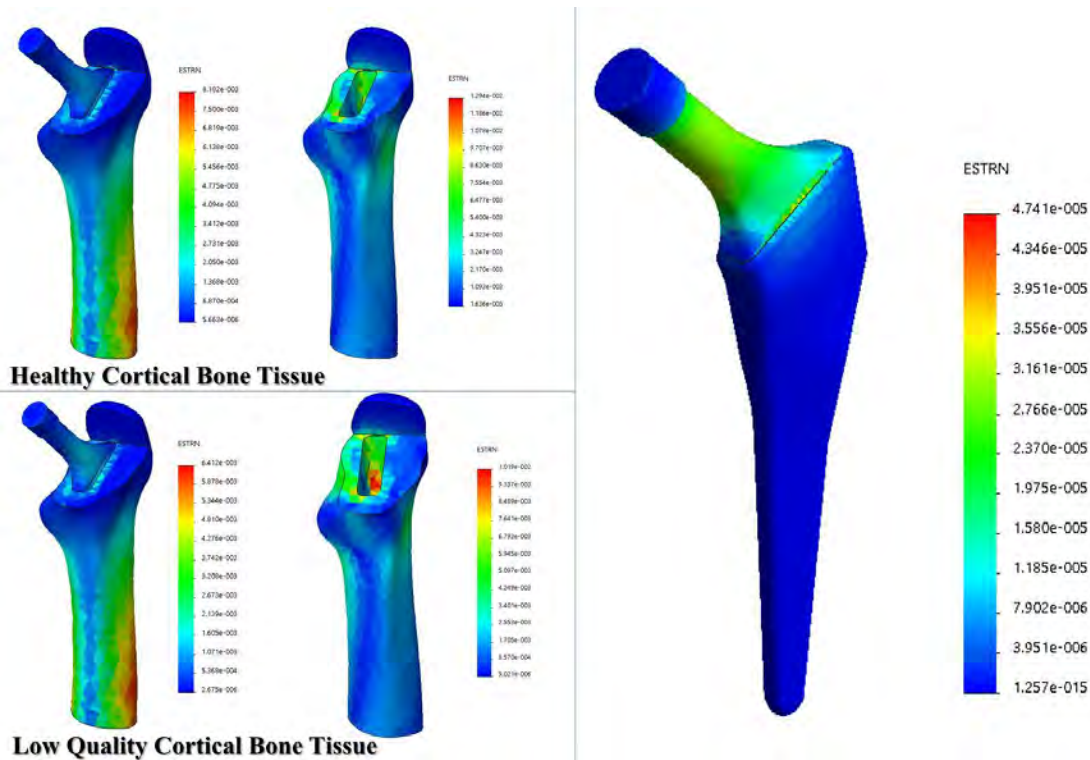
Figure 4.63. Strain results distribution in case of 3000 N load applied

4.5.   Chapter conclusion

Comparing the results obtained from the FEA studies between the assembly that contains standard hip stem and custom hip stem we can notice a considerable improvement in the stress results following the femoral custom hip stem. A personalized geometry may discharge in a more optimal way the loads that can occur inside the hip joint articulation. At the same time we can observe also that the bone quality influences the results and the stress at the joint level, young patients responding better to external loads than elderly that can suffer of bone loss or other associative pathology.

Although virtual simulations can provide significant information on the mechanical behavior of prostheses they cannot accurately reproduce real situations due to the complexity of the human body and the uniqueness of each individual. However, they are especially used in the prototyping phase of a design, helping the concept engineer to decide which design can be studied further and in which design should invest for the in vivo experiments.

Due to the large number of THRs performed in the last decade, but also due to the increasing number of surgeries expected to be realized in the coming years, the use of the patient's femoral landmarks to develop femoral prosthetic components can be an important stage in orthopedics, and the implementation of an accessible manufacturing method for such prostheses can generate a new approach in this medical sector.

Figure 4.64. Comparison of stress results

CHAPTER 5

DEVELOPING BONE SEGMENTATION AND VIRTUAL PROTOTYPING MEDICAL SOFTWARE

5.1. Main stages in developing a bone segmentation software

Figure 5.1. Stages to develop a bone segmentation software

5.1.1. *Software feasibility analysis*

The project aim was to develop a software that allows the user to upload DICOM files obtained by MRI or CT patients' scan and performing bone segmentation by displaying a CAD model of the bone structure which allows the user to manipulate it in order to perform image processing operations. The development of this software was done in collaboration with doctors from *Imagerie Médicale Clinique du Parc*, Lyon, France, which provide CT scans of patients with various health conditions regarding the hip joint, but also useful information from the orthopedic surgeon and radiologist point of view.

The software will be used for didactic purposes, as a tool, for teaching students in medicine (future orthopedic surgeons in particular), but also for students in biomechanical engineering bone segmentation process in THR and virtual preoperative planning. For future doctors it is a way of planning THR surgery, to learn how to choose the most suitable hip prosthesis according to each patient's case.

In order to give an identity to the project a logo was made starting from the abbreviation of the project name NAOS (Numerical Analysis for Orthopedic Surgery) shown in *Figure 5.2*, but also a motto to create a greater impact, "Predicting orthopedic future".

The software must perform the following main functions:

a.   Opening DICOM files.
b.   Bone segmentation, 3D control.
c.   Multi Planar View of MPR view (coronal plane, axial plane, and sagittal plane).
d.   Contrast control for MPR view.
e.   3D pelvis visualization and rotation.

Figure 5.2. NAOS project logo

As technical resources a DELL portable laptop was used with the following main characteristics: Intel® Core ™ i7-7820HQ CPU 2.90GHz processor, 16.0GB RAM memory with a 64-bit operating system, Windows 10 Pro edition. Programming software used were Pthon 3.7.2. version with Visual Code Studio.
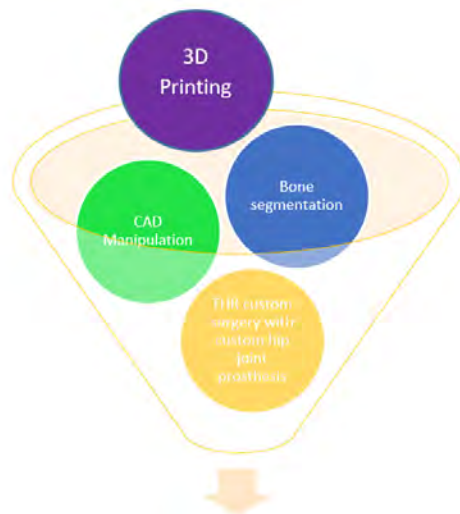
Figure 5.3. New product market principle

The software that follows the functions listed above can enter very difficult on this market segment, because the number of open source platforms and software that allows simple bone segmentation studies are quite a lot, but by implementing the idea of custom THR with custom hip joint prostheses may increase the interest of potential developers, and the introduction of additional 3D printing module for hip stem based on the femoral landmarks that the user identify can position this project in an area of interest.

This project can become an impact in terms of speculating "custom" THR idea in the orthopedic field and also in creating links with Additive Manufacturing Industry.

5.1.2. *Analyze and determine software requirements*

To create a global view and to define better this thesis part, was used a case diagram (UML) to express each part contribution, as shown in *Figure 5.5*.
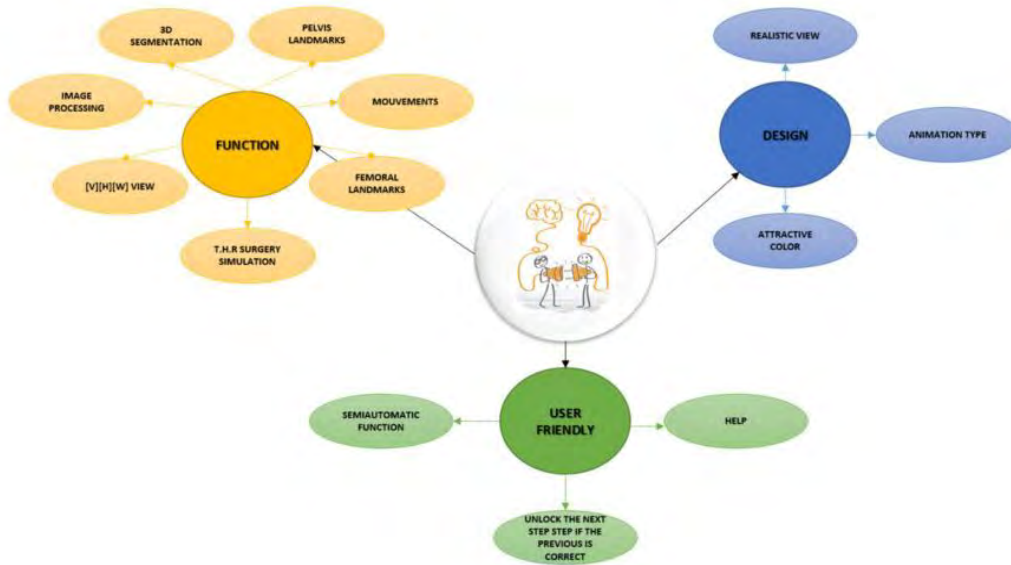
Figure 5.4. Brainstorming discussion with surgeons

Following the meetings held with the surgeons to finalize the structure and the needs of the users, was identified the main software development directions as shown in *Figure 5.4*.
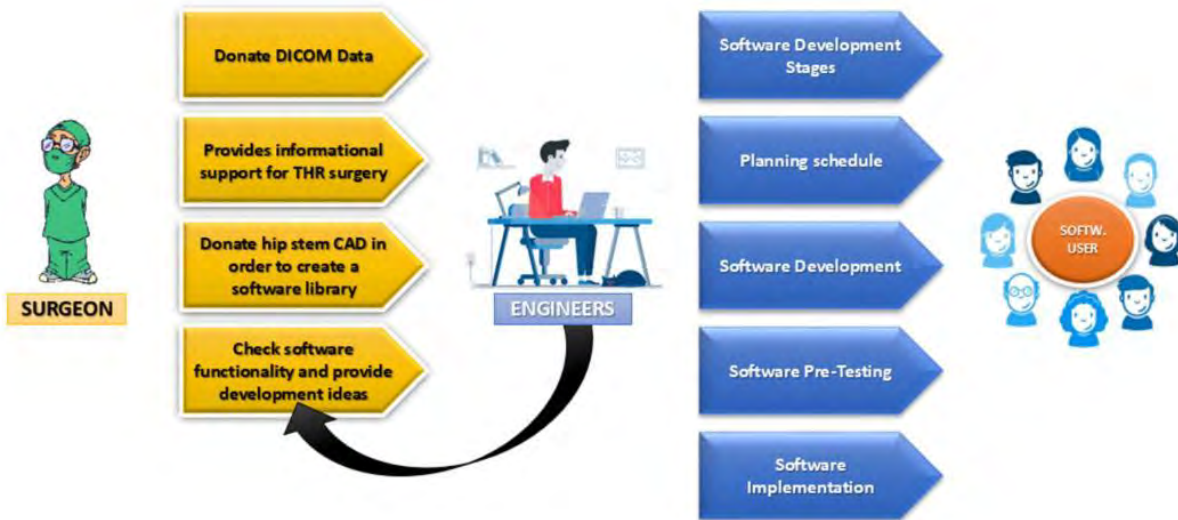
Figure 5.5. NAOS project case diagram

5.1.3. Industry best practices

At this stage a market research was done in order to have a clearer picture about this segment of the industry and this typology of medical providers. In this sense, after the market analysis were identified the following main global medical software providers:

a.   *NextGen Healthcare* (practice management, scheduling and also software that generates bills in this field).

b.   *Eclinical works* (unites and connect medical practice management, patient's records, also belling in one database).

c.   *McKesson* (a system that masters person index or MPI with patient data, equipment, scheduling, personnel and rooms).

d.   *Allscripts* (this company offers software solutions for every branch of the medical industry).

e.   *Athenahealth* (it is a cloud software, which tracks and identify issues in the workflow, but also improves it).

f.   *GE Healthcare* (improve performance with enhanced connectivity in terms of electronic data and offers portal to patients in order to provide secure web access).

g.   *Epic System Corporation* (this company develops various software for academic institutions, mid-size and large company groups).

In the same way, a market study about bone segmentation software was done, among which we mention the following:

a.   *OncoSpineSeg* (it is a software which uses computer aided diagnosis in order to identify metastatic disease in bones, but also other spine disorders).

b.   *BoneFinder®* (it is an automatic software which creates an outline and select the bone contour from 2D X-Rays).

c.   *TurtleSeg* (it is a 3D medical segmentation tool).

d.   *ImFusion* (it is a complex medical software, which can segment different structures in 2D or 3D image data).

e.   *Amira* (it is a very powerful and complex medical software, in which users can perform various medical image segmentation, but also manipulate the resulting structures).

Following these examples of software and companies that produce software for the medical industry, it provided valuable information on how to develop software in the medical industry, create and design an easy interface.

5.1.4. Software design

For the software interface the PyQT5 was used, a user-friendly software in which you can simply design your interface and export it as a code. The code can be converted in python language and easily integrate it into the initial software code.

5.1.5. Measuring and tracking software progress

In order to be able to manage the evolution of the project and the duration of each task, a project plan was made in which the time required to obtain each result was approximated in weeks as shown in *Figure 5.6*.

5.1.6. *Software development*

In order to develop the software, the Python programming language was used. Python is a programming language, which takes what the user writes, generically called code, and turns it into instruction to users' computer, in the end executing them. Python was used in association with Visual Code Studio, which is a source code editor that helps the user and gives support for debugging, code completion, refactoring or even syntax highlighting.
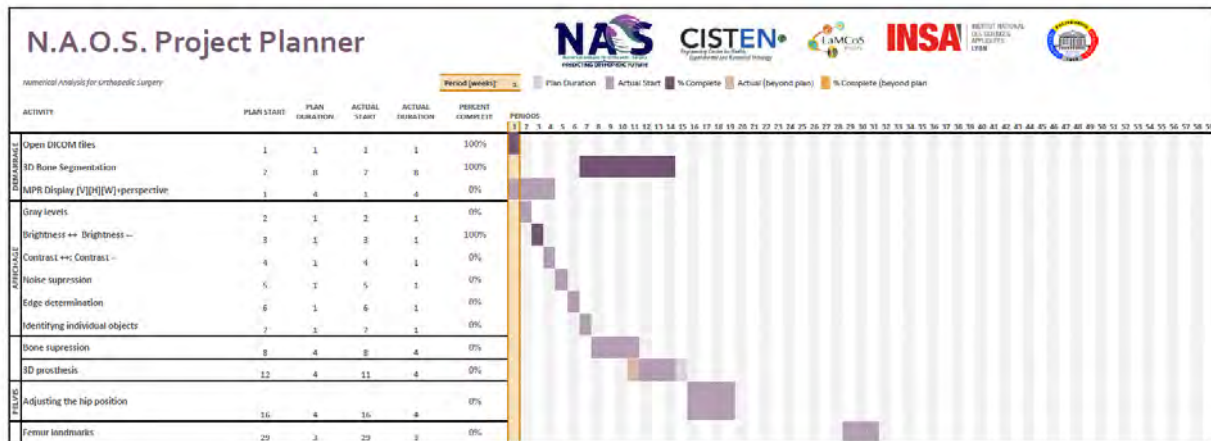
Figure 5.6. NAOS project planner

5.1.7. *Addressing software automation*

The software will be semi-automatic, requesting the user's intervention regarding the extraction or identification of the femur or pelvis, especially in the case of patients with hip joint diseases, in which the separation of the components that realize the hip joint cannot be distinguished with simple image processing algorithms.

5.1.8. *Software testing*

The software will be tested in the laboratory by users trained in this sense, by inserting CT sets from different patients, CT sets obtained from associated surgeons.

5.1.9. *Gradual implementation of software practices*

The software can be implemented and used in the institutional framework of the faculties, and later in the training school of the future orthopedic surgeons.

5.2. Developing the bone segmentation software modules

In order to simplify the software development process, NAOS software was divided into three modules (MPR view, bone extraction and hip stem customization) as shown in *Figure 5.7*, thus, three codes in the Python programming language will be realized, which will be subsequently implemented in the interface at the end of the process.
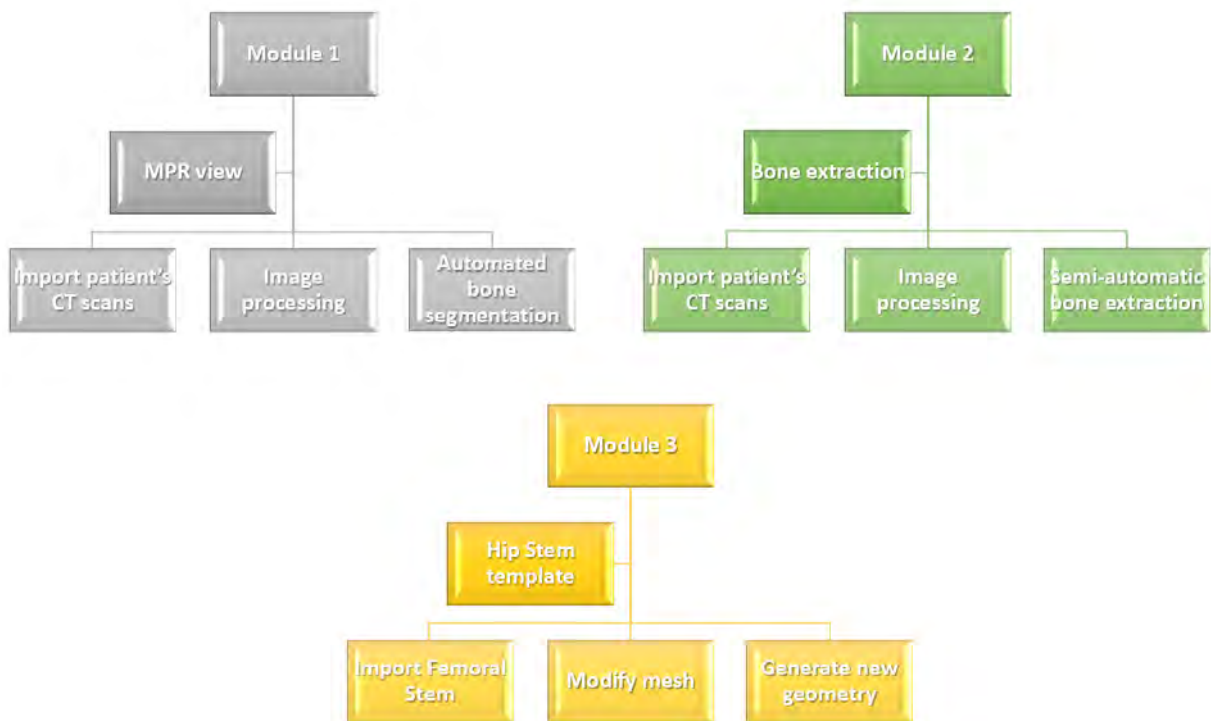
Figure 5.7. NAOS software modules

5.2.1. Developing the software's MPR view in Python language

In order to be able to develop the code, which is reading patient's CT scans and displaying them in the so-called MPR view, more precisely coronal plane, axial plane and sagittal plane, it is necessary to identify the useful patches that allow the display, or use of virtual libraries that helps to achieve the desired result. These patches can be installed via CMD (Command Prompt) with the help of pip, a standard package management system that manage software packages written in Python language.
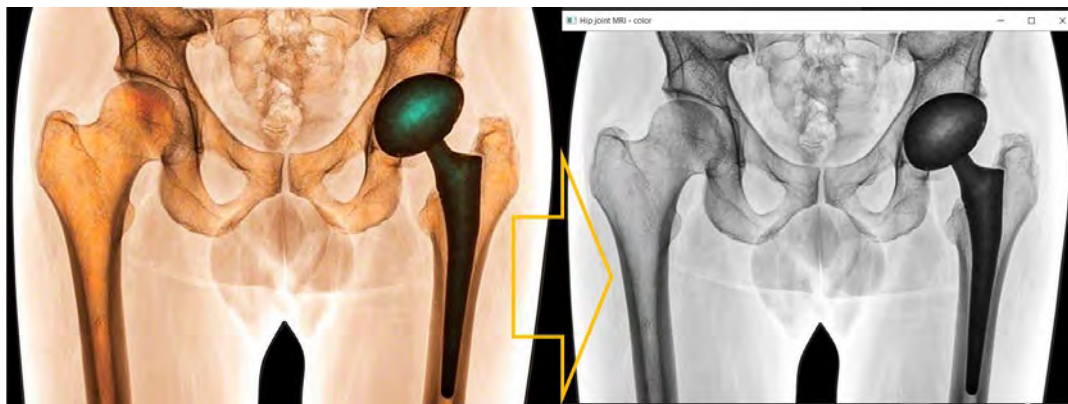
Figure 5.8. Patch testing in Python. Initial MRI file (left) and converted file to gray (right)

The following patches were used in the code development of the first software module:

a.   *Numpy* (*<pip install numpy>*) is a library for the Python programming language, which supports multidimensional arrays and large arrays, having a big collection of high-level mathematical functions that work on these arrays.

b.   *OpenCV* (*<python –m pip install opencv-python>*) is a library for the Python programming language, of computer functions specialized in real time computerized view. After installation, these functions were tested by downloading a colored MRI image, loading the file from Python dedicated folder path and convert it to gray (*Figure 5.8*).

c.   *PyDICOM* (*<pip install pydicom>*) this patch can read, storage and transfer medical image datasets. It is usually used by physicians, graduate students or scientists that develop software based on DICOM datasets and protocols.

d.   *VTK or The Visualization Toolkit* (*<python –m pip install vtk>*) is an open-source system software patch used for 3D computer graphics, visualization and image processing, especially in medical imaging.

e.   *Matplotlib* (*<python –m pip install –U matplotlib>*) is a 2D plotting library for Python programming language, which produce high quality figures in interactive environments.

f.   *Plotly* (*<pip install plotly>*) is a patch that will allow to perform 3D plotting.

g.   *Scikit-image* (*<pip install scikit-image>*) is a library which allows processing open source images in Python.

h.   *SciPy* (*<pyton –m pip install scipy>*) is a free library for the Python programming language used for technical and scientific calculation.

i.   *OS* (*<pyton –m pip install os-win>*) is a patch that provides a way to use operating system dependent functions, in a portable way.

j.   *Glob3* (*<pip3 install glob3>*) is a patch for Python programming language that finds pathnames and match them with a specific pattern according to the rules.

k.   *Cluster* (*<pip install numpy scipy scikit-learn>*) is a patch used in the Python language programming for comparing different clustering algorithms on various datasets for example, an open source data analyzing module.

l.   *Pylint* (*<pip install pylint>*) is a code source patch that bug and check the quality of the Python programming language.

m.   *Optimesh* (*<pip install optimesh>*) is a mesh optimization patch for Python programming language that mesh and smooth geometries.

n.   *Trimesh* (*<pip install trimesh>*) is a Python patch library used in loading triangular meshes.

o.   *Jupyter* (*<python –m pip install jupyter>*) is an open source patch for Python that offer services for interactive computing language, such as Python programming language.

These are the most important patches and virtual libraries used in software coding, which are also used for subsequent modules in certain operations. In order to facilitate the access code and the modification of the eventual errors that may appear, the code has been divided into different stages according to the operations that it executes.

The first stage is represented by accessing the patches we use and selecting the DICOM file path, the folder which contains patient's CT scans. The DICOM folder is selecting automatically the file path from the Python source folder as we can see in the following code lines:

```
import vtk
from glob import glob
```

<center>***</center>

file_path_variable = r'C:\Users\admin\Desktop\Python\Python\DICOM FOLDER\336923,4448 88'

The other option to select the CT datasets is to create a pop-up dialog window (*Figure 5.9*), where we can select manually the folder path each time we run the code, as we can see in the following code:

```
root = tkinter.Tk()
root.withdraw()

def search_for_file_path ():
    currdir = os.getcwd()
    tempdir = filedialog.askdirectory(parent=root, initialdir=currdir, title='Please select a directory')
    if len(tempdir) > 0:
        print ("You chose: %s" % tempdir)
    return tempdir
file_path_variable = search_for_file_path()
print ("\nfile_path_variable = ", file_path_variable)
```
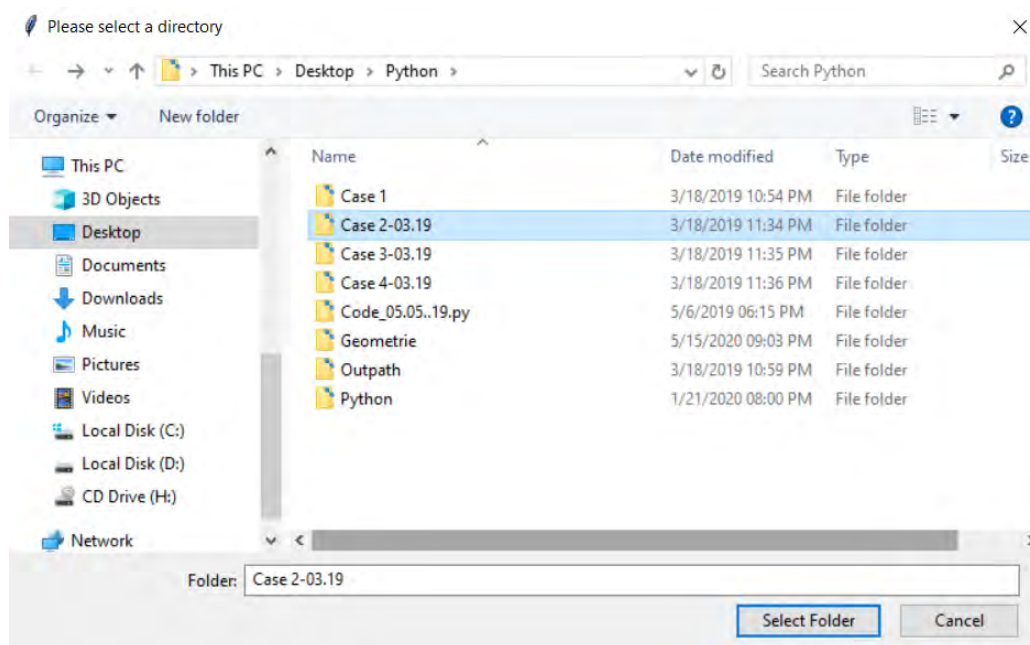

Figure 5.9. Select directory pop-up window for DICOM patients' files

The next step of the code is to read and import all the DICOM (*.dcm) files from the CT dataset from the patient that we want to analyze. In order to input the DICOM file, *vtkDICOMImageReader* class reference was used, at this stage the code is reading the files dimension, scaling, but also the spacing between the slices, at the end printing them as we can see in the following code lines:

```
reader = vtk.vtkDICOMImageReader()
```

```
reader.SetDirectoryName(file_path_variable)
reader.Update()
data_files = glob(file_path_variable + '/*.dcm')
W,H,D = reader.GetOutput().GetDimensions()
a1,b1 = reader.GetOutput().GetScalarRange()
spacing = reader.GetOutput().GetSpacing()
print("Range of image: %d--%d" %(a1,b1))
print(W,H,D)
print(spacing)
colors = vtk.vtkNamedColors()
```

In the next coding stage the MPR view windows were needing to be designed as shown in *Figure 5.10*, divided in four areas three representing the MPR view (coronal, axial and sagittal) and the fourth one displaying the perspective view after the bone segmentation.

Figure 5.10. Software window display

In this sense, were created four render windows and render Interactor by using the *vtkRenderWindow* class reference. Each viewport is having a specific position a specific size with a title that help the user to identify the type of view as we can observe in the following code lines:

```
# Render window

renWin = vtk.vtkRenderWindow()
renWin.SetSize(800, 800)
renWin2 = vtk.vtkRenderWindow()
renWin2.SetSize(800,800) # Size window
renWin2.SetPosition(800,0)
Viewport2 = [0.0, 0.0, 1.0, 1.0]
Renderer2 = vtk.vtkRenderer()
```

```python
renWin2.AddRenderer(Renderer2)
Renderer2.SetViewport(Viewport2)
iren2 = vtk.vtkRenderWindowInteractor()
iren2.SetRenderWindow(renWin2)

# Renderers / Viewport ranges [x_min, y_min, x_max, y_max]

Cor_Viewport = [0.0, 0.5, 0.5, 1.0] # Coronal view
Seg_Viewport = [0.5, 0.5, 1.0, 1.0] # Sagittal view
Axi_Viewport = [0.0, 0.0, 0.5, 0.5] # Axial view
Per_Viewport = [0.5, 0.0, 1.0, 0.5] # 3D view

Cor_Renderer = vtk.vtkRenderer()
renWin.AddRenderer(Cor_Renderer)
Cor_Renderer.SetViewport(Cor_Viewport)
Seg_Renderer = vtk.vtkRenderer()
renWin.AddRenderer(Seg_Renderer)
Seg_Renderer.SetViewport(Seg_Viewport)
Axi_Renderer = vtk.vtkRenderer()
renWin.AddRenderer(Axi_Renderer)
Axi_Renderer.SetViewport(Axi_Viewport)

Per_Renderer = vtk.vtkRenderer()
renWin.AddRenderer(Per_Renderer)
Per_Renderer.SetViewport(Per_Viewport)
Per_Renderer.SetBackground(.2, .2, .2)
```

<p style="text-align:center">***</p>

```python
# Titles

def winTitle3D(titre,debut,hauteur,NumRenderer):
    title = vtk.vtkTextActor() title.SetInput(titre)
    title.GetTextProperty().SetColor(colors.GetColor3d('White'))
    title.GetTextProperty().SetFontFamilyToArial()
    title.GetTextProperty().SetFontSize(16)
    title.GetTextProperty().BoldOn()
    title.SetDisplayPosition(debut,hauteur)
    NumRenderer.AddActor(title)

winTitle3D("CORONAL PLANE VIEW",115,425,Cor_Renderer)
winTitle3D("SAGITTAL PLANE VIEW",515,425,Seg_Renderer)
winTitle3D("AXIAL PLANE VIEW",132,25,Axi_Renderer)
winTitle3D("3D PLANE VIEW",545,25,Per_Renderer)
```

After creating the viewports, the next step is starting the bone segmentation process, in this sense was used *vtkMarchingCubes* class reference as a bone extractor, *vtkStripper* class reference, which is a filter that creates triangle strips and lines or poly-lines from input polygons, working with *vtk.vtkPolyDataMapper*. For the outline bone creation *vtkOutlineFilter* class reference was used, and in order to function, an actor was inserted to the perspective render viewport, finally the bone volume was defined with *vtkFixedPointVolumeRayCastMapper* (a caster software ray that render 3D volume in *vtkImageData*) and *vtkVolume* (representing volumetric objects in a render scene) class reference.
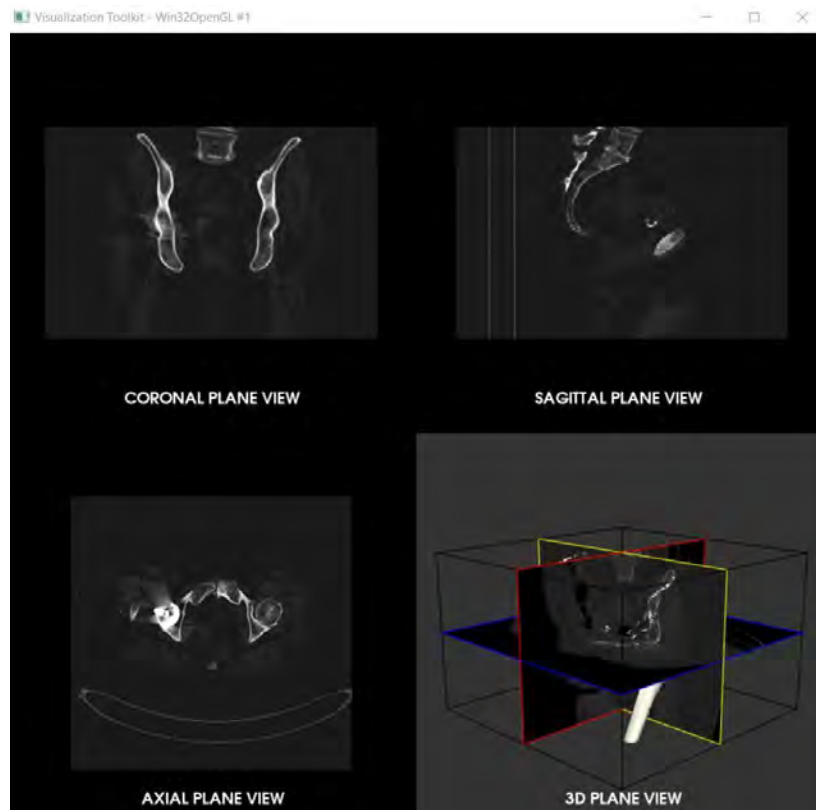
Figure 5.11. Software viewports display

Bone Segmentation

```
default_MAXvalue = 1000
default_MINvalue = 0
boneExtractor = vtk.vtkMarchingCubes()
boneExtractor.SetInputConnection(reader.GetOutputPort())
boneExtractor.SetValue(default_MINvalue, default_MAXvalue)

boneStripper = vtk.vtkStripper()
boneStripper.SetInputConnection(boneExtractor.GetOutputPort())

boneMapper = vtk.vtkPolyDataMapper()
boneMapper.SetInputConnection(boneStripper.GetOutputPort())
```

```
boneMapper.ScalarVisibilityOff()

bone = vtk.vtkActor() bone.SetMapper(boneMapper)
bone.GetProperty().SetDiffuseColor(colors.GetColor3d("Ivory"))

# Add actor to renderer

Per_Renderer.AddActor(bone)

# Create bone outline

outlineData = vtk.vtkOutlineFilter()
outlineData.SetInputConnection(reader.GetOutputPort())
outlineData.Update()
mapOutline = vtk.vtkPolyDataMapper()
mapOutline.SetInputConnection(outlineData.GetOutputPort())
outline = vtk.vtkActor()
outline.SetMapper(mapOutline)
outline.GetProperty().SetColor(colors.GetColor3d("Black"))

# Add actor to renderer

Per_Renderer.AddActor(outline)

aCamera = vtk.vtkCamera()
aCamera.SetViewUp(0, 0, -1)
aCamera.SetPosition(0.5, 0.5, -0.2)
aCamera.SetFocalPoint(0, 0, 0)
aCamera.ComputeViewPlaneNormal()
SE_Renderer.SetActiveCamera(aCamera)
SE_Renderer.ResetCamera()

# Bone volume definition

volumeMapper = vtk.vtkFixedPointVolumeRayCastMapper()
volumeMapper.SetInputConnection(reader.GetOutputPort())
volume = vtk.vtkVolume()
volume.SetMapper(volumeMapper)
```

Next coding step was to display the 3D view and for this was created a display axis definition in order to display XYZ axis, after axis definition, each plane view was defined: [YZ] corresponding to the sagittal plane, [XZ] corresponding to the coronal plane and [XY]

corresponding to the axial plane. To each plan was added an *InteractionEvent* in order to be able to move the planes along the axis.

```
def displayAXIS(reader,Renderer,colorx,colory,colorz,keyA):
    ipw = vtk.vtkImagePlaneWidget()
    ipw.SetInputConnection(reader.GetOutputPort())
    ipw.SetCurrentRenderer(Renderer)
    ipw.SetInteractor(iren)
    ipw.PlaceWidget()
    ipw.DisplayTextOn()
    ipw.EnabledOn()
    ipw.SetKeyPressActivationValue(keyA) prop
    = ipw.GetPlaneProperty()
    prop.SetColor(colorx,colory,colorz)
    ipw.SetLookupTable(ipw.GetLookupTable())

# Display X axis and its properties

ipwx = displayAXIS(reader,Per_Renderer,1,0,0,"x")
ipwx.SetPlaneOrientationToXAxes()
ipwx.SetSliceIndex(int(W/2))

# Display Y axis and its properties

ipwy = displayAXIS(reader,Per_Renderer,1,1,0,"y")
ipwy.SetPlaneOrientationToYAxes()
ipwy.SetSliceIndex(int(H/2))

# Display Z axis and its properties

ipwz = displayAXIS(reader,Per_Renderer,0,0,1,"z")
ipwz.SetPlaneOrientationToZAxes()
ipwz.SetSliceIndex(int(D/2))

def move_YZ_plane(self, event): # Sagittal plane view
    dx = ipwx.GetSlicePosition()
    center = volume.GetCenter()
    delta_x = dx - center[0]
    reslice_sag.Update()
    matrix = reslice_sag.GetResliceAxes()
    matrix.SetElement(0, 3, center[0]+delta_x)
    SliderSAG.SetValue((center[0]+delta_x)/spacing[0])
    renWin2.Render()

def move_XZ_plane(self, event): # CoRonal plane view
```

```
      dy = ipwy.GetSlicePosition()
      center = volume.GetCenter()
      delta_y = dy - center[1]
      reslice_cor.Update()
      matrix = reslice_cor.GetResliceAxes()
      matrix.SetElement(1, 3, center[1]+delta_y)
      SliderCOR.SetValue((center[1]+delta_y)/spacing[1])
      renWin2.Render()


 def move_XY_plane(self, event): # Axial plane view
      dz = ipwz.GetSlicePosition()
      center = volume.GetCenter()
      delta_z = dz - center[2]
      reslice_ax.Update()
      matrix = reslice_ax.GetResliceAxes()
      matrix.SetElement(2, 3, center[2]+delta_z)
      SliderAX.SetValue((center[2]+delta_z)/spacing[2])
      renWin2.Render()
ipwx.AddObserver("InteractionEvent",  move_YZ_plane)
ipwy.AddObserver("InteractionEvent",  move_XZ_plane)
ipwz.AddObserver("InteractionEvent", move_XY_plane)
```
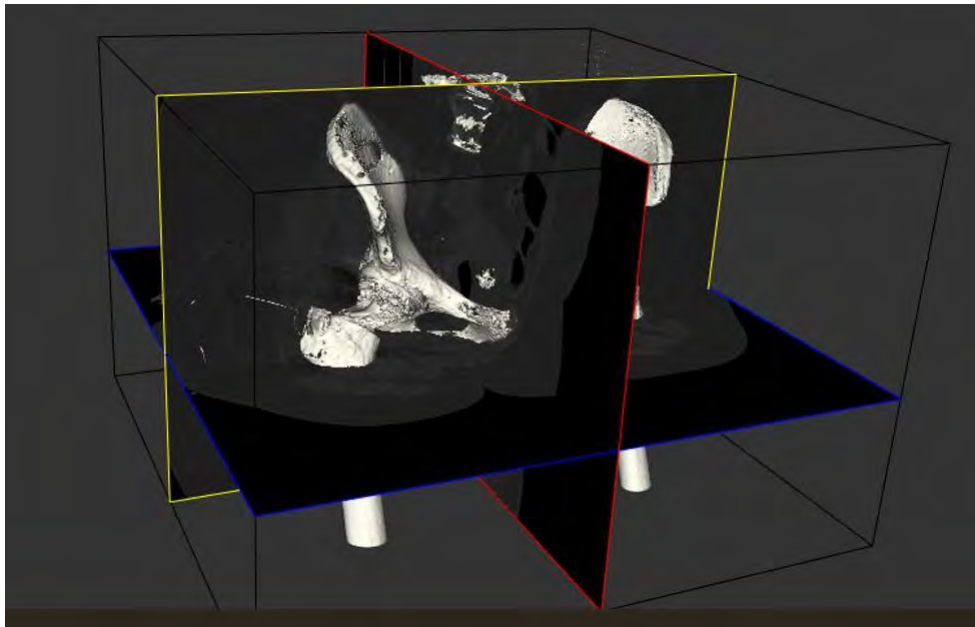

Figure 5.12. 3D view

The MPR 3D view planes are correlated with each other, by acting the mouse scroll button in the interior MPR planes (blue framed plane goes for the axial plane view, yellow framed plane goes for the coronal plane view and a red framed plane goes for the sagittal plane view), by moving the mouse the user can observe that the DICOM changes in the plane view window.

Once the 3D view display was set up, next coding part was to display the other 2D viewports: coronal view, sagittal view, and axial view. In this sense a text mapper and actor were created to display the picking results, as shown in the following code lines:

```
textMapper = vtk.vtkTextMapper()
tprop = textMapper.GetTextProperty()
tprop.SetFontFamilyToArial()
tprop.SetFontSize(15)
tprop.BoldOff()
tprop.ShadowOn()
tprop.SetColor(1, 1, 1)

textActorAX = vtk.vtkActor2D()
textActorAX.VisibilityOff()
textActorAX.SetMapper(textMapper)

pickerAX = vtk.vtkCellPicker()
```

Going further, was created text function in Python and defined for the previous text mapper used to display the picking results, as shown in the following code:

```
def annotatePickAX(object, event):
    global pickerAX, textActorAX, textMapper, pointAX
    if pickerAX.GetCellId() < 0:
        textActorAX.VisibilityOff()
    else:
        selPt = pickerAX.GetSelectionPoint() pickPos =
        pickerAX.GetPickPosition()
        textMapper.SetInput("(%.1f, %.1f, %.1f)"%pickPos)
        textActorAX.SetPosition(selPt[:2])
        textActorAX.VisibilityOn()

# Create point geometry(the coordinate)

        points = vtk.vtkPoints()
        p = pickPos
```

<p style="text-align:center">***</p>

```
# Display

        mapperPT = vtk.vtkPolyDataMapper()
        mapperPT.SetInputData(point)
        pointAX = vtk.vtkActor()
        pointAX.SetMapper(mapperPT)
```

```
        pointAX.GetProperty().SetPointSize(10)
        pointAX.GetProperty().SetColor(0, 0, 1)
        SW_Renderer.AddActor(pointAX)
pickerAX.AddObserver("EndPickEvent", annotatePickAX)
```

To view the desired orientation, a matrix was generated for each defined plane, after obtaining the volume center, as following:

```
center = volume.GetCenter() axial
= vtk.vtkMatrix4x4()
axial.DeepCopy((1, 0, 0, center[0],
         0, 1, 0, center[1],
         0, 0, 1, center[2],
         0, 0, 0, 1))


coronal = vtk.vtkMatrix4x4()
coronal.DeepCopy((1, 0, 0, center[0],
          0, 0, 1, center[1],
          0, -1, 0, center[2],
          0, 0, 0, 1))


sagittal = vtk.vtkMatrix4x4()
sagittal.DeepCopy((0, 0,-1, center[0],
           1, 0, 0, center[1],
           0,-1, 0, center[2],
           0, 0, 0, 1))
```

In the next part the slices were extracted in the desired orientation with the help of *vtkImageReslice* class reference, which reslice the volume along a set axes for each view as in the following code lines:

```
reslice_ax = vtk.vtkImageReslice()
reslice_ax.SetInputConnection(reader.GetOutputPort())
reslice_ax.SetOutputDimensionality(2)
reslice_ax.SetResliceAxes(axial)
reslice_ax.SetInterpolationModeToLinear()
reslice_sag = vtk.vtkImageReslice()
reslice_sag.SetInputConnection(reader.GetOutputPort())
reslice_sag.SetOutputDimensionality(2)
reslice_sag.SetResliceAxes(sagittal)
reslice_sag.SetInterpolationModeToLinear()
reslice_cor = vtk.vtkImageReslice()
reslice_cor.SetInputConnection(reader.GetOutputPort())
```

```
reslice_cor.SetOutputDimensionality(2)
reslice_cor.SetResliceAxes(coronal)
reslice_cor.SetInterpolationModeToLinear()
```

In order to control the grayscale level a lookup table was used to set the image intensity range and the color saturation, mapping the image through lookup table and display the image as in the following code:

```
# Grayscale lookup table

table = vtk.vtkLookupTable()
table.SetRange(0, 1000)
table.SetValueRange(0.1, 1.0)
table.SetSaturationRange(0.0, 0.0)
table.SetRampToLinear()
table.Build()

# Mapping image through lookup table

color_ax = vtk.vtkImageMapToColors()
color_ax.SetLookupTable(table)
color_ax.SetInputConnection(reslice_ax.GetOutputPort())

color_sag = vtk.vtkImageMapToColors()
color_sag.SetLookupTable(table)
color_sag.SetInputConnection(reslice_sag.GetOutputPort())

color_cor = vtk.vtkImageMapToColors()
color_cor.SetLookupTable(table)
color_cor.SetInputConnection(reslice_cor.GetOutputPort())

# Display images

actor_ax = vtk.vtkImageActor()
actor_ax.GetMapper().SetInputConnection(color_ax.GetOutputPort())
SW_Renderer.AddActor(actor_ax)
SW_Renderer.AddActor2D(textActorAX)


actor_sag = vtk.vtkImageActor()
actor_sag.GetMapper().SetInputConnection(color_sag.GetOutputPort())
Sag_Renderer.AddActor(actor_sag)

actor_cor = vtk.vtkImageActor()
actor_cor.GetMapper().SetInputConnection(color_cor.GetOutputPort())
```

```
Cor_Renderer.AddActor(actor_cor)

iren.SetPicker(pickerAX)
```
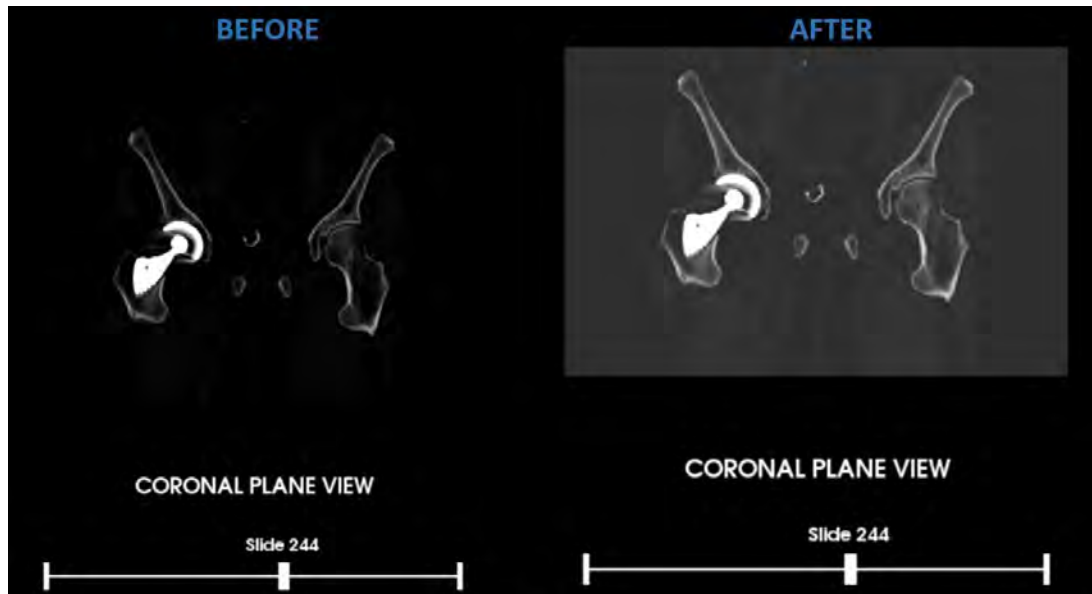

Figure 5.13. Brightness control

Each plane view gains different functions, in this sense in any plane view the user can zoom in the image by scrolling in or click right the mouse button and move it up, or zoom out by scrolling out or click right the mouse button and move it down.
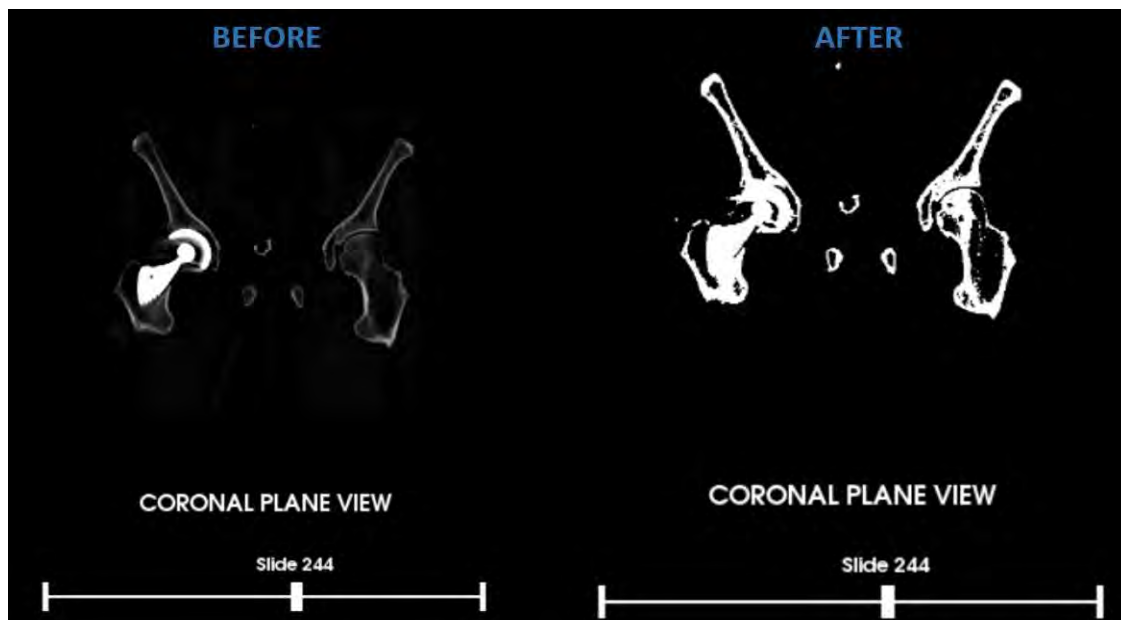
Figure 5.14. Contrast control

The brightness control can be modified by clicking the left button of the mouse and move it up and down inside the viewport and the contrast control can be modified by clicking the left button of the mouse and move it left and right in the viewport.

In order to control better the bone segmentation process based on the patients' medical condition and what we need to extract, a Housfield Units slider widget was added so in this way we can select a minimum and a maximum value in which the bone extractor can action:

```
def vtkSliderCallbackHUMax(obj, event):
    SliderMaxHU = obj.GetRepresentation()
    position = int(round(SliderMaxHU.GetValue()))

    if position <= int(round(SliderMinHU.GetValue())):
        max_val = int(round(SliderMinHU.GetValue())) + 10
        SliderMaxHU.SetValue(max_val)
    elif position < int(round(SliderMinHU.GetValue())):
        position = position
```
<div align="center">***</div>

```
# 3D view updating

    boneExtractor.SetValue(0, position)
    renWin.Render()

def winSliderHU(debut,fin,hauteur,minV,maxV,setV):
    slider = vtk.vtkSliderRepresentation2D()
    slider.SetMinimumValue(minV)
    slider.SetMaximumValue(maxV)
    slider.SetValue(setV)
    slider.GetPoint1Coordinate().SetCoordinateSystemToDisplay()
    slider.GetPoint1Coordinate().SetValue(debut, hauteur)
    slider.GetPoint2Coordinate().SetCoordinateSystemToDisplay()
    slider.GetPoint2Coordinate().SetValue(fin, hauteur)
```
<div align="center">***</div>

```
# Maximum Hounsfield slider widget

SliderMaxHU, SliderMaxHUWidget = winSliderHU(25,375,300,a1,b1,default_MAXvalue)
SliderMaxHUWidget.AddObserver("EndInteractionEvent", vtkSliderCallbackHUMax)
```
<div align="center">***</div>
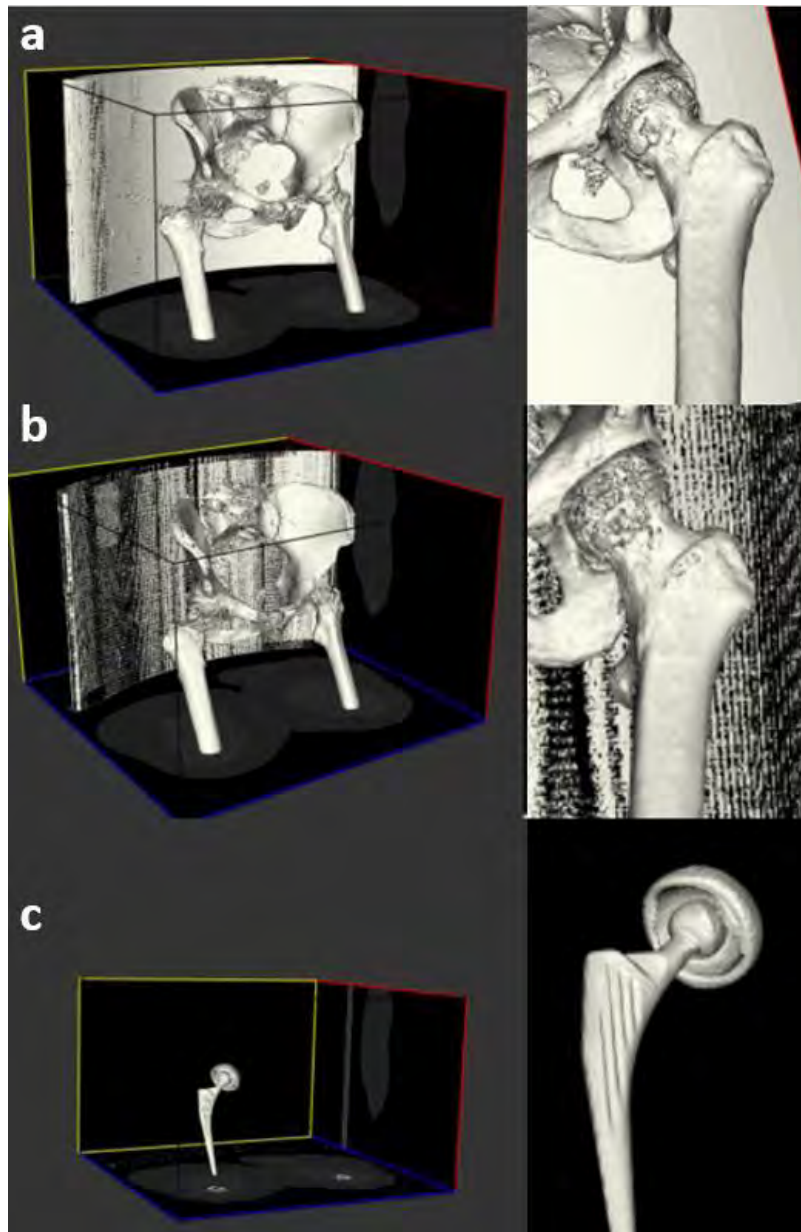
Figure 5.15. a. Bone extractor value 200HU; b. Bone extractor value 300HU; c. Bone extractor value 2000HU

Following the same principle as in the case of the Hounsfield slider widget, we create slider widget for each MPR view, which permits us to visualize all the *.dcm files from the patients' CT datasets that were imported:

```
def winSlider(debut,fin,hauteur,minV,maxV):
    slider = vtk.vtkSliderRepresentation2D()
    slider.SetMinimumValue(minV)
slider.SetMaximumValue(maxV)
slider.SetValue((minV+maxV)/2)
```

```python
slider.GetPoint1Coordinate().SetCoordinateSystemToDisplay()
slider.GetPoint1Coordinate().SetValue(debut, hauteur)
slider.GetPoint2Coordinate().SetCoordinateSystemToDisplay()
slider.GetPoint2Coordinate().SetValue(fin, hauteur)
```

***

```python
def vtkSliderCallbackCOR(obj, event):
SliderCOR = obj.GetRepresentation()

position = int(round(SliderCOR.GetValue()))
cor_rot = SliderZAXIS.GetValue()

# Update Coronal Plane view

center = volume.GetCenter()
reslice_cor.Update()
matrix = reslice_cor.GetResliceAxes()

# 3D view updating

ipwy.SetSliceIndex(int(position))
ipwy.SetPoint1(0.5*W*spacing[1]-
0.5*W*spacing[1]*np.sin((cor_rot+90)*np.pi/180),   (position-
0.5*H)*spacing[1]+0.5*H*spacing[1]+0.5*H*spacing[1]*np.cos((cor_rot+90)*np.pi/180), D*
spacing[1])
ipwy.SetPoint2(0.5*W*spacing[1]+0.5*W*spacing[1]*np.sin((cor_rot+90)*np.pi/180),   (posit
ion-0.5*H)*spacing[1]+0.5*H*spacing[1]-
0.5*H*spacing[1]*np.cos((cor_rot+90)*np.pi/180), 0          )
ipwy.SetOrigin(0.5*W*spacing[1]-
0.5*W*spacing[1]*np.sin((cor_rot+90)*np.pi/180),   (position-
0.5*H)*spacing[1]+0.5*H*spacing[1]+0.5*H*spacing[1]*np.cos((cor_rot+90)*np.pi/180), 0
     )
ipwy.UpdatePlacement()

# 3D view updating

reslice_cor.Update()
matrix = reslice_cor.GetResliceAxes()
matrix.SetElement(0, 0, np.sin((cor_rot+90)*np.pi/180))
matrix.SetElement(1, 2, np.sin((cor_rot+90)*np.pi/180))
matrix.SetElement(1, 0, -np.cos((cor_rot+90)*np.pi/180))
matrix.SetElement(0, 2, np.cos((cor_rot+90)*np.pi/180))
if position >= H/2:
matrix.SetElement(1, 3, center[1]+spacing[1]*(position-H/2))
```

```
else:
matrix.SetElement(1, 3, center[1]-spacing[1]*(H/2-position))
renWin.Render()

def vtkSliderCallbackAX(obj, event):
SliderAX = obj.GetRepresentation()

position = int(round(SliderAX.GetValue()))
ax_rot = SliderAXRot.GetValue()
```

***

```
# Coronal view slider

SliderCOR, SliderCORWidget = winSlider(25,375,700,0,H)
SliderCORWidget.AddObserver("EndInteractionEvent", vtkSliderCallbackCOR)
```

***

Following the same code flow as in the previsions case the oblique MPR view was created for each plane view, in this way the user can eventually correct the patient posture during the tomography examination, helping him to evaluate better the patient medical condition. In order to correlate the MPR views with the slider and also with the 3D view, for each axis the plane views were resliced with the help of *vtkImageReslice* class reference and create a 3D display for each plane view.
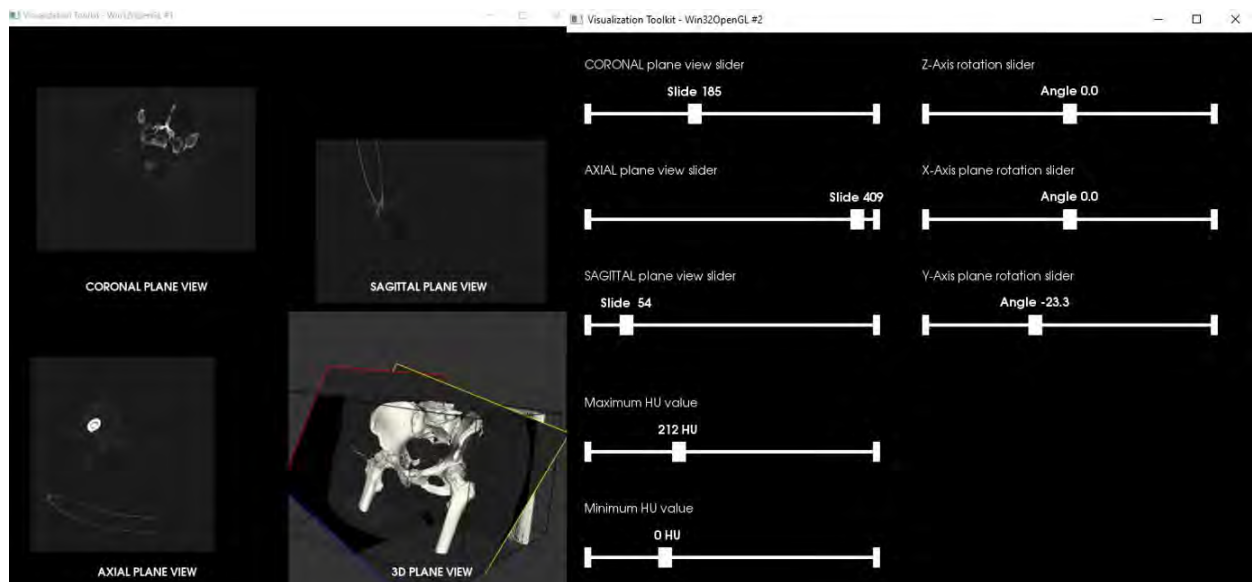
Figure 5.16. Code running visualization
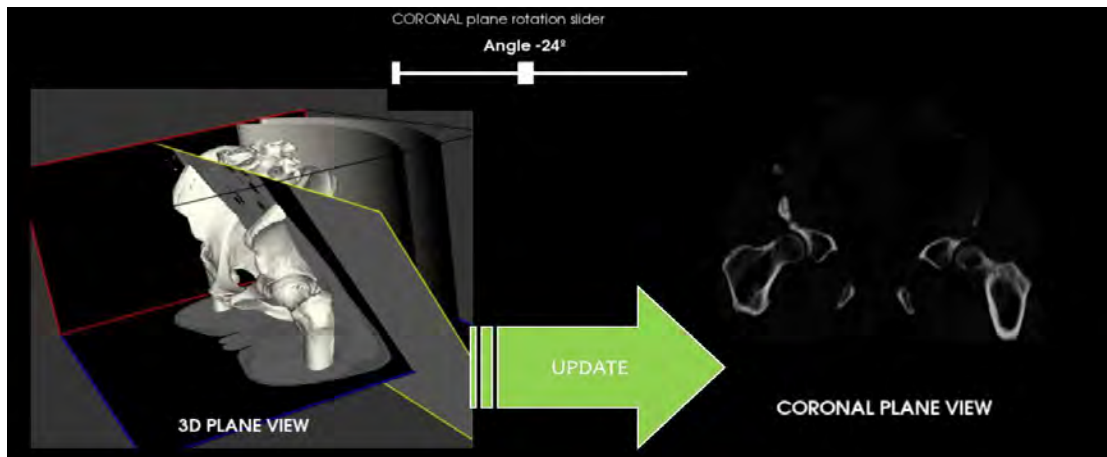
Figure 5.17. Coronal plane rotation slider interaction

To verify if the code can realize the bone segmentation on different medical cased patients, the debugging was run for three case patients:
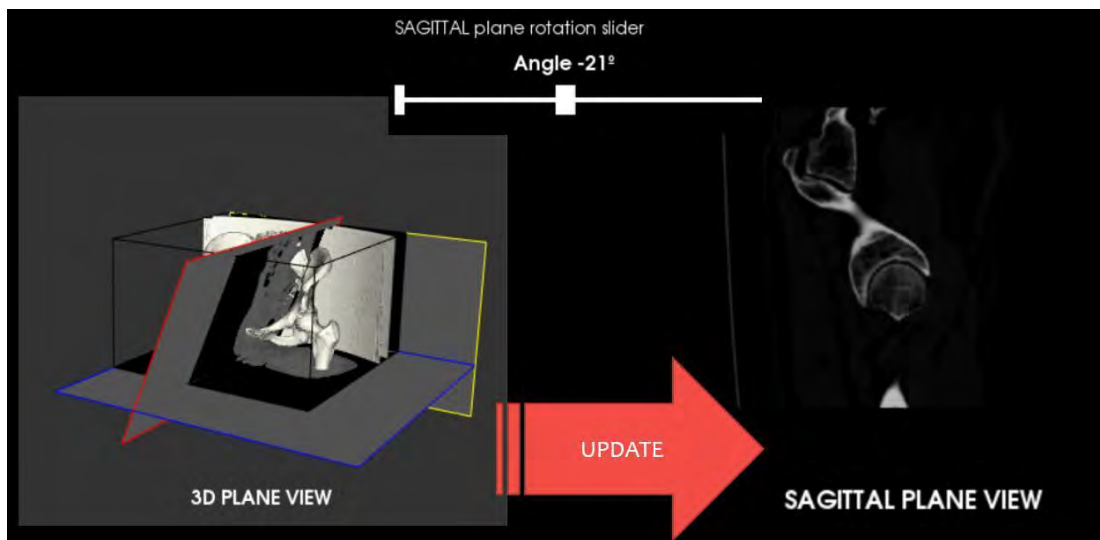
Figure 5.18. Sagittal plane rotation slider interaction

For each slider widget an identification text was added as following:

```
def winTitle(titre,debut,hauteur,NumRenderer):
title = vtk.vtkTextActor() title.SetInput(titre)
title.GetTextProperty().SetColor(colors.GetColor3d('White'))
title.GetTextProperty().SetFontFamilyToArial()
title.GetTextProperty().SetFontSize(14)
title.SetDisplayPosition(debut,hauteur)
NumRenderer.AddActor(title)
```

winTitle("CORONAL plane view slider",25,750,Renderer2)
winTitle("Z-Axis rotation slider",425,750,Renderer2)
winTitle("AXIAL plane view slider",25,625,Renderer2)

winTitle("X-Axis plane rotation slider",425,625,Renderer2)
winTitle("SAGITTAL plane view slider",25,500,Renderer2)
winTitle("Y-Axis plane rotation slider",425,500,Renderer2)
winTitle("Maximum HU value",25,350,Renderer2)
winTitle("Minimum HU value",25,225,Renderer2)
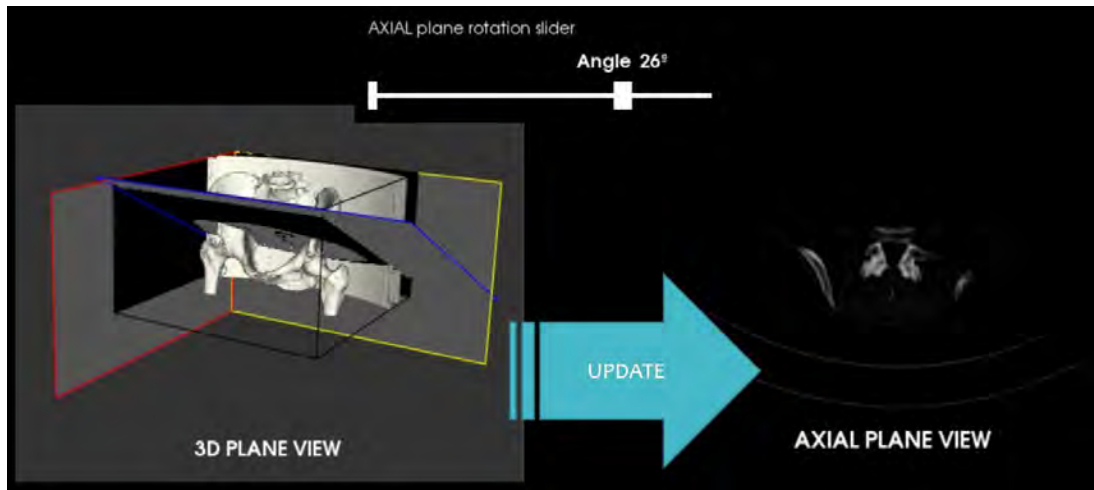
Figure 5.19. Axial plane rotation slider interaction

a.   Patient with hip stem prosthesis
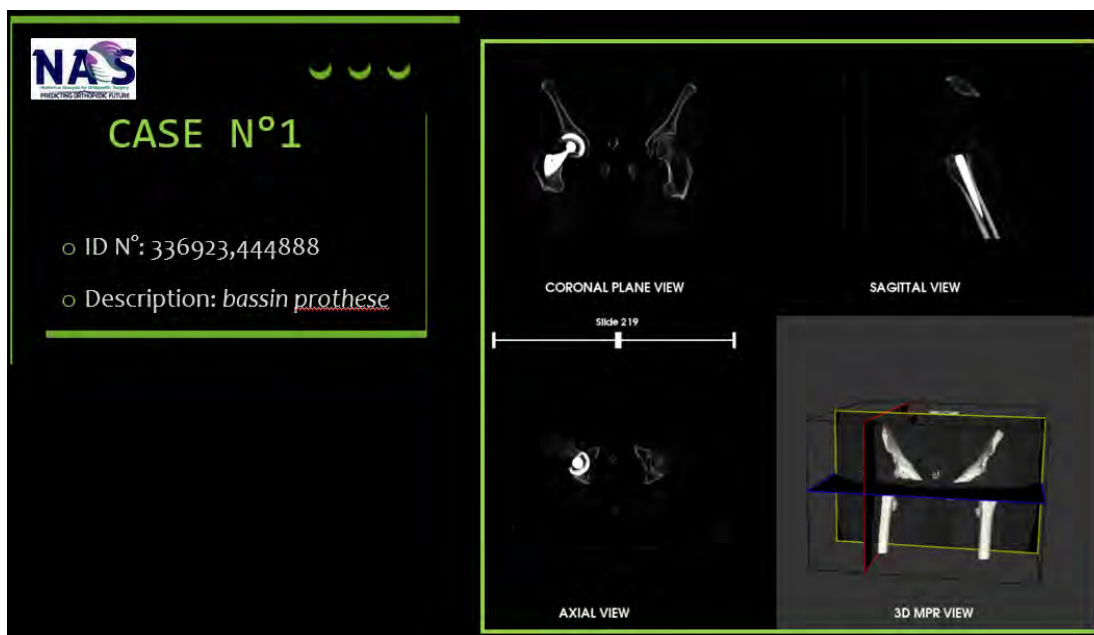
Figure 5.20. MPR visualization in case of a patient with THR

b.   *Patient with arthritis*
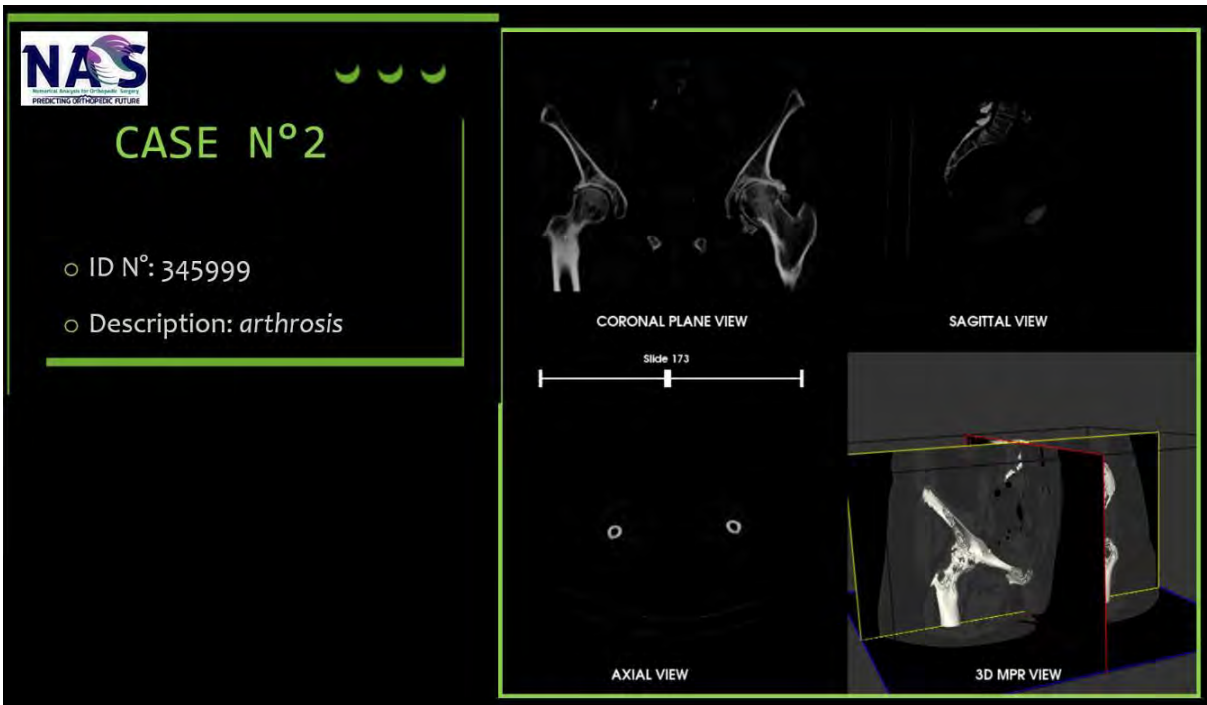
Figure 5.21. MPR visualization in case of a patient diagnosed with arthritis

c.   *Patient with healthy hip joint*
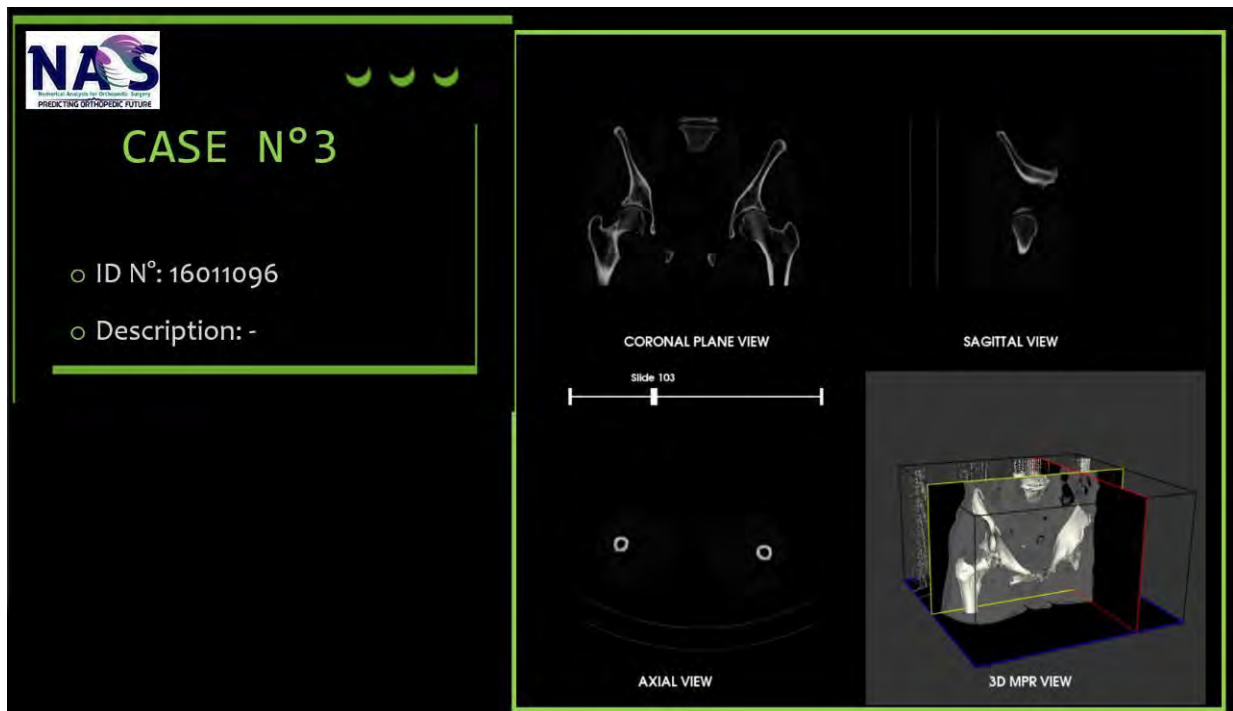
Figure 5.22. MPR visualization in case of a patient with healthy hip joint

5.2.2. *Developing the bone isolation module*

This software module was made with the help of image processing algorithms, namely bone segmentation based on region growing, this method being a contour-based segmentation, which find the boundaries between different regions and connect the threshold if they share similarities. One of the most important property of a region is the homogeneity and consists of main criterion in region growing bone segmentation process because it divides in different areas of homogeneity. In this case because was considering for CT scans, the homogeneity criterion is based on gray level. It starts with a selected voxel or a selected group of voxels and increases all the neighboring voxels, if one of these voxels meets the same criterion as the selected one, it will be added to the group of voxels already formed. The process is repeated until there are no voxels add into the group because they don't share the same criterion with the other voxels.

Following the same idea, a code was developed with the help of the following python libraries: *os*, *numpy*, *SimpleITK*, *glob*, *matplotlib*, *pyplot* and *vtk* (*vtkConstants*). The DICOMs path is defined, in this way the user can select the patient's CT scans datasets, but as in the previous code case we must define a lower value and an upper value, the best practice being between 200 and 2000HU, in order to select only the bone tissue.

Because we want to select the voxels, a function which allows to display the CT scan slides and recover the selected voxel by clicking inside the displayed image but also delete them was developed as in the following code:

```
def sitk_show(img, idxSlice):

    def on_click(event):
        if radio.value_selected == my_list[0]:
        if event.inaxes is ax:
            global coords, imgSegmented, boneSegmented
            ix, iy = event.xdata, event.ydata
            coords.append((int(round(ix)), int(round(iy)), int(sliderSliceNumber.val)))
            ax.scatter(ix,iy, alpha=0.75)
            plt.draw()
            img = SimpleITK.ConnectedThreshold(image1=imgOriginal,
                            seedList=coords,
                            lower=lowerValue,
                            upper=upperValue,
                            replaceValue=1)
            imgOriginalIntensity = SimpleITK.Cast(SimpleITK.RescaleIntensity(imgOriginal), i
mg.GetPixelID())
            imgSegmented = SimpleITK.LabelOverlay(imgOriginalIntensity, "cubehelix_r")
            dicomImages = SimpleITK.GetArrayFromImage(imgSegmented[:,:,int(sliderSliceNu
mber.val)])

            boneSegmented = []
            boneSegmented = SimpleITK.Cast(img, imgOriginal.GetPixelID())
```

```
ax.imshow(dicomImages)
fig.canvas.draw_idle()

if 'imgSegmented' in globals():
    return coords, imgSegmented, boneSegmented


if radio.value_selected == my_list[1]:
    if event.inaxes is ax:
        global coords_segm
        ix, iy = event.xdata, event.ydata
        coords_segm.append((int(round(ix)), int(round(iy)), int(sliderSliceNumber.val)))
        ax.scatter(ix,iy,color='red', alpha=0.75, s=radius*20)
        plt.draw()
        return coords_segm
```

An update function has been defined to be able to return to the initial conditions in case we want to segment or delete the chosen voxels preparing the dataset for a new selection. After defining the previous function, two buttons were created, one button is acting the bone segmentation process, and the other button is creating a pop-up window with the visualization of the 3D model, as following:

```
segmentationAx = plt.axes([0.27, 0.08, 0.15, 0.05])
buttonSegment = Button(segmentationAx, 'Run Segmentation', color=axcolor, hovercolor='0.8
25')


visualizationAx = plt.axes([0.65, 0.08, 0.15, 0.05])
buttonVisualization = Button(visualizationAx, 'Visualization', color=axcolor, hovercolor='0.82
5')
```
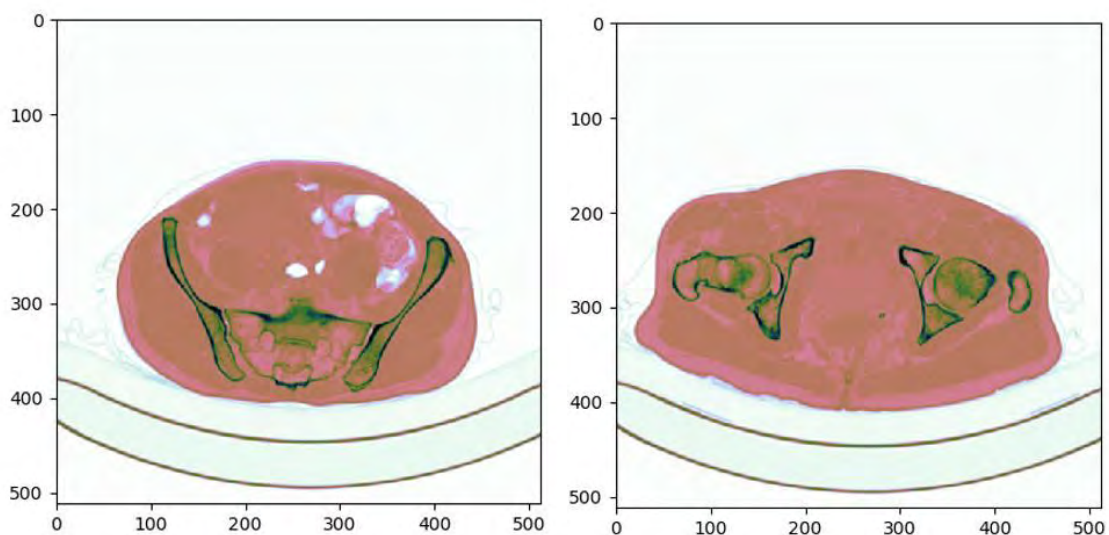

Figure 5.23. CT dataset visualization in the axial plane

For a better CT dataset visualization in the axial plane, the "*cubehelix_r*" color theme was chosen, in this way the user can easily identify the difference between the soft tissues (light pink) and the bone tissue (dark green).

In order to run the desired process for each button was defined an event that which proceeds the bone segmentation by applying the *Region Growing* algorithm, and another one that open the visualization of the bone segmentation results, as following:

```
def segment(event):
    global dicomImages, imgSegmented, img, boneSegmented
    ax.clear()
    for i in range (len(coords_segm)):
        x0 = coords_segm[i][0]
        y0 = coords_segm[i][1]
        z0 = coords_segm[i][2]
        for x in range(x0-radius, x0+radius+1):
            for y in range(y0-radius, y0+radius+1):
                for z in range(z0-radius, z0+radius+1):
                    deb = radius*radius - (x0-x)*(x0-x) - (y0-y)*(y0-y) - (z0-z)*(z0-z)
                    if (deb)>=0:
                        imgOriginal[x,y,z] = int(0)
    img = SimpleITK.ConnectedThreshold(image1=imgOriginal,
                    seedList=coords,
                    lower=lowerValue,
                    upper=upperValue,
                    replaceValue=1)
    imgOriginalIntensity = SimpleITK.Cast(SimpleITK.RescaleIntensity(imgOriginal), img.GetPixelID())
    imgSegmented = SimpleITK.LabelOverlay(imgOriginalIntensity, img)
    dicomImages = SimpleITK.GetArrayFromImage(imgSegmented[:,:,int(sliderSliceNumber.val)])

    boneSegmented = []
    boneSegmented = SimpleITK.Cast(img, imgOriginal.GetPixelID())

    ax.imshow(dicomImages)
    fig.canvas.draw_idle()
    return dicomImages, imgSegmented, boneSegmented

    def visualization(event):
        def numpy2VTK(img,spacing=spacing):
            importer = vtk.vtkImageImport()
            img_data = img.astype('uint8')
            img_string = img_data.tostring() # type short
            dim = img.shape
            importer.CopyImportVoidPointer(img_string, len(img_string))
```

```
importer.SetDataScalarType(VTK_UNSIGNED_CHAR)
importer.SetNumberOfScalarComponents(1) extent =
importer.GetDataExtent()
importer.SetDataExtent(extent[0], extent[0] + dim[2] - 1,
   extent[2], extent[2] + dim[1] - 1, extent[4], extent[4] +
dim[0] - 1) importer.SetWholeExtent(extent[0], extent[0] +
                      dim[2] - 1,
           extent[2], extent[2] + dim[1] - 1,
           extent[4], extent[4] + dim[0] - 1)
importer.SetDataSpacing(spacing[0], spacing[1], spacing[2])
return importer
```
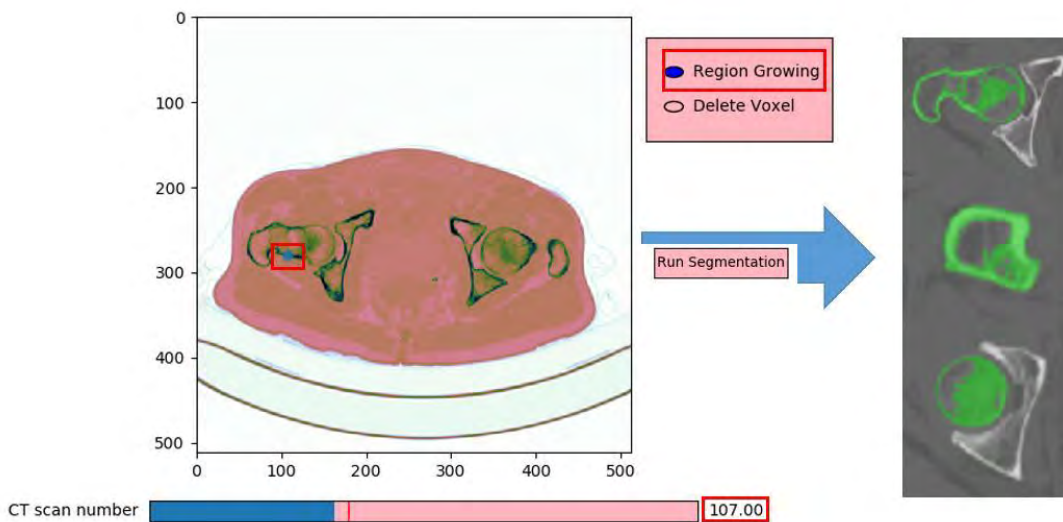

Figure 5.24. Bone segmentation with Region Growing method

The results visualization was made with the help of *VTK library*, first we converted the *simpleITK* image in *numpy*, the segmented bone is returning at the initial values and then was used a *numpy* to *VTK* function to import the segmented region. As in the previous subchapter code a rendering window and a renderer was created with a *vtkRenderWindowInteractor* class reference.

As in the case of the MPR view code, also this code has been checked to see if it works for patients with different medical conditions: healthy hip joint, patient with THR surgery and patient with arthritis. The results can be observed in *Figure 5.25*.

Following the code testing, certain limitations can be observed in the case of patients with poor bone quality (case b. and c. from *Figure 5.27*) because of the mechanical wear of the hip joint, the femur and pelvis appearing connected to each other, so the algorithm perceives the pelvis as part of the same group of voxels. The obtained results can be subsequently exported and used in dedicated software, in which the surface can be refined with other algorithms, it can be used in virtual biomechanical studies, or it can be used to perform a 3D virtual preoperative planning for the patient.
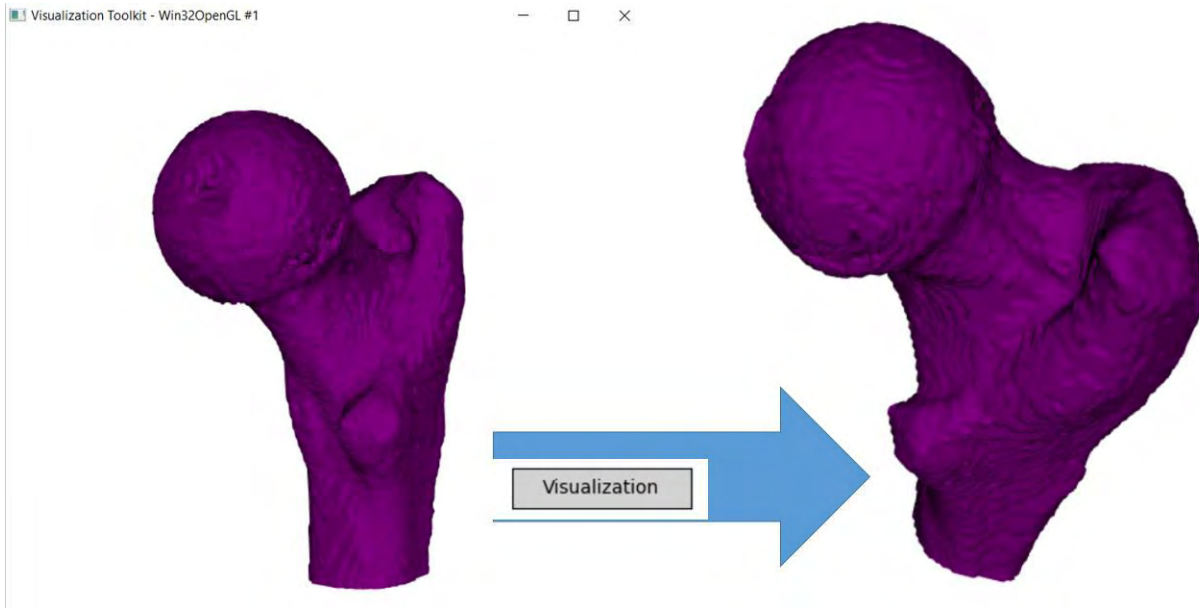
Figure 5.25. Bone segmentation results visualization with VTK

5.2.3. Developing the custom hip stem geometry

For the hip stem geometry modification Gmsh open source software was used, which is a software that generates three-dimensional meshes. The software contains instruments that allows to transform the imported CAD model, but also can generate the model's script, allowing the users to modify it and generate the model based on the changes that the user made in the script. In this sense the 3D model of a hip stem was used as a template to be modified and make possible a geometrical personalization based on patient's CT landmarks. The file extension used to import the femoral stem model was *.stp, a three-dimensional graphic extension used by CAD software to collect the image data in format ASCII, as the standards are defined in ISO-10303-21.
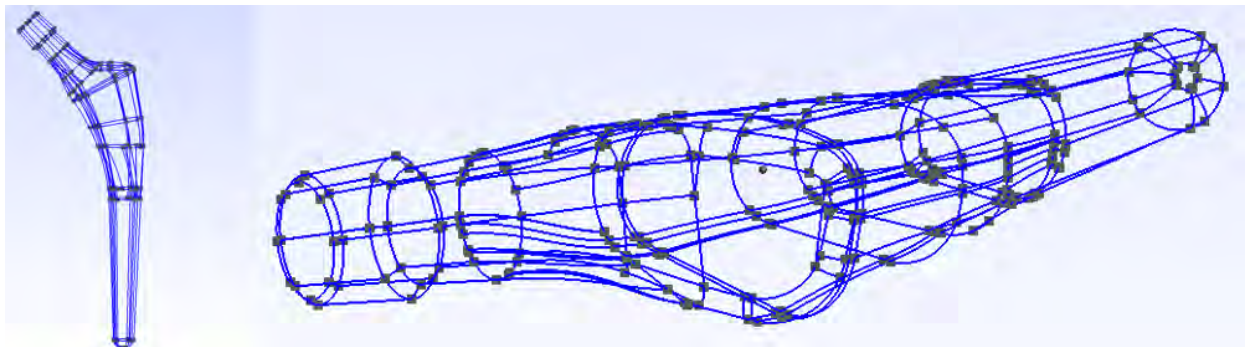
Figure 5.26. Femoral hip stem template imported in Gmsh
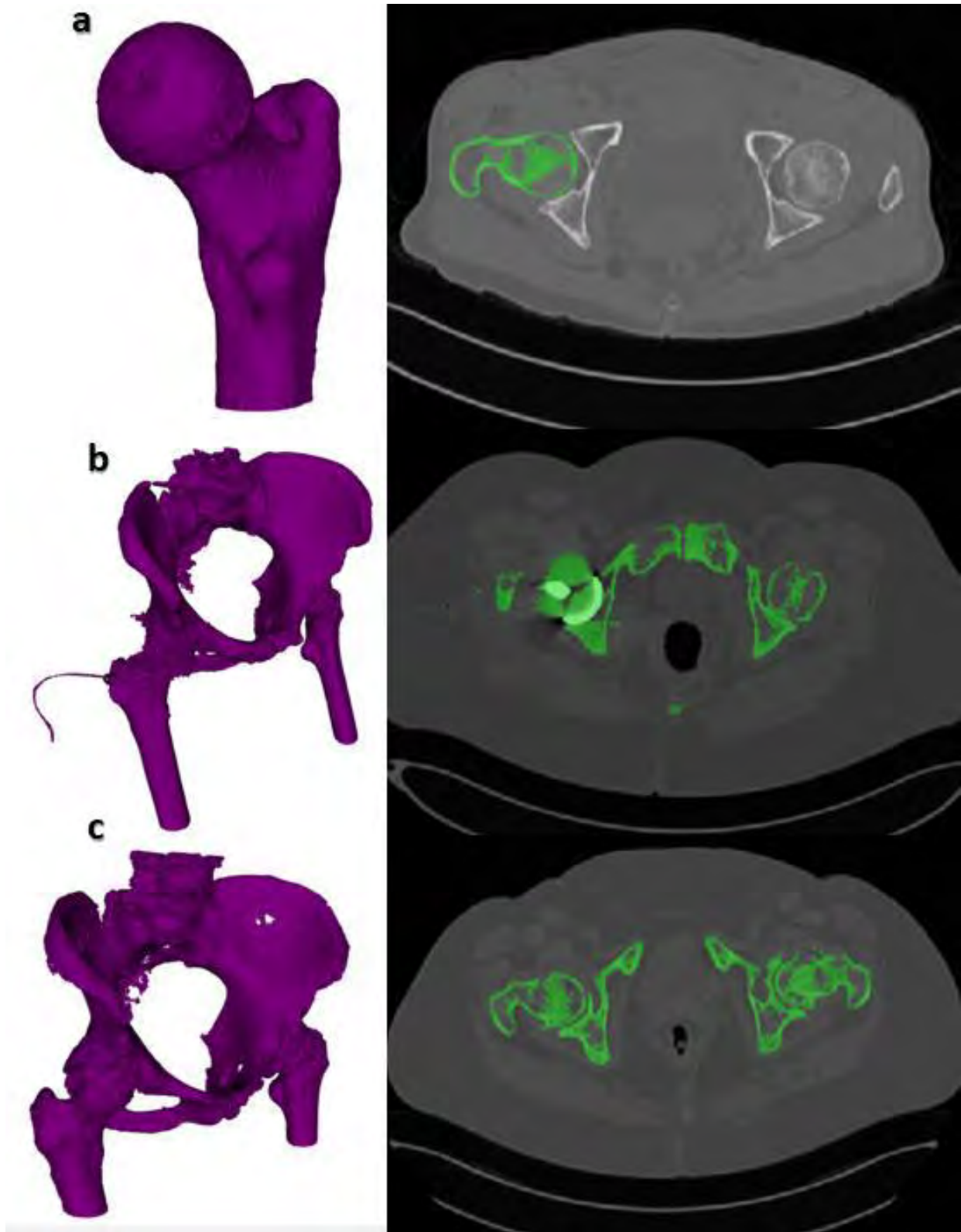
Figure 5.27. a. Healthy hip joint; b. Patient with THR surgery; c. Patient with arthritis

After importing the hip stem geometry, by following the *Geometry* menu, we can access the *Edit Script* option which pops-up a *Notepad* window that contains all the image data from the CAD file. The script contains 15716 code line divided in:

a.   *Cartesian Point* (vertex or control point)
#CARTESIAN_POINT('ControlPoint',(4.65733268297,0.723814595911,3.40468924644))

b.   *Direction* (axis direction, vector direction)
#DIRECTION('Axis2P3DDirection',(0.697824494384,-0.161105478742,-0.697915467487))

c.   *Axis placement* (for plane or circle)
#AXIS2_PLACEMENT_3D('Plane Axis2P3D',#52,#53,#54)

d.   *Oriented edge*
#ORIENTED_EDGE('',*,*,#65,.F.)

e.   *Advanced faces*
#ADVANCED_FACE('Corps principal',(#15269),#15168,.T.)

f.   *Spline curves*
#B_SPLINE_CURVE_WITH_KNOTS('',4,(#528,#529,#530,#531,#532),.UNSPECIFIED.,.F.,.U.
,(5,5),(26.4073012454,30.8113551361),.UNSPECIFIED.)

g.   *Spline surface*
#1524=B_SPLINE_SURFACE_WITH_KNOTS('',5,4,((#1525,#1526,#1527,#1528,#1529),(#1530,#1531,#1532,#1533,#1534),(#1535,#1536,#1537,#1538,#1539),(#1540,#1541,#1542,#1543,#1544),(#1545,#1546,#1547,#1548,#1549),(#1550,#1551,#1552,#1553,#1554)),.UNSPECIFIED.,.F.,.F.,.U.,(6,6),(5,5),(0.,8.18367565731),(0.,4.37645950379),.UNSPECIFIED.)

h.   *Edge curves*
#EDGE_CURVE('',#62,#64,#60,.T.)

i.   *Edge loop*
#EDGE_LOOP('',(#13180,#13181,#13182,#13183,#13184))

j.   *Face outer bound*
#FACE_OUTER_BOUND('',#5209,.T.)

k.   *Lines*
#LINE('Line',#1405,#1407)

l.   *Planes*
#PLANE('',#939) ;

m.   *Vertex points*
#VERTEX_POINT('',#14546)

All the graphic entities listed above contribute to the generation of the femoral hip stem geometry used as a template in this study. To personalize the geometry, it was opted for the geometric transformation in three directions as represented in *Figure 5.28*.

To transform the geometry of the stem, it was necessary to identify the vertices that can be modified and those that will remain unchanged, more precisely to which vertices will be applied changes of the coordinates in order to obtain the desired transformation.

In case of the first transformation, the femoral stem radius, the following vertex were identified with the following positions:

-        Point 117(-23.4407, 2.8781, 112.4325);
-        Point 118(-20.9599, 9.1927, 113.5393);
-        Point 122(-21.2802, -1.3301, 113.7101);
-        Point 140(-16.2971, 2.001, 100.6147);
-        Point 141(-13.8797, 6.752, 101.0112);

- Point 145(-15.0426, -1.9493, 100.8936);
- Point 161(-10.2846, 5.5323, 92.1);
- Point 163(-12.5404, 1.5397, 92.1);
- Point 168(-11.7806, -2.1925, 92.1).
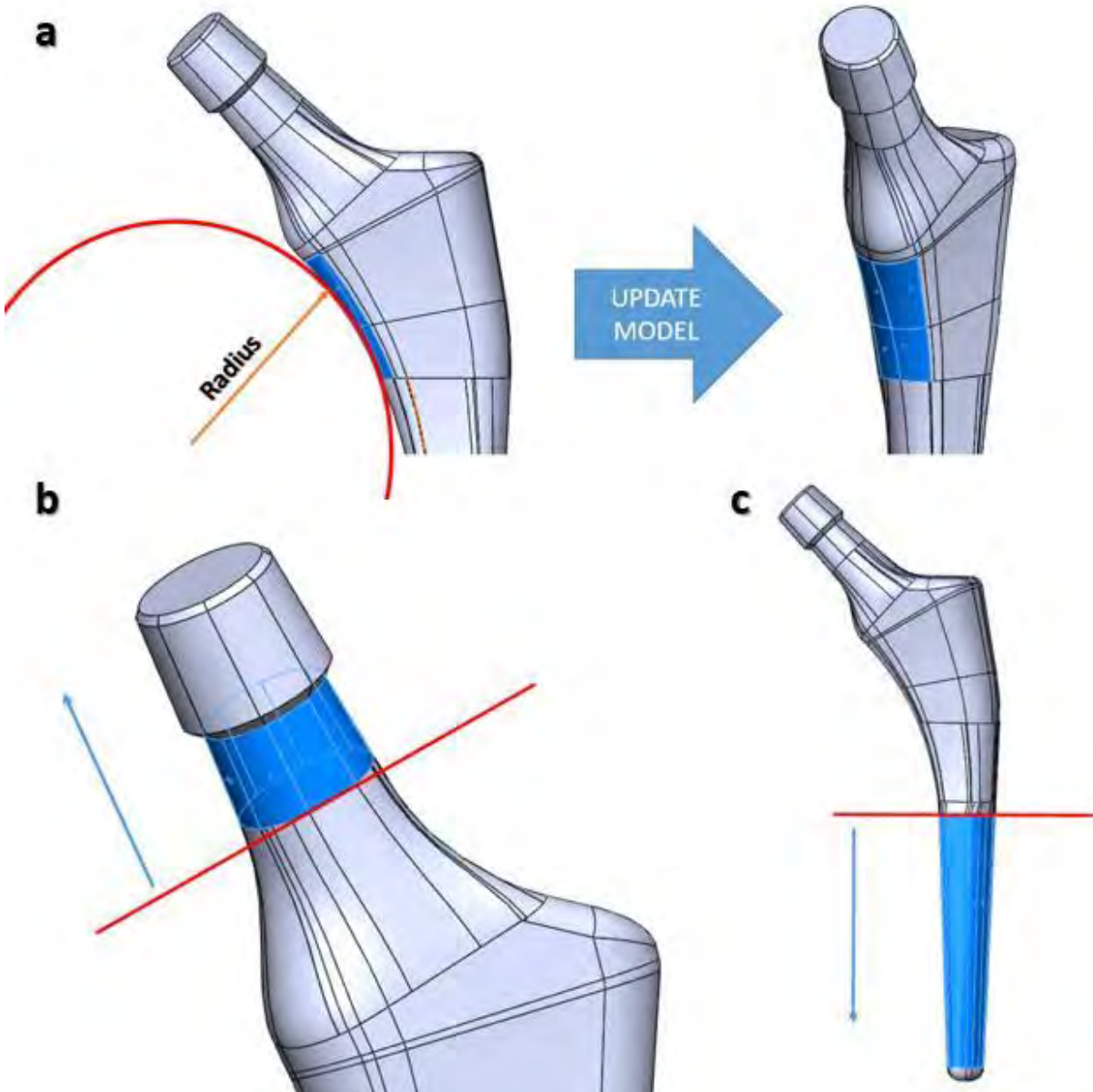
Figure 5.28. Hip stem geometrical transformation. a. Femoral stem anatomical radius; b. Femoral stem neck length; c. Femoral stem length

To control the transformation the vertices were identified first and then all the control points used to build the splines and the surfaces. After the identification, changes were applied only at the X coordinate, in this way we can increase or decrease the femoral stem radius contact with the

femur canal radius so that it can match. For example, if the user wants to modify by adding 2 mm to point 140, 141 and 145, in the script was made the following changes:
#7981=CARTESIAN_POINT('Vertex',(-16.2971940902+n,2.00104382031,100.614777388));
#7971=CARTESIAN_POINT('Vertex',(-13.8797224724+n,6.75206133508,101.011261194));
#8218=CARTESIAN_POINT('Vertex',(-15.0426453526+n,-1.94930566629,100.893684639)).

Where *n* represents the length with which the femoral stem must be enlarged in each Cartesian point.
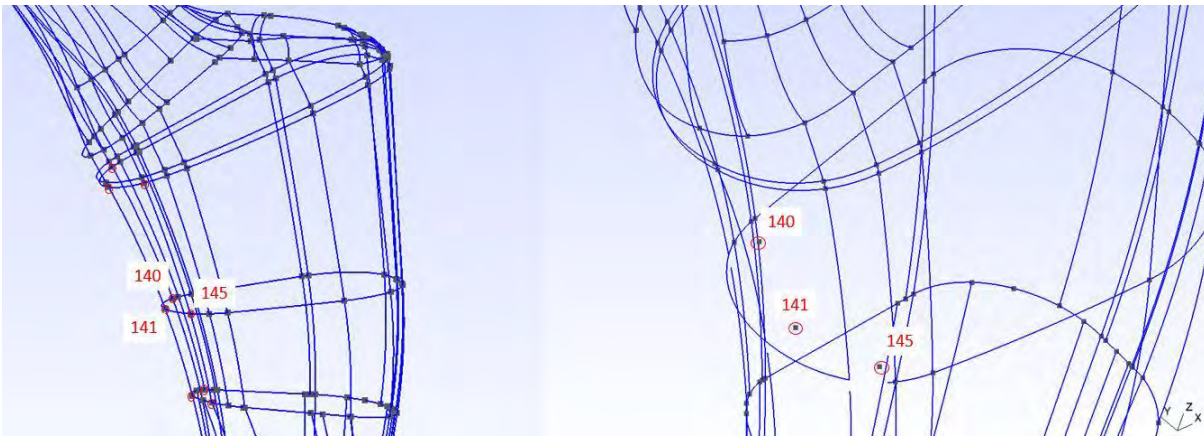
Figure 5.29. Applied transformation for vertices 140, 141 and 145 (before and after)

The result of the X coordinate modification for vertices 140, 141 and 145 can be visualized in *Figure 5.29*.

Consequently, the new coordinates of vertices 140, 141 and 145 will be:
#7981=CARTESIAN_POINT('Vertex',(-14.2971940902,2.00104382031,100.614777388));
#7971=CARTESIAN_POINT('Vertex',(-11.8797224724,6.75206133508,101.011261194));
#8218=CARTESIAN_POINT('Vertex',(-13.0426453526,-1.94930566629,100.893684639)).

In case of the stem neck length transformation all the superior part that includes also the hip stem head vertices were identified together with their control points that determine the formation of splines and surfaces, while the lower part of the stem neck was blocked, the coordinates remained unchangeable.

In case of this transformation of the neck stem length, the following vertex were identified with the following coordinates:
  – Point 28(-37.0473, 2.9041, 140.0129);
  – Point 29(-34.0351, 3.8373, 142.8093);
  – Point 31(-32.2724, 11.4708, 142.8096);
  – Point 32(-34.5701, 13.6298, 140.0138);
  – Point 33(-37.5821, 12.6968, 137.2176);
  – Point 35(-39.5917, 9.1239, 136.033);
  – Point 36(-39.345, 5.0633, 137.217).

The following vertices were identified, and transformation was applied to the Z coordinates:

#1097=CARTESIAN_POINT('Vertex',(-37.0473352176,2.90414160829,140.012912783+n));
#1099=CARTESIAN_POINT('Vertex',(-34.0351352957,3.83730337812,142.809310778+n));
#1217=CARTESIAN_POINT('Vertex',(-32.272494585,11.4708834985,142.809600617+n));
#1272=CARTESIAN_POINT('Vertex',(-34.5701453038,13.6298915176,140.013868093+n));
#1327=CARTESIAN_POINT('Vertex',(-37.582170833,12.6968845126,137.217608742+n));
#1409=CARTESIAN_POINT('Vertex',(-39.591728501,9.1239783367,136.033076343+n));
#1461=CARTESIAN_POINT('Vertex',(-39.3450748045,5.06336513667,137.217041655+n)) .

Where n represents the length with which the femoral stem must be enlarged.
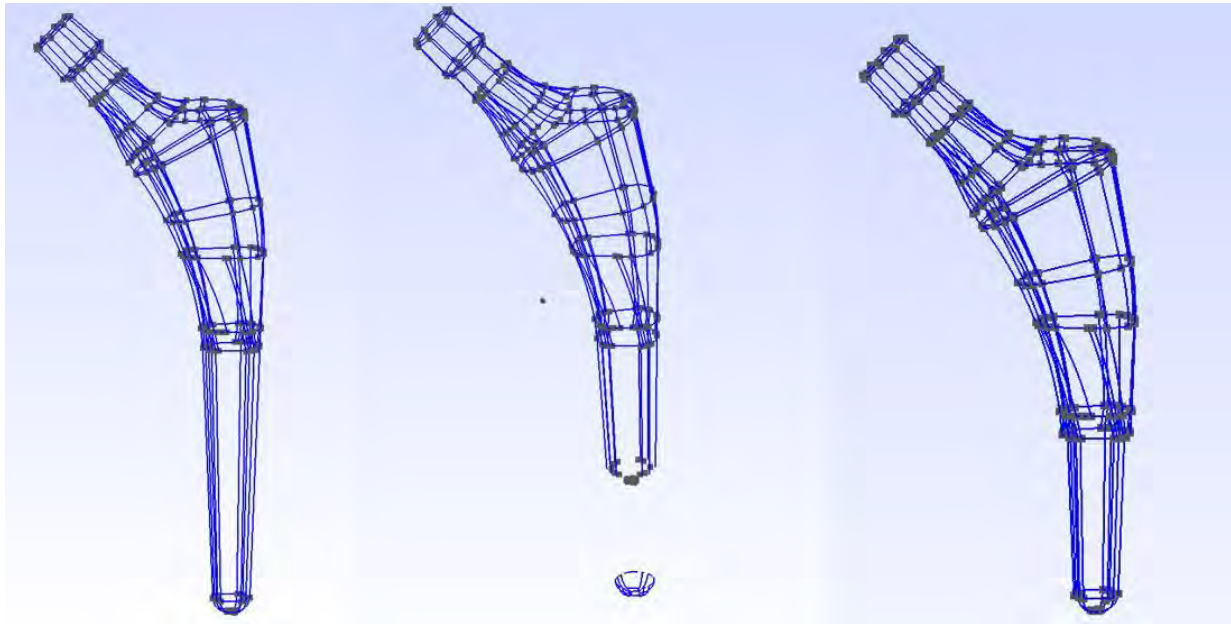
Figure 5.30. Femoral stem length shortness with 30 mm

In case of the hip stem length was proceeded in the same manner, the following points were identified and the position of each one: 247, 248, 250, 253, 254, 255, 256, 262, 261, 270, 271, 272, 273, 274, 275, 276, 277, 280, 281 and 285. After identifying the vertices and control points, the transformation was applied at the Z coordinate as in the following example:

#12838=CARTESIAN_POINT('Vertex',(-3.10855130771,3.58356650813,3.46586217414+n));
#12840=CARTESIAN_POINT('Vertex',(-4.00414578389,2.50580829015,3.42603159097+n));
#12905=CARTESIAN_POINT('Vertex',(1.92463874916,4.40217251366,3.46095521427+n));
#13080=CARTESIAN_POINT('Vertex',(-4.68114201934,1.17571956364E-015,3.41372327772+n));
#13158=CARTESIAN_POINT('Vertex',(-3.10855165354,-3.58356618407,3.46586217965+n));
#13160=CARTESIAN_POINT('Vertex',(1.92463428259,-4.40217459775,3.46095516911+n));
#13223=CARTESIAN_POINT('Vertex',(-4.00414318503,-2.50581279493,3.42603170808+n));
#13523=CARTESIAN_POINT('Vertex',(3.28038888121,-3.48088716487,3.41477095162+n));
#13525=CARTESIAN_POINT('Vertex',(4.68971213303,2.7043440419E-015,3.40443672749+n));
#14169=CARTESIAN_POINT('Vertex',(3.28038802621,3.48088803573,3.41477098887+n)).

Where n represents the length with which the femoral stem must be enlarged.

If these vertices and control points are modified for example, with 30 mm the obtained results will look like in *Figure 5.30*.

The script coordinate points which are supposed to be changeable can be imported in an excel file, where an algorithm that changes only the desired coordinates. After the script is changed it can be saved in a *.txt file and opened with Gmsh. Different other CAD software can be also used to change the file extension so it can be imported into dedicated software that prepare surfaces for the 3D printing process.

5.3.   Interface proposal for the medical software

A relatively user-friendly alternative to a software interface is the PyQt, which represents a Python binding for the Qt toolkit with the GUI cross-platform. The interface can be generated by Qt Designer software, where the user can add different type of widgets.

In order to start creating an interface example for the medical software a new main window was created in Qt Designer and a new resource file, where the user can add all the icons that he would like to use in the interface. In order to generate a resource file the NAOS logo was copied in the interface folder in *.jpg extension, after the file extension was changed in *NAOS.qrc* and used as a resource.

After the project was created with Qt Designer the user can start to add widgets on the main window such as: tool bars, adding actions to be used on the toolbar (generate 3D view, refresh, new study, import, exit) but also choosing the icon paths in order to be shown, adding containers to the MPR view and also sliders for each frame or text boxes.

Figure 5.31. Icons created for the NAOS interface. a. 3D view generation; b. Refresh button; c. New study button; d. Import DICOM path; e. Exit software

The following windows were created and renamed as follows:
–   NAOS_MainWindow, dimensions and location: [(0,0),1367x891];
–   NAOS_CentralWidget, dimensions and location: [(0,26),1367x840];
–   NAOS_MenuBar, dimensions and location: [(0,0),1367x26];
–   NAOS_StatusBar, dimensions and location: [(0,866),1367x25];
–   NAOS_scrollArea, dimensions and location: [(11,11),1345x818];
–   NAOS_tabWidget, dimensions and location: [(11,11),1321x794].

In addition, three tab widgets were created with the following name and dimensions:
–   MPR_tab, dimensions and location: [(0,0),1315x769];
–   BoneSegmentation_tab, dimensions and location: [(0,0),1315x769];

    – CustomHipStem_tab, dimensions and location: [(0,0),1315x769].

    The first tab can contain the multi-planar representation view (coronal view, axial view, and sagittal view), in addition the perspective or 3D view. For each view frame sliders were designed in order to move from one DICOM to another, but also two sliders for the HU units and a toolbox with display slice planes. The bone segmentation tab contains one frontal view, the coronal plane view in this study case, two buttons for the *region growing* algorithm and *delete region growing*, a DICOM slider in order to verify the segmentation quality, and a view segmentation button that generates a new window in which the user can visualize the three dimensional piece. The custom stem tab can contain a figure in which there are represented the parameters that the user can change and three boxes in which you can insert the dimension.
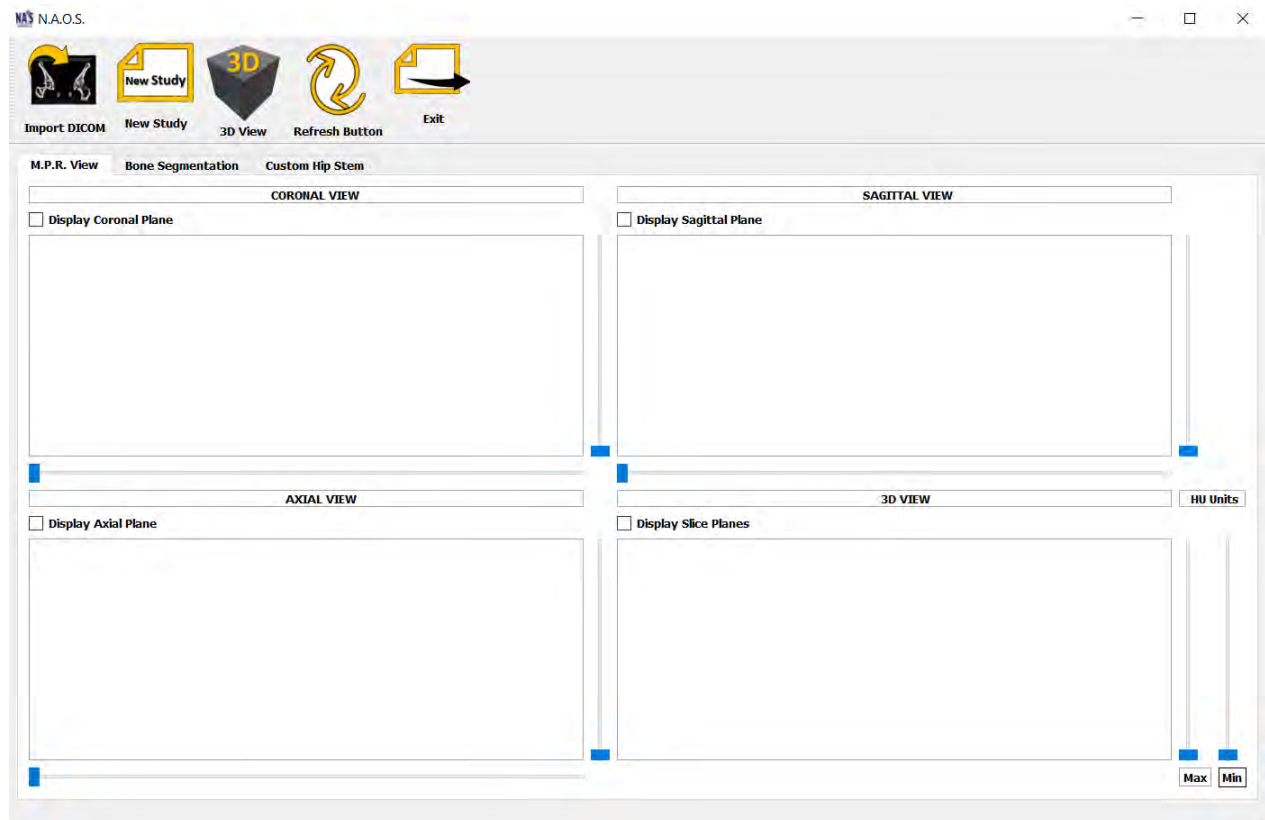
Figure 5.32. NAOS interface proposal generated with Qt Designer

    To be read by Python, the project must be exported in *.ui extension. The file can be converted in *.py in Command Prompt by typing the file path first, and after using the following command: pyuic5 –x *File name*.ui –o *File name.py*. The interface than can be opened with Python and Visual Code and adapted for the existing code.

5.4. Chapter conclusions

The development of a software[1] that can be used for a didactic purpose can be a laborious work that which combines project management knowledge with software engineering, biomechanics, industrial engineering, and a minimum of medical knowledge. The MPR view offers the possibility to examine patients' CT scans and generate the 3D view in order to analyze the perspective of the bone segmentation, the bone segmentation code apply the region growing algorithm and permits the bone extraction in a semi-automatic way and the stem customization script permits the user to create personalized hip stem geometry in each patient case.

Such a software can build the way for customization in terms of hip stem prostheses, and can offer an alternative to analyze patients, but also a cheaper manufacturing way due to additive manufacturing appearance, and due to the continuous technological development process.

---

[1] This chapter contains passages from the original code to prevent intellectual theft.

CHAPTER 6

ADDITIVE MANUFACTURING OF A CUSTOM FEMORAL STEM

The additive manufacturing or commonly known as 3D printing is a technology that is not as new as we think, but which, in the last decades, has become increasingly accessible to most people, allowing, and stimulating the innovation by increasing efficiency in many areas due to the design freedom and sometimes for low production costs.

3D printing technology can be used as a rapid prototyping in medical education also, both in veterinary medicine and in human medicine, orthopedics, dentistry, ophthalmology, etc. In order to be used successfully, the 3D printing in medicine uses a 3D scanned model by high-performance equipment such as CT scanners or tomography medical equipment.

6.1. Additive manufacturing (AM) in medical field *[99, 122, 123]*

In the 1980s, the first patent application for the rapid prototyping method was filed by Dr. Kodama from Nagoya Municipal Industrial Research Institute, Japan, describing his rapid prototyping system as a recipient filled with material, such as photopolymer that reacts when is exposed at the UV light by hardening the components and building the model up slice by slice.

Later in the 1983s the first Stereolithography device was invented by Charles Hull and putting the basis of the 3D System Corporation, one of the biggest organizations that work in the field of 3D printing nowadays. In 1984 Charles Hull files the patent for an SLA device – Stereolithography Apparatus, the technology created based on a combined laser projector that is hardening each layer of the photosensitive resin. Later on in the 1986 after his company becomes the first company of additive manufacturing or 3D printing in the world creates also a rapid prototyping system as a commercial version with the name of SIA-1, which was started to be sale with the beginning of 1988.

Carl Robert Deckard invents in 1989 the rapid prototyping (RP) process with Selective Laser Sintering (SLS), which represents a new 3D printing process by using nonmetallic powders and melting it with a laser beam in order to create objects. In the same year, another researcher Steven Scott Crump, the co-founder of Stratasys Inc. invented another 3D printing process, fused deposition modelling or FDM and using an extruder to create a layer-with-layer object. After obtaining the patent for the FDM process in 1992, the company started to bring this technology into people homes at an acceptable cost by introducing plastic materials such as PLA (Polylactic Acid or Polylactide) or ABS (Acrylonitrile Butadiene Styrene) in a heated extruder that melts the material and transform it in a viscous liquid.

Starting with the 1999s the additive manufacturing is taking place in the medical field with the purpose of printing organs. In this year the first organ, a human skeleton was built in the laboratory by 3D printing it and was covered with human cells. The technology brought to market by the Wake Forest Institute for Generative Medicine opened the door for new strategy and methods in the organs projection field by including also the additive manufacturing process.

Later on, MCP Technologies introduce in 2000 the selective laser melting technology, which opens the way for the 3D model printing that requires processing into metallic materials.

Due to the advance 3D printing technology the researchers create the first functional animal kidney in 2002, this was a functional miniature kidney capable of filtering and producing diluted urine.

In 2005 an ambitious project was started, an open-source for the 3D printing called RepRap, led by Adrian Bowyer from the University of Bath, Great Britain as an alternative response at the expensive additive manufacturing technology on the market. In this sense he created a 3D printer capable to auto replicate the majority of its components. Starting with 2006 the first SLS equipment is becoming viable conducting to the mass personalization of the products from the industrial field and later on for the prostheses.

One of the major change in the prosthetic industry was done in 2008 when a patient started to use a prosthetic leg which was 3D printed by parts knee, sole foot, all the complex articulations that after were assembled in one functional prosthetic leg. The work in bio printing was continued by the Organovo Company that in 2009 using the technology implemented by Gabor Forgacs is using the 3D printer in order to print the first 3D blood vessel.

The first 3D printed jaw prosthesis was created by a team of Dutch doctors and engineers in 2012, by using a 3D printer manufactured by LayerWise. The custom inferior jaw prosthesis was later on implanted to an 83 year old woman suffering from a chronic bone infection. Technology has been at the beginning at that time, and in the following years, was oriented towards the growth of new bone tissue on the prosthesis.

The most commonly used 3D prints in medicine are for products intended for outside use of the human body, such as orthopedic boots or exoprostheses, but printed products can be used also for educational or research purposes. The reason why 3D medical printing is more oriented in this direction is because the implantation or manufacture of the endoprostheses requires a sterile controlled environment, tests and preliminary experiments in order to be approved, because the human body easily rejects prosthesis and this can have catastrophic results on the patient's life.

Very widespread lately is the 3D printing of human organs in their real form or in section for study purpose in medical universities, bioengineering or for exposition in medical offices. In the medical education field, different components of the human body, parts of the human skeleton or exact representations of human organs extracted from the patients' CT scans, can be printed. Thus, medicine can benefit from the advantages of 3D printing because it can create from plastic materials, for educational purposes, component parts of animals or the human body, which can help the process of understanding their functional based on tomography or ultrasound scans. Through the additive manufacturing process, prototypes can be obtained for various medical products such as dental devices, orthopedics (orthopedic surgical guides or surgical prostheses) even hearing aids.

Thus, additive manufacturing in medicine facilitates and stimulates innovation, creating the possibility for doctors and researchers working in the medical field to rapid prototype, test completely and customize medical prostheses. They can plan medical procedures and evaluate possible behavioral scenarios in the field of surgery based on anatomical models and can prototype medical devices that aim to improve the function of organs that have associated or degenerative diseases. Last but not least, perhaps one of the most substantial advantages is that it accelerates the production time of medical products aimed for clinical trials and can replace traditional methods of study, such as the studies realized on human corpses.

6.2. Custom hip stems additive manufacturing

Using the custom virtual hip stem model described in the previous chapters, a prototype was obtained using additive manufacturing with the help of fused deposition modelling process technology. The FDM 3D printing technology is one of the most commonly used in rapid prototyping process because of the accessible cost of the equipment and the large possibility of material printing.

Table 6.1. Smartfil Medical 3D filament properties

Properties	Value	U. M. in SI	ISO Certification
Material density	1.05	g/cm^3	ISO 1183
Charpy Impact Strength	124	kJ/m^2	ISO 179
Flexural Modulus	2600	MPa	ISO 178
Flexural Strength	75	MPa	ISO 178
Notched Izod Impact	15	kJ/m^2	ISO 180
Tensile Yield Strength	36.5	MPa	ISO 527
Tensile Modulus * at 23 °C	2550	MPa	ISO 527
Heat Distortion Temperature	98	°C	ISO 75
Vicat Softering Temperature	101	°C	ISO 306

The material used in this process was the natural Smartfil Medical 3D filament produced by Smart Materials 3D company, an ABS, high quality material specially designed for medical applications [124]. This filament is a USP class VI or ISO 10993-1 certified, which guarantees that this filament is biocompatible with the human body [125, 126]. This class allows the material to enter in contact with the human body for a certain period of time. This high quality material allows the user to make model parts with a high degree of detail and without major deformations.

The Smartfil Medical filament physical, mechanical and thermal properties are listed in *Table 6.1*. The Smartfil Medical filament printing properties are listed in *Table 6.2*.

Table 6.2. Smartfil Medical filament printing properties

Properties	Value
Printing temperature	240°± 10°C
Hot pad	80°-100°C
Printing speed	40-50 mm/s

CREATOR PRO Flash Forge was used to manufacture the custom hip stem. In order to obtain smooth surfaces, the model mesh containing 1212 vertices and 4091, was refined and prepared by using MeshLab software. This process involved the use of filters (refining mesh algorithms) to clean and repair the model mesh by removing the duplicate faces or vertices. Two faces are considered equal if they are composed of the same set of vertices, regardless of the vertices order.
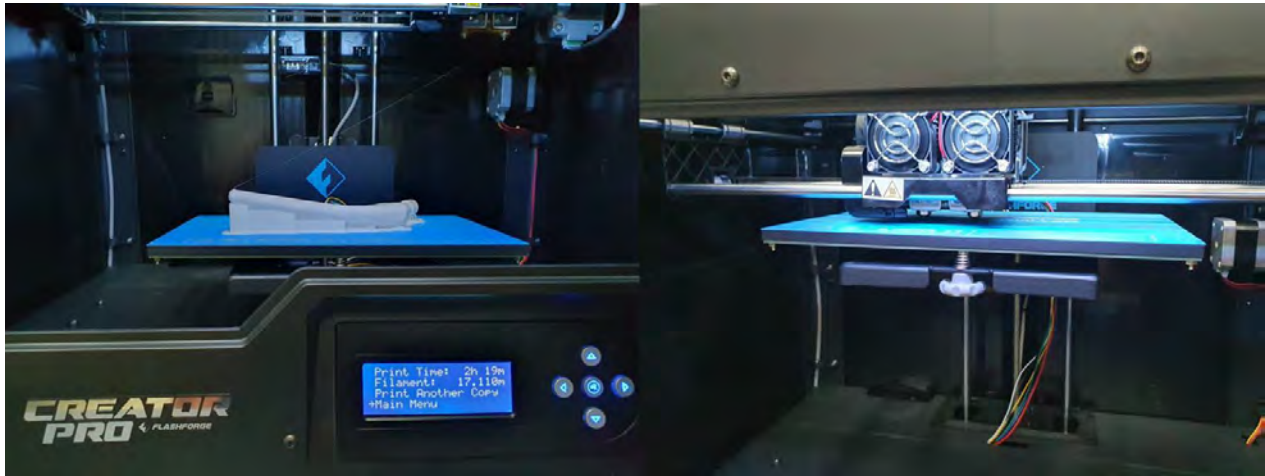
Figure 6.1. Custom stem prototype (left) and calibrating Creator PRO Flash Forge pad (right)

By applying this different filter, the number of faces decreased to 2567. A high mesh quality was created to have a smooth surface. This is preferable in order to obtain more accurate model, instead of reducing the mesh.

The model was imported in Flash Print software, then it was rotated with 90°, to position it parallel with the machine platform pad, which will be manufactured (*Figure 6.2).*
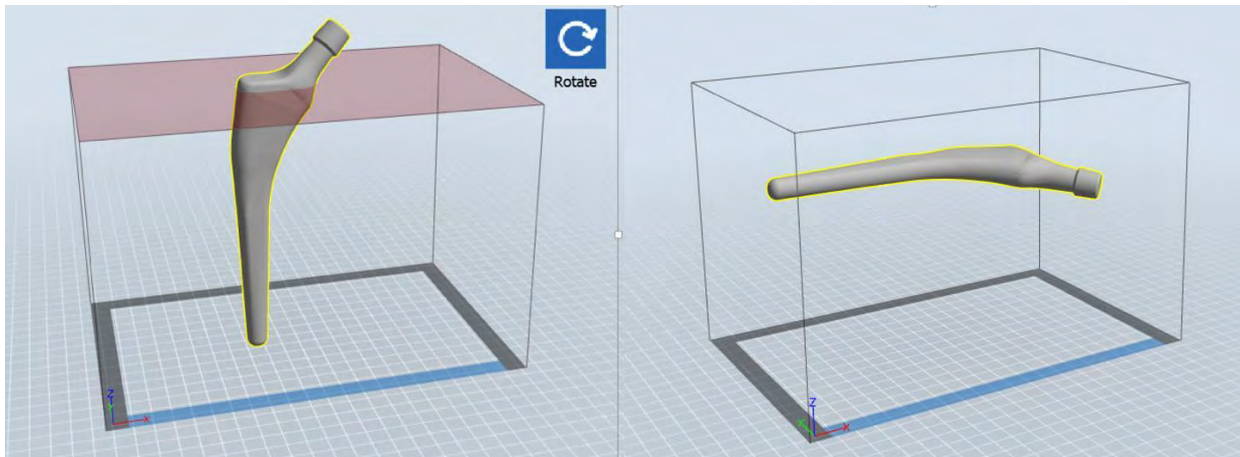
Figure 6.2. Custom stem prototype printing position in Flash Print software. Initial imported model position (left); Model position after 90° rotation in relation with the 3D printer pad

The model was centered on the platform and position at 4 mm above it. This was done to create a raft support in order to eliminate the sticking of the material to the platform, due to the irregular shape of the model. The sticking of the material can affect the printing of proper layers. The raft support contained pillars of 3 mm in size and an overhang threshold of 45° (*Figure 6.3*).

An important step was the printer settings input, because the material can be optimally printed under certain condition [127]. The layer height was about 0.18mm and the first layer height was set to 0.27mm. The shell setting was chosen as follows: 2 perimeter shells, 3 top solid layers and 3 bottom solid layers.
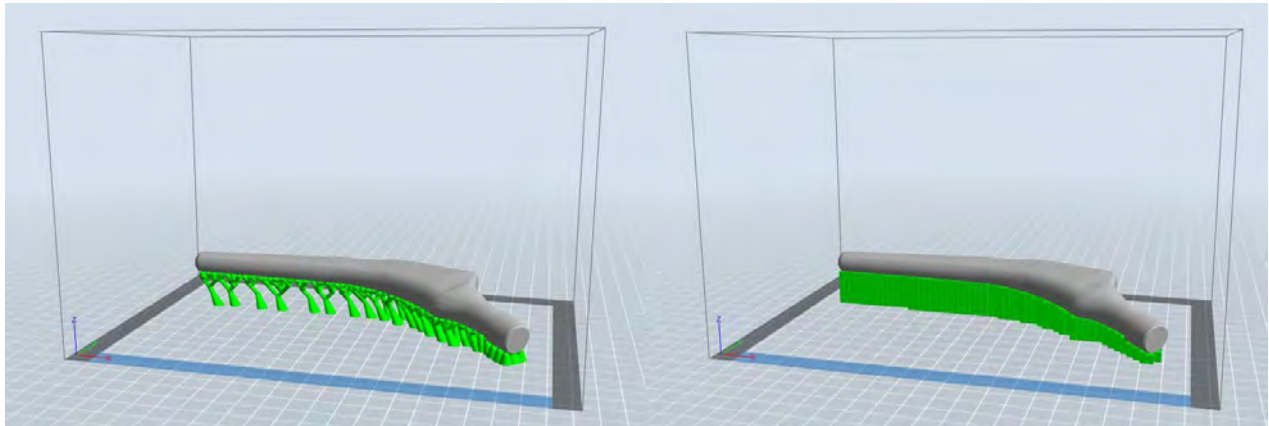
Figure 6.3. Generating a raft support with minimal material use (left); Generating a raft support allowing the layers, printing without problems and the easy detachment of the hip stem prototype after printing (right)

The infill was chosen as follows: the fill density of 30% and hexagon fill pattern (*Figure 6.5)*. The print speed was 60mm/s and the travel speed 80mm/s.

Figure 6.4. Comparison of the manufactured prototype and a commercial hip stem (Linea Anatomical hip system Tornier©)
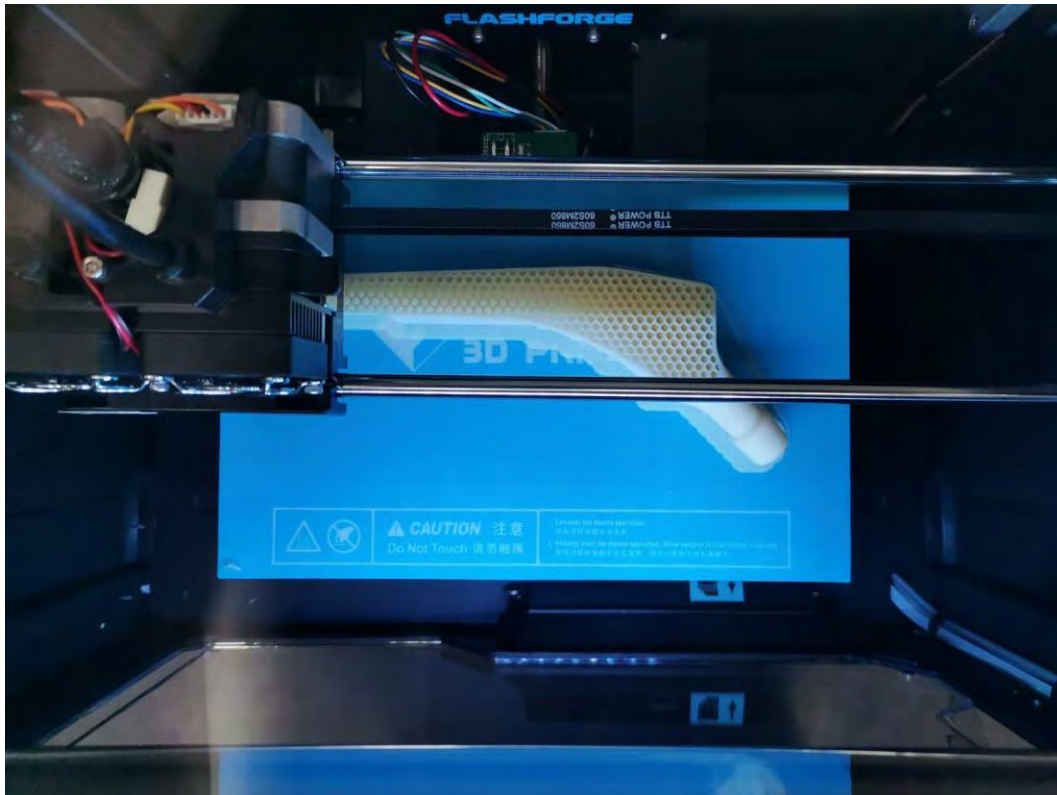
Figure 6.5. Custom hip stem prototype 30% hexagon fill pattern
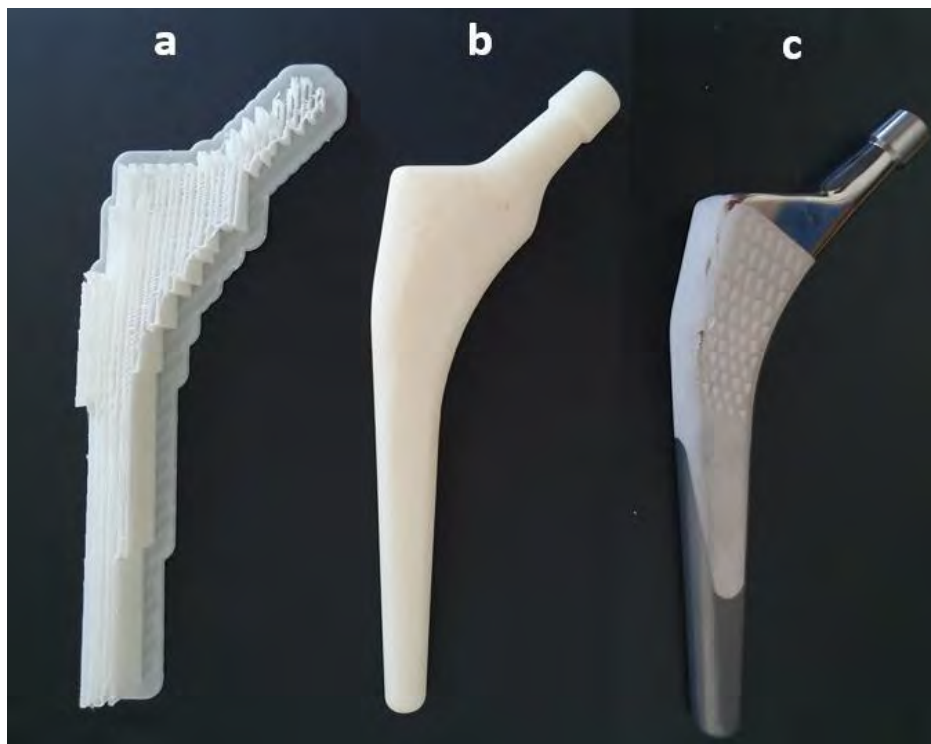
Figure 6.6. a. Custom stem prototype raft; b. Custom hip stem prototype; c. Linea Anatomical hip system Tornier©

The temperature at extruder level was 240°C (this temperature allows the optimal melting of the material, so that the layers can be built without problems) and at platform level 90°C (this temperature allows the material shelf so that it does not come off during the printing). The prototype manufacturing process took 3 hours and 50 minutes and was used 14.852 m of *Smart* filament.

The final prototype is slightly larger than a commercial hip stem, as it can be observed in *Figure 6.6.* By using the Smartfil Medical material for additive manufacturing of the custom hip stem a well-defined prototype was obtained.

6.3.   Custom hip stem compression test

In order to perform the compression test, the Instron® 8872 equipment was used, being one of the most used servo-hydraulic testing equipment that allows users to test products at static or dynamic testing simulations demands. Having the actuator positioned in the upper crosshead and also a t-slot platform on the lower part, this equipment can be an optimal laboratory device in order to test biomedical product applications or biocompatible materials with the human body.
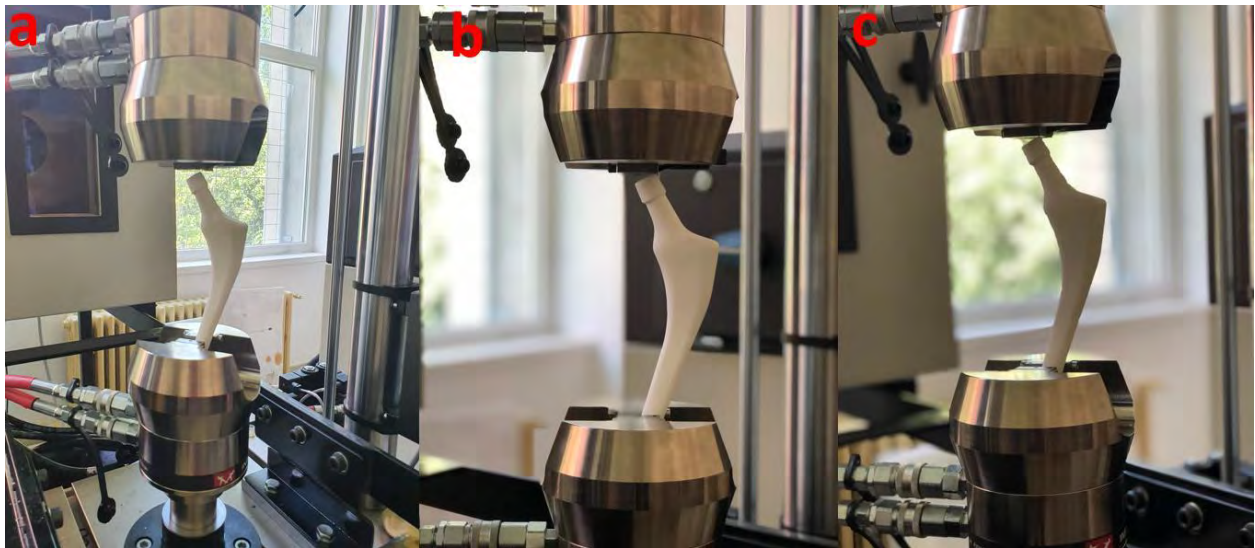
Figure 6.7. Compression test of custom stem prototype on Instron® 8872 before load applied. a. PLA custom stem sample 1; b. Medical Smartfil custom stem sample 2; c. Medical Smartfil custom stem sample 3

The compression test accomplished by Instron® 8872 system is optimal for testing biomedical products at static loads, having an axial force capacity going up to ±25 kN, using Dynacell patented loading cell, having options for extra-height or standard frame and a variety of fixtures, grips or other additional accessories.

In order to realize the compression test, three custom stem prototypes were 3D printed, two with Smartfil Medical and one in PLA material. All prototype samples have the same geometric characteristics, same infill settings and same hexagon pattern with a 30% infill the only difference being the material from which it was printed (PLA was printed at a 205°C extruder temperature and 50°C hot pad temperature, the ABS printing settings can be visualized in *Table 6.2*).

Attempts were made to position the custom femoral stem during the test as it should be positioned anatomically in the human body after a THR surgery, thus following the stem

positioning an increasing force was applied on the custom femoral stem head in the same way that the prosthesis takes over the weight of the patient's body. For the custom femoral stem sample printed with PLA filament the displacement has been set to 0.5mm/min, for the custom femoral stem samples made of Medical Smartfil the displacement was increased to 1mm/min.

6.3.1. Compression test Results

The results showed a maximum force supported by custom hip stem sample made of PLA material (specimen 1) of 0.796kN, for the custom hip stem sample made of Medical Smartfil (specimen 2) of 0.753kN and for specimen 3 of 0.749kN. This means that specimen 1 can support the equivalent body weight of 79.6kgf, specimen 2 of 75.3kgf and specimen 3 of 74.9kgf with only 30% material infill.

The graphic results of the compression test for all samples are shown in *Figure 6.8*.
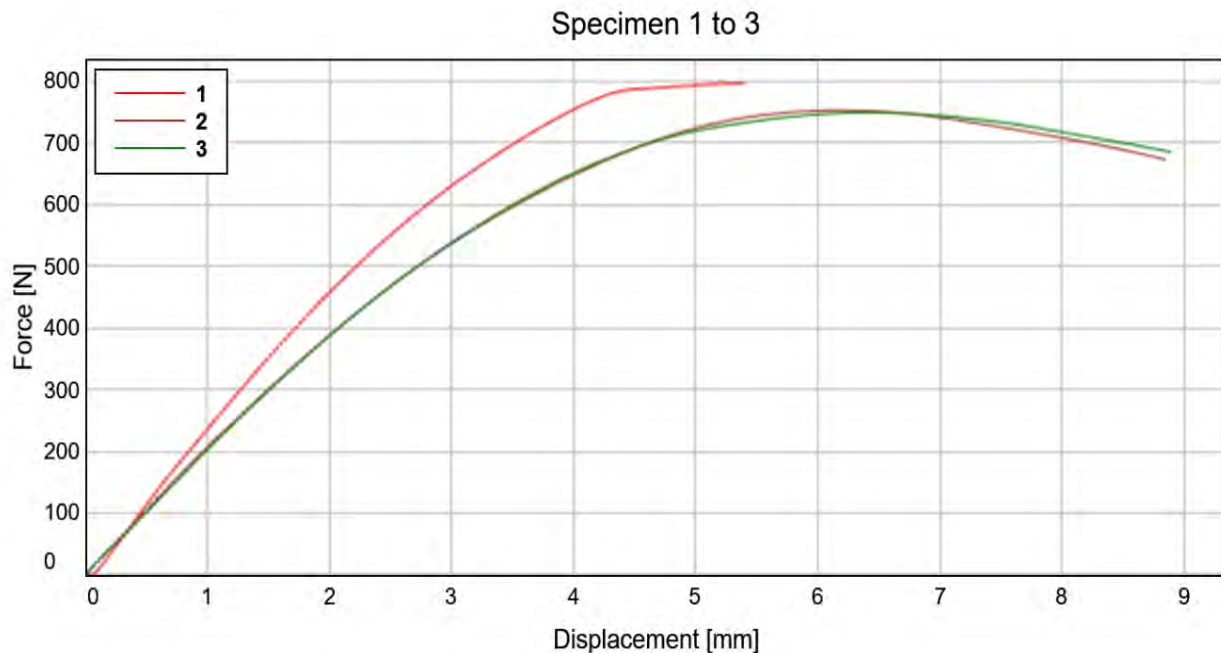
Figure 6.8. Custom hip stems compression test results

The results of the compression test indicate the appearance of a buckling phenomenon in the lower part of the custom femoral stem as indicated in *Figure 6.9* where we can observe the appearance of cracks in that solicited area of the stem.

The samples were not destroyed during the compression test and a rapid return to the initial geometry of the samples was observed, especially in the case of samples printed with the Medical Smartfil material, a material that can withstand large deformations.

Although the maximum force may appear small comparing to standard hip stem prosthesis manufactured with titanium alloy we should take into consideration that the custom stem infill was set to 30%, with hexagon pattern type, the possibilities can be multiple in order to increase the resistance of the product to external loads.
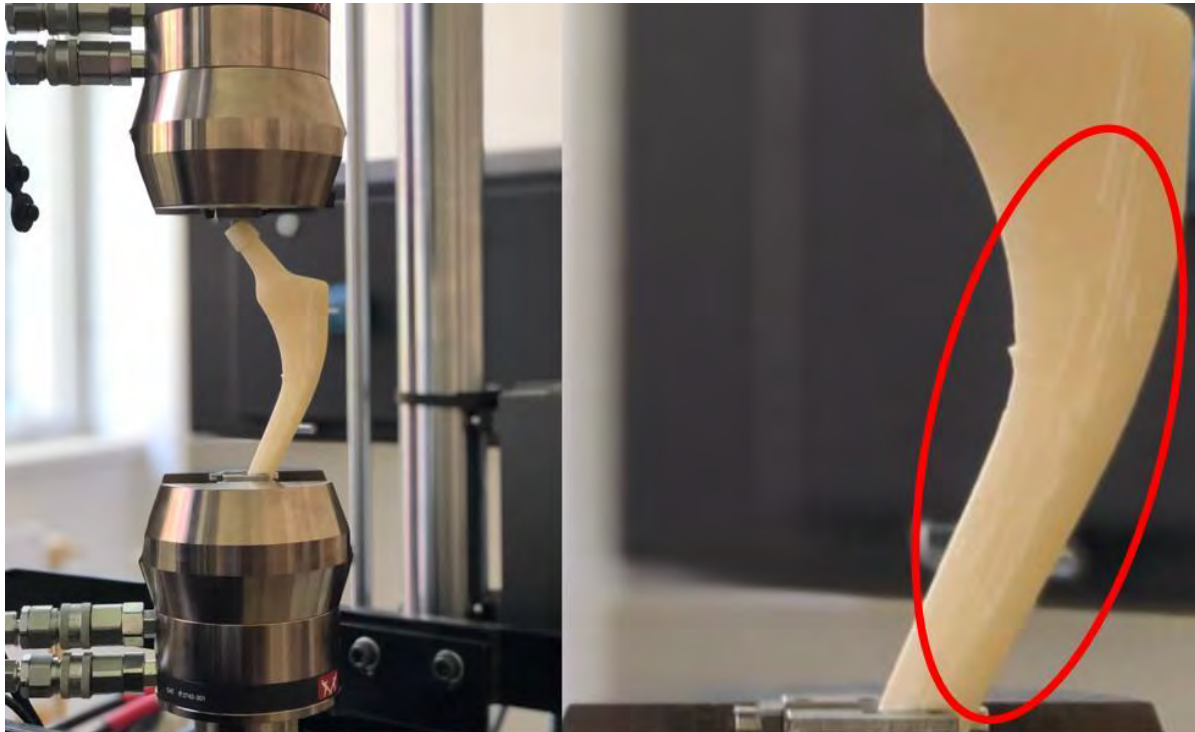
Figure 6.9. Custom femoral stem sample 2 during the compression test

6.4. Chapter conclusion

Even if the prostheses currently available on the market has reached an all-time level of development, the unique anatomy of each individual is still a challenge. More than that, injuries of different degrees of complexity in young people, arise the necessity to use a prosthesis that can function properly for a long period of time, so the need to advance the research on custom prostheses are paramount.

A prototype of the custom hip stem with 30% fill, using the hexagon pattern of deposition was obtained by additive manufacturing with Medical Smartfil ABS, which represents an ideal option due to its properties. When compared to a commercial hip stem, the manufactured prototype a slightly difference in dimension can be observed. The well-defined form of the prototype is a result of the good compatibility of the use of Medical Smartfil ABS and printing settings. Future studies will focus on studying the mechanical behavior of custom hip stems manufactured by additive prototyping. The future goal will be to analyze the geometry impact and percentage of pattern filling on the mechanical behavior of the custom hip stem. This will represent a second step in developing a custom hip stem similar to the bone, in terms of its mechanical behavior.

CHAPTER 7

FINAL CONCLUSIONS

Nowadays, virtual prototyping is gaining more and more importance in the field of bioengineering and medical sector due to facility that offers in terms of analyzing patients' conditions, simulating different daily life activities and surgery planning. The human body is a complex organic machine which although it may have common features, seen up close, it has so many peculiarities that give us uniqueness both as an individual and as an organism, peculiarities that can make a difference if we talk about the surgical approach in the orthopedic field.

This work is based on medical studies of the anatomical morphology of the human hip joint, but also causes of the hip joint pain and related illnesses in order to provide a complex understanding of how the quality of a patient can be improved from an engineering point of view. Due to the frequency with which the number of Total Hip Replacement surgeries is increasing in the last years either due to pathology, an unhealthy lifestyle that involves a poor diet or morbid obesity, even due to excessive physical activity, the age at which patients may undergo THR surgery decreases each year. This causes doctors and engineers to work together to improve the life quality of the patients who have undergone a THR, by increasing the life of a prosthesis so that the patient goes through fewer revision surgeries during his life.

In this study, a 3D preoperative planning of THR surgery methodology was presented using specific algorithms for extracting bones from patients' CT scans to measure the femoral landmarks that are used to template and choose a suitable femoral stem. Based on these patients' morpho-anatomical landmarks a femoral stem was geometrically optimized so that it can fuse on the patient's femoral curvature and present its anatomical features, in order to restore the function and the motion center of the hip that the patient had initially. Such optimization can reduce post-operative complications that have as cause stem geometry and prosthetic component placement inside the human body. The virtual prototyping methodology of the custom femoral stem presents a clear and explicit approach through which a custom femoral stem can be obtained from the CT scans of a patient which has to undergo a THR surgery.

The results of the FEA simulation show better mechanical behavior for the custom hip stem, how the loads are discharging, and small displacement compared to a standardized prosthesis and can be a start in terms of geometric validation of custom hip prostheses. Although FEA analyzes are still limited in terms of simulating the complexity of the human hip joint, however, they can provide vital information about prosthesis failure or the appearance of cracks, fracture subsequent, in the patient's femur.

The thesis also aimed to develop a preoperative planning medical software coded in Python with the help of VTK library which is intended for use in academia or research as a tool in analyzing patients medical condition at the joint level by importing CT scans and using the bone segmentation algorithms in order to obtain patients' femur from which the femoral landmarks can be subsequently obtained with the purpose of using this landmarks in order to change the geometry of a femoral stem and customize it for the patient.

Such a process can pave the way for personalization in the prosthetic industry by using it simultaneously with the additive manufacturing process in order to decrease the fabrication costs and make it more affordable for the patients that needs to undergo THR. Simplifying the customization process by developing medical software that works simultaneously with industrial

equipment and technologies such as additive manufacturing printing machines can lead to a new approach in the field of orthopedics.

7.1. The contributions brought into the doctoral thesis

Following the approach of a virtual preoperative planning (VPP) of THR surgery, it was aimed to develop a methodology of bone segmentation process by using dedicated medical software. In this sense, starting from patients' CT scans obtained from Imagerie Médicale Clinique du Parc clinic, Lyon, the DICOM files were imported in Simpleware ScanIP. The use of specific image processing algorithms described in the thesis conducts to a fast bone segmentation process by obtaining optimal bone models that can be used in virtual research studies. By using the *Threshold* image processing algorithm with a lower value that corresponds to +400HU and an upper value that corresponds to +2000HU allows the extraction of bone tissue only, eliminating most of the soft tissue, the *Region Growing* algorithm allows the user to select other voxels which belongs, for example, to the femoral bone region, the *Paint with threshold* instrument select the voxels manually, that the previsions algorithms didn't identified them in order to create a full solid model, the *Island removal* algorithm eliminates the residual voxels around the model and the *Close morphological* algorithm unifies the eventually gabs that may occur between the voxels . The use of these image processing algorithms listed above leads to a rapid bone segmentation of the femoral bone and pelvis from the CT scans.
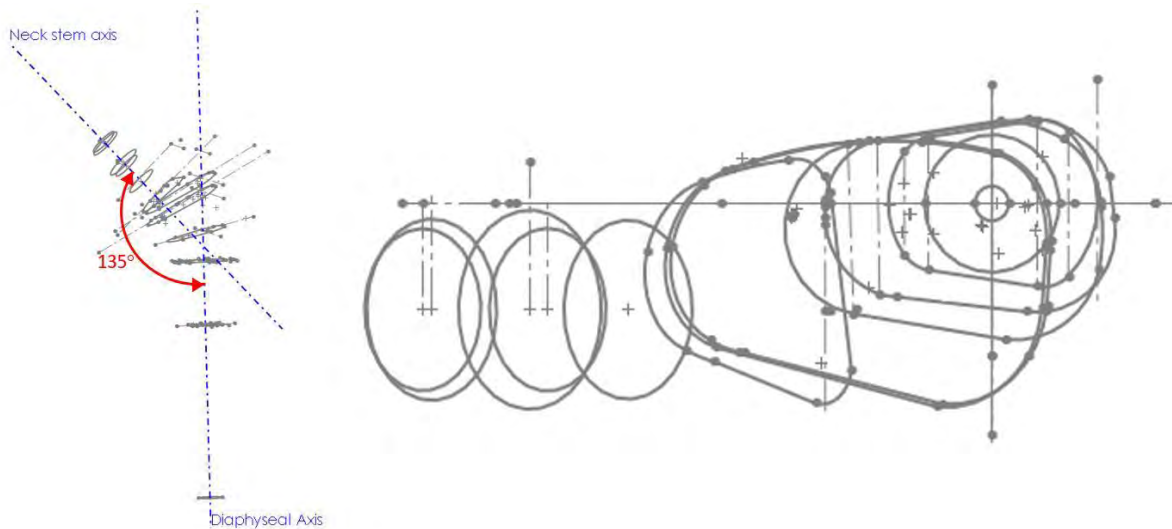
Figure 7.1. Custom femoral stem cross-sections

The process of identifying patient's femoral landmarks by using VPP and their implementation in order to develop a custom stem prosthesis that fits to patients' needs from the geometrical point of view, it aimed to emphasize the uniqueness of each human body and treating each individual as a unique different case, focusing on his personal medical needs from this point of view. Although the process of obtaining a standardized prosthesis using patients' femoral landmarks may seem difficult a hip prosthesis was made starting from a standard one with changeable parameters, which can be modified according to the medical situation of the individual in dedicated CAD software.

Creating a code meant to read and import data from patients' CT scans, allowing to analyze the medical condition of the individual in coronal, sagittal and axial view, but also allowing to generate a 3D representation by choosing a minimum and a maximum value on the Hounsfield unit scale allows a fast three-dimensional generation and update of the view. The oblique MPR view can be used to solve visualization problems regarding the incorrect positioning of the patient on the tomographic table, so that the analyzed parts are located in the same plane.
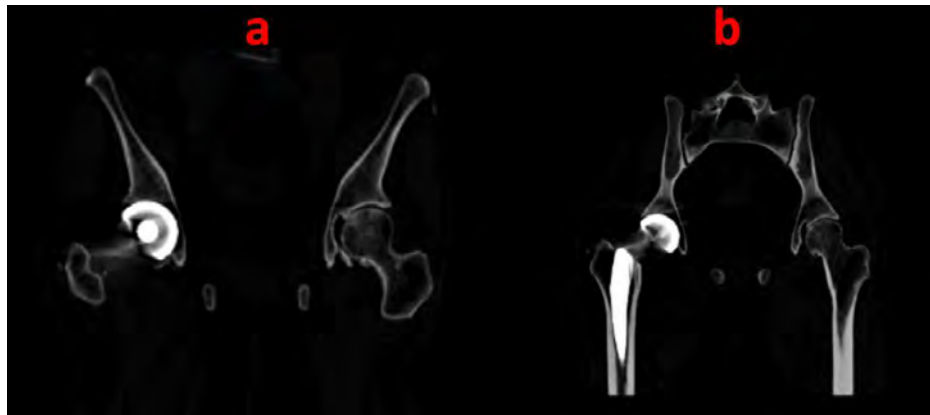
Figure 7.2. Coronal view of a patient CT scan. a. Coronal plane view set to 0°; b. Coronal plane view set to 27°

Based on the image processing algorithm called *Region Growing* a code was developed for a semi-automatic bone extraction. The patients' CT scans are imported and read by the code after choosing the optimal DICOM slide. The user can click on a voxel and apply the algorithm that as a result will include all neighboring voxels that have the same properties as the selected voxel into a region. This helps to obtain a femoral or a pelvic model that can be used in virtual studies.

The bone segmentation software together with the extraction and identification module for the patient's bone part was performed by consulting accredited medical staff from the orthopedic and radiological field, developing thus, a progress monitoring plan for the medical software. In this sense a software feasibility analysis was conducted in order to establish the software performing functions, such as: opening DICOM files, the bone segmentation process and the 3D control, the MPR view that contains the coronal plane, the sagittal plane and the axial plane, the brightness and contrast control inside the MPR view and the 3D pelvis visualization and rotation. For analyzing and determine the software requirements constant meetings were held with medical staff to evaluate and suggest different medical approaches.

To decide the best approach, a marketing study was conducted to analyze and extract the best options in terms of software development. Software development and design were performed in the Python programming language used with Visual Code Studio, and for the software interface proposal was used PyQT5, a software used to design interface widgets and buttons that can be exported in Python language further. In order to measure and track the software progress a project plan was used, where the approximate timings for developing each function were inserted and discussed at each meeting with the medical staff. The automation of the bone segmentation and extraction process was semi-automated, developing a code based on the Region Growing image processing algorithm, which runs in the software background.

Transforming the custom stem used as template into a script and the individualization of vertices, Cartesian points used as control points, spline lines and surfaces created between them,

which can be included in certain geometric transformations meant to customize a hip stem prosthesis is a way to implement a patient's femoral landmark in an attempt to automate this laborious customization process and to make it accessible so that a future implementation in this field can be attempted.

Table 7.1. Summarized presentation of the main thesis objectives

Objectives	Obtained Results	Results published in relevant scientific papers and/or presented in the academic environment
O₁	Method of personalizing of a hip stem by using patient's femoral anatomical landmarks.	REM 2018, German-French-Moroccan Summer School 2018 *Custom hip implant optimization*
O₂	Development of a software dedicated to the analysis and planning of a THR surgery in the orthopedic field.	Rapport du doctorant au Comité de suivi de thèse 4ᵉᵐᵉ année
O₃	Manufacturing of the customized hip stem prosthesis using FDM technology.	Materiale Plastice (Mater. Plast.) 2020 *Custom Hip Stem Additive Prototyping using Smart Materials*
OS₁	Bone segmentation methodology using specific image processing algorithms.	U.P.B. Sci. Bull. 2019 *Method of extracting hip joint bones from C.T. images in order to perform static F.E.A. study*
OS₂	Method of finishing organic virtual model surfaces obtained from bone segmentation process to reduce the complexity of the model and to simplify virtual simulations.	Séminaire TMI du 5 Juillet 2018 *Optimization of personalized prostheses*
OS₃	Methods of performing virtual THR surgical simulations using CAD software with FEA extension module and VPP.	5th SGEM Conf. 2018 *Reducing early intraprosthetic dislocation by using personalized hip joint prosthetic design and virtual preoperative planning*
OS₄	Virtual simulation performed in order to describe the mechanical behavior of an organic model by using Reverse Engineering methods.	IMSCI 2019 *F.E.A. study of a patient's prosthetic hip by using Reverse Engineering Method*
OS₅	Development of a bone extraction code by using specific image processing algorithms in Python programming language.	Scientific Report N°4
OS₆	Development of a user-friendly interface proposal for a medical software.	Scientific Report N°5

The software codes were tested for several medical cases in order to observe the segmentation capacity, according to the patients' medical conditions and satisfactory results were obtained. In the future, a gradual implementation in the academic environment is desired to be tested by medical students studying radiology and orthopedic surgery.

The 3D printing of human organs and prosthesis in the experimental environment, it is not a new concept in the orthopedic field, but the realization of a study meant to unify the development of medical software in order to prepare a THR surgery by using the virtual environment, the customization of the stem according to the individual femoral landmarks which can be fabricated by using the AM technology can improve a patient's life after THR intervention by reducing postoperative complications related to stem geometry, that occurs due to the choice of an inappropriate standard stem or the bad positioning of the femoral component. It can also be a cheaper alternative for the manufacture of customized prostheses for special cases of THR and the eventual implementation of such a system of production can lead to the elimination of "*prostheses banks*", the production of only necessary stem prostheses not leading to product expiration and possible recycling of the medical products.

In *Table 7.1* a summarized presentation of the main thesis objectives along with personal contributions exposed in publications are shown.

7.2. List of the original works published in international indexed journals or conferences

1. **19th International Conference on Research and Education in Mechatronics (REM), Delft, Netherlands**, 7-8 June 2018, Date Added to IEEE Xplore: 31 July 2018, Publisher: IEEE, Information: Electronic ISBN: 978-1-5386-5413-2, USB ISBN: 978-1-5386-5412-5, Print on Demand (PoD) ISBN: 978-1-5386-5414-9.
Authors: **Patricia Isabela Brãileanu**, Ionel Simion, Benyebka Bou- Saïd, Nicoleta Crişan
Paper: *Custom hip implant optimization*
DOI: 10.1109/REM.2018.8421805
Indexing: IEEE Xplore

2. **5th International Multidisciplinary Scientific Conference on Social Sciences & Arts SGEM**, Albena, Bulgaria, August 24 - September 2 / 2018.
Authors: **Patricia Isabela Brãileanu**, Loredana Manasia, Ionel Simion, Benyebka Bou- Saïd, Gina Florica Stoica
Paper: *Reducing early intraprosthetic dislocation by using personalized hip joint prosthetic design and virtual preoperative planning*
DOI: http://doi.org/10.5593/sgemsocial2018/5.3
Currently WOS indexing pending
Indexing: Clarivate Analytics, Scopus - Elsevier international indexing database, Google Scholar, Proquest, EBSCO, Crossref DOI, Russian citation SCI, British Library, Mendeley Elsevier

3. **U.P.B. Sci. Bull., Series D, Vol. D, Iss. 2, 2019, pp. 153-164.**
Authors: **Patricia Isabela Brãileanu**, Ionel Simion, Benyebka Bou-Saïd, Gina Florica Stoica
Paper: *Method of extracting hip joint bones from C.T. images in order to perform static F.E.A. study*

Indexing: Ulrich's International Periodicals Directory, Scopus, INSPEC, Metadex, Elsevier Sciences's Bibiliographic Database, Engineering Village, Cambridge Scientific Abstracts, Compendex.

4. **ICEGD 2019, Craiova Romania, published in JIDEG, May 2019, vol. 14, no. 1, pp. 221-226**
Authors: **P. I. Braileanu**, I. Simion, and B. Bou-Said
Paper: *Researching and trends in optimizing hip joint prosthesis*
Indexing: ROAD Directory of Open Access scholarly Resources, DOAJ Directory of Open Access Journals, Copernicus, Applied Science & Technology Source (EBSCO), Applied Science & Technology Source Ultimate (EBSCO), Engineering Source (EBSCO), STM Source (EBSCO), ProQuest SciTech collection, ProQuest Technology collection, Google Scholar.

5. **13th International Multi-Conference on Society, Cybernetics and Informatics (IMSCI 2019),** July 6-9, 2019, Orlando, Florida, USA, Conf. Proceedings, Vol. I, pp. 65-70.

Authors: **Patricia I. Brăileanu**, Ionel Simion, Benyebka Bou- Saïd, Maria Gratiela Ianoș, Oliver Tayot, Bertrand Bordet
Paper: *F.E.A. study of a patient's prosthetic hip by using Reverse Engineering Method*
Indexing: Scopus - Elsevier international indexing database, DOAJ - Directory of Open Access Journals

6. **Materiale Plastice (Mater. Plast.), Vol. 57 No.2,** June 2020, 152-158
Authors: **Patricia I. Brăileanu**, Ionel Simion, Benyebka Bou- Saïd, Delia Alexandra Prisecaru, Nicoleta Crișan
Paper: *Custom hip stem additive prototyping using Smart Materials*
ISSN 2668-8220
DOI https://doi.org/10.37358/MP.20.2.5361
Currently WOS indexing pending
Indexing: Web of Science, Scopus - Elsevier international indexing database, LetPub Boston, SCImago Journal & Country Rank, CAS – division of the American Chemical Society, Electronic Journals Library, ROAD - the Directory of Open Access scholarly Resources, developed with the support of the Communication and Information Sector of UNESCO.

7. **JIDEG, June 2020, Vol. 15, Iss. 1, pp. 35-40**
Authors: F. Harmon, **P. I. Brăileanu**
Paper: *Rapid prototyping of a custom upper limb bionic prosthesis*
Indexing: ROAD - Directory of Open Access scholarly Resources, DOAJ - Directory of Open Access Journals, Copernicus, Applied Science & Technology Source (EBSCO), Applied Science & Technology Source Ultimate (EBSCO), Engineering Source (EBSCO), STM Source (EBSCO), ProQuest SciTech collection, ProQuest Technology collection, Google Scholar.

7.3. Seminars and Poster Sessions participation not indexed

1. **German-French-Moroccan Summer School 2018, TRIBOLOGY TODAY – From Research Labs to Industry, Marrakesh, Morocco**, April 8-14, 2018
Authors: **Patricia I. Brăileanu**
Scientific coordinators: Benyebka Bou- Saïd, Ionel Simion
Poster Title: *Optimization of personalized prostheses*

2. **Séminaire TMI, LaMCoS, INSA Lyon**, July 5, 2018
Authors: **Patricia I. Brăileanu**
Scientific coordinators: Benyebka Bou- Saïd, Ionel Simion
Presentation Title: *Optimization of personalized prostheses*

7.4. Scientific Reports

1. **Scientific Report n°1, UPB**: "*Notions regarding the optimization of custom prosthesis*"
Authors: **Patricia I. Brăileanu**
Scientific coordinators: Benyebka Bou- Saïd, Ionel Simion
Evaluation Committee: Prof. PhD. Eng. Ionel Simion, Conf. PhD. Eng. Victor Adîr, Conf. PhD. Eng. Daniel Dobre, Prof. PhD. Eng. Sorin Cănănău

2. **Scientific Report n°2, UPB**: "*Research on custom prosthesis optimization*"
Authors: **Patricia I. Brăileanu**
Scientific coordinators: Benyebka Bou- Saïd, Ionel Simion
Evaluation Committee: Prof. PhD. Eng. Ionel Simion, Conf. PhD. Eng. Victor Adîr, Conf. PhD. Eng. Daniel Dobre, Prof. PhD. Eng. Gina Florica Stoica

3. **Scientific Report n°3, UPB**: "*Reducing THR postoperative complications by using customized femoral stems*"
Authors: **Patricia I. Brăileanu**
Scientific coordinators: Benyebka Bou- Saïd, Ionel Simion
Evaluation Committee: Prof. PhD. Eng. Ionel Simion, Conf. PhD. Eng. Victor Adîr, Conf. PhD. Eng. Daniel Dobre, Prof. PhD. Eng. Gina Florica Stoica

4. **Scientific Report n°4, UPB**: "*Bone density extraction from DICOM files in order to develop a femoral bone density map*"
Authors: **Patricia I. Brăileanu**
Scientific coordinators: Benyebka Bou- Saïd, Ionel Simion
Evaluation Committee: Prof. PhD. Eng. Ionel Simion, Conf. PhD. Eng. Victor Adîr, Conf. PhD. Eng. Daniel Dobre, Prof. PhD. Eng. Gina Florica Stoica

5. **Scientific Report n°5, UPB**: "*Considerations regarding the research of customized prosthesis*"
Authors: **Patricia I. Brăileanu**
Scientific coordinators: Benyebka Bou- Saïd, Ionel Simion
Evaluation Committee: Prof. PhD. Eng. Ionel Simion, Conf. PhD. Eng. Victor Adîr, Conf. PhD. Eng. Daniel Dobre, Prof. PhD. Eng. Gina Florica Stoica

6. **Rapport du doctorant au Comité de suivi de thèse 4eme année, INSA Lyon** : *Optimization of personalized prostheses*
Authors: **Patricia I. Brăileanu**
Scientific coordinators: Benyebka Bou- Saïd, Ionel Simion
Evaluation Committee: MdC. Jarir Mahfoud from LaMCoS, DCS and Prof. PhD. Eng. Nicolas Riviere from LMFA

7.5.   Perspectives and research directions

The methodology of optimization and customization of the femoral hip stem presented in this work can be used as a basis in future research studies for automating the process so that it becomes an accessible option when planning a THR surgery. Software development can continue to become more user-friendly with medical users and containing more femoral landmarks that can be implemented to change the geometry of the femoral stem so that the traditional preoperative planning methods of THR surgery will completely move into a virtual environment. Thus, the virtual environment being much more permissive, it can be used for planning and simulating a THR intervention, making it much more suitable for everyone.

The customization of the femoral stem can continue moving from the geometric side on the part of the material used to be fabricated with the help of AM technology. The human femur contains a variety of densities along it, being a nonhomogeneous material of two bone tissues which is reinforcing where the femur is more solicited during various activities and thins where the external loads are not high. A study on the extraction of the femoral density from patients' CT scans can be used as a basis in developing a new material that can present gradient properties and can be 3D printed on a custom prosthesis. Continuation of this hip stem customization study by creating a smart material that mimics human tissue can revolutionize the medical field by opening a new era regarding orthopedic prostheses.

REFERENCES

[1] Fuangrod Todsaporn, Khawne Amnach, Wataru Mitsuhashi, Computer-Aided pre-operative planning system for total hip replacement by using 2D x-ray images, 2008 SICE Annual Conference, 20-22 Aug. 2008, Tokyo, Japan, IEEE, DOI 10.1109/SICE.2008.4654851.

[2] Surgical technique. Hip prosthesis. Linea Anatomic Tornier, www.tornier.com.

[3] Glyn O Philips, Advances in Tissue Banking, Vol. 6, World Scientific Publishing Co. Pte. Ltd, ISBN 981-238-088-4, Singapore, 1998.

[4] William H. Harris, Wear and Periprosthetic Osteolysis. The problem, Clinical orthopaedics and related research, December 2001, Vol. 393, pp. 66-70.

[5] Gavin Ring, John O'Mullane, Alan O'Riordan, Ambrose Furey, Trace metal determination as it relates to metallosis of orthopaedic implants: Evolution and current status, Clinical Biochemistry, Vol. 49, Issues 7-8, May 2016, pp. 617-635.

[6] Ivan Landor, Pavel Vavrik, Antonin Sosna, David Jahoda, Henry Hahn and M. Daniel, Hydroxyapatite porous coating and the osteointegration of the total hip replacement, Arch Orthop Trauma Surg., 2007, No.127, 81–89, DOI https://doi.org/10.1007/s00402-006-0235-1.

[7] *** Osso VR, Virtual Reality Surgical Training & Assessment Platform, https://ossovr.com/.

[8] Philippe Hernigou, Steffen Quiennec, Isaac Guissou, Hip hemiarthroplasty: from Venable and Bohlman to Moore and Thompson, International Orthopaedics (SICOT), 2014, No. 38, pp. 655–661, DOI https://doi.org/10.1007/s00264-013-2153-5.

[9] Francesco Baino, Chiara Vitale-Brovarone, Three-dimensional glass-derived scaffolds for bone tissue engineering: Current trends and forecasts for the future, Journal of Biomedical Materials Research, 2011, Vol.97A, Issue 4, pp. 514-535, DOI https://doi.org/10.1002/jbm.a.33072.

[10] Nägerl H, Kubein-Meesenburg D, Fanghänel J., Elements of a general theory of joints. 2. Introduction into a theory of synarthrosis, Anatomischer Anzeiger, 1990, Vol.171 (5), pp. 323-333.

[11] M. Khan, S. N. Redman, R. Williams, G. P. Dowthwaite, S. F. Oldfield, C. W. Archer, The Development of Synovial Joints, Current Topics in Developmental Biology, 2007, Vol. 79, pp. 1-36, DOI https://doi.org/10.1016/S0070-2153(06)79001-9.

[12] E. Allander, O. J. Björnsson, Ó. Ólafsson, N. Sigfússon, J. Thorsteinsson, Normal Range of Joint Movements in Shoulder, Hip, Wrist and Thumb with Special Reference to Side: a Comparison between Two Populations, International Journal of Epidemiology, September 1974, Vol. 3, Issue 3, pp. 253-261, DOI https://doi.org/10.1093/ije/3.3.253.

[13] R. D. Crowninshield, R. C. Johnston, J. G. Andrews, R. A. Brand, A biomechanical investigation of the human hip, Journal of Biomechanics, 1978, Vol. 11, Issues 1-2, pp. 75-85, DOI https://doi.org/10.1016/0021-9290(78)90045-3.

[14] Radu N. Cârmaciu, Cezar TH. Ninculescu, Leila Torsan, The human anatomy and physiology (Anatomia și fiziologia omului), Editura didactică și pedagogică, 1994, ISBN 973-30-0489-8.

[15] Diane Lee, The Pelvic Girdle. An approach to the examination and treatment of the lumbopelvic-hip region, Publisher Churchill Livingstone, 2004, ISBN 978-0-443-07373-1.

[16] Kevin T. Patton, Gary A. Thibodeau, Anatomy & Physiology 9th Edition, Publisher Elsevier, 2015, ISBN 978-323-34139-4.

[17] Steven D. Waldman, Pain Review, Publisher Saunders Elsevier, 2009, ISBN 978-1-4160-5893-9.

[18] Nüesch Eveline, Dieppe Paul, Reichenbach Stephan, Williams Susan, Iff Samuel, Jüni Peter et al., All cause and disease specific mortality in patients with knee or hip osteoarthritis: population based cohort study, BMJ, 2011, Vol. 342, DOI https://doi.org/10.1136/bmj.d1165.

[19] H. Malchau, G. Garellick, P. Herberts, The Evidence from the Swedish Hip Register. In: The Well-Cemented Todal Hip Arthroplasty, Springer, 2005, Berlin, Heidelberg, ISBN 978-3-540-24197-3, pp. 291–299.

[20]   J. A. P. Da Silva, G. M. Hall, The effects of gender and sex hormones on outcome in rheumatoid arthritis, Baillière's Clinical Rheumatology, 1992, Vol. 6, Issue 1, pp. 193-219, DOI https://doi.org/10.1016/S0950-3579(05)80344-9.

[21]   Robert M. Stecher, Heredity of joint diseases, Eugenics Quarterly, 1954, Vol. 1:1, pp. 16-20, DOI: 10.1080/19485565.1954.9987159.

[22]   Magliano, Obesity and arthritis, Menopause International, 2008, Vol. 14(4), pp. 149–154, DOI https://doi.org/10.1258/mi.2008.008018.

[23]   Buckwalter J.A., Felson D.T., Post-Traumatic Arthritis: Definitions and Burden of Disease. In Post-Traumatic Arthritis, Springer, Boston, 2015, DOI https://doi.org/10.1007/978-1-4899-7606-2_2.

[24]   Allaire, S. H., Li, W., & LaValley, Work Barriers Experienced and Job Accommodations Used by Persons with Arthritis and Other Rheumatic Diseases. Rehabilitation Counseling Bulletin, 2003, Vol. 46(3), pp. 147–156, DOI https://doi.org/10.1177/00343552030460030301.

[25]   Saag KG, Cerhan JR, Kolluri S, et. al., Cigarette smoking and rheumatoid arthritis severity, Annals of the Rheumatic Diseases, 1997, Vol. 56, pp. 463-469., DOI http://dx.doi.org/10.1136/ard.56.8.463.

[26]   D. P. M. Symmons, P. Prior, D. L. Scott, R. Brown, C. F. Hawkins, Factors influencing mortality in rheumatoid arthritis, Journal of Chronic Diseases, 1986, Vol. 39, Issue 2, pp. 137-145, DOI https://doi.org/10.1016/0021-9681(86)90070-6.

[27]   E. D. Harris, Rheumatoid Arthritis — Pathophysiology and Implications for Therapy, N Engl J Med, 1990, Vol. 322, pp. 1277-1289, DOI: 10.1056/NEJM19900503322180.

[28]   Harris WH, Etiology of osteoarthritis of the hip, Clinical Orthopaedics and Related Research, 1986, Vol. 213, pp. 20-33.

[29]   Freeman, Peter A. M.A., MB., Peter M.B., T. Wallace M.B., Total Hip Joint Replacement in Osteoarthrosis and Polyarthritis A Statistical Study of the Results, Clinical Orthopaedics and Related Research®: September 1973, Vol.95, Issue, pp. 224-230.

[30]   https://www.cdc.gov/arthritis/data_statistics/national-statistics.html, Last viewed on 03/01/2020.

[31]   https://www.cdc.gov/arthritis/data_statistics/disparities.htm, Last viewed on 03/01/2020.

[32]   Jacqueline Finch, The ancient origins of prosthetic medicine, The Art of Medicine, 2011, Vol. 377, Issue 9765, pp. 548–549.

[33]   Hsin-Yi Kathy Cheng, Chun-Li Lin, Shih-Wei Chou, Yan-Ying Ju, Yin-Chou Lin, May-Kuen Wong, The importance of the great toe in balance performance, 2007, Proceedings of the Fifth IASTED International Conference on Biomechanics, BioMech, Vol. 59–63.

[34]   Martin M. Malawer, Robert M. Henshaw, Kristen Kellar-Graney, Overview of Endoprosthetic Reconstruction, 2009, available at: http://sarcoma.org/publications/OTOS_Book/13282_ON-3.pdf, Accessed: 2019-01-03.

[35]   Richard A. Brand, Michael A. Mont, M. M. Manring, Biographical Sketch: Themistocles Gluck (1853–1942), Clin Orthop Relat Res. 2011 Jun, Vol. 469(6), pp. 1525–1527.

[36]   Stephen Richard Knight, Randeep Aujla, Satya Prasad Biswas, Total Hip Arthroplasty – over 100 years of operative history, Orthopaedic Reviews 2011, Vol. 3:e16, pp. 72–74.

[37]   T. W. R. Briggs, S. A. Hanna, B. Kayani, S. Tai, R. C. Pollock, S. R. Cannon, G. W. Blunn, R. W. J. Carrington, Metal-on-polyethylene versus metal-on-metal bearing surfaces in total hip arthroplasty, The Bone & Joint Journal, Sep 2015, Vol. 97(B), No. 9, pp. 1183–1191.

[38]   Andrew J. Ruys, Alumina Ceramics: Biomedical and Clinical Applications, Woodhead Publishing Series in Biomaterials, 2018, ISBN 978-0-08-102443-0, pp. 151–152.

[39]   Philippe Hernigou (2014). Smith–Petersen and early development of hip arthroplasty, Int Orthop., 2014 Jan., Vol. 38(1), pp. 193–198.

[40]   William Waugh, John Charnley: The Man and The Hip, The New England Journal of Medicine, Aug. 23, 1990, Los Angeles, CA 90024, Vol. 323, No. 8, pp. 553–554.

[41]   Jianxi Lu, Orthopedic Bone Cements, Biomechanics and Biomaterials in Orthopedics, Springer, 2016, Editor Dominique G. Poitout, Springer-Verlag London, ISBN 978-1-84882-663-2, pp. 123–138.

[42] C.J. Hedbeck, R. Blomfeldt, G. Lapidus, H. Törnkvist, S. Ponzer, J. Tidermark, Unipolar hemiarthroplasty versus bipolar hemiarthroplasty in the most elderly patients with displaced femoral neck fractures: a randomised, controlled trial, Int. Orthop., Feb. 8, 2011, Vol. 35(11), pp. 1703–1711.

[43] *** Statistics Hip Report (Raport statistici șold 2010, Registrul Național de Endoprotezare, Perioada analizată 2003-2010), www.rne.ro.

[44] P. Babaniamansour, M. Ebrahimian-Hosseinabadi, A. Zargar-Kharazi, Designing an Optimized Novel Femoral Stem, J Med Signals Sens., Jul-Sep 2017, Vol. 7(3), pp. 170–177.

[45] G. Schmidig, A. Patel, I. Liepins, M. Thakore, DC. Markel, The effects of acetabular shell deformation and liner thickness on frictional torque in ultrahigh-molecular-weight polyethylene acetabular bearings, J Arthroplasty, Jun 2010, Vol. 25(4), pp. 644–653.

[46] Gerhard J. A. Drescher, Prosthetic liner for an acetabular prosthesis, Patent No. US8177851B2, May 15, 2012.

[47] Sujit Kumar Tripathy, Tarun Goyal, Ramesh Kumar Sen, Management of femoral head osteonecrosis: Current concepts, Indian J Orthop., Jan-Feb 2015, Vol. 49(1), pp. 28–45.

[48] Xu Haiying, Zhang Wei, Fan Kai, Fu Pengfei, TC4 Titanium Alloy Microstructure and Properties Influenced by High Frequency Scan of Electron Beam, Rare Metal Materials and Engineering, 2017, Vol. 46, Issue 6, pp. 1457–1462.

[49] W.V. Christian, L.D. Oliver, D.J. Paustenbach, M.L. Kreider, B.L. Finley, Toxicology-based cancer causation analysis of CoCr-containing hip implants: a quantitative assessment of genotoxicity and tumorigenicity studies, J Appl Toxicol., 2014, Vol. 34, Issue 9, pp. 939–967.

[50] Orhun K. Muratoglu, Steven M. Kurtz, Alternate Bearing Surface in Hip Replacement, Hip Replacement. Current Trends and Controversies, Editor Raj K. Sinha, 2002, ISBN 0-8247-0789-3, Issue 9, pp. 1–46.

[51] S. Pramanik, A. K. Agarwal, K. N. Rai, Chronology of Total Hip Joint Replacement and Materials Development, Trends Biomater. Artif. Organs, 2005, Vol. 19(1), pp. 15–25.

[52] Catarina A. Oliveira, Isabel S. Candelária, Pedro B. Oliveira, Antonio Figueiredo, Filipe Caseiro-Alves, Metallosis: A diagnosis not only in patients with metal-on-metal, prostheses, Eur J Radiol Open., 2015, Vol. 2, pp. 3–6.

[53] E. J. McPherson, L. D. Dorr, T. A. Gruen, M. T. Saberi, Hydroxyapatite-Coated Proximal Ingrowth Femoral Stems, Clinical Orthopaedics, 1995, Vol. 315, pp. 223–230.

[54] Andrew J. Ruys, Alumina Ceramics: Biomedical and Clinical Applications, Woodhead Publishing Series in Biomaterials, 2018, ISBN 978-0-08-102443-0, pp. 151–152.

[55] Jung Taek Kim, Jeong Joon Yoo, Implant Design in Cementless Hip Arthroplasty, Hip Pelvis, June 2016, Volume 28, Issue 2, Pages 65–75.

[56] Philippe Hernigou, Gildasio Daltro, Charles Henri Flouzat Lachaniette, Xavier Roussignol, Martin Mukisi Mukasa, Alexandre Poignard, Fixation of the Cemented Stem: Clinical Relevance of the Porosity and Thickness of the Cement Mantle, Open Othop. J., February 2009, Volume 3, Pages 8–13.

[57] Perka, Carsten, Fischer, Ulrike, Taylor, William R., Matziolis, Georg, Developmental Hip Dysplasia Treated with Total Hip Arthroplasty with a Straight Stem , JBJS, February 2004 – Vol. 86, Issue 2, pp. 312-319.

[58] G. Lecerf, M.H. Fessy, R. Philippot, P. Massin, F. Giraud, X. Flecher, J. Girard, P. Mertl, E. Marchetti, E. Stindel, Femoral offset: Anatomical concept, definition, assessment, implications for preoperative templating and hip arthroplasty, Revue de Chirurgie Orthopédique et Traumatologique, May 2009, Vol. 95, Issue 3, pp. 248-257, DOI https://doi.org/10.1016/j.otsr.2009.03.010.

[59] J. S. Siopack, H. E. Jergesen, Total hip arthroplasty, West J. Med, 1995 Mar., vol. 162(3), pp. 243 – 249.

[60] Coventry Mark B., Beckenbaugh, Robert D., Nolan, Declan R., Ilstrup, Duane M., 2,012 Total Hip Arthroplasties: A Study of Postoperative Course and Early Complications, J.B.J.S., 1974 March, vol. 56, issue 2.

[61]   C.Fabry, J. Langlois, M. Harmadouche, R. Bader, Intra-prosthetic dislocation of dual-mobility cups after total hip arthroplasty: potential causes from a clinical and biomechanical perspective, International Orthopaedics, May 2016, vol. 40, issue 5, pp. 901 – 906.

[62]   *** Swedish Hip Arthroplasty Register (2011) Annual report, http://www.shpr.se/en/Publications/DocumentsReports.aspx.

[63]   R. Bouchet, N. Mercier, D. Saragaglia, Posterior approach and dislocation rate: A 213 total hip replacements case-control study comparing the dual mobility cup with a conventional 28-mm metal head/polyethylene prosthesis, Orthopaedics & Traumatology: Surgery & Research, Feb. 2011, vol. 97, issue 1, pp. 2–7.

[64]   Bradford S. Waddell, Ivan De Martino, Thomas Sculco and Peter Sculco, Total Hip Arthroplasty Dislocations Are More Complex Than They Appear: A Case Report of Intraprosthetic Dislocation of an Anatomic Dual-Mobility Implant After Closed Reduction, Ochsner Journal June 2016, Vol. 16 (2), pp. 185–190.

[65]   *** Postoperative issues – CISTEN, Last viewed 16/06/2020, http://cisten.org/en/.

[66]   Anne Van Riet, Jo De Schepper, Hendrik Pieter Delport, Arthroscopic psoas release for iliopsoas impingement after total hip replacement, Acta orthopaedica Belgica, 2011,Vol. 77, Issue 1, pp. 41-6 .

[67]   Malik, Aamer, Maheshwari, Aditya, Lawrence D., Impingement with Total Hip Replacement, JBJS: August 2007, Vol. 89, Issue 8, pp. 1832-1842, DOI 10.2106/JBJS.F.01313.

[68]   JÄger, M., Wild, A., Westhoff, B. et al., Femoroacetabular impingement caused by a femoral osseous head–neck bump deformity: clinical, radiological, and experimental results, J Orthop Sci., 2004, Vol. 9, pp. 256–263, DOI https://doi.org/10.1007/s00776-004-0770-y.

[69]   Isaacson MJ, Bunn KJ, Incavo SJ., Trochanteric impingement: is it a source of pain after THR?, Arthroplast Today, 2015, Vol. 1(3), pp. 73-75, DOI 10.1016/j.artd.2015.05.004.

[70]   Alina Adriana Feiler, Ana-Maria Ungureanu, Handbook of radiology and medical imaging. Thorax (Manual de radiologie și imagistică medicală. Toracele), Vol. 1, Publisher Victor Babeș, ISBN 978-606-8054-83-4.

[71]   S. Eggli, M. Pisan, M. E. Müller, The value of preoperative planning for total hip arthroplasty, J Bone Joint Surg [Br], 1998, Vol. 80-B, pp. 382-90.

[72]   McGee HMJ, Scott JHS, A simple method of obtaining equal leg length in total hip arthroplasty, Clin Orthop, 1985, Vol. 194, pp. 269-70.

[73]   Hoikka V, Santavirta S, Eskola A, et al., Methodology for restoring functional leg length in revision total hip arthroplasty. J Arthroplasty, 1991, Vol. 6, pp. 189-93.

[74]   Richmond Caroline, Sir Godfrey Hounsfield, BMJ, 2004, 329:687.

[75]   Lee W. Goldman, Principles of CT and CT Technology, J. Nucl. Med. Technol, September 2007, Vol. 35, No. 3, pp. 115-128, DOI 10.2967/jnmt.107.042978.

[76]   I. T. Haider, P. Schneider, A. Michalski, W. B. Edwards, Influence of geometry on proximal femoral shaft strains: Implications for atypical femoral fracture, Bone, 2018, Vol. 110, pp. 295 – 303.

[77]   I. Otomaru, M. Nakamoto, M. Takao, N. Sugano, Y. Kagiyama, H. Yoshikawa, Y. Kagiyama, H. Yoshikawa, Y. Tada, Y. Sato, Automated preoperative planning of femoral component for total hip arthroplasty (THA) from 3D CT images, J. Biomechanical Science and Eng., 2008, Vol. 4, pp. 478–489.

[78]   T. Scheerlinck, Primary hip arthroplasty templating on standard radiographs a stepwise approach, Acta Orthop. Belg., 2010, Vol. 76, pp. 432–442.

[79]   J. P. Crutcher, Preoperative Planning for Total Hip Arthroplasty, Operative Techniques in Orthopaedics, 2000, Vol. 10, No. 2, pp. 102–105.

[80]   Y. S. Lee, S. H. Oh, J. K. Seon, E. K. Song, T. R. Yoon, 3D femoral neck anteversion measurements based on the posterior femoral plane in ORTHODOC® system, Med. Bio. Eng. Comput., 2006, Vol. 44, pp. 895–906.

[81]   P.N.Tuan, N.V.Tuong, P.P Trinh, Measuring geometric parameters of proximal femur by using reverse engineering, 5th World Conference on Applied Sciences, Engineering & Technology, 2016, Vol. 13, pp. 183–188.

[82]   S. Bangare, A. Dubal, P. S. Bangare and S. Patil, Reviewing otsu's method for image thresholding, in Int. Journal of Applied Engineering Research, January 2015, Vol. 10, No. 9, pp. 21777-21783.

[83]   X. Yang, X. Shen, J. Long and H. Chen, An improved median-based Otsu image thresholding algorithm, in AASRI Procedia, 2012, Vol. 3, pp. 468-473.

[84]   A. R. Amanda and R. Widita, Comparison of image segmentation of lungs using methods: connected threshold, neighborhood connected and threshold level set segmentation, in Journal of Physics: Conference Series, Vol. 694, conference 1.

[85]   M. M. Abdelsamea, An enhancement neighborhood connected segmentation for 2D-cellular image, in International Journal of Bioscience, Biochemistry and Bioinformatics, 2011, Vol. 1, No. 4, pp. 256-260.

[86]   H. Rahman and Md. R. Islam, A version of watershed algorithm for color image segmentation, in The AIUB Journal of Science and Engineering (AJSE), August 2013, Vol. 12, No. 1, pp. 105-115.

[87]   S. J. Park, J. H. Kim, S. H. Lee and K. G. Kim, Comparative assessment of 3D region growing methods for lung airway segmentation: evaluation with pathological and normal cases, in IFMBE Proceedings, August 2006, Vol. 14, No. 4, pp. 2525-2531.

[88]   X. Jiang, R. Zhang and S. Nie, Image segmentation based on level set method, in Physics Procedia, 2012, Vol. 33, pp. 840-845.

[89]   S.Trukham, A. Nedzved and S. Ablameyko, Region growing segmentation of CT-image by the analysis of 3D local neighborhood, in Pattern Recognition and Information Processing (PRIP'2014): Proceedings of the 12th International Conference, 28–30 May 2014, Minsk, Belarus, pp. 285-289.

[90]   J. Fripp, S. Crozier, S. K. Warfield and S. Ourselin, Automatic Segmentation and Quantitative Analysis of the Articular Cartilages From Magnetic Resonance Images of the Knee, in IEEE Transactions on Medical Imaging, Jan. 2010, Vol. 29, No. 1, pp. 55-64, DOI 10.1109/TMI.2009.2024743.

[91]   Li Y, Hong B, Gao S, Liu K., Bone segmentation in human CT images, Journal of Biomedical Engineering, 2004 Apr, Vol. 21(2), pp. 169-173, PMID: 15143532.

[92]   J. Lee, Digital Image Enhancement and Noise Filtering by Use of Local Statistics, in IEEE Transactions on Pattern Analysis and Machine Intelligence, March 1980, Vol. PAMI-2, No. 2, pp. 165-168, DOI 10.1109/TPAMI.1980.4766994.

[93]   Lei Huang,Qian Kemao,Bing Pan,Anand Krishna Asundi, Comparison of Fourier transform, windowed Fourier transform, and wavelet transform methods for phase extraction from a single fringe pattern in fringe projection profilometry, Optics and Lasers in Engineering, February 2010,Vol. 48, Issue 2, pp. 141-148, DOI https://doi.org/10.1016/j.optlaseng.2009.04.003.

[94]   Harley H. L. Chan, Jeffrey H. Siewerdsen, Allan Vescan, Michael J. Daly, Eitan Prisman, Jonathan C. Irish, 3D Rapid Prototyping for Otolaryngology—Head and Neck Surgery: Applications in Image-Guidance, Surgical Simulation and Patient-Specific Modeling, PLoS One., 2015, Vol. 10(9): e0136370., PMCID: PMC4557980, DOI 10.1371/journal.pone.0136370.

[95]   Broder, J., Imaging of nontraumatic abdominal conditions, J. Broder (Ed.) Diagnostic Imaging for the Emergency Physician. Elsevier, New York, 2011, pp. 445–577.

[96]   K.T. Schuetze,P.S. Shiakolas,S.N. Muthukrishnan,R.V. Nambiar,K.L. Lawrence, A study of adaptively remeshed finite element problems using higher order tetrahedra, Computers & Structures, 17 January 1995, Vol. 54, Issue 2, pp. 279-288, DOI https://doi.org/10.1016/0045-7949(94)00320-3.

[97]   Ravera, Emiliano Crespo, Marcos Guarnieri, Fabio Braidot, Stress in Human Pelvis throughout the Gait Cycle: Development, Evaluation and Sensitivity Studies of a Finite Element Model, 2014, DOI 10.13140/2.1.4877.5367.

[98]   P. I. Brãileanu, I. Simion, B. B. Saïd and N. Crișan, Custom hip implant design optimisation, 2018 19th International Conference on Research and Education in Mechatronics (REM), Delft, 2018, pp. 58-63, DOI 10.1109/REM.2018.8421805.

[99]   P.I. Braileanu, I. Simion, B. Bou-Said, D.A. Prisecaru, N. Crisan, Custom Hip Stem Additive Prototyping Using Smart Materials, Mater. Plast., Vol. 57, No. 2, pp. 152-158, 2020, DOI https://doi.org/10.37358/MP.20.2.5361.

[100]   Nicola, C., Alessandro, N., Arcangelo, P., Giovanni Francesco, S., & Francesco, N., Parametric model of lumbar vertebra, Journal of Industrial Design and Engineering Graphics, 2010, Vol. 5(2), pp. 15-18, Retrieved from http://sorging.ro/jideg/index.php/jid/article/view/71.

[101]   Jae-Young Rho,Liisa Kuhn-Spearing,Peter Zioupos, Mechanical properties and the hierarchical structure of bone, Medical Engineering & Physics, March 1998, Vol. 20, Issue 2, pp. 92-102, DOI https://doi.org/10.1016/S1350-4533(98)00007-1.

[102]   Jae Young Rho,Richard B. Ashman,Charles H. Turner, Young's modulus of trabecular and cortical bone material: Ultrasonic and microtensile measurements, Journal of Biomechanics, February 1993, Vol. 26, Issue 2, pp. 111-119, DOI https://doi.org/10.1016/0021-9290(93)90042-D.

[103]   Morgan EF, Unnikrisnan GU, Hussein AI, Bone Mechanical Properties in Healthy and Diseased States. Annu Rev Biomed Eng, 2018, Vol. 20, pp. 119–143, DOI 10.1146/annurev-bioeng-062117-121139.

[104]   Jameson, John Robert, Characterization of Bone Material Properties and Microstructure in Osteogenesis Imperfecta/Brittle Bone Disease, Dissertations (2009 -), Paper 413, http://epublications.marquette.edu/dissertations_mu/413.

[105]   Ramin Oftadeh, Miguel Perez-Viloria, Juan C. Villa-Camacho, Ashkan Vaziri, Ara Nazarian, Biomechanics and Mechanobiology of Trabecular Bone: A Review, J Biomech Eng, 2015 Jan, Vol. 137(1), pp. 0108021–01080215, DOI 10.1115/1.4029176, PMCID: PMC5101038.

[106]   Birnbaum, K., Sindelar, R., Gärtner, Material properties of trabecular bone structures, J.R. et al. Surg Radiol Anat (2002), 23: 399. https://doi.org/10.1007/s00276-001-0399-x.

[107]   B. Depalle, R. Chapurlat, H. Walter-Le-Berre, B. Bou-Said, H. Follet, Finite element dependence of stress evaluation for human trabecular bone, 4th International Conference on the Mechanics of Biomaterials and Tissue (ICMOBT4), Journal of the Mechanical Behavior of Biomedical Materials, August 2012, DOI http://dx.doi.org/10.1016/j.jmbbm.2012.08.012.

[108]   D. Mitton, Chrsitian Roux and Pascal Laugier, Bone Quantitative Ultrasound-Bone Overview, Publisher Springer Science+Business Media B. V., 2011, DOI 10.1007/978-94-007-0017-8_1.

[109]   Bruno Vidal ,Rita Cascão,Mikko A. J. Finnilä,Inês PVidal B, Cascão R, Finnila¨ MAJ, Lopes IP, Saarakkala S, Zioupos P, et al., Early arthritis induces disturbances at bone nanostructural level reflected in decreased tissue hardness in an animal model of arthritis, 2018, PLoS ONE 13(1): e0190920, DOI https://doi.org/10.1371/journal.pone.0190920.

[110]   Havaldar R, Pilli SC, Putti BB., Insights into the effects of tensile and compressive loadings on human femur bone, Adv Biomed Res., 2014, Vol. 3:101, DOI doi:10.4103/2277-9175.129375.

[111]   Mohamed J. Mirzaali, J. Jakob Schwierdzik, Suwanwadee Thaiwichai, James P.Best, Johann Michler, Philippe K. Zysset, UweWolfram, Mechanical properties of cortical bone and their relationships with age, gender, composition and microindentation properties in the elderly, Bone, December 2016, Vol.93, pp. 196-211.

[112]   Taylor WR, Heller MO, Bergmann G, Duda GN., Tibio-femoral loading during human gait and stair climbing, J Orthop Res., 2004, Vol. 22(3), pp.625-632, DOI doi:10.1016/j.orthres.2003.09.003.

[113]   Hsin-Yi Lin, Joel D. Bumgardner, Changes in surface composition of the Ti–6Al–4V implant alloy by cultured macrophage cells, Applied Surface Science, March 2004, Vol. 225, Issues 1-4, pp. 21-28.

[114]   Hans van Viet, Software Enngineering: Principles and Practice, Publisher Wiley, 2007.

[115]   Van der Linden, F. and M¨uller, J. (1995), Creating Architectures with Building Blocks, IEEE Software, Vol. 12(6), pp. 51-60.

[116]   Weller, E. (1993), Lessons from Three Years of Inspection Data. IEEE Software, Vol. 10(5), pp. 38-45.

[117]   John M. Zelle, Python Programming. An introduction to computer science, Franklin, Beedle & Associates, Inc., 2004.

[118]   Michał Jaworski, Tarek Ziadé, Expert Python Programming: Become a master in Python by learning coding best practices and advanced programming concepts in Python 3.7, Publisher Packt, ISBN 978-1-78980-889-6.

[119]   D. Gansawat, W. Jiratticharoen, S. Sotthivirat, K. Koonsanit, W. Narkbuakaew, P. Yampri, W. Sinthupinyo, Integration of image processing from the Insight Toolkit (ITK) and the Visualization Toolkit

(VTK) in Java Language for Medcial Imaging Applications, ICBME 2008, Proceedings 23, pp. 586-589, 2009.

[120]   Feng Dong, Gheorghita Ghinea, Sherry Y. Chen, User Centered Design for Medical Visualization, Publisher Medical Information Science Reference, Hershey, New York, ISBN 978-1-59904-777-5.

[121]   Laurent Massoptier, Romain Viard, Innovative imaging to improve radiotherapy treatments, Publisher SUMMER, ISBN 978-1-291-60417-7.

[122]   Amit Bandyopadhyay, Susmita Bose, Additive Manufacturing Second Edition, Publisher CRC Press Taylor & Francis Group, 2019, ISBN 978-1-138-60925-9.

[123]   Declan M. Devine, Polymer-Based Additive Manufacturing. Biomedical Applications, Publisher Springer, 2019, ISBN 978-3-030-24531-3.

[124]   Delia Alexandra Prisecaru, Daniel Besnea, Edgar Moraru, Sorin Cananau, Additive Manufactured Bioplastics for Conceptual Models of Knee Customized Prostheses, Mat. Plast., Vol. 56, no.4, 2019, pp.957-963.

[125]   Zoltan Fabian, Kristof Kadar, Lajos Patonay, Krisztian Nagy, Application of 3D Printed Biocompatible Plastic Surgical Template for the Reconstruction of a Nasoalveolar Cleft with Preoperative Volume Analysis, Mat. Plast., Vol. 56, no.2, 2019, pp.413-415.

[126]   Nagib R., Szuhanek C., Moldoveanu B., Negrutiu M.L., Sinescu C., BRAD S., Custom Designed Orthodontic Attachment Manufactured Using a Biocompatible 3D Printing Material, Mat. Plast., Vol. 54, no.4, 2017, pp.757-758.

[127]   Miclaus R., Repanovici A., Roman N., Biomaterials: Polylactic Acid and 3D Printing Processes for Orthosis and Prosthesis, Materiale Plastice, Vol. 54, no.1, 2017, pp.98-102.

[128] *** Solidworks, https://help.solidworks.com/2017/english/

[129]   Patricia Isabela Brăileanu, Loredana Manasia, Ionel Simion, Benyebka Bou- Saïd, Gina Florica Stoica, Reducing early intraprosthetic dislocation by using personalized hip joint prosthetic design and virtual preoperative planning, Published in: 5th International Multidisciplinary Scientific Conference on Social Sciences & Arts SGEM, August 24 - September 2 / 2018, DOI http://doi.org/10.5593/sgemsocial2018/5.3.

[130]   Patricia Isabela BRĂILEANU, Ionel SIMION, Benyebka BOU-SAÏD, Gina Florica Soica, Method of extracting hip joint bones from C.T. images in order to perform static F.E.A. study, Publisher U.P.B. Sci. Bull., Series D, Vol. D, Iss. 2, 2019, pp. 153-164, ISSN 1454-2358.

[131]   P. I. Braileanu, I. Simion, and B. Bou-Said, Researching and trends in optimizing hip joint prosthesis, JIDEG, vol. 14, no. 1, pp. 221-226, May 2019.

[132]   Patricia I. Brăileanu, Ionel Simion, Benyebka Bou- Saïd, Maria Gratiela Ianoş, Oliver Tayot, Bertrand Bordet, F.E.A. study of a patientțs prosthetic hip by using Reverse Engineering Method, Proceedings of The 13th International Multi-Conference on Society, Cybernetics and Informatics (IMSCI 2019) July 6-9, 2019-Orlando, Florida, USA, Vol. I, pp. 65-70.

LIST OF FIGURES

Brăileanu Patricia – Isabela 185

Brăileanu Patricia – Isabela   187

Brăileanu Patricia – Isabela

Brăileanu Patricia – Isabela 189

Brăileanu Patricia – Isabela   190

LIST OF TABLES

Brăileanu Patricia – Isabela 192